Sediment dynamic, slope instability and potential tsunami hazard at the outer Thai shelf margin, Mergui Ridge, Andaman Sea

DISSERTATION

Zur Erlangung des Doktorgrades
an der Mathematisch-Naturwissenschaftlichen Fakultät
der Christian-Albrechts-Universität zu Kiel

vorgelegt von
Julia Maria Schwab

Kiel, 2017

Referent:	Prof. Dr. Sebastian Krastel
Koreferent:	Prof. Dr. Karl Stattegger
Tag der mündlichen Prüfung:	31.05.2017

Zum Druck genehmigt:

……..

Der Dekan

Hiermit erkläre ich, dass ich die vorliegende Dissertation selbständig und ohne Zuhilfenahme unerlaubter Hilfsmittel angefertigt habe. Die Doktorarbeit stellt abgesehen von der Beratung durch meinen Betreuer nach Inhalt und Form meine eigene Arbeit dar. Bisher ist die Arbeit noch nicht an anderer Stelle im Rahmen eines Prüfungsverfahrens vorgelegt worden. Die Arbeit ist unter Einhaltung der Regeln guter wissenschaftlicher Praxis der Deutschen Forschungsgemeinschaft entstanden.

Kiel, den

Julia Schwab

Abstract

The Thai Andaman Sea coast, located in the vicinity of the Sunda Trench, has been repeatedly struck by tsunamis, one of them being the catastrophic and highly destructive 2004 Indian Ocean Tsunami, which was caused by an extreme earthquake at the Sunda Trench. More than 227000 people lost their lives during this catastrophe, 8200 of them in Thailand alone. Based on tsunami event layers retrieved at the Thai coast, the geological record shows that this was not the first tsunami that hit the area, and possible predecessors to the 2004 Tsunami have been identified in the geological record for the last two millennia. Most of the tsunamis worldwide are of tectonic origin, but it is well known, that earthquakes are not the only source for tsunamis. Submarine landslides can cause destructive tsunamis as well. Submarine landslides occur when a slope becomes unstable and fails. The stability of a slope depends largely on the sedimentary conditions, as these conditions govern the properties and the morphology of the sedimentary deposits. Thereby they dictate, whether failure preconditioning factors, such as rapid sedimentation, overpressure buildup or the presence of weak layers are developed. In order to assess the tsunami potential that may arise from a specific slope it is hence crucial to know the sedimentary processes and conditions that shape a margin. Moreover, it is important to know the failure history in order to estimate the frequency of failures and their dimensions. All this information may also help to assess the potential for future failures and for landslide tsunamis. The outer Thai shelf margin in the Andaman Sea has previously not been investigated in detail with respect to sediment dynamics and associated slope stability. Therefore, it was unknown so far, whether submarine mass wasting at this margin does occur and whether it may add to the tsunami hazard potential for the adjacent coasts. In order to examine the sedimentary development of this slope and in order to evaluate the state of the slope with respect to its stability and tsunami potential a new multibeam bathymetry and high resolution 2D multichannel reflection seismic data set was acquired during three subsequent research cruises (MASS I, MASS II and MASS III) in 2006, 2007 and 2011 from the Mergui Ridge area at the Thai outer shelf approximately 250km west off Phuket.

The analysis of the newly acquired data shows that the Mergui Ridge, an area of low sedimentary input, is today shaped by bottom currents. This can be concluded from the presence of drift deposits adjacent to areas of low sedimentation or erosion of old sediments. Along-slope currents, fluctuating with the monsoon seasons and potentially also internal waves may be responsible for shaping the margin today. After a phase of uplift and subaerial exposure at the end of the Late Miocene, marked by a pronounced erosive unconformity, the Mergui Ridge shelf area subsided in the Pliocene to its recent position in up to 800m water depth. Tectonic deformation today is ongoing but on a smaller scale than in the past. This geological development is reflected in the older sedimentary deposits present in the Mergui Ridge area. This led to the deposition of a sedimentary unit characterized by indicators of local erosion when the ridge was in shallow water. Today a thin drape of undisturbed sediments partially covers these older sediments.

Within the sediments of the Mergui Ridge area, seventeen mass transport deposits have been identified. Most of these deposits occur within drift deposits. Their presence shows that the slope has been unstable and failures have taken place repeatedly. The presence of fluids, instability of drift deposits and ongoing tectonic activity are considered as most important preconditioning factors; this setting may lead to failures in the future. Based on their mostly relative small dimension with volumes between approximately 0.3 and 14km^3, and the large water depth where the failures occur, it is unlikely for most of these failures to have been tsunamigenic, but triggering of tsunamis by such failures cannot be excluded.

Based on the thickness of hemipelagic layers between events, the recurrence of these failures seems to be long, especially compared to the recurrence of tectonic tsunamis. A simple numerical modeling of landslide tsunami propagation and estimation of run up heighs based on geometrical parameters of the previously identified mass transport deposits of up to between 1.0 and 25.8m shows that landslides in the area may produce tsunamis. However, modeled tsunamis represent worst case scenarios and wave heights may be overestimated in the simple model.

Zusammenfassung

Die thailändische Küste der Andamanensee, westlich des Sundagrabens gelegen, war schon mehrfach von Tsunamis betroffen. Einer dieser Tsunamis war der katastrophale und höchst zerstörerische Tsunami im Dezember 2004, der mehr als 227000 Menschen das Leben kostete, davon alleine 8200 in Thailand. Tsunamiablagerungen, eingeschaltet in die Sedimente der thailändischen Küste, zeigen, dass der Tsunami von 2004 nicht der erste Tsunami war, der die Küste getroffen hat, sondern dass in den letzten zweitausend Jahren mehrere solcher Tsunamis stattgefunden haben könnten. Die weltweit häufigsten Tsunamis werden durch Erdbeben verursacht, jedoch sind Erdbeben nicht der einzige Auslöser für Tsunamis. Auch untermeerische Hangrutschungen können zerstörerische Tsunamis verursachen. Die Stabilität/Instabilität eines Hanges und das Auftreten von Hangrutschungen werden erheblich von den vorherrschenden Sedimentationsprozessen beeinflusst, da diese Prozesse die Eigenschaften und die Morphologie der abgelagerten Sedimente bestimmen und damit, ob Vorbedingungen geschaffen werden die zum Versagen eines Hanges führen können. Solche Vorbedingungen sind zum Beispiel hohe Sedimentationsraten, der Aufbau von Porenüberdruck im Sediment oder die Ablagerung von instabilen Lagen in den Sedimenten. Um das Tsunamipotential durch Rutschungen an einem bestimmten Hang abzuschätzen ist es daher essentiell die Sedimentationsbedingungen und -prozesse im Bereich dieses Hanges zu kennen. Darüber hinaus ist es wichtig, das Auftreten von Hangrutschungen, auch in der geologischen Vergangenheit zu analysieren, um die Häufigkeit von Hangrutschungen und ihre Dimensionen einzuschätzen, und um von diesen Kenntnissen ausgehend das Potential für zukünftige Rutschungen und dadurch mögliche Tsunamis zu beurteilen. Der äußere Schelfrand in der thailändischen Andamanensee ist bisher im Hinblick auf die Sedimentdynamik und die damit assoziierte Hangstabilität nicht detailliert untersucht worden. Daher war bisher auch unbekannt, ob submarine Hangrutschungen in diesem Gebiet auftreten, und ob solche Hangrutschungen ein Tsunamipotential für die angrenzenden Küstengebiete beitragen. Um die sedimentäre Entwicklung dieses Gebietes und den Zustand des Kontinentalhanges in Bezug auf die Hangstabilität und das Tsunamipotential zu untersuchen, wurde ein neuer Fächerecholot-Datensatz und ein hochauflösender 2D Reflexionsseismik-Datensatz während drei Forschungsausfahrten (MASS I, MASS II und MASS III) 2006, 2007 und 2011 im Gebiet des Mergui Rückens, der den thailändischen äußeren Kontinentalhang etwa 250 km westlich vor Phuket bildet gewonnen.

Die neugewonnenen Daten zeigen, dass die Morphologie des Mergui Rückens, ein Gebiet von geringem Sedimenteintrag, rezent durch Bodenströmungen geformt wird. Dies kann aus dem Auftreten von Driftsedimenten im Arbeitsgebiet geschlossen werden, sowie aus dem Vorhandensein von Bereichen die durch Erosion geprägt sind und oder in denen keine Sedimentation stattfindet. Es ist möglich, dass monsuninduzierte Strömungen entlang des Schelfrandes und eventuell auch das Auftreten von internen Wellen die Morphologie und Dynamik des Schelfrandes im Gebiet des Mergui Rückens prägen. Die bekannte geologische Entwicklung des Gebietes wird aus den identifizierten älteren seismischen Einheiten ersichtlich. Nach einer Hebungsphase im späten Miozän, während der der Mergui Rücken oberhalb des Meeresspiegels lag, und die zur Ausbildung einer deutlichen Erosionsdiskordanz führte, fand im Pliozän tektonisch bedingte Subsidenz statt und das Gebiet senkte sich auf seine heutige Lage in bis zu 800m Wassertiefe ab. Tektonische Deformation findet auch rezent noch statt aber, in einem sehr viel kleineren Ausmaß. Während der initialen Phase der Subsidenz wurden Sedimente abgelagert, die intern Hinweise auf eine Ablagerung im Flachwasserbereich zeigen. Diese werden von einer

geringmächtigen ungestörten Ablagerung überdeckt, die ein Absinken unterhalb den Einflussbereichs des Meeresspiegels zeigt.

Siebzehn Ablagerungen die möglicherweise von Hangrutschungen stammen wurden im vorliegenden Datensatz identifiziert. Die meisten dieser Ablagerungen sind in die Driftsedimente eingelagert. Das Vorhandensein dieser Ablagerungen zeigt, dass der Schelfrand instabil ist, und dass hier wiederholt Hangversagen aufgetreten ist. Fluide in den Sedimenten, die generelle Instabilität von Driftsedimenten und rezent andauernde tektonische Aktivität sind potentielle Vorbedingungen für Hangversagen im Arbeitsgebiet und könnten auch in der Zukunft zu Hangrutschungen führen. Das Volumen der meisten identifizierten Hangrutschungen ist relativ klein (0.3 bis zu 14km^3), und vermutlich sind die Rutschungen auch meist in großen Wassertiefen aufgetreten. Daher ist es relativ wahrscheinlich, dass die meisten dieser Rutschungen keinen Tsunami ausgelöst haben. Der Datensatz lässt es aber nicht zu, ein Tsunamipotential grundsätzlich auszuschließen. Die Mächtigkeit hemipelagischer Sedimente zwischen den einzelnen Hangrutschungs-ablagerungen zeigt jedoch auch, dass die Frequenz von Rutschungsereignissen gering ist, vor allem im Verhältnis zur Frequenz von erdbebeninduzierten Tsunamis. Die vorläufige vereinfachende Modellierung zeigte, dass Hangrutschungen, die im Arbeitsgebiet auftreten, Tsunamis produzieren könnten. Jedoch sind die modellierten Hangrutschungen Worst-Case-Szenarien und errechnete Run ups die zwischen bis zu 1.0 und 25.8m liegen, könnten im angewendeten vereinfachenden Modell überschätzt sein.

Content

Outline of the Thesis 2
1. **Introduction** 4
1.1. Motivation 4
1.2. Submarine Landslide Tsunamis 6
1.3. Slope Stability on Continental Margins 8
References 11
2. **Regional setting of the working area** 18
2.1. Physiography 18
2.2. Hydrography 19
2.3. Tectonic development and sedimentation 21
2.3.1. Mergui Basin 23
2.3.2. Mergui Ridge 24
2.3.3. East Andaman Basin 25
References 26
3. **Objectives** 30
4. **Data and Methods** 32
4.1. Multibeam Bathymetry data 32
4.2. Supplementary bathymetry data 33
4.3. High resolution 2D multichannel reflection seismic data 33
4.3.1. Acquisition of reflection seismic data 33
4.3.2. Processing of reflection seismic data 33
4.3.3. Interpretation of reflection seismic data 35
4.4. ECCO2 dataset 38
4.5. Tsunami Modeling 40
4.5.1. Initial wave calculation 41
4.5.2. Tsunami propagation numerical modeling 42
4.5.3. Run-up estimation 42
References 43
5. **Sediment dynamic in the Mergui Ridge area at the outer continental margin off western Thailand, Andaman Sea: Manuscript I** 46
6. **Submarine mass wasting and associated tsunami risk offshore western Thailand, Andaman Sea, Indian Ocean: Manuscript II** 84
7. **Modeling of Potential Landslide Tsunami Hazards Off Western Thailand (Andaman Sea): Manuscript III** 108
8. **Conclusions and Outlook** 122
References 125
Acknowledgements 126

Outline of the Thesis

Chapter 1 is an introductory chapter. The motivation for the work thesis work is described. Introductory information on submarine landslides and slope instability is outlined.

Chapter 2 describes the setting of the working area at the outer shelf margin off western Thailand. This includes physiography, hydrography and the geological development of the working area.

Chapter 3 describes specific objectives and research topics addressed with the work of this thesis.

Chapter 4 describes data and methods used in this thesis.

Chapter 5 contains Manuscript I, in preparation to submission: Sediment Dynamic in the Mergui Ridge Area at the outer continental margin off Western Thailand, Andaman Sea. Schwab, Julia; Böttner, Christoph; Gross, Felix; Krastel, Sebastian. To be submitted to Marine Geology.

This chapter focusses on the sedimentary development and dynamics of the working area at the Mergui Ridge. The geological history of the working area is worked out, the morphology and nature of recent sediment deposits are interpreted and possible processes shaping the margin today are discussed.

Chapter 6 contains Manuscript II, published: Submarine mass wasting and associated tsunami risk offshore western Thailand, Andaman Sea, Indian Ocean. Schwab Julia M.; Krastel, Sebastian; Grün, Mathias; Gross, Felix; Pananont, Passakorn; Jintasaeranee, Pachoenchoke; Bunsomboonsakul, Suratta; Weinrebe, Willi; Winkelmann, Daniel. (2012); Natural Hazards and Earth System Science; 12; 8; 2609–2630; doi:10.5194/nhess-12-2609-2012.

This chapter focusses on the investigation of slope failures in the outer western Thai Shelf area. Mass transport deposits are identified, their volumes and recurrences are examined and the potential for landslide tsunamis that may have arisen or may arise from the working area is assessed.

Chapter 7 contains Manuscript III, published: Modeling of Potential Landslide Tsunami Hazards Off Western Thailand (Andaman Sea). Schwab, Julia, Krastel Sebastian; Heidarzadeh Mohammad; Brune, Sascha (2014); S. Krastel et al. (eds.); Submarine Mass Movements and Their Consequences; Advances in Natural and Technological Hazards Research 37; Springer International Publishing Switzerland 2014; doi: 10.1007/978-3-319-00972-8.

This chapter describes a numerical modeling approach that was applied in order to preliminarily assess the tsunami hazard potential that may arise from landslides in the working area.

Chapter 8 presents the main conclusions drawn from the thesis work. Furthermore the chapter gives an outlook on potential future research, suggested based on the results obtained in this thesis.

1. Introduction

Tsunamis are recurring natural disasters that can have most devastating impact on coastal communities. This has become especially obvious in recent years by the catastrophic 2004 Indian Ocean Tsunami, where more than 227000 people were killed (NGDC/WDS, 2016) and by the 2011 Tohoku Tsunami in Japan, that caused around 19000 deaths (NGDC/WDS, 2016). Both tsunamis have been triggered by earthquakes. In Southeast Asia, tsunamis are a recurring phenomenon due to seismic activity at the Sunda Trench which is repeatedly causing disasters, such as also for example the tsunamis of 2006 and 2010. These tsunamis caused both several hundred casualties on Java and on Mentawai Island respectively (NGDC/WDS, 2016).

However, earthquakes are not the only cause for tsunamis. Submarine landslides, arising from slope failures at continental margins, can also pose geohazards that have consequences for humans. They may threaten coastal communities by producing tsunamis of catastrophic extend as well, as this has been the case for example 1998 in Papua New Guinea (Tappin et al., 2001; Synolakis et al., 2002; Tappin et al., 2008) where a landslide tsunami caused wave heights of 10-15m around Sissano Lagoon area (Tappin et al., 2008) and about 2200 people died (McSaveney et al., 2000). Moreover, submarine landslides are capable not only of producing tsunamis but also to damage sea floor infrastructure by their moving sediment masses (Bruschi et al., 2006). It has been hypothesized that submarine landslides may also have an impact on climate by releasing methane from the subsurface (Maslin et al., 2004; Beget and Addison, 2007). Mass failure events are hard to predict (Harbitz et al., 2013; Urlaub et al., 2013) particularly in areas where no or only little information about sedimentary conditions of the continental margin is available. Hence it is necessary to obtain detailed knowledge of sedimentary processes and the stability of individual shelf and slope areas in order to gain insight into potential causes, frequency and dimensions of previous slope failures, their hazard potential and also in order to obtain information about the potential for future slope failures. Ideally, suchknowledge may be used to assess tsunami potential and preparedness for coastal areas.

1.1. Motivation

Thailand is one of the countries that have been hit the hardest by the 2004 Indian Ocean Tsunami, caused by an extreme earthquake with a magnitude of 9.1 (NGDC, 2016) at the nearby Sunda Trench subduction zone. It has affected the Thai coast in several ways. More than 8200 citizens of Thailand lost their lives during the catastrophe (Telford and Cosgrave, 2006). Besides tremendous damage and loss for the coastal communities, coastal ecosystems have been damaged, such as mangrove forests (Römer et al., 2010) and other components of the ecosystem that are important for the coastal communities (Kaiser et al., 2013). Also in nearshore areas, a minor effect of the Tsunami on the sedimentary environment has been found (Feldens et al., 2012) such as resuspension of sediment (Milker et al., 2013) and deposition of event layers (Feldens et al., 2009; Sugawara et al., 2009; Sakuna et al., 2012; Sakuna-Schwarz et al., 2015). A database of reported historic tsunamis in Southeast Asia, compiled by Løvholt et al. (2012) contains 153 reported incidents, most of them from the 17th century onward. It shows that tsunamis

in the area are a recurrent phenomenon. Also in the geologic record, based on tsunami deposits identified in coastal areas of western Thailand and Sumatra, potentially destructive predecessors of the 2004 Indian Ocean Tsunami in the last two millennia have been identified (Jankaew et al. 2006; Monecke et al., 2008; Fujino et al., 2009; Brill et al. 2011; 2012).

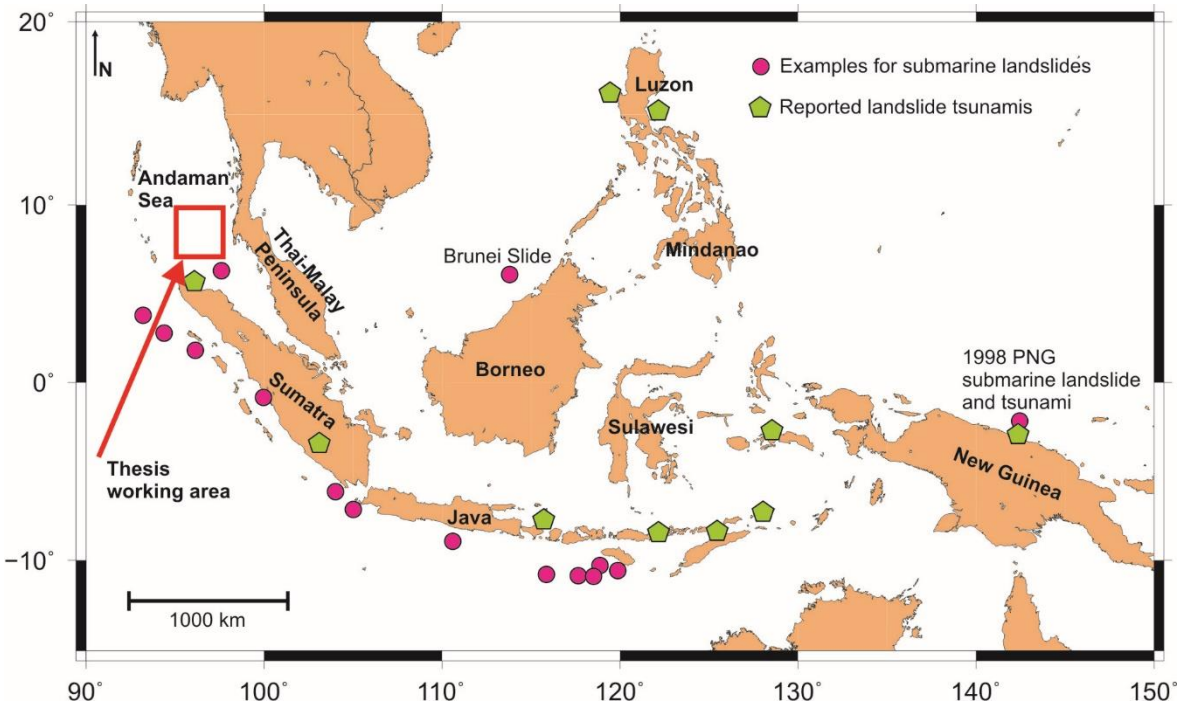

Figure 1: Map of Southeast Asia, showing working area of the thesis, and several locations of submarine landslides identified in geophysical data, as well as locations of reported landslide tsunamis in the area. Compiled from Gee et al. (2007), Tappin et al. (2008), Lin et al. (2009), Brune et al. (2010) and Løvholt et al. (2012).

The source statistics of the Løvholt et al. (2012) compilation show, that different triggers for the recorded tsunamis have been reported. Most of the events are attributed to earthquakes and volcanoes. However, earthquakes and volcanoes are not the only source for tsunamis in Southeast Asia. In fact, nine tsunami events in the database have been caused by landslides or landslides together with earthquakes (Figure 1). Well known examples of landslide tsunamis around Southeast Asia are, among others, the 1992 Flores Island tsunami (Yeh et al., 1993; Imamura et al., 1995), and the 1998 Papua New Guinea Tsunami (Tappin et al., 2001; Synolakis et al., 2002; Tappin et al., 2008). Several submarine landslide deposits have been identified in geophysical datasets in Southeast Asia (Figure 1), such as the large-scale Brunei slide off Northwestern Borneo (Gee et al., 2007), deposits in the Indonesian Sunda Arc (Brune et al., 2010 and references therein). Also, southwest off the Thai-Malay Peninsula submerged submarine landslides with a minimum age of 20-30ka have been found (Lin et al., 2009). Sumner et al. (2013) showed that mass wasting events at the Sumatran margin during the last centuries are scarce and that their age cannot be correlated with earthquake records for the last 200 years. This may imply that slope failures in the area can have causes and triggers other than earthquakes.

An area in Southeast Asia that previously has not been investigated with respect to sediment dynamics and associated slope stability is the Thai outer continental margin off western Phuket, the Andaman Sea shelf break. No high resolution bathymetric and subsurface data have been available, and no knowledge existed whether, in addition to

the tsunami risk that arises for Thailand from large earthquakes along the Sunda Trench, submarine mass wasting at the continental margin may add to the tsunami hazard potential. In 2006 the interdisciplinary project TRIAS (Tracing Tsunami Impacts On- and Offshore in the Andaman Sea Region, see Schwarzer et al., 2010 for a more detailed description) was started as a Thai-German cooperation. The project was funded jointly by the National Research Council of Thailand (NRCT) and the German Research Foundation (DFG). The overall aim of this project was, in the aftermath of the Tsunami of 2004, to investigate tsunami related issues in the Andaman Sea, ranging from tsunami triggering, tsunami impact on shelf, coast and land, to economic and social consequences of tsunamis for the coastal communities. During two project phases in 2006 and 2007 six subprojects of TRIAS addressed the following major topics: Improvement of risk management such as early warning to prevent or mitigate future tsunami events, factors determining resilience respectively vulnerability of coastal areas to tsunamis (TRAIT subproject); attenuation of tsunami wave energy in the coastal realm and the role of natural and artificial barriers to wave attenuation (TAPFOR subproject); influence of loaded tsunami backflow to biosphere, ecosystems and sea floor topography and sedimentary cover (ORCAS and TUNWAT subprojects); tsunami recurrence and its sedimentary evidence on-and offshore in the recent past (TRIAS COAST, TUNWAT subprojects) and the MASS-Andaman Sea subproject aiming to assess where and how tsunamis may be triggered in the previously unstudied Andaman Sea shelf break region. The primary aims of the MASS subproject were to determine the current state of the Andaman Sea Shelf break off the west coast of Thailand, to assess its stability and the potential for slope failures and for tsunamis that may arise from slope failures. In the first project phase, during two research cruises (MASS I and MASS II) multibeam bathymetry and sub-bottom profiler data were acquired. Jintasaeranee et al. (2012) investigated these data and found several indicators for slope instabilities such as a rugged, potentially unstable zone at the shelf break, indicators for fluid venting and several small- scale scars and slumps. Jintasearanee et al. (2012) did not conclude a tsunami potential from the identified failures and due to the limited data set they could not investigate the subsurface. In order to obtain a more detailed picture of the state of the slope, a subsequent cruise (MASS-III) was carried out in 2011 and new high resolution 2D multichannel reflection seismic data were collected. Within the framework of the MASS-Andaman-Sea project the aim of this thesis is a joint interpretation of the multibeam bathymetry and the 2D high resolution multichannel reflection seismic data from the Andaman Sea shelf break in order to determine sediment transport processes that shape the margin and in relation to that to asses the slope stability.The occurrence of and possible causes for recent and older, buried slope failures are examined and and their tsunami potential is preliminarily assessed.

1.2. Submarine Landslide Tsunamis

Whereas large scale, ocean-wide tsunamis are mostly triggered tectonically, submarine landslides are also an important cause for tsunamis, although they occur only infrequently (Harbitz et al., 2014). In fact, landslides, both submarine and subaerial, may be the second most frequent trigger for tsunamis worldwide (Harbitz et al., 2014). Over the last decades, submarine landslides as causes for tsunamis have received increasing attention, especially after the 1998 Papua New Guinea landslide tsunami (Tappin et al., 2001; Synolakis et al., 2002; Tappin et al. 2008). Several historic, locally destructive tsunami hazards have been attributed to submarine slope failures. Among them are the 1929 Grand Banks tsunami (Hasegawa and Kanamori, 1987; Fine et al., 2005), the 1994 Skagway Harbor Tsunami (Kulikov et al., 1996) and the 1979 Nice tsunami (Assier-Radciewicz, 2000).

Landslide tsunamis are surface waves that are generated by impulsive disturbance of the seafloor during a mass wasting event, resulting in transfer of momentum from the landslide mass to the overlying water column (Mohammed and Fritz, 2012). The characteristics of the initial tsunami wave are dependent on landslide properties. Among others, the following landslide parameters are important: Volume (length, width and thickness), slide dynamics (initial acceleration and velocity) and retrogressive behavior (Løvholt et al., 2015 and references therein). Water depth where the landslides do occur is also an important factor for tsunami potential, which decreases with increasing water depth. As a very generalized rule, the critical water depth for tsunami generation can be assumed to be ~1000m or less at a minimum landslide volume of ~2km^3 Greene et al. (2006). Initial tsunami wave height increases with landslide volume (Murty, 2003) and initial acceleration. Tsunami wavelength increases with landslide velocity and runout distance (Løvholt et al., 2015 and references therein). Moreover, the flow behavior of a landslide during the failure process can influence the resulting tsunami wave as well (Harbitz et al., 2014). If a mass failure is slow and disintegrates during the sliding process it may cause smaller waves than a sudden large block failure. On the other hand, abrupt deceleration of a landslide may produce large surface elevations (Masson, 2006). Especially slumps may be tsunamigenic (Masson et al., 2006; Løvholt et al. 2015). Retrogressive failures may stretch the tsunami if the time lag between individual failures is large, whereas positive interference may increase the wave amplitudes on short time lags (Løvholt et al., 2015).

In contrast to earthquake tsunamis, which can have far field effects due to their high energy content and threaten large areas, landslide tsunamis spread from a relatively small source and their effects are locally constrained due to fast energy dissipation (Helal and Mehanna, 2008). However, their relatively small source areas result in shorter wavelengths compared to earthquake tsunamis, which may result in extreme run-ups in the near-field (Okal and Synolakis, 2004). For example, during the 1998 Papua New Guinea Landslide tsunami wave heights of up to 15m have been observed (McSaveney et al., 2000; Okal and Synolakis, 2004). Moreover, investigations of prehistoric examples of large scale mass wasting events showed that landslides of extreme volumes such as the Storegga Slide off Norway, may trigger tsunamis that can have also significant far-field effects (Harbitz et al., 2014). The Storegga Slide may have caused wave heights exceeding 20m in places, as deduced from tsunami deposits that have been observed in Iceland, Norway, Scotland and on the Faroe Islands (Bondevik et al., 2003 and references therein). Similarly, the BIG'95 landslide, another prehistoric event that is among the largest landslides in the Mediterranean (Lastras et al., 2004; Urgeles et al., 2006) may have had widespread effects in the Mediterranean. Tsunami run-up heights of 9m and more have been modeled for this event (Igleasias et al., 2012; Løvholt et al., 2013). Moreover, tsunamigenic landslides may be triggered by earthquakes, that trigger a tsunami themselves (Hampton et al., 1996; Harbitz et al., 2006). Such coseismic triggering may add local peaks to the seismic tsunami by the landslide (Synolakis et al., 2002), as it has been suggested for the 2011 Tohoku tsunami (Tappin et al., 2014), where, according to Tappin et al. (2014) local wave heights of up to 40m cannot be explained by the seismic event alone.

1.3. Slope Stability on Continental Margins

Submarine landslides arising from failures of the continental slope are among the key transport processes of sediment from the continental margins into the deep-sea realm (Hühnerbach and Masson, 2004; Masson et al. 2006; Talling et al., 2012; Urlaub et al., 2013). The term “submarine landslide” is used in the following as a general denomination for all mass movements generated by submarine slope failures, as in Masson et al. (2006) and Talling et al. (2012). Unlike subaerial landslides, submarine landslides on open continental slopes can have extreme characteristics such as large volumes (several thousand km^3; Dingle, 1977; Haflidason et al., 2004), occurrence on low slope gradients (<2°; Urlaub et al., 2012 and references therein) and long runout distances (several hundred km; Dingle, 1977; Haflidason et al., 2004).

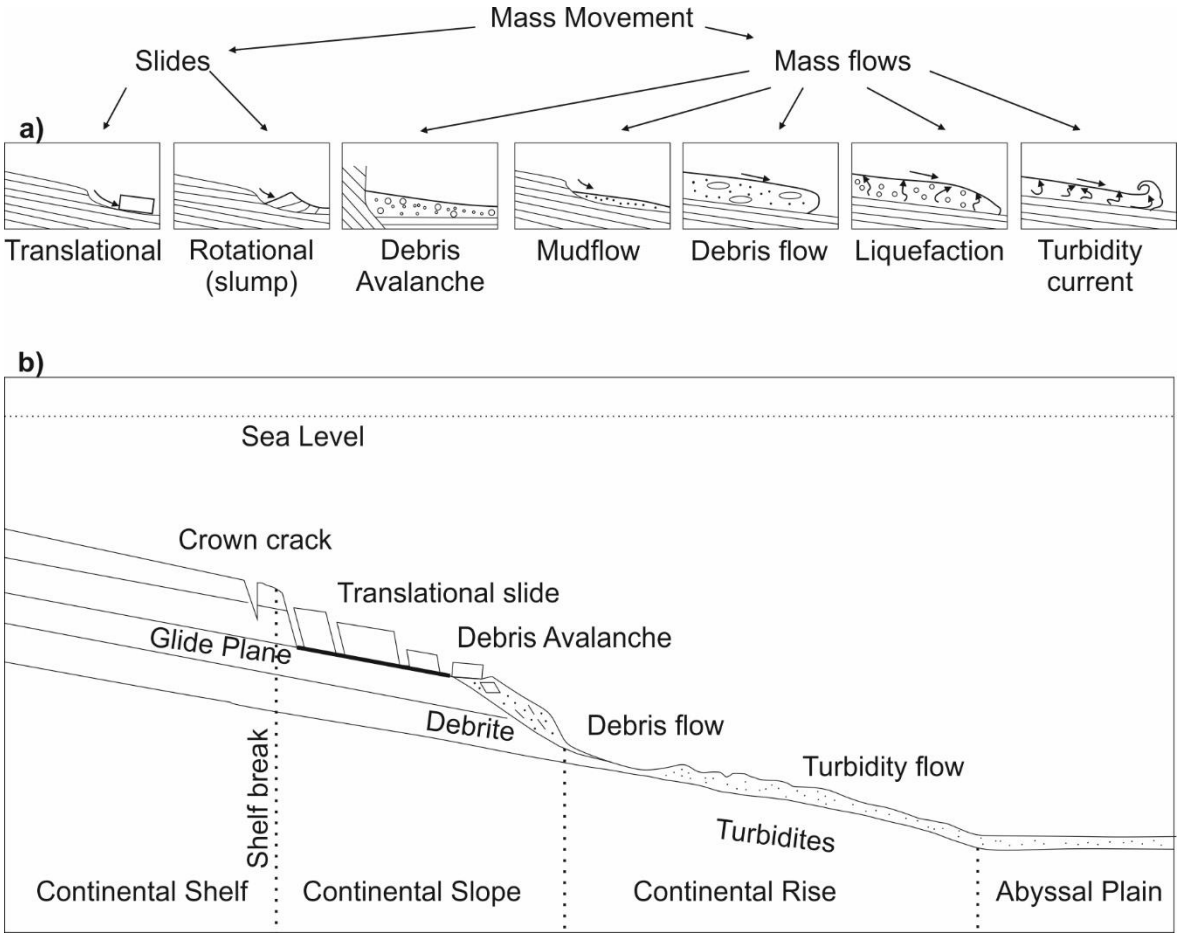

Figure 2: a) Classical mass movement nomenclature based on Varnes (1958), discerning between landslides, moving as coherent bodies and sediment loaded mass flows containing sea water. Modified from Lee et al. 2007. b) Conceptual sketch of transformation of a translational slide during the failure process. Modified from Smith et al. (2013).

Figure 2 gives and overview over different types of submarine landslides that have been discerned (Hampton et al., 1996; Mulder and Cochonat, 1996; Locat and Lee, 2002). End members range from coherent translational slides and rotational slumps that move along failure surfaces, to plastic debris flows that are characterized by laminar plastic flow of grains, to turbulent non-cohesive flow turbidity currents (Mulder and Cochonat, 1996; Masson et al., 2006). Typical morphological characteristics of failures include a headwall scarp with slide/slump below and depositis of debris acalanches, debris flows and/or turbidity currents subsequently further downslope (Mulder and Cochonat, 1996; Masson et al., 2006). Slope failures are often described to be retrogressive (Locat and Lee, 2002;

Masson et al., 2006). Accordingly, mass flow events may comprise different flow types, and transformation between different flow types may occur during the failure event (Talling et al., 2012). Submarine landslides are a phenomenon that is ubiquitous on continental margins, irrespective of the tectonic and geological setting (Hampton et al., 1996, Masson et al. 2006; Solheim et al., 2007; Lee et al. 2007; Harbitz et al., 2014), although most slopes possess an inherent stability (Masson et al., 2006). Hence, in order for a submarine slope to become unstable and fail, there has to exist a loading that cannot be resisted by the material strength of the sediment (Lee et al., 2007). This means that slope stability is dependent on the balance of stresses acting downslope and the resisting forces (Hampton; 1996; Lee et al, 2007).

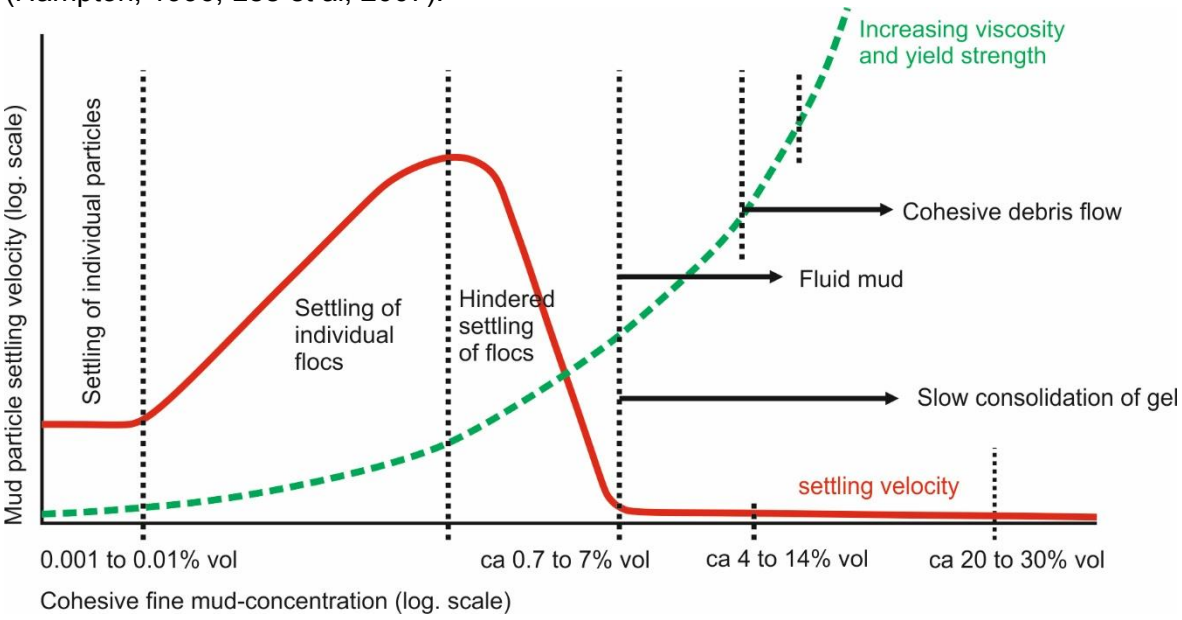

Figure 3: Dependence of mud particle settling velocity, viscosity/yield strength and resulting flow types from concentration of cohesive mud. Modified from Talling et al. (2012).

To gain knowledge about the state of a slope and its subsurface conditions it is important to obtain insight about the sedimentary processes that shape the margin, as these processes govern sedimentation rate, distribution and morphology as well as internal composition, type and texture of deposited sediments, and in turn, those characteristics may dictate whether preconditions for failure develop in a specific area.

A number of interacting environmental factors can lead to slope failure (Canals et al., 2004; Masson et al., 2006; Solheim et al., 2007; Smith et al., 2013). Common preconditioning factors and causes for submarine slope failure that have been suggested are: the presence of weak layers (Masson et al. 2006; Solheim et al. 2007; Locat et al. 2014), dissociation of gas hydrates within the sediment (McIver, 1982; Nixon and Grozic, 2007; Grozic, 2010) and pore fluid overpressure due to rapid sedimentation (Dugan and Sheahan, 2012). Generally, pore fluid overpressure seems to be the key factor that may lead to destabilization of sediment (Dugan and Sheahan, 2012). However, as submarine landslides are difficult to monitor, the exact nature and interplay of different triggers and preconditioning factors is not well understood yet (Urlaub et al., 2013; Talling et al., 2014). For example, headwalls of most large continental landslide are located at depths below the gas hydrate stability zone (Talling et al., 2014), or where gas hydrates seem to be absent (Urlaub et al., 2013) and large submarine landslides do occur in areas where the sedimentation rates are low (Urlaub et al., 2012). It has been suggested that cyclic fluctuations of climate during glacial-interglacial phases and the associated changes in sedimentation and sea level may induce landslide recurrence that is linked to these cycles (Bryn et al., 2005; Lee et al., 2009), hence implying a potential climate control on the

occurrence of submarine landslides as well (Tappin et al., 2010). However, on a global perspective, no statistically relevant dependence of landslide timing and frequency of cyclic environmental changes can be proved yet (Urlaub et al., 2013), as the current database of worldwide landslide events contains too few events that are not yet well enough dated (Pope et al., 2015). Earthquakes are the most often suggested final trigger for submarine landslides (Harbitz et al., 2014). On the other hand, frequent seismicity may lead to consolidation of sediment and hence increase stability of the slope (Locat and Lee, 2002). In fact, recent work by ten Brink et al. (2016) found a statistical correlation between earthquake frequency and the absence of slope failures on different continental margins. Moreover, frequent seismicity may also influence the size of submarine landslides that may be smaller in areas where earthquakes do occur frequently, implying a small landslide tsunami hazard potential from such margins (Völker et al., 2009, 2011). Generally, the presence of fine grained clay or mud sediment layers may favor buildup of excess pore pressure due to its low permeability (Bryn et al., 2005; Masson, 2006), and hence areas where fine grained material dominates may be especially susceptible for failure (Masson, 2006). Moreover, sedimentary properties do not only influence slope stability, but they also influence the dynamics of the failure process (Figure 3). Elverhoi et al. (2010) found that clay rich material tends to maintain coherence over long runout distances, moving at high velocities during a slope failure event whereas sand rich material tends to disintegrate. Talling et al., (2012) describes that even small changes in cohesive mud content can alter flow behavior (Figure 3) by changing fluid viscosity, yield strength and dissipation time of excess pore pressure by orders of magnitude. This in turn may have implications for the characteristic of landslide tsunamis, as these are influenced by the dynamics of the mass wasting event that creates them.

A specific example for potentially unstable sediments are contourite drifts, that are ubiquitous on continental margins (Rebesco et al., 2014 and references therein). They often exhibit a mounded geometry and are located on inclined slopes, which makes them prone to failure (Rebesco et al, 2014 and references therein). Drift deposits tend to be well sorted due to the action of steady bottom currents, and have a lower shear resistance than poorly sorted sediments. Drift deposits therefore may be especially prone to liquefaction during earthquakes (Laberg and Camerlenghi, 2008). Moreover, high sedimentation rates within areas of drift deposition may lead to rapid loading and development of excess pore pressure (Laberg and Camerlenghi, 2008). Pore fluid overpressure may be enhanced by migration of gas due to high organic content in the high productivity water masses at continental margins and by the migration of fluids into the upper sediment layers, which may further destabilize the sediment (Vorren et al. 1998, Stigall and Dugan, 2010). In fact, the interrelation between slope instability and the presence of contourites has been shown for several locations, the most prominent example being the Storegga Slide (Bryn et al. 2005).

Factors determining the morphology of contourite drifts are the interaction of bottom currents of specific characteristics (velocity, flow depth and flow direction) with the physiographic and geologic setting (Rebesco et al., 2014 and references therein). The location and velocity of bottom currents governs sediment transport, size sorting andwinnowing of small grain size particles as well as erosion of previously deposited sediment (McCave, 2008). Important for the interaction of currents with the sea floor is the Coriolis force. It deflects currents and steers bottom currents towards or away from the margins depending on the flow direction. Coriolis force may lead to intensification of a flow at a margin and its impact on sedimentation/erosion (Faugères et al. 1999). Locally, bottom currents can be modified by topographic obstacles which may lead to an increase in current velocity and the creation of erosional features such as erosive terraces, moats

or marginal valleys around obstacles, as shown in Figure 4 (Hernández-Molina et al., 2008). Additionally, the formation of erosive terraces may occur in areas where bottom current velocity is intense (Hernández-Molina et al., 2008). The formation of such terraces may be linked to the location of water mass boundaries where along slope bottom currents are modified by turbulences, such as internal waves (Preu et al., 2013). Figure 4 gives an overview of typical contourite drift features.

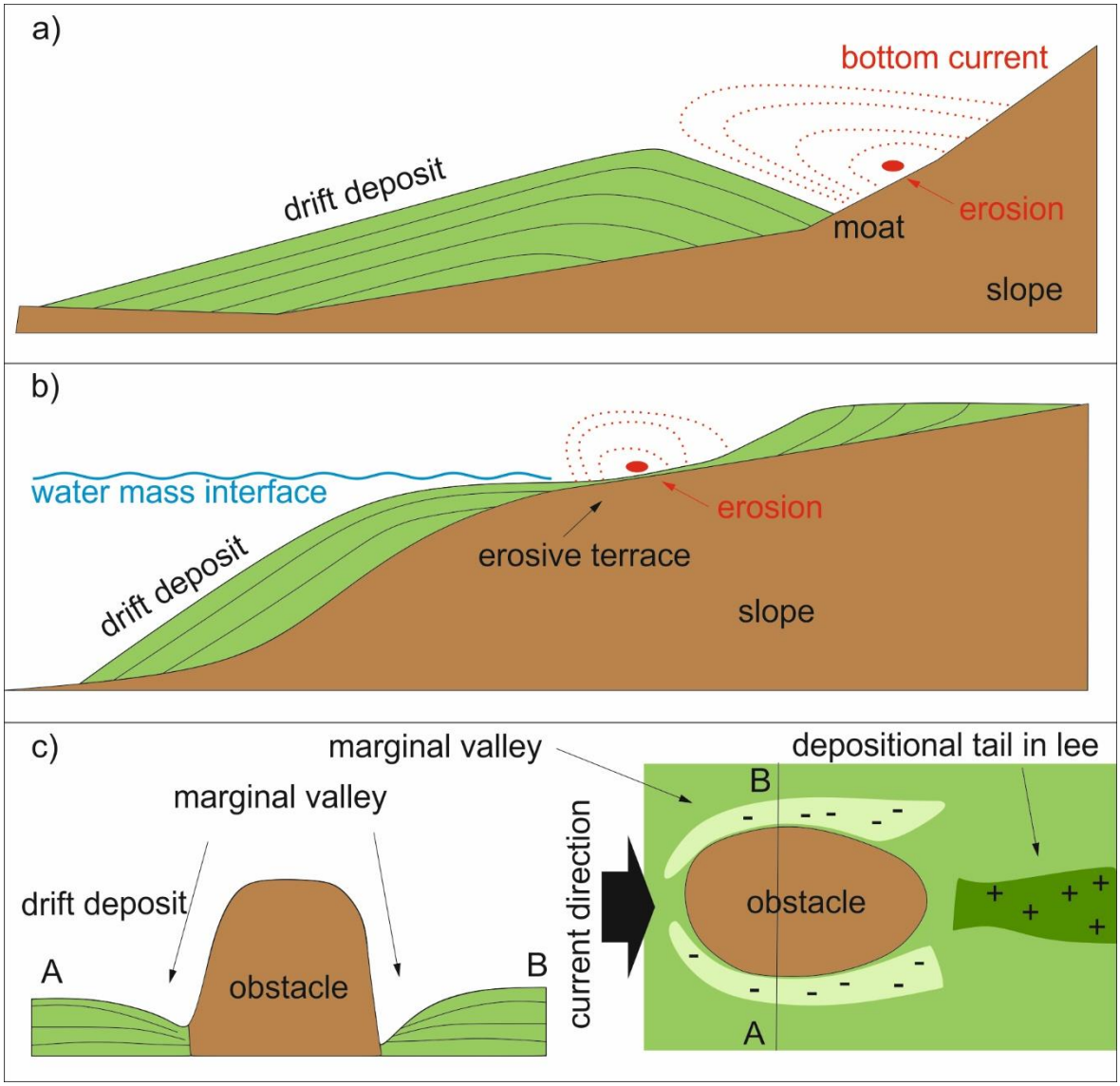

Figure 4: Conceptual sketch of typical contourite features. a) Plastered drift with main deposition away from core of bottom current. b) drift deposition with formation of erosive terrace at water mass boundary. c) Formation of marginal valley and depositional tail due to bottom current flow around obstacle. Modified from Hernández-Molina et al. (2008) and Preu et al. (2013).

References

Assier-Rzadkiewicz, S., Heinrich, P., Sabatier, P.C., Savoye, B., Bourillet, J.F., 2000. Numerical Modelling of a Landslide-generated Tsunami: The 1979 Nice Event. Pure appl. geophys. 157 (10), 1707–1727. 10.1007/PL00001057.

Beget, J.E., Addison, J.A., 2007. Methane gas release from the Storegga submarine landslide linked to early Holocene climate change: A speculative hypothesis. The Holocene 17 (3), 291–295. 10.1177/0959683607076435.
Bondevik, S., Mangerud, J., Dawson, S., Dawson, A., Lohne, Ø., 2003. Record-breaking height for 8000-year-old tsunami in the North Atlantic. Eos Trans. AGU 84 (31), 289. 10.1029/2003EO310001.
Brill, D., Brückner, H., Jankaew, K., Kelletat, D., Scheffers, A., Scheffers, S., 2011. Potential predecessors of the 2004 Indian Ocean Tsunami — Sedimentary evidence of extreme wave events at Ban Bang Sak, SW Thailand. Sedimentary Geology 239 (3–4), 146–161. 10.1016/j.sedgeo.2011.06.008
Brill, D., Klasen, N., Jankaew, K., Brückner, H., Kelletat, D., Scheffers, A., Scheffers, S., 2012. Local inundation distances and regional tsunami recurrence in the Indian Ocean inferred from luminescence dating of sandy deposits in Thailand. Nat. Hazards Earth Syst. Sci. 12 (7), 2177–2192. 10.5194/nhess-12-2177-2012.
Brink, U.S. ten, Andrews, B.D., Miller, N.C., 2016. Seismicity and sedimentation rate effects on submarine slope stability. Geology, G37866.1. 10.1130/G37866.1.
Brown, B., 2007. Coral reefs of the Andaman Sea - an integrated perspective. Oceanography and Marine Biology: an Annual Review 45, 173–194. 10.1201/9781420050943.ch5.
Brune, S., Babeyko, A.Y., Ladage, S., Sobolev, S.V., 2010. Landslide tsunami hazard in the Indonesian Sunda Arc. Nat. Hazards Earth Syst. Sci. 10 (3), 589–604. 10.5194/nhess-10-589-2010.
Bruschi, R., Bughi, S., Spinazzè Maurizio, Torselletti, E., Vitali, L., 2006. Impact of debris flows and turbidity currents on Impact of debris flow and turbidity currents on seafloor structures. Norwegian Journal of Geology 86, 317–337.
Bryn, P., Berg, K., Stoker, M., Haflidason, H., Solheim, A., 2005. Contourites and their relevance for mass wasting along the Mid-Norwegian Margin. Marine and Petroleum Geology 22 (1-2), 85–96. 10.1016/j.marpetgeo.2004.10.012.
Canals, M., Lastras, G., Urgeles, R., Casamor, J., Mienert, J., Cattaneo, A., Batist, M. de, Haflidason, H., Imbo, Y., Laberg, J., Locat, J., Long, D., Longva, O., Masson, D.G., Sultan, N., Trincardi, F., Bryn, P., 2004. Slope failure dynamics and impacts from seafloor and shallow sub-seafloor geophysical data: case studies from the COSTA project. Marine Geology 213 (1-4), 9–72. 10.1016/j.margeo.2004.10.001.
Dingle, R.V., 1977. The anatomy of a large submarine slump on a sheared continental margin (SE Africa). Journal of the Geological Society 134 (3), 293–310. 10.1144/gsjgs.134.3.0293.
Dugan, B., Sheahan, T.C., 2012. Offshore sediment overpressures of passive margins: Mechanisms, measurement, and models. Rev. Geophys. 50 (3). 10.1029/2011RG000379.
Elverhoi, A., Breien, H., Blasio, F.V. de, Harbitz, C.B., Pagliardi, M., 2010. Submarine landslides and the importance of the initial sediment composition for run-out length and final deposit. Ocean Dynamics 60 (4), 1027–1046. 10.1007/s10236-010-0317-z.
Faugères J. -C., Stow D. A. V., Imbert, P., Viana A., 1999. Seismic features diagnostic of contourite drifts. Marine Geology 162 (1), 1–38. 10.1016/S0025-3227(99)00068-7.
Fine, I., Rabinovich, A.B., Bornhold, B.D., Thomson, R., Kulikov, E.A., 2005. The Grand Banks landslide-generated tsunami of November 18, 1929: preliminary analysis and numerical modeling. Marine Geology 215 (1-2), 45–57. 10.1016/j.margeo.2004.11.007.
Fujino, S., Naruse, H., Matsumoto, D., Jarupongsakul, T., Sphawajruksakul, A., Sakakura, N., 2009. Stratigraphic evidence for pre-2004 tsunamis in southwestern Thailand. Marine Geology 262 (1-4), 25–28. 10.1016/j.margeo.2009.02.011.
Gee, M.J.R., Uy, H., Warren, J., Morley, C.K., Lambiase, J.J., 2007. The Brunei slide: A giant submarine landslide on the North West Borneo Margin revealed by 3D seismic data. Marine Geology 246 (1), 9–23. 10.1016/j.margeo.2007.07.009.
Greene, H.G.G., Murai, L.Y., Watts, P., Maher, N.A., Fisher, M.A., Paull, C.E., Eichhubl, P., 2006. Submarine landslides in the Santa Barbara Channel as potential tsunami sources. Nat. Hazards Earth Syst. Sci. 6 (1), 63–88. 10.5194/nhess-6-63-2006.
Grozic, J.L.H., 2010. Interplay Between Gas Hydrates and Submarine Slope Failure, in: Mosher, D.C., Shipp, R.C., Moscardelli, L., Chaytor, J.D., Baxter, C.D.P., Lee, H.J., Urgeles, R. (Eds.), Submarine Mass Movements and Their Consequences. Springer Netherlands, Dordrecht, pp.11–30.
Haflidason, H., Sejrup, H.P., Nygård, A., Mienert, J., Bryn, P., Lien, R., Forsberg, C.F., Berg, K., Masson, D.G., 2004. The Storegga Slide: architecture, geometry and slide development. Marine Geology 213 (1-4), 201–234. 10.1016/j.margeo.2004.10.007.

Hall, R., 2012. Late Jurassic–Cenozoic reconstructions of the Indonesian region and the Indian Ocean. Tectonophysics 570–571 (0), 1–41. 10.1016/j.tecto.2012.04.021.
Hampton, M.A., Lee, H.J., Locat, J., 1996. Submarine landslides. Reviews of Geophysics 34 (1), 33. 10.1029/95RG03287.
Harbitz, C.B., Løvholt, F., Geir, P., Masson, D.G., 2006. Mechanisms of tsunami generation by submarine landslides: a short review. Norwegian Journal of Geology 86, 255–264.
Harbitz, C.B., Løvholt, F., Bungum, H., 2014. Submarine landslide tsunamis: How extreme and how likely? Nat Hazards 72 (3), 1341–1374. 10.1007/s11069-013-0681-3.
Harders, R., Kutterolf, S., Hensen, C., Moerz, T., Brueckmann, W., 2010. Tephra layers: A controlling factor on submarine translational sliding? Geochem. Geophys. Geosyst. 11 (5). 10.1029/2009GC002844.
Hasegawa, H.S., Kanamori, H., 1987. Source Mechanism of the Magnitude 7.2 Grand Banks Earthquake of November 1929: Double Couple or Submarine Landslide? Bulletin of the Seismological Society of America 77 (6), 1984–2004.
Helal, M., Mehanna, M., 2008. Tsunamis from nature to physics. Chaos, Solitons & Fractals 36 (4), 787–796. 10.1016/j.chaos.2007.08.044.
Hernández-Molina, F.J., Llave, E., Stow, D., 2008. Continental Slope Contourites, in: M. Rebesco and A. Camerlenghi (Ed.), Developments in Sedimentology: Contourites, Volume 60. Elsevier, pp.379–408.
Hsu, M.-K., Hsieh, C.-H., Ro, C.-H., Yang, J., 2014. Nonlinear Internal Waves in the Andaman Sea. ISPRS Journal of Photogrammetry and Remote Sensing 18 (3), 161–173.
Hühnerbach, V., Masson, D.G., 2004. Landslides in the North Atlantic and its adjacent seas: an analysis of their morphology, setting and behaviour. Marine Geology 213 (1-4), 343–362. 10.1016/j.margeo.2004.10.013.
Iglesias, O., Lastras, G., Canals, M., Olabarrieta, M., González, M., 2010. Numerical simulation of the potential tsunami generated by the BIG'95 debris flow, Northwestern Mediterranean Sea Numerical simulation of the potential tsunami debris flow, Northwestern Mediterranean Sea. Geophysical Research Abstracts 12.
Imamura, F., Gica, E., Takahashi, T., Shuto, N., 1995. Numerical Simulation of the 1992 Flores Tsunami: Interpretation of Tsunami Phenomena in Northeastern Flores Island and Damage at Babi Island, in: Imamura, F., Satake, K. (Eds.), Tsunamis: 1992–1994. Birkhäuser Basel, Basel, pp.555–568.
Jankaew, K., Atwater, B.F., Sawai, Y., Choowong, M., Charoentitirat, T., Martin, M.E., Prendergast, A.L., 2008. Medieval forewarning of the 2004 Indian Ocean tsunami in Thailand. Nature 455 (7217), 1228–1231. 10.1038/nature07373.
Jintasaeranee, P., Weinrebe, W., Klaucke, I., Snidvongs, A., Flueh, E.R., 2012. Morphology of the Andaman outer shelf and upper slope of the Thai exclusive economic zone. Journal of Asian Earth Sciences 46, 78–85. 10.1016/j.jseaes.2011.11.003.
Kaiser, G., Burkhard, B., Römer, H., Sangkaew, S., Graterol, R., Haitook, T., Sterr, H., Sakuna-Schwartz, D., 2013. Mapping tsunami impacts on land cover and related ecosystem service supply in Phang Nga, Thailand. Nat. Hazards Earth Syst. Sci. 13 (12), 3095–3111. 10.5194/nhess-13-3095-2013.
Kulikov, E.A., Rabinovich, A.B., Thomson, R.E., Bornhold, B.D., 1996. The landslide tsunami of November 3, 1994, Skagway Harbor, Alaska. Journal of Geophysical Research 101 (C3), 6609. 10.1029/95JC03562.
Laberg, J.S., Camerlenghi, A., 2008. The Significance of Contourites for Submarine Slope Stability, in: M. Rebesco and A. Camerlenghi (Ed.), Developments in Sedimentology: Contourites, Volume 60. Elsevier, pp. 537–556 10.1016/S0070-4571(08)10025-5
Lastras, G., Canals, M., Urgeles, R., Batist, M. de, Calafat, A., Casamor, J., 2004. Characterisation of the recent BIG'95 debris flow deposit on the Ebro margin, Western Mediterranean Sea, after a variety of seismic reflection data. Marine Geology 213 (1-4), 235–255. 10.1016/j.margeo.2004.10.008.
Lee, H.J., 2009. Timing of occurrence of large submarine landslides on the Atlantic Ocean margin. Marine Geology 264 (1-2), 53–64. 10.1016/j.margeo.2008.09.009.
Lee, H.J., Locat, J., Desgagnes, P., Parsons, J., McAdoo, B.G., Orange, D.L., Piug, P., Wong, F.L., Dartnell, P., Boulanger, E., 2007. Submarine mass movements on continental margins, in: Nittrouer, C.A., Austin, J., Field, M.E., Kravitz, J.H., Syvitsky, J.P.M., Wiberg, P.L. (Eds.), Continental margin sedimentation. From sediment transport to sequence stratigraphy. Blackwell, Malden, Mass.

Lin, Y.-n.N., Sieh, K., Stock, J., 2010. Submarine landslides along the Malacca Strait-Mergui Basin shelf margin: Insights from sequence-stratigraphic analysis. Journal of Geophysical Research 115 (B12), B12102.
Locat, J., Lee, H.J., 2002. Submarine landslides: advances and challenges. Can. Geotech. J. 39 (1), 193–212. 10.1139/t01-089.
Locat, J., Leroueil, S., Locat, A., Lee, H., 2014. Weak Layers: Their Definition and Classification from a Geotechnical Perspective, in: Krastel, S., Behrmann, J.-H., Völker, D., Stipp, M., Berndt, C., Urgeles, R., Chaytor, J., Huhn, K., Strasser, M., Harbitz, B.C. (Eds.), Submarine Mass Movements and Their Consequences: 6th International Symposium. Springer International Publishing, Cham, pp. 3–12.
Løvholt, F., Harbitz, C.B., Vanneste, M., Blasio, F.V. de, Urgeles, R., Iglesias, O., Canals, M., Lastras, G., Pedersen, G., Glimsdal, S., 2014. Modeling Potential Tsunami Generation by the BIG'95 Landslide. Springer International Publishing, Cham, 1 p.
Løvholt, F., Kühn, D., Bungum, H., Harbitz, C.B., Glimsdal, S., 2012. Historical tsunamis and present tsunami hazard in eastern Indonesia and the southern Philippines. J. Geophys. Res. 117 (B9), n/a-n/a. 10.1029/2012JB009425.
Løvholt, F., Pedersen, G., Harbitz, C.B., Glimsdal, S., Kim, J., 2015. On the characteristics of landslide tsunamis. Philosophical transactions. Series A, Mathematical, physical, and engineering sciences 373 (2053). 10.1098/rsta.2014.0376.
Maslin, M., Mikkelsen, N., Vilela, C., Haq, B., 1998. Sea-level –and gas-hydrate–controlled catastrophic sediment failures of the Amazon Fan. Geol 26 (12), 1107. 10.1130/0091-7613(1998)026<1107:SLAGHC>2.3.CO;2.
Maslin, M., Owen, M., Day, S., Long, D., 2004. Linking continental-slope failures and climate change: Testing the clathrate gun hypothesis. Geology 32 (1), 53. 10.1130/G20114.1.
Masson, D.G., Harbitz, C.B., Wynn, R.B., Pedersen, G., Løvholt, F., 2006. Submarine landslides: processes, triggers and hazard prediction. Philosophical Transactions of the Royal Society A: Mathematical, Physical and Engineering Sciences 364 (1845), 2009–2039. 10.1098/rsta.2006.1810.
McCave, I.N., 2008. Size Sorting During Transport and Deposition of Fine Sediments: Sortable Silt and Flow Speed, in: M. Rebesco and A. Camerlenghi (Ed.), Developments in Sedimentology : Contourites, Volume 60. Elsevier, pp.121–142.
McIver, R.D., 1982. Role of Naturally Occurring Gas Hydrates in Sediment Transport. AAPG Bulletin 66 (6), 789–792.
McSaveney, M.J., Goff, J.R., Darby, D.J., Goldsmith, P., Barnett, A., Elliott, S., Nongkas, M., 2000. The 17 July 1998 tsunami, Papua New Guinea: evidence and initial interpretation. Marine Geology 170 (1–2), 81–92. 10.1016/S0025-3227(00)00067-0.
Menemenlis, D., Campin, J.M., Heimbach, P., Hill, Lee, C., Nguyen, A., Schodlock, M., Zhang, H., 2008. ECCO2: High resolution Global Ocean and Sea Ice Data Synthesis. Mercator Ocean Quarterly Newsletter 31, 13–21.
Milker, Y., Wilken, M., Schumann, J., Sakuna, D., Feldens, P., Schwarzer, K., Schmiedl, G., 2013. Sediment transport on the inner shelf off Khao Lak (Andaman Sea, Thailand) during the 2004 Indian Ocean tsunami and former storm events: evidence from foraminiferal transfer functions. Nat. Hazards Earth Syst. Sci. 13 (12), 3113–3128. 10.5194/nhess-13-3113-2013.
Mohammed, F., Fritz, H.M., 2012. Physical modeling of tsunamis generated by three-dimensional deformable granular landslides. Journal of Geophysical Research 117 (C11), C11015. 10.1029/2011JC007850.
Monecke, K., Finger, W., Klarer, D., Kongko, W., McAdoo, B.G., Moore, A.L., Sudrajat, S.U., 2008. A 1,000-year sediment record of tsunami recurrence in northern Sumatra. Nature 455 (7217), 1232–1234. 10.1038/nature07374.
Morley, C.K., 2015. Cenozoic structural evolution of the Andaman Sea: Evolution from an extensional to a sheared margin. Geological Society, London, Special Publications. 10.1144/SP431.1.
Mulder, T., Cochonat, P., 1996. Classification of Offshore Mass Movements. SEPM JSR Vol. 66 (1), 43–57. 10.1306/D42682AC-2B26-11D7-8648000102C1865D.
Murty, T.S., 2003. Tsunami Wave Height Dependence on Landslide Volume. Pure appl. geophys. 160 (10-11), 2147–2153. 10.1007/s00024-003-2423-z.
National Geophysical Data Center / World Data Service (NGDC/WDS): Global Historical Tsunami Database. National Geophysical Data Center, NOAA. doi:10.7289/V5PN93H7 [last access: 15.06.2016].
Nixon, M.F., Grozic, J.L.H., 2007. Submarine slope failure due to gas hydrate dissociation: a preliminary quantification. Can. Geotech. J. 44 (3), 314–325. 10.1139/T06-121.

Okal, E.A., Synolakis, C.E., 2004. Source discriminants for near-field tsunamis. Geophys J Int 158 (3), 899–912. 10.1111/j.1365-246X.2004.02347.x.
Polachan, S., Racey, A., 1994. Stratigraphy of the Mergui Basin, Andaman Sea: (Implications for Petroleum Exploration). Journal of Petroleum Geology 17 (4), 373–406.
Pope, E.L., Talling, P.J., Urlaub, M., Hunt, J.E., Clare, M.A., Challenor, P., 2015. Are large submarine landslides temporally random or do uncertainties in available age constraints make it impossible to tell? Marine Geology 369, 19–33. 10.1016/j.margeo.2015.07.002.
Preu, B., Hernández-Molina, F.J., Violante, R., Piola, A.R., Paterlini, C.M., Schwenk, T., Voigt, I., Krastel, S., Spiess, V., 2013. Morphosedimentary and hydrographic features of the northern Argentine margin: The interplay between erosive, depositional and gravitational processes and its conceptual implications. Deep Sea Research Part I: Oceanographic Research Papers 75, 157–174. 10.1016/j.dsr.2012.12.013.
Rebesco, M., Hernández-Molina, F.J., Rooij, D.v., Wåhlin, A., 2014. Contourites and associated sediments controlled by deep-water circulation processes: State-of-the-art and future considerations. Marine Geology 352, 111–154. 10.1016/j.margeo.2014.03.011.
Römer, H., Kaiser, G., Sterr, H., Ludwig, R., 2010. Using remote sensing to assess tsunami-induced impacts on coastal forest ecosystems at the Andaman Sea coast of Thailand. Nat. Hazards Earth Syst. Sci. 10 (4), 729–745. 10.5194/nhess-10-729-2010
Schwarzer, K., Snidvongs, A., Richter, C., Brückner, H., Oumeraci, H., Sterr, H., Khokiattiwong, S., Weinrebe, W., 2010. Tracing Tsunami Impacts on- and offshore in the Andaman Sea Region (TRIAS). Abstract of the 3rd Tsunami Field Conference.
Shanmugam, G., 2016. Slides, Slumps, Debris Flows, Turbidity Currents, and Bottom Currents☆, in: Reference Module in Earth Systems and Environmental Sciences. Elsevier.
Smith, D.E., Harrison, S., Jordan, J.T., 2013. Sea level rise and submarine mass failures on open continental margins. Quaternary Science Reviews 82, 93–103. 10.1016/j.quascirev.2013.10.012.
Solheim, A., Forsberg, C.F., Yang, S., Kvalstad, T.J., Longva, O., Rise, L. The Role of Geological Setting and Depositional History in Offshore Slope Instability, in: Offshore Technology Conference, Houston, Texas, U.S.A. 2007-04-30.
Stigall, J., Dugan, B., 2010. Overpressure and earthquake initiated slope failure in the Ursa region, northern Gulf of Mexico. Journal of Geophysical Research 115 (B4). 10.1029/2009JB006848.
Sumner, E.J., Siti, M.I., McNeill, L.C., Talling, P.J., Henstock, T.J., Wynn, R.B., Djajadihardja, Y.S., Permana, H., 2013. Can turbidites be used to reconstruct a paleoearthquake record for the central Sumatran margin? Geology 41 (7), 763–766. 10.1130/G34298.1.
Synolakis, C.E., Bardet, J.-P., BORRERO, J.C., Davies, H.L., Okal, E.A., Silver, E.A., Sweet, S., Tappin, D.R., 2002. The slump origin of the 1998 Papua New Guinea Tsunami. Proceedings of the Royal Society A: Mathematical, Physical and Engineering Sciences 458 (2020), 763–789. 10.1098/rspa.2001.0915.
Talling, P., Clare, M., Urlaub, M., Pope, E., Hunt, J., Watt, S., 2014. Large Submarine Landslides on Continental Slopes: Geohazards, Methane Release, and Climate Change. oceanog 27 (2), 32–45. 10.5670/oceanog.2014.38.
Talling, P.J., Masson, D.G., Sumner, E.J., MALGESINI, G., 2012. Subaqueous sediment density flows: Depositional processes and deposit types. Sedimentology 59 (7), 1937–2003. 10.1111/j.1365-3091.2012.01353.x.
Tappin, D.R., 2010. Submarine mass failures as tsunami sources: their climate control. Philosophical transactions. Series A, Mathematical, physical, and engineering sciences 368 (1919), 2417–2434. 10.1098/rsta.2010.0079.
Tappin, D.R., 2010. Submarine mass failures as tsunami sources: their climate control. Philosophical Transactions of the Royal Society A: Mathematical, Physical and Engineering Sciences 368 (1919), 2417–2434. 10.1098/rsta.2010.0079.
Tappin, D. R., Watts, P., Grilli, S.T., 2008. The Papua New Guinea tsunami of 17 July 1998: anatomy of a catastrophic event. Nat. Hazards Earth Syst. Sci. 8 (2), 243–266.
Tappin, D.R., Watts, P., McMurtry, G.M., Lafoy, Y., Matsumoto, T., 2001. The Sissano, Papua New Guinea tsunami of July 1998 — offshore evidence on the source mechanism. Marine Geology 175 (1–4), 1–23. 10.1016/S0025-3227(01)00131-1.
Telford, J., Cosgrave, J., 2006. Joint Evaluation of the International Response to the Indian Ocean Tsunami: Synthesis Report. The Swedish International Development Cooperation Agency; Tsunami Evaluation Coalition, 191pp.
Urgeles, R., Leynaud, D., Lastras, G., Canals, M., Mienert, J., 2006. Back-analysis and failure mechanisms of a large submarine slide on the Ebro slope, NW Mediterranean. Marine Geology 226 (3-4), 185–206. 10.1016/j.margeo.2005.10.004.

Urlaub, M., Talling, P.J., Masson, D.G., 2013. Timing and frequency of large submarine landslides: implications for understanding triggers and future geohazard. Quaternary Science Reviews 72 (0), 63–82. 10.1016/j.quascirev.2013.04.020.

Urlaub, M., Talling, P.J., Masson, D.G., 2013. Timing and frequency of large submarine landslides: Implications for understanding triggers and future geohazard. Quaternary Science Reviews 72, 63–82. 10.1016/j.quascirev.2013.04.020.

Urlaub, M., Zervos, A., Talling, P.J., Masson, D.G., Clayton, C.I., 2012. How do ~2° Slopes Fail in Areas of Slow Sedimentation? A Sensitivity Study on the Influence of Accumulation Rate and Permeability of Submarine Slope Stability, in: Yamada, Y., Kawamura, K., Ikehara, K., Ogawa, Y., Urgeles, R., Mosher, D.C., Chaytor, J., Strasser, M. (Eds.), Submarine Mass Movements and Their Consequences. Springer Netherlands.

Varkey, M.J., Murty, V.S.N., Suryanarayana, A., 1996. Physical Oceanography of the Bay of Bengal and Andaman Sea. Oceanography and Marine Biology: an Annual Review 34, 1–70.

Völker, D., Scholz, F., Geersen, J.M., 2011. Analysis of submarine landsliding in the rupture area of the 27 February 2010 Maule earthquake, Central Chile. Marine Geology 288 (1-4), 79–89. 10.1016/j.margeo.2011.08.003.

Völker, D., Weinrebe, W., Behrmann, J.H., Bialas, J., Klaeschen, D., 2009. Mass wasting at the base of the south central Chilean continental margin: The Reloca Slide. Adv. Geosci. 22, 155–167.

Vorren, T.O., Laberg, J.S., Blaume, F., Dowdeswell, J.A., Kenyon, N.H., Mienert, J., Rumohr, J.A., Werner, F., 1998. The Norwegian–Greenland Sea Continental Margins: Morphology and Late Quaternary Sedimentary Processes and Environment. Quaternary Science Reviews 17 (1-3), 273–302. 10.1016/S0277-3791(97)00072-3.

Yeh, H., Imamura, F., Synolakis, C., Tsuji, Y., Liu, P., Shi, S., 1993. The Flores Island tsunamis. Eos Trans. AGU 74 (33), 369. 10.1029/93EO00381.

2. Regional setting of the working area

2.1. Physiography

The Andaman Sea is an active back-arc basin, located on the Sunda Plate (Figure 5a) behind the Sunda Trench subduction zone and the Andaman-Nicobar Island arc (Figure 5b). Several sub-basins and topographic highs characterize the morphology of the Andaman Sea. The western deep sea area is formed by the Central Andaman Basin (CAB), which is the location of the modern sea floor spreading, and the East Andaman Basin (EAB), an N-S elongated rift basin (Morley, 2015) with water depths of up to around 2500m. The Andaman Sea sub-basins are separated by the Alcock and Sewell seamounts, and the eastern boundary of the EAB is formed by the Mergui Shelf area, the western edge of the Sunda Shelf (Figure 5b). The Mergui Shelf is a drowned platform (Searle and Morley, 2010), extending from the Myanmar shelf in the north along the Thai-Malay Peninsula to the Malacca Strait in the south.

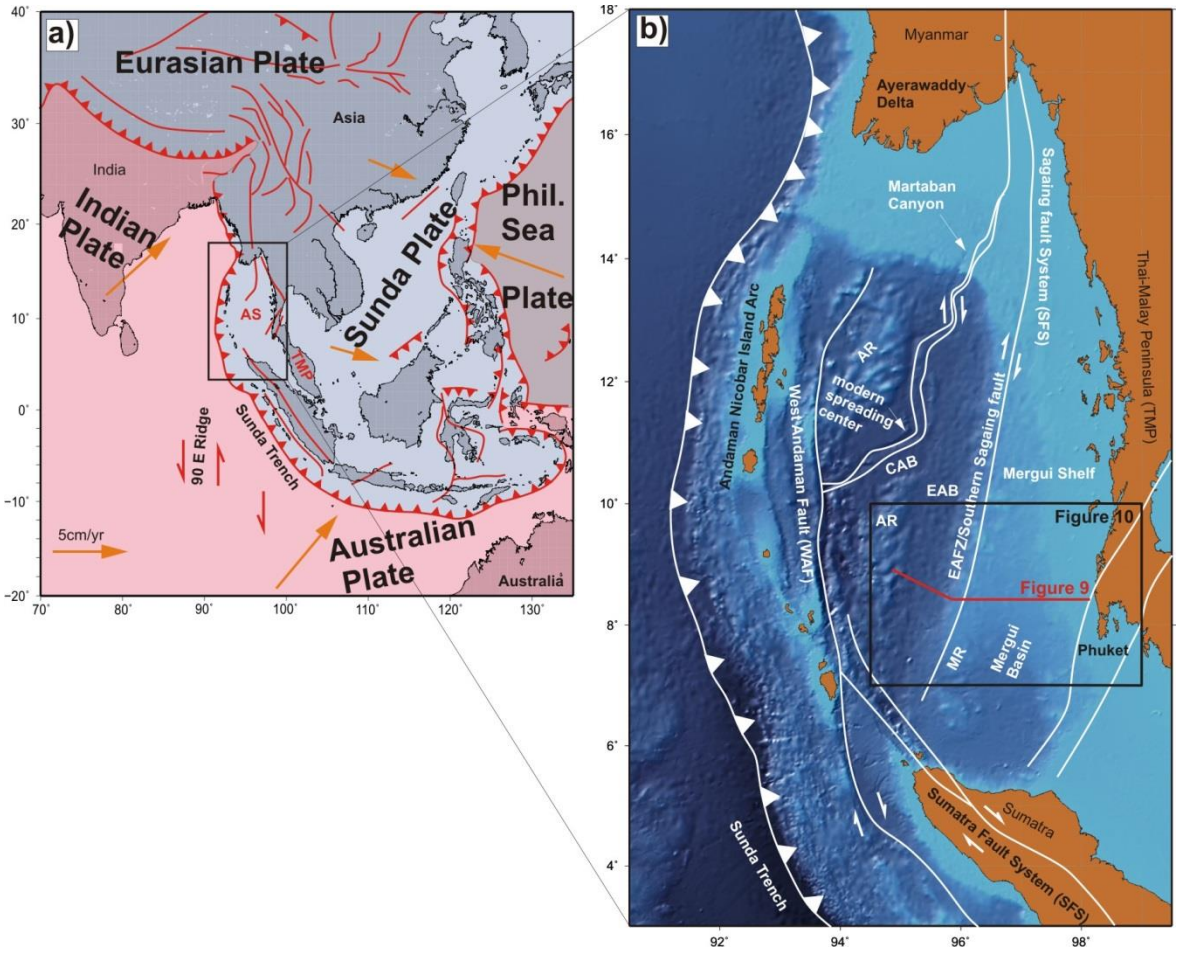

Figure 5: a) Plate tectonic setting of Southeast Asia. Modified from Sibuet et al., (2007) and Metcalfe et al., (2013). b) Physiographic setting of the Andaman Sea area and location of the working area of this study (black frame). AR: Alcock Rise; CAB: Central Andaman Basin; EAFZ: East Andaman Fault Zone; MR: Mergui Ridge; SR: Sewell Rise. Modified from Curray, 2005, Morley, 2012.Background bathymetry is from GEBCO (IOC et al., 2003).

South of approximately 12°30'N the shelf is broadening and deepening, and in this area the shelf edge is located in unusual water depths of about 600-800m. South of 8°30'N the Mergui Shelf is underlain by the Mergui Basin (MB), a sediment filled continental rift basin (Polachan and Racey, 1994). The Mergui Basin is separated from the East Andaman Basin by the Mergui Ridge, a roughly 500km long and 60km broad N-S elongated volcanic/metamorphic high (Curray, 2005) that forms the shelf edge in this area. At its western flank, towards the East Andaman Basin the slope steepens and water depths increases to up to 2500m. The target area of this thesis is located in the Mergui Basin/Mergui Ridge area between approximately 7°00'N to 8°45'N and 95°30'E to 97°50'E, with a main focus on the Andaman Sea shelf break, the western edge of Mergui Ridge (Figure 5b).

2.2. Hydrography

The circulation in the Andaman Sea is driven by the monsoon system with changing predominating wind directions twice a year over India/Southeast Asia. The change of wind directions leads to semi-annual reversal of surface current directions in the Mergui Ridge area (Wyrtki, 1961; Figure 6), and is also controlling the freshwater input in the Andaman Sea (Rodolfo, 1969). During the NE monsoon winds blow from the north/north east and during SW monsoon from the southwest. The strength of winds leads to peak rainfall amounts in the Ayerawaddy catchment area (Figure 6) in August (Rashid et al., 2007) and this in turn leads to main outflow of freshwater into the Andaman Sea in October (in total 482km^3 of freshwater per year; Millimann and Meade, 1983) and to the presence of a low salinity freshwater lens in the Andaman Sea (Rodolfo, 1969) with fluctuating salinity. During SW monsoon the surface circulation in the Andaman Sea is dominated by the SW monsoon current that enters the Andaman Sea from the north (Brown, 2007; Figure 6). According to Varkey et al. (1996) and Potemra et al. (1991) a cyclonic seasonal gyre develops in deeper parts of the water column (Figure 6). During the NE monsoon the flow of the North Equatorial Current is entering the Andaman Sea from the south via the Malacca Strait (Brown, 2007), and the surface circulation is described to be a clockwise (anticyclonic) gyre (Varkey et al., 1996; Potemra et al. 1991) with downward effect to 500m and 1000m (Varkey et al., 1996; Figure 6), and current speeds of up to 12cm/s at 500m water depth (Varkey et al., 1996). As well, Potemra et al. (1991) modeled gyral flow in 250m water depth indicating change of direction of the gyral flow from cyclonic (Jan-Mar) to anticyclonic (April-July) to cyclonic (August-October) and to anticyclonic again (November-December).

Regarding water masses, the surface layer characteristics in the upper 70-100m of the Andaman Sea are dominated by the large inflow of freshwater from the Ayerawaddy-Salween rivers (Rodolfo, 1969), that forms in the northern part of the Andaman Sea a freshwater lens with changing southward extent, depending on the season (Rodolfo, 1969). Beneath the surface layer water mass characteristics in the upper 1300m (Rodolfo, 1969) to 1500m (Nozaki and Alibo, 2003) are similar in the Andaman Sea and Bay of Bengal, with a salinity maximum layer between 300 and 600m water depth (Naqvi et al. 1994; Kim et al. 2015). The thickness of this layer varies seasonally (Varkey et al., 1996). Down to a depth of maximum 1800m lateral exchange between the two seas occurs over the shallow sills in the Andaman-Nicobar Ridge, the Ten Degree Channel (800m depth) and the Great Channel (1800m depth; Nozaki and Alibo, 2003), as well as the shallow

water (<200m) Malacca Strait (Keller and Richards, 1967; see Figure 6 for locations). At about 500m water depth, inflow into the Andaman Sea does occur in response to superficial outflow by monsoon surface currents (Rodolfo, 1969) during the NE Monsoon (Rodolfo, 1969). Below 1800m exchange is restricted (Rodolfo, 1969, Dutta et al. 2007), and the deep water of the Andaman Sea below 1500m consists of a uniform, well mixed water mass due to vigorous vertical mixing (Dutta et al., 2007) with renewal times of about 6yr (Okubo et al., 2004).

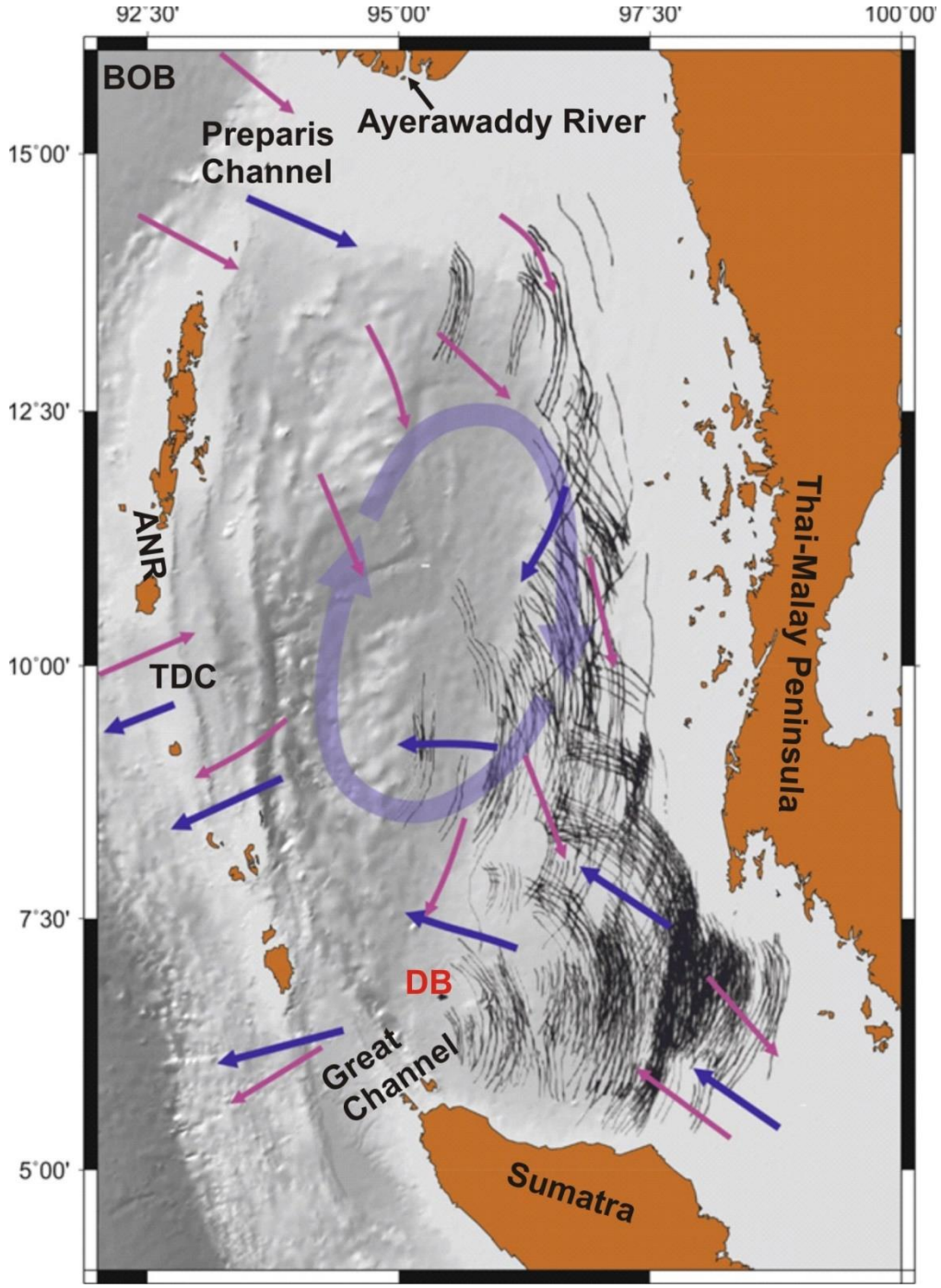

Figure 6: Important hydrographic features in the Andaman Sea area. Surface currents (blue and pink arrows are influenced by the monsoon and showing a reverse pattern in different monsoon seasons (pink arrows are NE monsoon and blue arrows are SW monsoon patterns). Modified from Brown (2007). The location of a seasonal gyre at 1000m water depth is indicated by the light blue arrow. Modified from Varkey et al. (1996). The black lines indicate surface expressions of internal waves in the Andaman Sea. Modified Huang et al. (2014). ANR: Andaman-Nicobar Ridge; BOB: Bay of Bengal; DB: Dreadnought Bank; TDC: Ten Degree Channel..

A process very important for the Andaman Sea circulation is the occurrence of internal waves. Internal waves have been shown to occur in many locations and in all oceans. They are ubiquitous and they have a profound effect on several processes in the oceans, such as nutrient supply (Wang et al., 2007), ocean mixing, climate (Melet et al., 2013) and sediment transport (Bogucki et al., 1997; Pomar et al., 2012) They also may pose potential hazards for ocean infrastructure (Osbourne and Burch, 1980) and are important for the distribution of heat and momentum in the global ocean (Ferrari and Wunsch, 2009). Large scale examples are known for example from the South China Sea and from the Strait of Luzon (Alford et al., 2015). Regular occurrence of internal waves in the Andaman Sea has been known for a long time and they have been scientifically recorded for the first time by Perry and Schimke (1965). The Andaman Sea is one of the locations where internal waves do occur regularly (Hyder et al., 2005). Here internal waves are created by tidal flow over sills and topographic highs (Apel, 1985); particularly energetic internal waves do arise around spring tides (Hyder et al., 2005). Internal waves with amplitudes of up to 80m, and propagation speed >2m/s have been observed (Jackson and Apel, 2002). These waves are generated in the eastern Andaman Sea over topographic highs and move eastward across the whole Andaman Sea. In the shallowing shelf area they have been observed to be deflected and to interfere with one another. The generation of secondary waves at the dreadnought bank (231 m water depth; Figure 6) close to the working area has been observed (Vlasenko and Alpers, 2005). In shallow areas of the Andaman Sea internal waves have been shown to impact on the ecosystem (Schmidt et al., 2012; Jantzen et al., 2013; Wall et al., 2012; 2015).

2.3. Tectonic development and sedimentation

Present day Southeast Asia is part of the Sunda Plate (Michel et al., 2000; Bird, 2003; Simons et al., 2007; Figure 5a). The Sunda Plate is surrounded by subduction zones, where the Asian, the Indian-Australian and the Pacific Sea plates converge (Michel et al., 2000; Metcalfe et al., 2013). At the Sunda Trench, the Indian Plate and the Australian plate are subducting below the Sunda Plate. The Sunda Plate is formed by an amalgamation of crustal blocks that rifted away from Gondwana and moved northward after breakup of the supercontinent and during the subduction of the Tethys oceans since the Late Paleozoic (Hall, 2012). The present day tectonic setting of the Sundaland area is closely connected to the convergence of the rigid Indian Plate with the Eurasian plate since 100Ma, which lead to collision of India with Eurasia since 50 – 45Ma ago (Rangin et al., 2013 and references therein) and to oblique convergence of the Indian Plate with the Sunda Plate (Curray, 2005). Figure 7 gives an overview over the plate tectonic development. Due to the northward drag of the Indian Plate and its oblique motion with respect to the Sunda Plate, plate kinematics are characterized by slip partitioning (Curray, 2005; McCaffrey, 2009), a concept that has been firstly described by Fitch (1972). The stress exerted on the overriding Sunda Plate by the highly oblique motion are partitioned in a trench normal component, taken up at the subduction zone (Sunda Trench) and a trench parallel component (Fitch, 1972; Curray, 2005; McCaffrey, 2009). The trench parallel motion is accommodated by the formation of a system of several approximately trench parallel strike-slip faults in the upper plate. These fault systems are the West Andaman fault (WAF), the Sumatra Fault (SF) and the Sagaing Fault (SGF) (Curray, 2005; Figure 5b), as well as an active sea floor spreading center in the Central Andaman Basin. There, production of oceanic crust is ongoing since about 4Ma (Curray, 2005, Kamesh Raju et al. 2004; Figure 5b). Located between the Sunda Trench and the Sagaing Fault-West Andaman Fault-Sumatra Fault strike-slip system a sliver-plate, the

Myanmar Plate (Curray, 1978; McCaffrey, 2009), is dragged northward with respect to Sundaland (Morley et al. 2011; Curray, 2005). This northward drag is accommodated by shearing and N-S strike slip deformation of the Myanmar Plate (Rangin et al., 2013).

The exertion of the stresses due to the regional tectonic regime led to the formation of numerous basins in Thailand (Polachan et al., 1991), and generally in Southeast Asia in the Lower Eocene to Oligocene (Hall and Morley, 2004; Hall, 2009; Pubellier et al. 2014 and references therein). Very common basin types are rift basins (Polachan et al., 1991). They are often characterized by the occurrence of low angle normal faults related to reactivation of older structures in the heterogeneous Sunda Plate basement (Morley et al., 2011; Pubellier et al., 2013; Morley, 2014). Accordingly, the development of the basins of the Andaman Sea (Central Basin, East Andaman Basin, Mergui Basin; see Figure 5b for locations) is linked to the development of the overall stress regime (Curray, 2005).

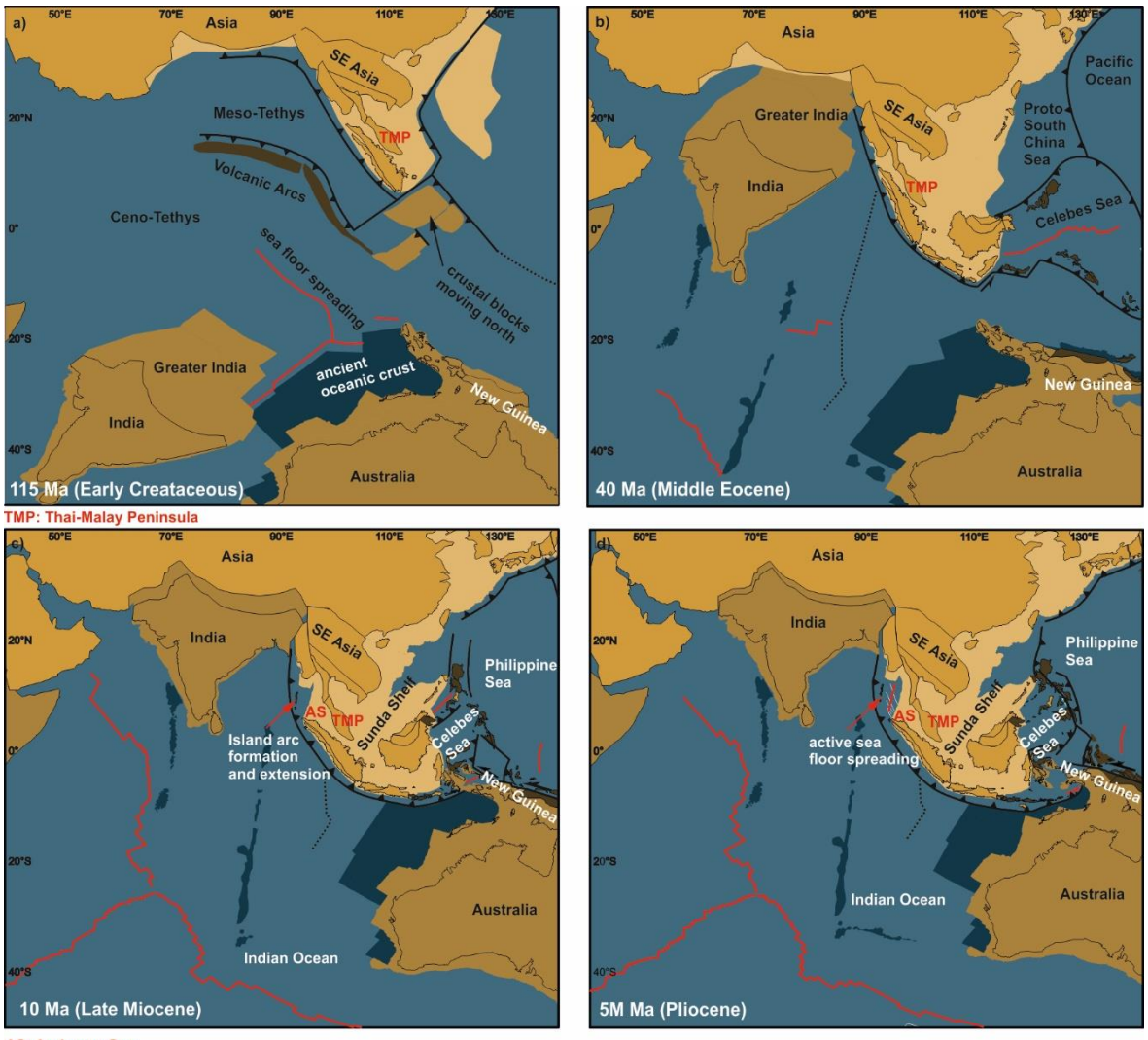

Figure 7: Plate tectonic development of Southeast Asia, influenced by the northward movement of India from the Early Cretaceous to the Pliocene Modified after Hall et al. (2012).

Some authors suggest a sequence of extensional phases to be responsible for the development of the Andaman Sea basins (Curray, 2005; Kamesh Raju, 2005; Chakraborty and Khan, 2009). According to Curray (2005), in a first extensional phase the Mergui Basin (see Figure 5b for location) opened as a series of N-S trending half grabens,

with rifting beginning around 32Ma (Early Oligocene). In response to increasingly oblique plate motions and changing convergence rates of the India-Australia Plate and the Sunda Plate the location of rifting also changed, which resulted in the opening of the East Andaman Basin by sea floor spreading and the formation of oceanic crust west of the Mergui Shelf/Mergui Ridge due to the extension from 15Ma on. After a spreading center jump (Kamesh Raju, 2005), in a later phase opening of the modern spreading center in the Central Andaman Basin took place since about 4Ma (Pliocene).

According to other authors (Srisuriyon and Morley 2014; Morley, 2015) the northward drag of the Myanmar Plate since the coupling of India with Western Myanmar became the key influence on the development of the Andaman Sea basins in the Early Miocene, and the beginning of opening of the East Andaman Basin and the Mergui Basin may have been coeval (Jha et al. 2008a, 2008b; Morley, 2012; Srisuriyon and Morley, 2014; Morley 2015). According to these authors, initial opening of both basins occurred in Late Eocene and Oligocene, when subduction related extensional processes dominated. Later deformation processes related to northward drag lead to a change from E-W extension in the Mergui Basin/East Andaman Basin area to NNW-SSE transtension. Moreover, according to Morley (2015) no oceanic crust has been produced in the East Andaman Basin but it is underlain by thinned continental crust. Until the Middle Miocene (Morley 2012) or Late Miocene (Jha et al., 2011) a strand of the Sagaing Fault, running southward along the western flank of the Mergui Shelf/Mergui Ridge (Figure 5), has been active, accommodating the stresses from the northward drag. This dextral strike slip fault zone is bounding the Mergui Ridge towards the East Andaman Basin. It is called the East Andaman Fault Zone (Polachan and Racey, 1994) or Southern Sagaing Fault (Morley, 2012). Deformation along this fault has created a series of downstepping westward dipping normal faults (Curray, 2005) at the western flank of Mergui Ridge. Abandonment of extension/transtension in the outer shelf area might be due to migration of the zone of stretching and establishment of the Sagaing Fault-West Andaman Fault-Sumatra Fault-system in the late Miocene and Pliocene (Srisuriyon and Morley, 2014).

2.3.1. Mergui Basin

The Mergui Basin today comprises a series of north-south trending half-grabens, underlying the shelf area off western Thailand (see Figure 5 for location). In the depocenters, the maximum thickness of sedimentary infill in the Mergui Basin reaches 6 to 7km (Morley and Racey, 2010). The sedimentary history of the Mergui Basin has been examined in detail by Polachan and Racey (1994) and Andreason et al. (1997). The oldest Eocene pre-rift sediments in the Mergui/Malacca shelf area consist of shallow water deposits of the Tampur Fm (Andreason et al. 1997). Nine formations (Figure 8) have been recognized within the overlying syn- and post-rift sediments in the Mergui Basin deposited since the onset of rifting (Polachan and Racey, 1996). The older Formations are onlapping on the Mergui Ridge that forms the western boundary of the Mergui Basin (Searle and Morley, 2010). According to Polachan and Racey (1994), Andreason et al. (1997), Morley and Racey (2010) and Srisuriyon and Morley (2014) the individual units in the Mergui Basin are:

Syn-rift sediments of the Upper Oligocene to early Lower Miocene, (or according to Morley, 2015 even the Eocene) consist of clastic sediments comprising fluviatile sandstones and conglomerates with pebble size lithoclasts, as well as delta plain and delta front deposits (Ranong Fm). Towards deeper parts of the basins deepwater shales were deposited (Yala Fm), and on structural highs the clastic syn-rift sediments pass into

carbonates. Late-rift sediments (Early Miocene) are shallow delta deposits in the basin margin areas (Payang Fm) and deepwater sediments towards the depocenters (Katang Fm) as well as carbonate units on structural highs (Tai Fm). Post rift sediments of the Middle Miocene consist of shallow marine deposits at the basin margins (Surin Fm), and glauconitic deep marine sediments in the deeper parts (Trang Fm). These are overlain by Late Miocene glauconitic shales and fine grained sandstones and occasionally limestones deposited in lower-fan environment (Thalang Fm). The Pliocene to recent sedimentary succession is made up by the Takua Pa Fm of calcareous and glauconitic shales and occasionally siltstones deposited in lower bathyal basin-plain environment. It is separated to the older units by a regional unconformity at 5.5Ma. Morley (2015) also suggests a Late Miocene age for an unconformity near Mergui Ridge that indicates a late uplift phase of the Mergui Ridge.

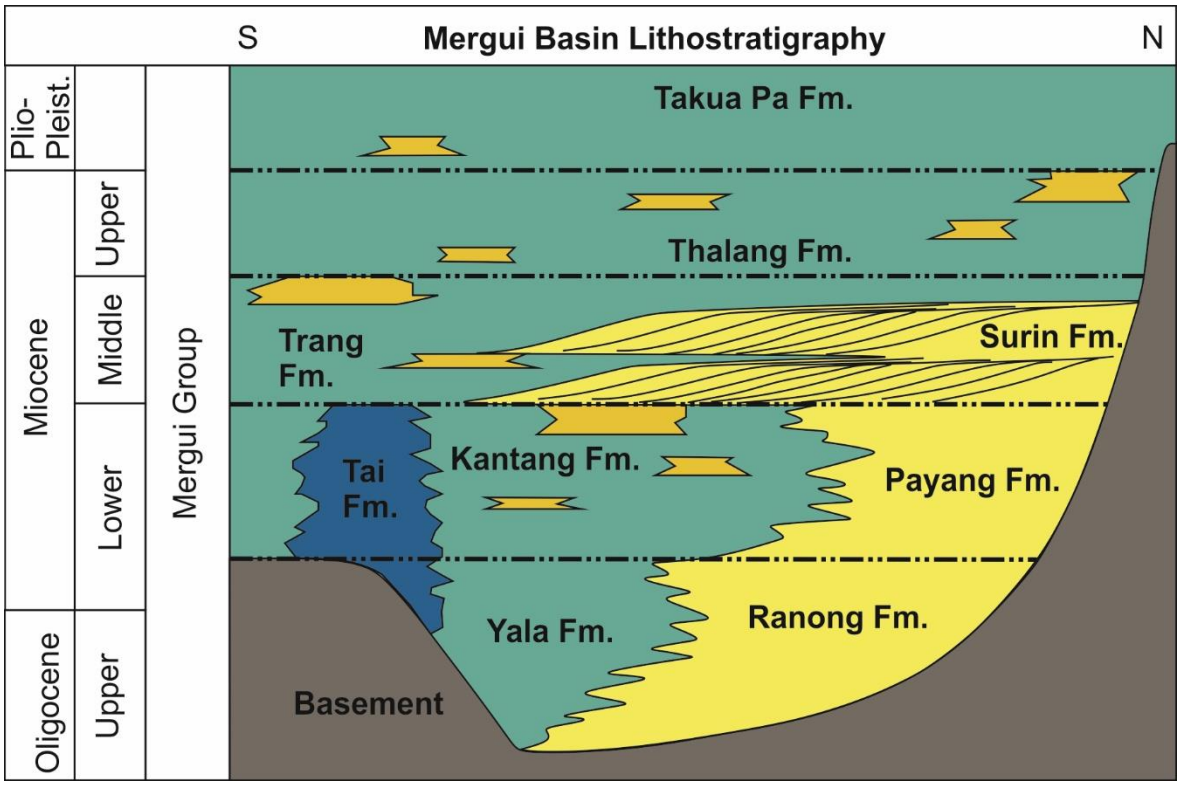

Figure 8: Lithostratigraphy of the Mergui Basin after Polachan and Racey (1994) and Morley and (Racey 2011). Modified from Morley and Racey (2010).

2.3.2. Mergui Ridge

The Mergui Ridge forms a separating horst between the East Andaman Basin and the Mergui Basin (Figure 9) and it is the westward depositional limit of the Mergui Basin (Andreason et al. 1997; Figure 9). The Mergui Ridge is an ancient structure, possibly a remnant of an old volcanic arc that has been subducted during the northward movement of India (Curray, 2005). Whereas the East Andaman Basin and the Mergui Basin both contain large volumes of sedimentary infill, the Mergui Ridge and the northward adjacent Mergui Shelf is a generally sediment starved area (Rodolfo 1969, Panchang, 2008, Morley

2012). Until the Late Miocene the Mergui Ridge has been an area of shallow water or even subaerial exposure (Andreason et al 1997, Morley 2015). The subaerial exposure has possibly been caused by buoyancy due to thermal underplating (Searle and Morley, 2010) and flexural isostatic response to the large volumes of sediment deposited east and west of the Mergui Ridge in the adjacent East Andaman and Mergui Basins (Searle and Morley, 2010). Today the Mergui Ridge is located in water depths of 600-800m which is unusually deep for a shelf margin. The submergence of Mergui Ridge is related to rapid subsidence during the Late Miocene/Pliocene (Andreason et al. 1997). Submergence may have been caused in response to creation of oceanic crust in the Central Andaman Basin, thermal subsidence (Srisuriyon and Morley, 2014) and/or dextral strike-slip deformation at the EAFZ/Southern Sagaing Fault during the Late Miocene (Jha et al. 2011). The recent morphology of the Mergui Ridge in the working area has been previously examined by Jintasearanee et al. (2012). They found a smooth outer shelf area and a rugged upper slope dissected by gullies and escarpments parallel to the slope. Moreover, they identified features such as a mud-dome, pockmarks, three prominent plateaus as well as gas charged sediment and small scale slumps.

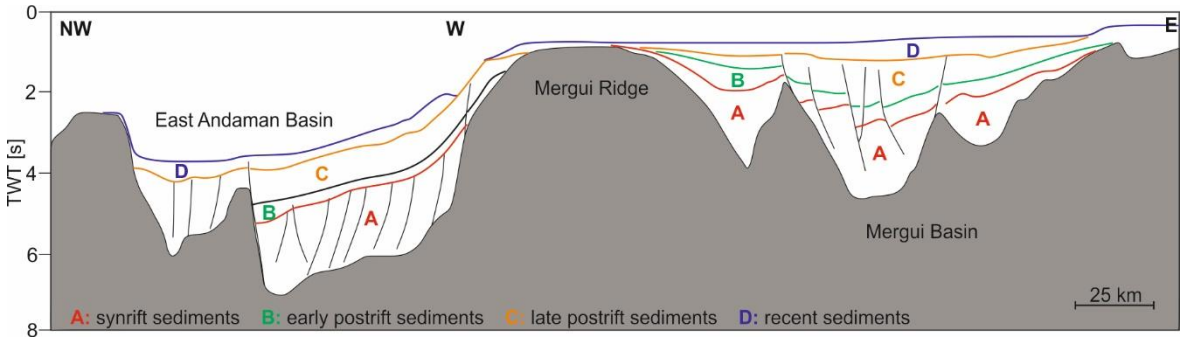

Figure 9: Profile across the Mergui Basin-East Andaman Basin transition (modified after Jha et al. 2008b). See Figure 5b for location of the Profile. Both basins show infill of sediments associated to rift phases. Sediments of the MB are pinching out towards the Mergui Ridge, where sedimentary cover is thin.

2.3.3. East Andaman Basin

The maximum thickness of sediments in the East Andaman Basin (EAB, see Figure 5b for location) is at least 4.6km (Curray, 2005). Whereas the sedimentary history of the East Andaman Basin has been described in quite detail (Polachan and Racey, 1994, Andreason et al. 1997, Srisuriyon and Morley 2014), the stratigraphy of the East Andaman Basin is known less well. Only recently a few studies have been published describing the sedimentary history of the East Andaman Basin to some extent (Jha et al. 2008a, 2008b; Jha et al., 2011; Morley 2015).

According to Jha et al. (2008a) the East Andaman Basin potentially contains a shallow marine pre-rift succession from the former Tethys passive margin that may have been deposited prior to the development of the present subduction zone at the Sunda Trench. This unit may correspond to the Oligocene shallow marine Tampur Formation described by Andreason et al. (1997). In the early phase of extension during Late Eocene/Early Miocene, when a shallow water environment prevailed prior to large scale extension and transition to a deep water environment in the Miocene (Morley, 2015) alluvial and fluvio-lacustrine sediments that pass into more marine sediments in the deeper basin area were deposited (Jha et al. 2008b). In the late syn-rift phase (Late Oligocene to Early Miocene) marine flooding caused by the thermal subsidence resulted in deposition of gradually

more marine sediments whereas the basin margin (Mergui Ridge) stayed subaerially exposed (Jah et al., 2010). According to Morley (2015) sediments in the East Andaman Basin are dissected by faults from the Oligocene to within Middle Miocene section, indicating the syn-rift stage. The overlying sedimentary layers are not or much less affected by faulting, thus representing the late-rift to post-rift stage since middle Miocene (Morley, 2015). Late post rift sediments were deposited during the subsidence phase of the Mergui Ridge area and they contain mass wasting and drift deposits (Jha et al, 2011). Since the Pliocene the East Andaman Basin is supplied with large amounts of clastic sediments from the Ayerawaddy-Salween River (Morley, 2015).

References

Alford, M.H., Peacock, T., MacKinnon, J.A., Nash, J.D., Buijsman, M.C., Centuroni, L.R., Chao, S.-Y., Chang, M.-H., Farmer, D.M., Fringer, O.B., Fu, K.-H., Gallacher, P.C., Graber, H.C., Helfrich, K.R., Jachec, S.M., Jackson, C.R., Klymak, J.M., Ko, D.S., Jan, S., Johnston, T M Shaun, Legg, S., Lee, I.-H., Lien, R.-C., Mercier, M.J., Moum, J.N., Musgrave, R., Park, J.-H., Pickering, A.I., Pinkel, R., Rainville, L., Ramp, S.R., Rudnick, D.L., Sarkar, S., Scotti, A., Simmons, H.L., St Laurent, Louis C, Venayagamoorthy, S.K., Wang, Y.-H., Wang, J., Yang, Y.J., Paluszkiewicz, T., Tang, T.-Y.D., 2015. The formation and fate of internal waves in the South China Sea. Nature 521 (7550), 65–69. 10.1038/nature14399.

Andreason, M.W., Mudford, B., St. Onge, J.E., 1997. Geologic Evolution and Petroleum System of the Thailand AndamanSea Basins. Proceedings of the Petroleum Systems of SE Asia and Australasia Conference.

Apel, J.R., Thompson, D.R., Tilley, D.G., van Dyke, P., 1985. Hydrodynamics and radar signatures of internal solitons in the Andaman Sea. Johns Hopkins APL Technical Digest 6 (4), 3330–3337.

Bird, P., 2003. An updated digital model of plate boundaries. Geochem. Geophys. Geosyst. 4 (3). 10.1029/2001GC000252.

Bogucki, D.J., Dickey, T., Redekopp, L.G., 1997. Sediment Resuspension and Mixing by Resonantly Generated Internal Solitary Waves. J. Phys. Oceanogr. 27, 1181–1196. 10.1175/1520-0485(1997)027<1181:SRAMBR>2.0.CO;2

Brown, B., 2007. Coral reefs of the Andaman Sea - an integrated perspective. Oceanography and Marine Biology: an Annual Review 45, 173–194. 10.1201/9781420050943.ch5.

Chakraborty, P.P., Khan, P.K., 2009. Cenozoic geodynamic evolution of the Andaman-Sumatra subduction margin: Current understanding. Island Arc 18 (1), 184–200. 10.1111/j.1440-1738.2008.00643.x.

Curray, J.R., 2005. Tectonics and history of the Andaman Sea region. Journal of Asian Earth Sciences 25 (1), 187–232. 10.1016/j.jseaes.2004.09.001.

Curray, J.R., Moore, D.G., Lawver, L.A., Emmel, F.J., Raitt, R., Henry, M., Kieckhefer, R., 1978. Tectonics of the Andaman Sea and Burma. AAPG Bulletin, 189–197.

Ferrari, R., Wunsch, C., 2009. Ocean Circulation Kinetic Energy: Reservoirs, Sources, and Sinks. Annu. Rev. Fluid Mech. 41 (1), 253–282. 10.1146/annurev.fluid.40.111406.102139.

Fitch, T.J., 1972. Plate Convergence, Transcurrent Faults, and Internal Deformation Adjacent to Southeast Asia and the Western Pacific. Journal of Geophysical Research 77 (23), 4432–4460.

Hall, R., 2009. Hydrocarbon basins in SE Asia: understanding why they are there. Petroleum Geoscience 15 (2), 131–146. 10.1144/1354-079309-830.

Hall, R., 2012. Late Jurassic–Cenozoic reconstructions of the Indonesian region and the Indian Ocean. Tectonophysics 570–571 (0), 1–41. 10.1016/j.tecto.2012.04.021.

Hall, R. and Morley, C. K., 2004. Sundaland Basins, in: Continent-Ocean Interactions Within East Asian Marginal Seas (eds P. Clift, W. Kuhnt, P. Wang and D. Hayes), American Geophysical Union, Washington, D. C..10.1029/149GM04

Hyder, P., Jeans, D., Cauquil, E., Nerzic, R., 2005. Observations and predictability of internal solitons in the northern Andaman Sea. Applied Ocean Research 27 (1), 1–11. 10.1016/j.apor.2005.07.001.

Jackson, C.R., Apel, J.R., 2002. An Atlas of Internal Solitary-like Waves and their Properties. Global Ocean Associates, 16 pp.
Jantzen, C., Schmidt, G.M., Wild, C., Roder, C., Khokiattiwong, S., Richter, C., 2013. Benthic reef primary production in response to large amplitude internal waves at the Similan Islands (Andaman Sea, Thailand). PloS one 8 (11), e81834. 10.1371/journal.pone.0081834.
Jha, P., 2008a. Evolution and Hydrocarbon Occurrences of Rift Basins at the Western Margin of Sunda Platform and Relations with East Andaman Basin, in: Geo India 2008 Conference and Exhibition. South Asian Geosciences Exhibition and Conference, Greater Nioda, New Dheli, India. 16-19 September.
Jha, P., Ros, D., Deglialessandrini, A., Kishore, M., 2008b. Speculative Petroleum System & Play Model of East Andaman Basin from Regional Geology and Basin Evolution Concepts: the Exploration Challenges of an Extreme Frontier Area, in:8th Biennial International Conference and Exposition on Petroleum Geophysics. 8th Biennial International Conference and Exposition on Petroleum Geophysics, Hyderabad.
Jha, P., Ros, D., Kishore, M., 2011. Seismic & Sequence Stratigraphic Framework and Depositional Architecture of Shallow and Deepwater Postrift Sediments in East Andaman Basin: An overview, in:Geo India 2011 Conference and Exhibition. South Asian Geosciences Exhibition and Conference, Greater Nioda, New Dheli, India. 12-14 January.
Jintasaeranee, P., Weinrebe, W., Klaucke, I., Snidvongs, A., Flueh, E.R., 2012. Morphology of the Andaman outer shelf and upper slope of the Thai exclusive economic zone. Journal of Asian Earth Sciences 46, 78–85. 10.1016/j.jseaes.2011.11.003.
Kamesh Raju, K.A., 2005. Three-phase tectonic evolution of the Andaman backarc basin. Current Science 89 (11), 1932–1937.
Kamesh Raju, K.A., Ramprasad, T., Rao, P., Ramalingeswara Rao, B., Varghese, J., 2004. New insights into the tectonic evolution of the Andaman basin, northeast Indian Ocean. EPSL 221 (1-4), 145–162. 10.1016/S0012-821X(04)00075-5.
Keller, G. H., Ric, A.F., 1967. Sediments of the Malacca Strait, Southeast Asia. SEPM JSR Vol. 37. 10.1306/74D7166D-2B21-11D7-8648000102C1865D.
Kim, T., Obata, H., Gamo, T., 2015. Dissolved Zn and its speciation in the northeastern Indian Ocean and the Andaman Sea. Front. Mar. Sci. 2, 2720. 10.3389/fmars.2015.00060.
McCaffrey, R., 2009. The Tectonic Framework of the Sumatran Subduction Zone. Annu. Rev. Earth Planet. Sci. 37 (1), 345–366. 10.1146/annurev.earth.031208.100212.
Melet, A., Hallberg, R., Legg, S., Polzin, K., 2013. Sensitivity of the Ocean State to the Vertical Distribution of Internal-Tide-Driven Mixing. J. Phys. Oceanogr. 43 (3), 602–615. 10.1175/JPO-D-12-055.1.
Metcalfe, I., 2013. Gondwana dispersion and Asian accretion: Tectonic and palaeogeographic evolution of eastern Tethys. Journal of Asian Earth Sciences 66 (0), 1–33. 10.1016/j.jseaes.2012.12.020.
Michel, G.W., Becker, M., Angermann, D., Reigber, C., Reinhart, E., 2000. Crustal motion in E-and SE-Asia from GPS measurements. Earth Planet Sp 52 (10), 713–720. 10.1186/BF03352270.
Milliman, J.D., Meade, R.H., 1983. World-Wide Delivery of River Sediment to the Oceans. The Journal of Geology 91 (1), 1–21.
Morley, C.K., 2012. Discussion of tectonic models for Cenozoic strike-slip fault-affected continental margins of mainland SE Asia. Journal of Asian Earth Sciences (0). 10.1016/j.jseaes.2012.10.019.
Morley, C.K., 2014. The widespread occurrence of low-angle normal faults in a rift setting: Review of examples from Thailand, and implications for their origin and evolution. Earth-Science Reviews 133, 18–42. 10.1016/j.earscirev.2014.02.007.
Morley, C.K., 2015. Cenozoic structural evolution of the Andaman Sea: Evolution from an extensional to a sheared margin. Geological Society, London, Special Publications. 10.1144/SP431.1.
Morley, C.K., Racey, A., 2010. Tertiary stratigraphy, in: Ridd, M.F., Barber, A.J., Crow, M.J. (Eds.), The Geology of Thailand.
Naqvi, W.A., Charles, C.D., Fairbanks, R.G., 1994. Carbon and oxygen isotopic records of benthic foraminifera from the Northeast Indian Ocean: implications on glacial-interglacial atmospheric CO2 changes. EPSL 121 (1–2), 99–110. 10.1016/0012-821X(94)90034-5.
Nozaki, Y., Alibo, D.S., 2003. Importance of vertical geochemical processes in controlling the oceanic profiles of dissolved rare earth elements in the northeastern Indian Ocean. EPSL 205 (3-4), 155–172. 10.1016/S0012-821X(02)01027-0.
Osborne, A.R., Burch, T.L., 1980. Internal Solitons in the Andaman Sea. Science 208 (4443), 451–460. 10.1126/science.208.4443.451.

Panchang, R., Ningam, R., Ravi Prasad, G., Rajagopalan, G., Ray, D., Koyihla, U., 2008. Relict faunal testimony for sea-level fluctuations off Myanmar (Burma). Journal of the Paleontological Society of India 53 (2), 185–195.
Perry, R.B., Schimke, G.R., 1965. Large-amplitude internal waves observed off the northwest coast of Sumatra. J. Geophys. Res. 70 (10), 2319–2324. 10.1029/JZ070i010p02319.
Polachan, S., Pradidtan, S., Tongtaow, C., Janmaha, S., Intarawijitr, K., Sangsuwan, C., 1991. Development of Cenozoic basins in Thailand. Marine and Petroleum Geology 8 (1), 84–97. 10.1016/0264-8172(91)90047-5.
Polachan, S., Racey, A., 1994. Stratigraphy of the Mergui Basin, Andaman Sea: (Implications for Petroleum Exploration). Journal of Petroleum Geology 17 (4), 373–406.
Pomar, L., Morsilli, M., Hallock, P., Bádenas, B., 2012. Internal waves, an under-explored source of turbulence events in the sedimentary record. Earth-Science Reviews 111 (1-2), 56–81. 10.1016/j.earscirev.2011.12.005.
Potemra, J.T., Luther, M.E., O'Brien, J.J., 1991. The seasonal circulation of the upper ocean in the Bay of Bengal. J. Geophys. Res. 96 (C7), 12667. 10.1029/91JC01045.
Pubellier, M., Morley, C.K., 2014. The basins of Sundaland (SE Asia): Evolution and boundary conditions. Marine and Petroleum Geology 58, 555–578. 10.1016/j.marpetgeo.2013.11.019.
Rangin, C., Maurin, T., Masson, F., 2013. Combined effects of Eurasia/Sunda oblique convergence and East-Tibetan crustal flow on the active tectonics of Burma. Journal of Asian Earth Sciences 76 (0), 185–194. 10.1016/j.jseaes.2013.05.018.
Rashid, H., Flower, B., Poore, R., Quinn, T., 2007. A ~25ka Indian Ocean monsoon variability record from the Andaman Sea. Quaternary Science Reviews 26 (19-21), 2586–2597. 10.1016/j.quascirev.2007.07.002.
Rodolfo, K.S., 1969. Bathymetry and Marine Geology of the Andaman Basin, and Tectonic Implications for Southeast Asia. Geol Soc America Bull 80 (7), 1203. 10.1130/0016-7606(1969)80[1203:BAMGOT]2.0.CO;2.
Schmidt G. M., Phongsuwan N, Jantzen C, Roder C, Khokiattiwong S, Richter C, 2012. Coral community composition and reef development at the Similan Islands, Andaman Sea, in response to strong environmental variations. Mar Ecol Prog Ser 456, 113–126.
Searle, M.P., Morley, C.K., 2010. Tectonic and thermal evolution of Thailand in the regional context of SE Asia, in: Ridd, M.F., Barber, A.J., Crow, M.J. (Eds.), The Geology of Thailand.
Sibuet, J.-C., Rangin, C., Lepichon, X., SINGH, S., Cattaneo, A., Graindorge, D., Klingelhoeffer, F., LIN, J., Malod, J.-A., Maury, T., 2007. 26th December 2004 great Sumatra–Andaman earthquake: Co-seismic and post-seismic motions in northern Sumatra. EPSL 263 (1-2), 88–103. 10.1016/j.epsl.2007.09.005.
Simons, W.J.F., Socquet, A., Vigny, C., Ambrosius, B.A.C., Haji Abu, S., Promthong, C., Subarya, C., Sarsito, D.A., Matheussen, S., Morgan, P., Spakman, W., 2007. A decade of GPS in Southeast Asia: Resolving Sundaland motion and boundaries. Journal of Geophysical Research 112 (B6), B06420. 10.1029/2005JB003868.
Srisuriyon, K., Morley, C.K., 2014. Pull-apart development at overlapping fault tips: Oblique rifting of a Cenozoic continental margin, northern Mergui Basin, Andaman Sea. Geosphere 10 (1), 80–106. 10.1130/GES00926.1.
Varkey, M.J., Murty, V.S.N., Suryanarayana, A., 1996. Physical Oceanography of the Bay of Bengal and Andaman Sea. Oceanography and Marine Biology: an Annual Review 34, 1–70.
Vlasenko, V., Alpers, W., 2005. Generation of secondary internal waves by the interaction of an internal solitary wave with an underwater bank. Journal of Geophysical Research 110 (C2). 10.1029/2004JC002467.
Wall, M., Putchim, L., Schmidt, G.M., Jantzen, C., Khokiattiwong, S., Richter, C., 2015. Large-amplitude internal waves benefit corals during thermal stress. Proceedings. Biological sciences / The Royal Society 282 (1799), 20140650. 10.1098/rspb.2014.0650.
Wall, M., Schmidt, G.M., Janjang, P., Khokiattiwong, S., Richter, C., 2012. Differential impact of monsoon and large amplitude internal waves on coral reef development in the Andaman Sea. PLoS ONE 7 (11), e50207. 10.1371/journal.pone.0050207.
Wang, Y.-H., Dai, C.-F., Chen, Y.-Y., 2007. Physical and ecological processes of internal waves on an isolated reef ecosystem in the South China Sea. Geophys. Res. Lett. 34 (18). 10.1029/2007GL030658.
Wyrtki, K., 1961. Physical Oceanography of the Southeast Asian waters: Scientific Results -Marine Investigations of the South China Sea and the Gulf of Thailand. Naga Report 2. The University of California, Scripps Institution of Oceanography, 225 pp.

3. Objectives

The overall objective of this thesis is to investigate the sediment dynamics in the working area and to investigate the slope stability at the outer continental Margin off western Thailand as well as potential associated tsunami hazards. More specifically, this thesis aims to:

- **Investigate the morphology and sediment dynamic of the working area by constraining the sedimentary evolution and sediment dynamic in the outer continental margin area of the Mergui Ridge**

  This objective is addressed by the analysis of a high resolution 2D multichannel reflection seismic data set in combination with multibeam bathymetry from the outer Thai Shelf area at Mergui Ridge.

  The seismic units in the data set are identified and their stratigraphic relationships are analyzed in order to deduce the sedimentary evolution of the working area and to place the development of the working area into the overall regional geological context.

  Surface morphological features are identified and characterized in order to identify the sedimentary processes that shape the margin today. Characteristic morphological features are related to the current regime in order constrain the sediment dynamics of the working area.

- **Assess the slope stability in the working area**

  Based mainly on the 2D multichannel reflection seismic data set, areas that show indications for previous failures are identified. Individual mass wasting deposits are mapped and their volume is estimated in order to quantify their tsunami potential.

  The distribution of mass transport deposits in the background sediments is examined in order to estimate recurrence of failures. Based on the findings on the overall sedimentary regime, possible preconditioning factors and triggers are identified. Moreover, potential locations of future failures are determined.

- **Obtain preliminary insight into the tsunami potential of slope failures**

  The mass transport deposits identified in the geological data set are the basis for a preliminary modeling of landslide tsunamis in the area.

  The tsunamigenic potential of landslides is assessed by the creation of failure scenarios that are based on landslides with geometrical parameters similar to those identified in the reflection seismic data.

  A simplifying numerical model is applied to calculate tsunami propagation and run up at the coast. This data give first insights into potential tsunami hazards that may arise from failures similar to those identified in this thesis.

4. Data and Methods

During the research cruises MASS I, MASS II and MASS III in 2006, 2007 and 2011 (RV Chakratong Tongyay) a new data set from the Mergui Ridge Thai continental margin has been acquired, consisting of high resolution multibeam bathymetry and high resolution 2D multichannel reflection seismic lines (Figure 10).

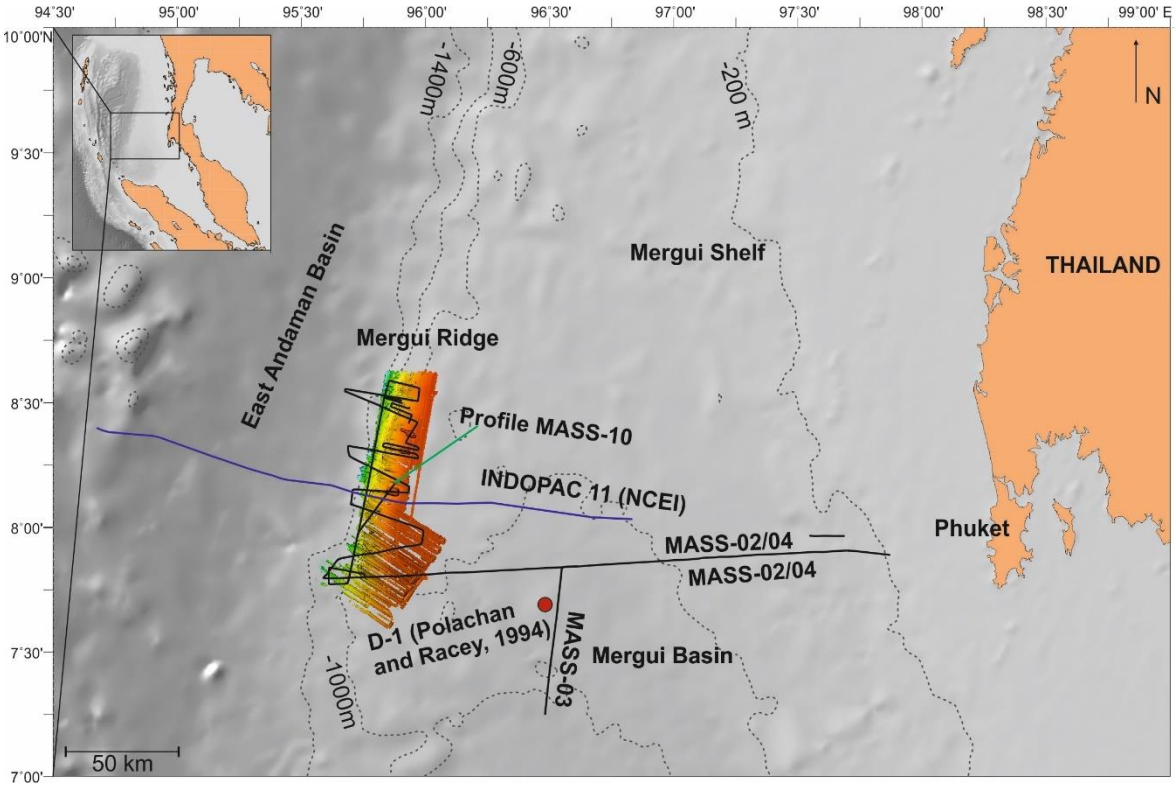

Figure 10: 2D multichannel reflection seismic and multibeam bathymetry dataset used in this thesis: Multibeam bathymetry (colored area) originally published by P. Jintasaeranee and high resolution 2D multichannel reflection seismic obtained during MASSIII cruise (black lines). Additionally, the location of the D-1 well (Polachan and Racey 1994) and bathymetry data (blue line) from INDOPAC 11 cruise (NCEI) is indicated. Background bathymetry (grey) from GEBCO (IOC et al., 2003).

4.1. Multibeam Bathymetry data

The multibeam bathymetry (about 3000km^2) was obtained during MASS I and MASS II cruises in 2006 and 2007 in water depths between approximately 500m and 1600m. The bathymetric dataset was originally processed and published by Jintasearanee et al. (2012) and provided for this work by P. Jintasearanee. The bathymetry was measured using a portable Seabeam 1050 multibeam echo sounder, operating at a frequency of 50Hz and providing 126 individual beams with a horizontal resolution of 1.5° and a maximum swath width of up to 153°. The data have been processed with MB-System and gridded with a final resolution of 50m grid cell size. Additionally, for the work in this thesis a backscatter map was created with MB-System. Interpretation, analysis and visualization of bathymetry data was done with GlobalMapper (Blue Marble Geographics) and GMT (Wessel et al., 2013).

4.2. Supplementary bathymetry data

GEBCO (IOC et al. 2003) and SRTM30 (Becker et al., 2009) data were used to supplement the multibeam bathymetry dataset. Moreover, for the modeling study (Manuscript III), the GEBCO bathymetry grid between 4°50'N to 10°38'N and 94°40'E to 99°40'E was used as modeling domain. A 32arcs grid cell size was used for calculation of the propagation of tsunami waves. Additionally, bathymetry from a seismic line from INDOPAC 11 cruise (1977) was used in order to obtain an idea of morphology at deeper parts of the EAB shelf slope. This profile is available at NCEI (National Centers for Environmental Information World Data Service for Geophysics at https://www.ngdc./noaa.gov/mgg/mggd.html).

4.3. High resolution 2D multichannel reflection seismic

39 high resolution 2D multichannel reflection seismic lines have been obtained during MASS cruise III in 2011. In total about 630km reflection seismic data were collected during the cruise (Figure 10).

4.3.1. Acquisition of reflection seismic data

The data have been acquired using a micro GIGun (2×0.1l/ Generator 0.1l, Injector 0.1l) that was operated with a pressure of about 120bar and a shot rate of 5 to 6s, depending on water depth. For recording a 150m long digital Geometrics GeoEel streamer was used. The streamer contains in total 96 channels with two hydrophones each, in 12 individual sections of 8 channels per section. The channel distance is 1.56m. The received acoustic signal was digitized by analog-digital converters (bottles), mounted between streamer sections. The streamer was toed in a distance of 36.5m behind the ship and three Oyo Geospace Bird Remote Units, attached to the streamer in in distances of 37.5m, 87.5m and 150m behind stern were used to maintain stable floating and depth control of the receiver unit. A shotpoint distance of 10m was achieved at a vessel speed of 4kn. The main signal frequency was 200Hz. The signals were digitized at 4kHz and the recording length of the received signal was 3s.

4.3.2. Processing of reflection seismic data

The processing of the high resolution 2D multichannel reflection seismic was carried out by M. Grün and F. Gross. Vista Seismic Processing (Schlumberger) and WinGeoApp (H.Keil) were used to carry out standard processing steps: Preprocessing of the data included conversion from SEG-D into SEG-Y format as well as the application of an Ormsby bandpass filter for noise reduction (15/30Hz low pass and 800/1200Hz high

pass). Subsequently geometry corrections were applied with WinGeoapp in order to account for the distances from the GPS device that was used for navigation recording and the positions of source and receiver. In the next step midpoint binning was carried out by choosing a bin size containing a minimum fold of 20 traces per bin, resulting in bin sizes of 2m in inline direction and 20m in crossline direction. Improvement of signal-to-noise-ratio was obtained by applying a despiking algorithm to reduce unwanted spikes in the seismic data that may be due to for example electrical disturbances in the cables and/or ship noise and breaking waves. In order to reduce unwanted coherent linear noise and side scattered energy, especially in the area around platforms, a standard fan shaped FK filtering was applied to eliminate unwanted energy. For profile MASS-10 (see Figure 10 for location), an additional FK filter was applied to account for the strong scattering of energy around the platform. Furthermore, correction for amplitude decrease due to spherical divergence of the signal was carried out. In the next step, zero offset sections were created by dynamic NMO (normal move out) correction applying a constant sound velocity of 1.500m/s due to the lack of availability of a reliable velocity model, and the traces were CMP-stacked (min. 20 traces) according to the chosen 2x20m bins. After CMP stacking for some of the profiles static correction was necessary out to account for residual statics. In a final step the data were time migrated in order to reposition reflections to their true reflection points. This was obtained by time FD-migration (finite difference migration) at a fixed sound velocity of 1500m/s. The vertical resolution of the processed data is between maximum 3 to 5m governed by the signal wavelength (300 - 500Hz), and the lateral resolution is between ~30m and 50m.

4.3.3. Interpretation of reflection seismic data

Age correlation

Interpretation of the seismic data was done with IHS Kingdom. Most of the seismic lines are located at the Mergui Ridge –East Andaman basin transition (Figure 10). Two additional profiles are available from the Mergui Basin, profile MASS-02/04 running from east to west across the basin and profile MASS-03 running from north-south in the southern part of the basin (Figure 10).

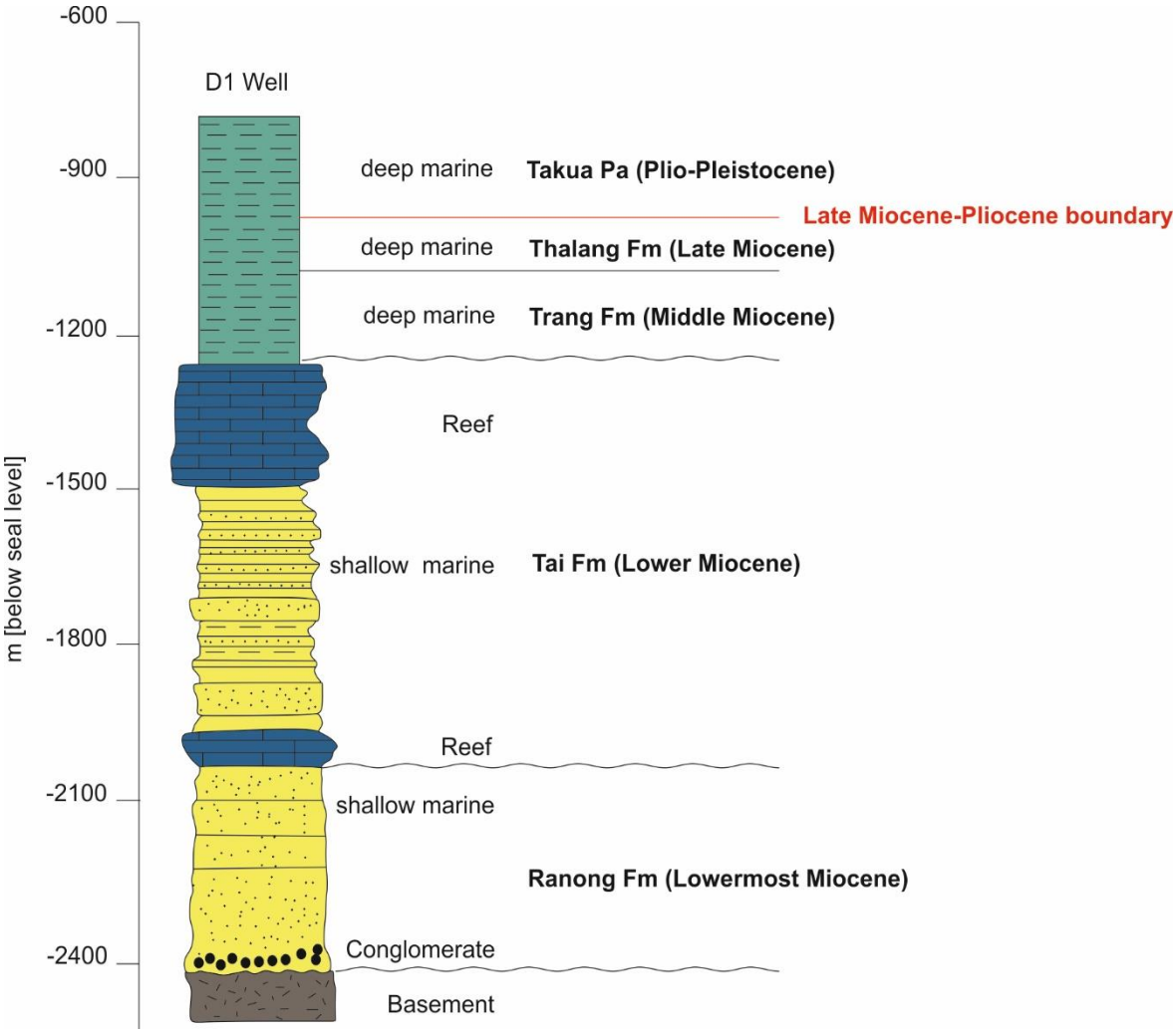

Figure 11: Lithology of borehole D-1 in the Mergui Basin (Polachan and Racey, 1994). See Figure 10 for location. Modified after Polachan and Racey (1994).

These two profiles were used for stratigraphic correlation. Stratigraphic placement of the seismic units was obtained by correlation to borehole data of the D-1 well in the Mergui Basin, as shown in Polachan and Racey (1994; their Figure 16) which is located about 3km from the north-south profile MASS-03 (Figure 10).The D-1 well (Polachan and Racey, 1994, Figure 11) is located at a water depth of ~800m. The D-1 well contains a Plio-Pleistocene unit of about 200m thickness (Figure 11, see Figure 10 for location). This corresponds to ~0.2ms TWT at a sound velocity of 2000m/s, which is the approximate sound velocity in the upper subsurface layers within the Mergui Basin (Curray, 2005). Approximately 0.2ms below the seafloor, at the location of the D-1 well a change of amplitudes from low amplitudes above to high amplitudes below occurs. This boundary

coincides with the Late Miocene-Pliocene boundary in the well and has been interpreted as the Late Miocene-Pliocene boundary in the data set.

Identification and volume estimation of Mass transport deposits

The Mass Transport Deposits (MTD) in the working area were identified based on their internal and external seismic characteristics, which are chaotic to transparent internal reflectors as well as irregular top and base.

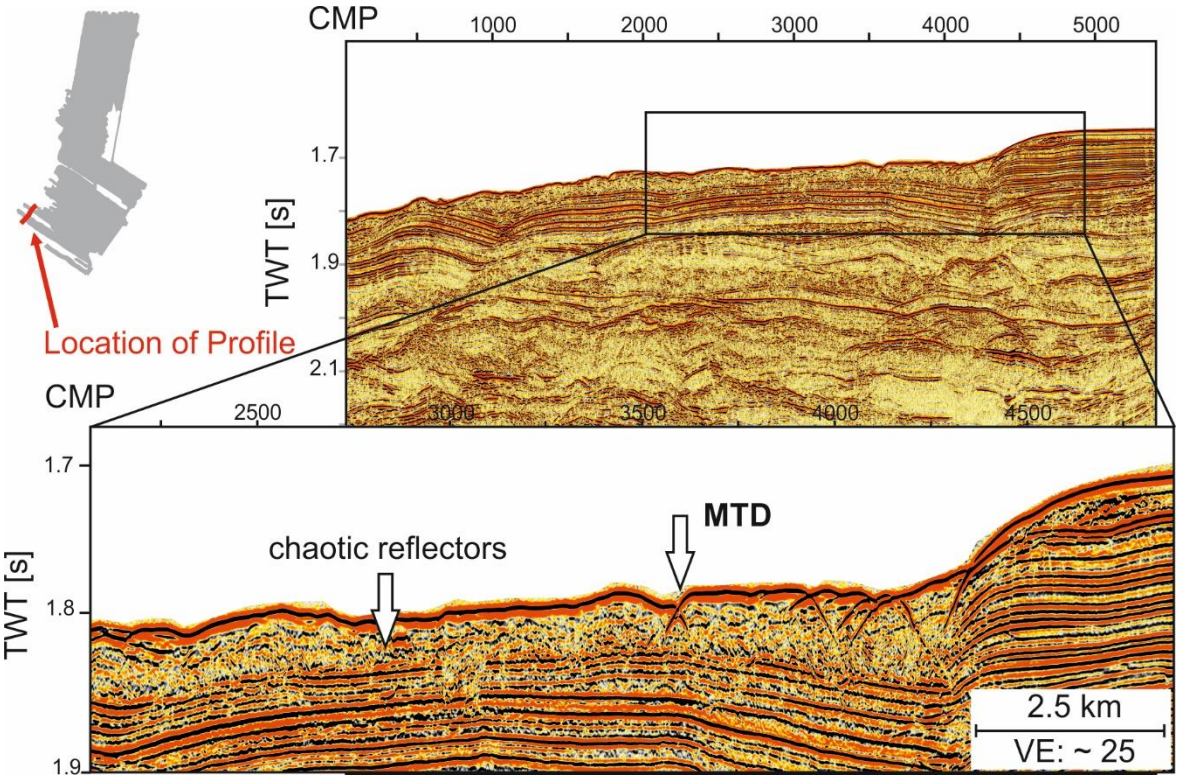

Figure 12: Example for seismic characteristic of identified Mass Transport Deposits (MTD). MTDs are characterized by chaotic internal reflectors and irregular top and base.

Figure 12 gives an example for a superficial MTD in the southern working area. Estimation of volumes of the MTDs identified in the working area is based on picked top and base horizons of the identified MTDs. Top and base time grids were created within kingdom suite by interpolation between the horizons (“FlexGridding” algorithm) within a polygon, defined as the outline of the MTDs (Figure 13). Subsequently an isopach map of the MTDs was created by assuming a constant sound velocity of 1500m/s, and volume was calculated within the constraints of the defined polygon.

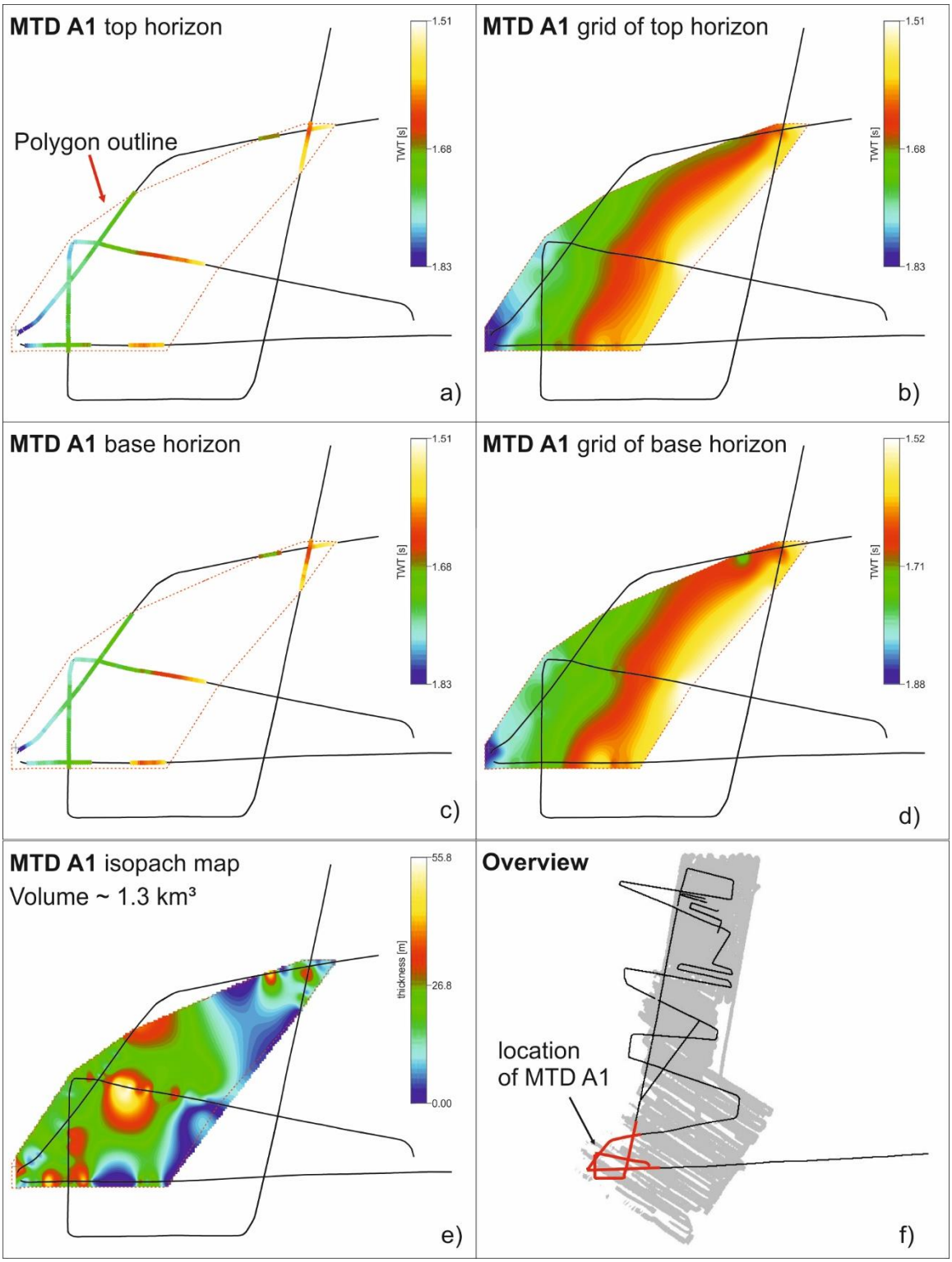

Figure 13: Example (MTD A1) of grids created for estimation of landslide volumes. a) Picked top horizons and polygon outlining landslide extent as derived from seismic lines. b) Interpolated grid of top horizon. c) and d) base horizon and corresponding grid. e) Isopach map of MTD A1. f) Location of MTD A1. Black lines: location of seismic profiles.

4.4. ECCO2 dataset

In order to relate the observations of the sediment dynamics from the reflection seismic/multibeam dataset to the hydrography of the working area, current velocity data from “ECCO2 Estimating the Circulation and Climate of the Ocean, Phase II: High Resolution Global-Ocean and Sea-Ice Data Synthesis” were used (Figure 14).

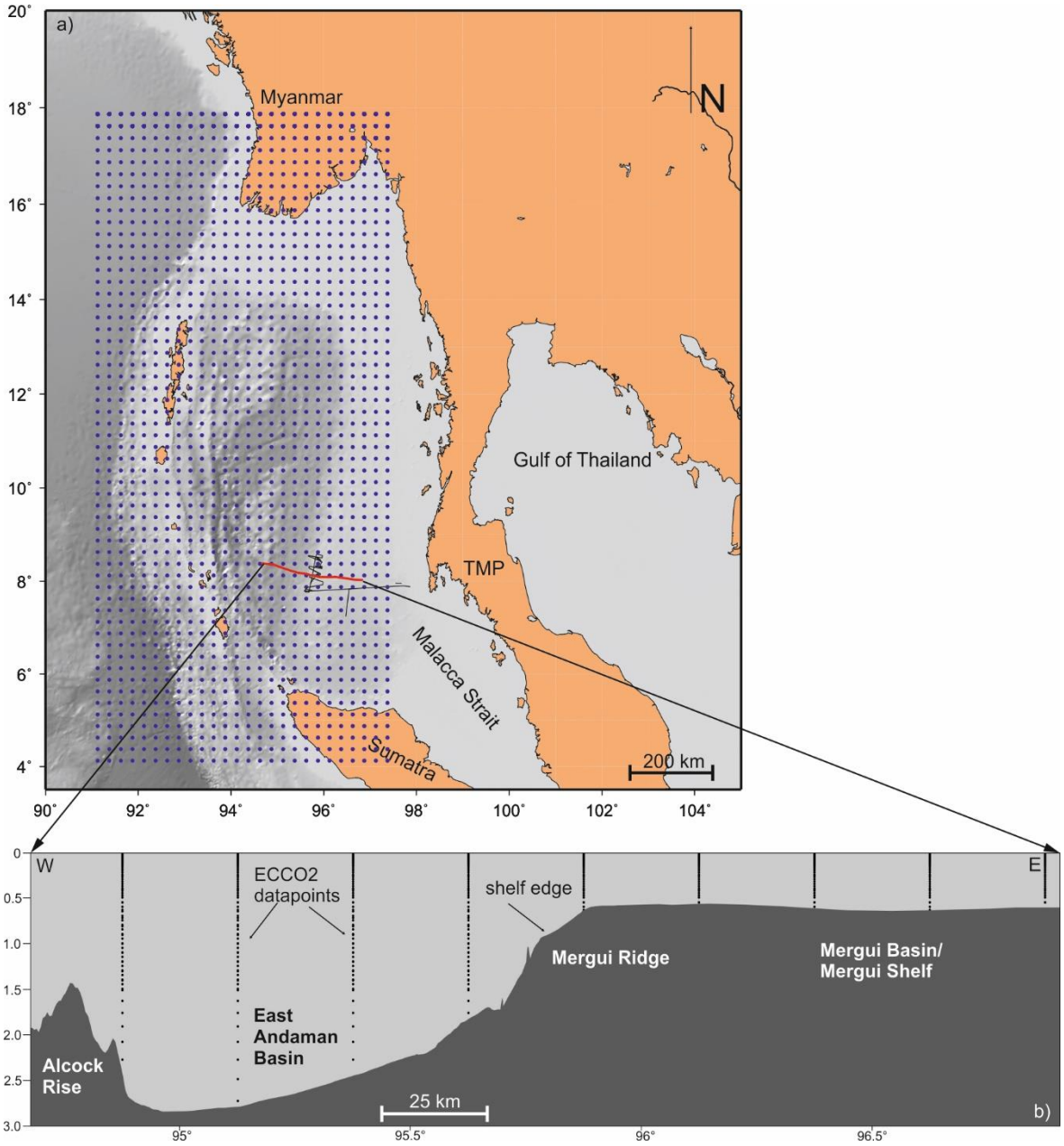

Figure 14: a) Map showing the area of the Andaman Sea where current velocity data from ECCO2 have been used (blue dots). Distance between the data points is 0.25°. Red frame: Main focus of this study. Black lines: Cruise track (MASSIII). Red line: Location of INDOPAC bathymetry profile (NCEI), applied for visualization of bottom current properties. b) Bathymetry Profile (INDOPAC, NCEI) across the Mergui Ridge shelf edge with indication of locations of adjacent ECCO2 (Menemenlis et al., 2008) data points, applied for visualization of bottom current properties along the profile. Background bathymetry from GEBCO (IOC et al., 2003).

ECCO2 is a part of WOCE (World Ocean Circulation Experiment), originally launched in 1998. The ECCO2 dataset is an assimilation of modelled and observed data, provided by NASA (Menemenlis et al. 2008; available at http://ecco2.jpl.nasa.gov/). It combines global in situ and remote observational data with the global circulation model “MITgcm”

(Massachusetts Institute of Technology General Circulation Model, Marshall et al. 1997), simulating ocean flow at all depths and resulting in a global grid of data points with a horizontal spacing of 0.25° and vertical 50 layers, containing modeled current velocities, temperature and salinity (Menemenlis et al. 2008; Wunsch and Heimbach, 2009). The data are originally provided as monthly mean for each year. For this thesis an eleven year average (2003-2013, arithmetic mean) of current velocity in zonal (uvel) and meridional (vvel) direction for each month, calculated with MathWorks® MATLAB 2011a was examined. The MATLAB calculation of the eleven year average was carried out by C. Böttner. The data were investigated and visualized with ODV (Schlitzer, 2016).

4.5. Tsunami Modeling

Several hypothetical landslide tsunami scenarios are modeled. These scenarios are based on landslide geometrical parameters taken from the landslide deposits identified the acoustic dataset. The approach for modeling tsunami waves triggered by submarine landslides in the working area follows the method of Brune (2009) and Brune et al. (2010a, 2010b) who modeled tsunamis arising from landslides of comparable dimensions in the Sunda Trench area. The modeling method comprises three separate steps (Figure 15) for 1) obtaining initial wave parameters 2) applying a numerical model for tsunami wave propagation and 3) estimation of run-up for distinct locations by empirical formulas. S. Brune provided the FORTRAN script that was used for the modeling (see Brune, 2009; Brune et al., 2010a; 2010b). In this script; calculation of initial wave parameters after the formulations of Watts et al. (2003; 2005) and Grilli and Watts (2005) are implemented as well as input of these initial parameters into the numerical model calculation of tsunami propagation (TUNAMI-N2) that was developed by F. Imamura (Goto et al., 1997).

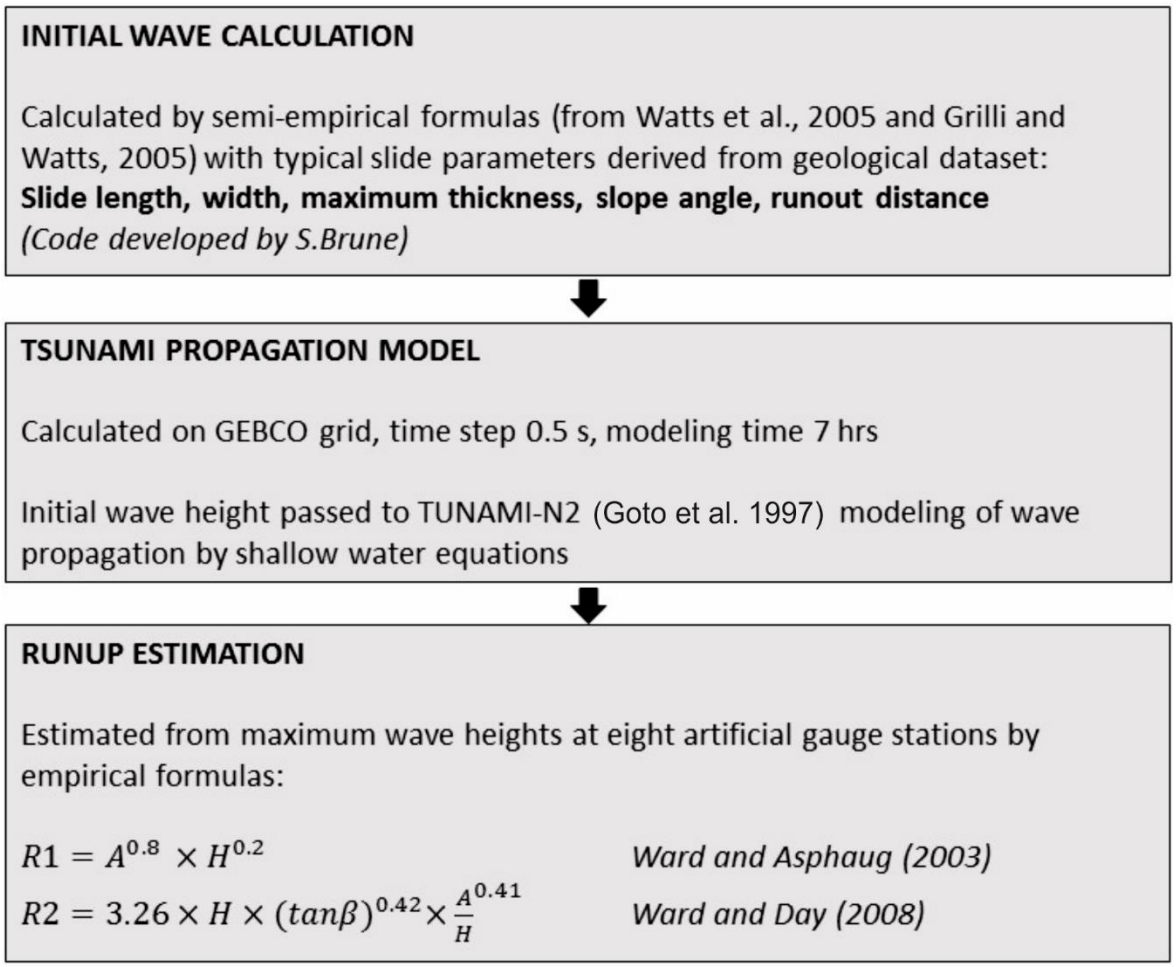

Figure 15: Modelling flow. R1: empirical formula to calculate run-up at the coast line from tsunami wave height an artificial gauge after Ward and Asphaug (2003); R2 empirical formula to calculate run up heights after Ward and Day (2008) A: tsunami wave height measured at water depth H; β: angle at the slope between gauge and the coast line.

4.5.1. Initial wave calculation

The parameters of the initial tsunami wave generated by rotational slumps is calculated after Brune et al. (2009) and Brune et al. (2010a; 2010b) with a method suggested by Watts et al. (2003), Watts et al. (2005) and Grilli and Watts (2005). Based on laboratory and numerical experiments these authors developed a set of semi-empirical, analytical formulas for the calculation of initial wave properties of rotational slumps. In their approach, they are firstly considering only one horizontal dimension (1HD) where the mass failure is simplified as an elliptical shape and its movement is regarded as a center of mass movement along an assumed parabolic failure surface with a radius of curvature, calculated from slump geometrical parameters (Figure 16). Angular displacement at the moment of maximum velocity is then calculated from travel distance (S0) and radius of curvature. In subsequent calculation steps initial acceleration, maximum velocity and characteristic time of motion (t0) are calculated. t0 is designating the end of buildup of the initial wave during the phase of initial acceleration of the mass failure. t0 marks also the point of time where the tsunami wave parameters are transferred to the tsunami propagation model as starting conditions. Subsequently approximation of the sea surface deformation by the mass movement is done. From the initial wave height (η1HD) and characteristic wavelength λ, two symmetric/Gaussian curves with positive amplitude +η1HD in the direction of the slide movement and negative amplitude –η1HD in the opposite direction and a distance of the center points of these two curves of one characteristic wavelength lambda are calculated (after Synolakis et al., 2002; Watts et al., 2005). Subsequently they transform this curve in two horizontal dimensions (2HD) according to Watts et al. (2005), yielding an initial wave height η2HD.

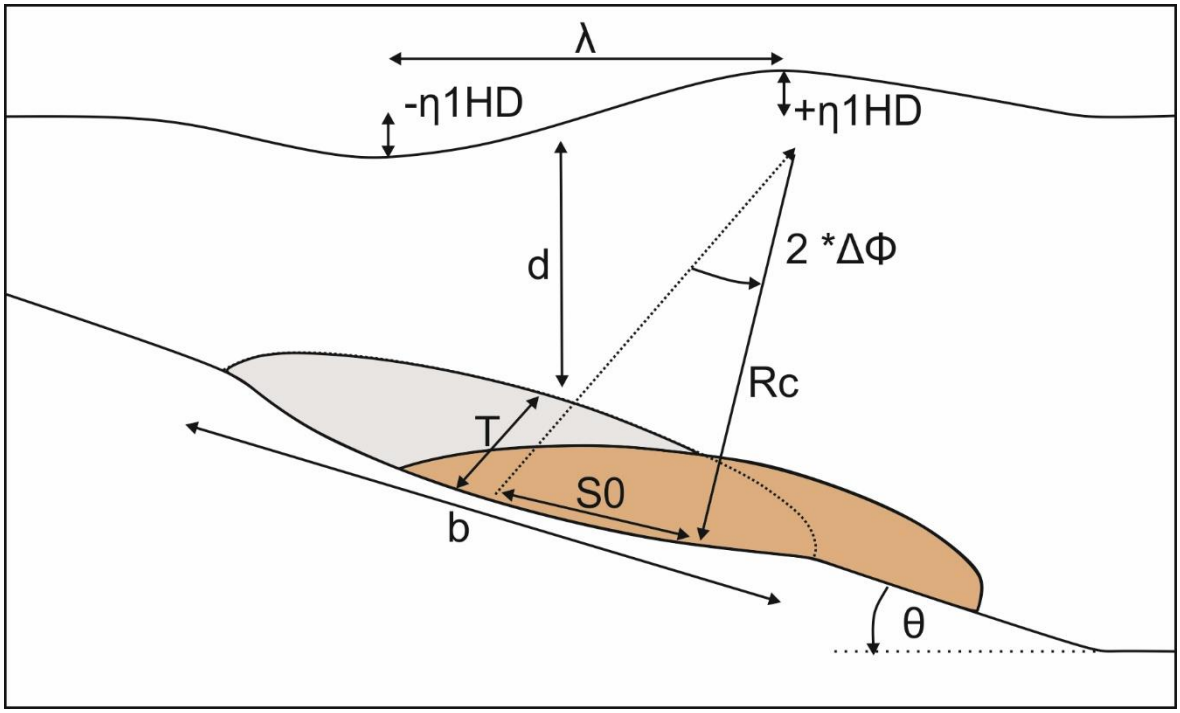

Figure 16: Parametrization Scheme after Watts et al. (2003), modified from Brune et al. (2010b), supplement. D is submergence depth, b slide length, so is travel distance, slide height is T, slope angle is θ, slump radius of curvature is Rc, angular displacement at moment of maximum velocity is ΔΦ. +ηhd and –ηhd are the wave heights calculated from these parameters (Watts et al. 2005, Brune et al 2009, 2010a, 2010b), as well as the characteristic wavelength λ.

4.5.2. Tsunami propagation numerical modeling

The initial wave distribution (with η2HD) at time point t0 is transferred to the TUNAMI-N2 numerical model for calculation of tsunami wave propagation. TUNAMI-N2 is a widely applied numerical model, originally developed by F. Imamura (Goto et al., 1997). In the model finite difference discretization for the solution of the nonlinear shallow water equations is applied. For the discretization in space and time the staggered leap-frog numerical scheme is applied and the upwind scheme for the convective terms. The modeling of tsunami wave propagation was carried out for each scenario for a total time of 25200s (7 hours) at time steps of 0.5s. For bathymetry, the GEBCO (IOC et al., 2003) grid in the domain 4°50'N to 10°38'N and 94°40'E to 99°40'E was used, resolved to 32arcs.

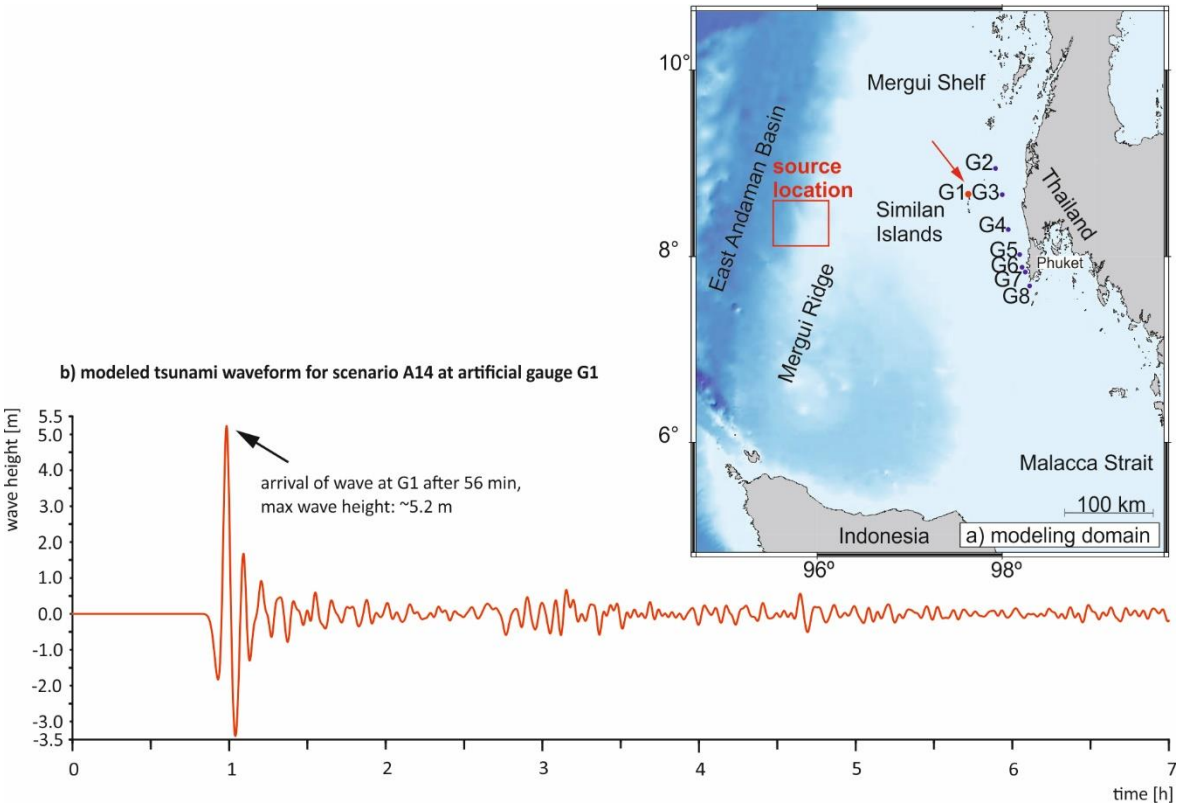

Figure 17: Example of tsunami wave height over modeled time interval (7 h) at gauge station G1.

4.5.3. Run-up estimation

Tsunami wave heights near the coast are calculated for at eight artificial gauge locations positioned in water depths between 24 and 51m (G1-G8, Figure 17). Figure 17 is showing the locations of the gauges as well as an example for the development of the tsunami wave for one scenario over the modelled time interval (7h). Following Brune (2009), we did not model run-up/inundation of the coast, due to the lack of high resolution bathymetry that would be necessary for robust inundation modeling results. Instead, from the gauge locations G1 to G8 the maximum wave heights during the modeled time period were identified, and from these maximum wave heights run-up was estimated by empirical formulas (R1 and R2 in Figure 15) as in Ward and Asphaug (2003) and Ward and Day

(2008), for the coast near the gauge stations. Whereas the estimation of wave height by R1 is only depending on water depth and tsunami wave height at the gauge locations, R2 takes account also of the slope angle between the gauge station and the shore line.

References

Becker, J.J., Sandwell, D.T., Smith, W.H.F., Braud, J., Binder, B., Depner, J., Fabre, D., Factor, J., Ingalls, S., Kim, S.-H., Ladner, R., Marks, K., Nelson, S., Pharaoh, A., Trimmer, R., Rosenberg, J. von, Wallace, G., Weatherall, P., 2009. Global Bathymetry and Elevation Data at 30 Arc Seconds Resolution: SRTM30_PLUS. Marine Geodesy 32 (4), 355–371. 10.1080/01490410903297766.

Brune, S., 2009. Landslide generated tsunamis: numerical modeling and real-timeprediction. PhD Thesis, University of Potsdam, 94pp.

Brune, S., Ladage, S., Babeyko, A.Y., Müller, C., Kopp, H., Sobolev, S.V., 2010a. Submarine landslides at the eastern Sunda margin: observations and tsunami impact assessment. Nat Hazards 54 (2), 547–562. 10.1007/s11069-009-9487-8.

Brune, S., Ladage, S., Babeyko, A.Y., Müller, C., Kopp, H., Sobolev, S.V., 2010b. Supplement to: Submarine landslides at the eastern Sunda margin: Observations and tsunami impact assessment. Nat Hazards 54 (2), 547–562. 10.1007/s11069-009-9487-8.

ECCO2 Estimating the Circulation and Climate of the Ocean, Phase II: High Resolution Global-Ocean and Sea-Ice Data Synthesis" http://ecco2.jpl.nasa.gov/

Goto, C., Shuto, N., Imamura, F., 1997. Numerical Method of Tsunami Simulation with the Leap-Frog Scheme. Intergovernmental Oceanographic Commission, manuals and guides 35. UNESCO.

Grilli, S.T., Watts, P., 2005. Tsunami Generation by Submarine Mass Failure. I: Modeling, Experimental Validation, and Sensitivity Analyses. J. Waterway, Port, Coastal, Ocean Eng. 131 (6).

IOC, IHO, BODC (2003) Centenary edition of the GEBCO digital atlas, published on CDROM on behalf of the Intergovernmental Oceanographic Commission and the International Hydrographic Organization as part of the general bathymetric chart of the oceans. British Oceanographic Data Centre, Liverpool

Jintasaeranee, P., Weinrebe, W., Klaucke, I., Snidvongs, A., Flueh, E.R., 2012. Morphology of the Andaman outer shelf and upper slope of the Thai exclusive economic zone. Journal of Asian Earth Sciences 46, 78–85. 10.1016/j.jseaes.2011.11.003.

Marshall, J., Adcroft, A., Hill, C., Perelman, L., Heisey, C., 1997. A finite-volume, incompressible Navier Stokes model for studies of the ocean on parallel computers. J. Geophys. Res. 102 (C3), 5753–5766. 10.1029/96JC02775.

Menemenlis, D., Campin, J.M., Heimbach, P., Hill, Lee, C., Nguyen, A., Schodlock, M., Zhang, H., 2008. ECCO2: High resolution Global Ocean and Sea Ice Data Synthesis. Mercator Ocean Quarterly Newsletter 31, 13–21.

NCEI: National Centers for Environmental Information World Data Service for Geophysics at at https://www.ngdc.noaa.gov/mgg/mggd.html.

Polachan, S., Racey, A., 1994. Stratigraphy of the Mergui Basin, Andaman Sea: (Implications for Petroleum Exploration). Journal of Petroleum Geology 17 (4), 373–406.

Schlitzer, R., Ocean Data View, http://odv.awi.de,2016

Synolakis, C.E., Bardet, J.-P., Borrero, J.C., Davies, H.L., Okal, E.A., Silver, E.A., Sweet, S., Tappin, D.R., 2002. The slump origin of the 1998 Papua New Guinea Tsunami. Proceedings of the Royal Society A: Mathematical, Physical and Engineering Sciences 458 (2020), 763–789. 10.1098/rspa.2001.0915.

Ward, S.N., Asphaug, E., 2003. Asteroid impact tsunami of 2880 March 16. Geophys J Int 153 (3), F6–F10. 10.1046/j.1365-246X.2003.01944.x.

Ward, S.N., Day, S.J., 2008. Tsunami Balls: A Granular Approach to Tsunami Runup and Inundation. Communications in Computational Physics 3 (1), 222–249.

Watts, P., Grilli, S.T., Kirby, J.T., Fryer, G.J., Tappin, D.R., 2003. Landslide tsunami case studies using a Boussinesq model and a fully nonlinear tsunami generation model. Nat. Hazards Earth Syst. Sci. 3, 391–402.

Watts, P., Grilli, S.T., Tappin, D.R., Fryer, G.J., 2005. Tsunami Generation by Submarine Mass Failure. II: Predictive Equations and Case Studies. J. Waterway, Port, Coastal, Ocean Eng. 131 (6), 298–310.

Wessel, P., Smith, W.H.F., Scharroo, R., Luis, J., Wobbe, F., 2013. Generic Mapping Tools: Improved Version Released. Eos Trans. AGU 94 (45), 409–410. 10.1002/2013EO450001.
Wunsch, C., Heimbach, P., Ponte, R., Fukumori, I., 2009. The Global General Circulation of the Ocean Estimated by the ECCO-Consortium. Oceanog. 22 (2), 88–103. 10.5670/oceanog.2009.41.

5. Sediment dynamic in the Mergui Ridge area at the outer continental margin off western Thailand, Andaman Sea

MANUSCRIPT I

Julia Schwab[1], Christoph Böttner[1], Felix Gross[1], Sebastian Krastel[1]

[1] *Institute of Geosciences, Christian-Albrechts-Universität zu Kiel, Kiel, Germany*

To be submitted to Marine Geology

Sediment dynamic in the Mergui Ridge area at the outer continental margin off western Thailand, Andaman Sea

Julia Schwab, Christoph Böttner, Felix Gross, Sebastian Krastel

Abstract

The sedimentary development and the processes that shape the outer shelf margin off western Thailand have not been examined in detail yet. Therefore, a new dataset consisting of high resolution 2D multichannel reflection seismic and high resolution multibeam bathymetry has been used in order to identify and analyze sedimentary units, their stratigraphic placement, and morphodynamics. These data have been interpreted with respect to the oceanographic regime in order to gain insight into the hydrographic processes that shape the margin. Within the dataset, sedimentary packages from the edge of the Mergui Ridge show indicators of sea level fluctuations, indicative of submergence of the ridge. Several drift deposits and other morphologic indicators of the interaction of bottom currents, such as the presence of an erosive zoane at the edge of the ridge and moats around topographic obstacles have been identified. These findings show that the youngest sediments in the working area are shaped by the subsidence of the Mergui Ridge that occurred in the Pliocene and subsequently by bottom currents, leading to the deposition of drift deposits on top of the Mergui Ridge, and off its western flank. The present-day configuration of sedimentary features in the working area may be explained by the interaction of alongslope currents that are influenced by the monsoon seasons as well as the occurrence of internal waves that may interact with the sea floor at the western part of the Mergui Ridge.

5.1. Introduction

Despite large sedimentary input into the Andaman Sea via the Ayerawaddy river (Figure M1-1; Robinson et al., 2007), the eastern Andaman (Mergui) shelf is a sediment starved margin. The Mergui Ridge, which is situated at the outer continental margin off western Thailand (Figure M1-1) belongs to this sediment starved area. The overall sedimentary setting of the Mergui Ridge, and the processes that lead to the deposition of the sedimentary succession have not been analyzed in detail yet. Such an analysis, however, is essential in order identify the processes that influence the sediment dynamics in the Mergui Ridge area. So far, drift deposits in the area have been found by Schwab et al. (2012) who examined the slope stability in the area. Slope instability has been related to these drift deposits. Beside the reconstruction of the sedimentary development of the Mergui Ridge area by interpreting a seismic and multibeam bathymetric dataset, the aim of this study is to relate the current sediment dynamics to the circulation patterns in the Andaman Sea. Special focus will be drawn on drift deposition. Several recent studies from other areas in the world relate morphodynamics and drift deposition to influences by the oceanographic regime through the joint interpretation of geological/geophysical and hydrological data (Preu et al., 2013; Hernández-Molina et al., 2014; Ercilla et al., 2015). Focus of this study is on monsoon influenced (bottom) currents and potential interaction of

internal waves with the sedimentary succession of the outer shelf. Specific points to be addressed are: I) Identification and analysis of seismic units in the Mergui Ridge area by means of high resolution 2D multichannel reflection seismic data set in order to establish the sedimentary development of the area. II) Linking the sedimentary architecture imaged by multibeam bathymetry and high-resolution reflection seismic data to circulation patterns and the oceanographic regime.

5.1.1. Working Area and Physiography of the Andaman Sea

The Andaman Sea (Figure M1-1) is a semi-enclosed, pull-apart back arc basin (Curray, 2005) with active sea floor spreading in its central part as a result of subduction of the Indian Plate below the Asian Plate along the Sunda Trench (Curray et al., 1978; Kamesh Raju et al. 2004; Curray, 2005). The associated island arc with the Andaman and Nicobar Islands forms the western boundary of the Andaman Sea and separates it from the Bay of Bengal. The western deep sea area of the Andaman Sea comprises two sub-basins, the Central Andaman Basin (CAB) and the East Andaman Basin (EAB), separated by two topographic highs, the Alcock rise (AR) and the Sewell rise (SR). The Central Andaman Basin (CAB) is the location of the modern sea floor spreading center. The adjacent East Andaman Basin (EAB) is an N-S elongated basin with water depths of up to 3000m; it extends from the shelf of Myanmar in the North to Sumatra in the south (Figure M1-1).

The eastern part of the Andaman Sea is underlain by the Mergui Shelf (MS). The Mergui Shelf is a broad drowned platform (Searle and Morley, 2010) with water depths of up to 800m that extends from the Myanmar Shelf/Ayerawaddy delta in the north, southward along the Thai-Malay Peninsula to the Malacca Strait area. Off western Thailand, the shelf broadens and exhibits a two-step morphology with an inner shelf break at approximately 200 m water depth and an outer shelf terrace that breaks at approximately 600-800 m water depth. Most parts of the outer shelf terrace is underlain by the sediment filled continental Mergui Rift basin (MB) (Polachan and Racey, 1994; Andreason et al., 1997); only the westernmost part of the Shelf is underlain by the Mergui Ridge (MR), a basement high (Polachan and Racey, 1994; Curray, 2005). The Mergui Basin roughly comprises a V-shape, opening and deepening to the south, where it merges with the North Sumatra Basin (Polachan et al., 1991). The outer shelf edge and boundary of the Mergui Basin is formed by the roughly 50 km broad and 200 km long Mergui Ridge (MR), a volcanic/metamorphic ridge (Curray, 2005), separating the Mergui Basin from the East Andaman Basin. The Mergui Ridge is connected at its northern end with the Mergui Shelf. The western edge of Mergui Ridge is the target area of this study (Figure M1-1).

5.1.2. Geological setting

The Mergui Ridge has been in shallow water depths or even been subaerially exposed for most of its time of existence until the Late Miocene (Andreason et al 1997; Morley 2015). In contrast, it is located today in water depths of 600-800m, which is unusual for a shelf edge. The submergence of the Mergui Ridge is related to rapid subsidence during the Late Miocene/Pliocene (Andreason et al., 1997) controlled by the tectonic development of

the area. Even today, subsidence is ongoing at rates of up to 0.35mm/yr in the southern Mergui Basin (Lin et al., 2010). The primary drivers for deformation and basin evolution in the Andaman Sea area are the oblique subduction of the Indian-Australian Plates at the Sunda Trench (Polachan et al., 1991; Curray, 2005; Diehl et al. 2013) and the northward drag of India with respect to Southeast Asia (Rangin et al. 2013; Morley, 2015) since the India - (Eur)Asia collision, approximately 59My ago (Lee and Lawver, 1995; Rangin et al., 2013). Oblique subduction has been resulting in strain partitioning in the overriding plate (Fitch, 1972), and ultimately in the accommodation of stresses by the formation of a modern spreading center with active production of oceanic crust, several linked arc parallel dextral strike slip fault systems (Sagaing Fault System, West Andaman Fault and Sumatra Fault, Michel et al., 2001; Nielsen et al., 2004; Curray, 2005; Socquet et al., 2006; Chakraborty and Khan, 2009) and the formation of a sliver plate (Myanmar or Burma Platelet), which is dragged northward with respect to Sundaland (Rangin et al. 2013 and references therein, Figure M1-1). This northward drag is accommodated by shearing of the Myanmar Plate and N-S strike slip deformation (Rangin et al., 2013).

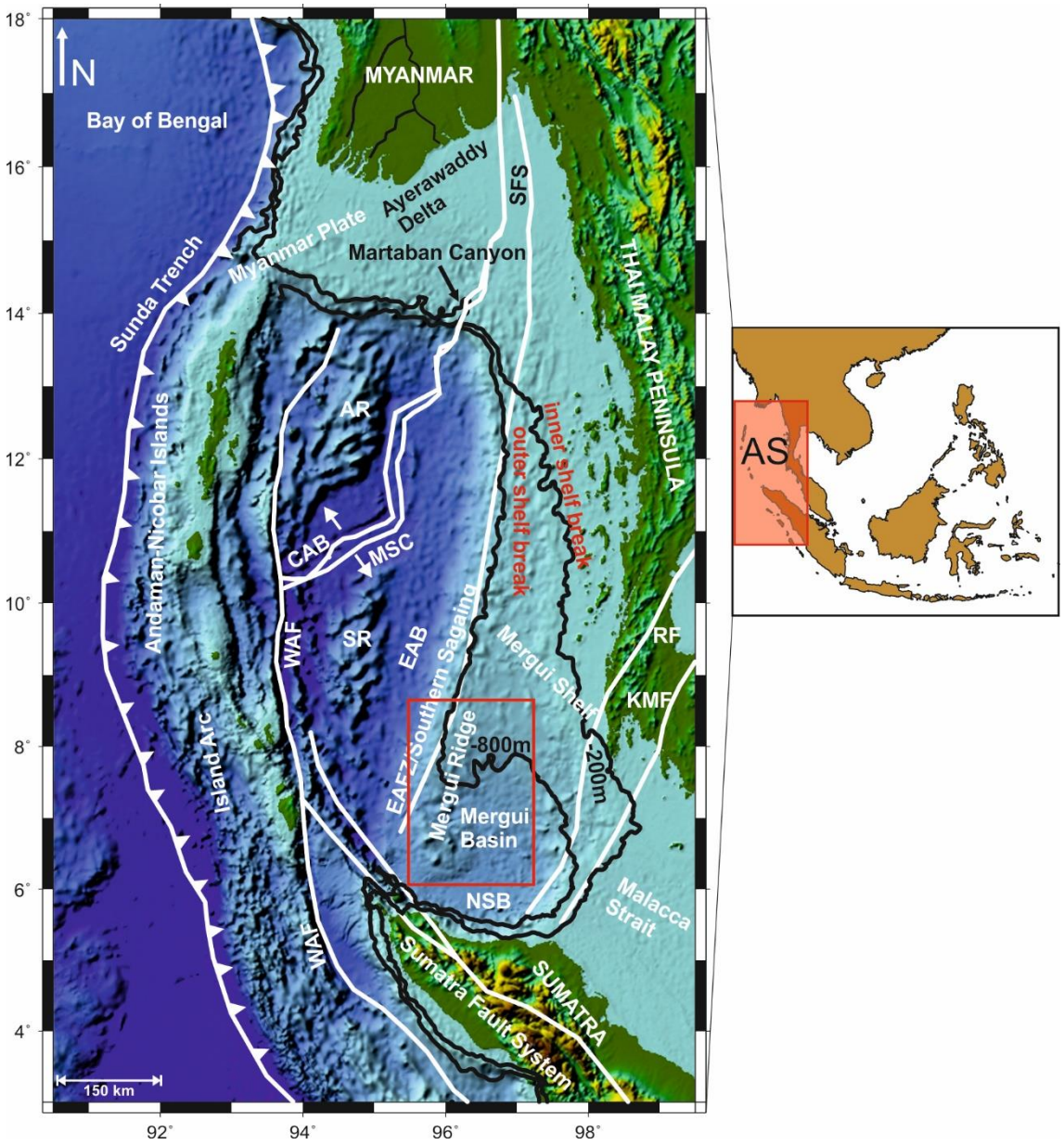

Figure M1- 1: Physiography and tectonic elements of the Andaman Sea, compiled from Curray (2005) and Morley (2015). The bathymetry is from GEBCO (IOC et al. 2003). Abbreviations are as follows: AS: Andaman Sea, NSB: North Sumatra Basin; EAFZ: East Andaman Fault Zone; WAF: West Andaman Fault Zone; SR: Sewell Rise; CAB: Central Andaman Basin; MSC: Modern Spreading Center; EAB: East Andaman Basin; SFS: Sagaing Fault Zone; KMF: Khlong Marui Fault, RF: Ranong Fault.

For the development of the sub-basins of the Andaman Sea (Central Andaman Basin, East Andaman Basin and Mergui Basin), multi stage models have been suggested (Kamesh Raju et al., 2004, Curray, 2005; Khan and Chakraborty, 2009). Curray (2005) describes the opening of the Mergui Basin and the East Andaman Basin as a sequence of extensional phases with changing locations of rifting in response to increasingly oblique plate motions and changing convergence rates of Indian and Sundaland plates (Curray, 2005) since the Oligocene with opening of the Mergui Basin starting at 32Ma (Early Oligocene) as a series of N-S trending half-grabens. The opening of East Andaman Basin took place since around 15Ma (Early/Middle Miocene) and the opening of the recent spreading center in the Central Andaman Basin since about 4Ma (Pliocene). Other studies (Srisuriyon and Morley, 2014; Morley and Alvey, 2015; Morley, 2015) stress the

importance of the impact of the northward drag after coupling of India with Western Myanmar, which took place since the Early Miocene (Morley and Racey, 2010). A more coeval onset of opening of the Mergui Basin and the East Andaman Basin is suggested in some studies (Jha et al., 2008a; 2008b; Morley, 2012; Srisuriyon and Morley, 2014; Morley, 2015). According to Morley (2015) an initial extensional phase occurred during the Late Eocene and Oligocene in E-W direction. During this time subduction related extensional processes dominated (Morley, 2015). In the Early Miocene deformation processes related to the northward drag became more important, leading from E-W extension in the Mergui Basin/East Andaman Basin area to transtensional NNW-SSE deformation (Morley 2015; Morley and Alvey, 2015). A now inactive transtensional dextral strike slip fault that is bounding the Mergui Ridge towards the East Andaman Basin was formed during that time: This fault was active until the Middle Miocene (Morley 2012; 2015), or Late Miocene (Jha et al., 2011). Abandonment of extension/transtension in the outer shelf area might be due to migration of the zone of stretching and establishment of the linked Sagaing-West Andaman-Sumatran fault system in the Late Miocene and Pliocene (Srisuriyon and Morley, 2014). Subsequently the shelf drowned, probably related to the creation of oceanic crust and onset of thermal subsidence following the cessation of extension and/or transtension (Srisuriyon and Morley, 2014). The onset of sea floor spreading in the Central Andaman Basin at around 4My ago (Kamesh Raju et al., 2004; Curray, 2005) may as well be responsible for subsidence of the shelf, possibly by intensifying transtensional movement along the South Sagaing Fault, even during the Late Miocene (Jha et al., 2011). The Mergui Ridge remained elevated relative to its surroundings during the Neogene (Racey, 2010), possibly due to buoyancy caused by thermal underplating (Searle and Morley, 2010) and flexural isostatic response to the establishment of depocenters in the East Andaman Basin and the Mergui Basin (Searle and Morley, 2010). The Mergui Ridge probably was an area of shallow water in the Early Miocene (Morley, 2015) and may have been exposed to the sea surface until Late Miocene/Pliocene (Andreason et al., 1997), acting as a sediment source for clastic material for the western part of the Mergui Basin (Racey, 2010). During Middle Miocene to Recent, there might have been mild inversion and uplift phases due to regional compression caused by far field effects caused by collision of Australia with related fragments along the southeastern margin of Australia/Borneo (Doust and Sumner, 2007). A late uplift phase of the Mergui Ridge may have occurred in the Late Miocene, leading to formation of a local unconformity at the basin ridge transition (Morley, 2015).

The sedimentation history of the Mergui Basin has been examined in detail by Polachan (1988), Polachan and Racey (1994), Andreason et al. (1997) and Srisuriyon and Morley (2014). The maximum sediment thickness in the N-S trending halfgrabens making up the Mergui Basin is about 6-7km (Morley and Racey, 2010). Syn-rift sediments (Upper Oligocene to early Lower Miocene, or even Eocene after Morley, 2015) consist of clastic sediments comprising fluviatile sandstones and conglomerates containing pebble size lithoclasts (Polachan and Racey, 1994; Morley and Racey 2010), as well as delta plain and delta front deposits (Ranong Fm). Towards deeper parts of the basins, deepwater shales were deposited (Yala Fm). In the southern part of the Mergui Basin the Eocene to Oligocene syn-rift section is onlapping on the Mergui Ridge (Morley, 2015). Late- and post- rift sediments of Miocene age are shallow delta deposits in the basin margin areas and deepwater sediments towards the depocenters as well as carbonate units on structural highs. The youngest Plio-Pleistocene to recent sedimentary succession is made up by the Takua Pa Fm of calcareous and glauconitic shales and occasionally siltstones deposited in lower bathyal basin-plain environment (Polachan and Racey, 1994).

The Mergui Ridge marks the westward depositional limit of sedimentation in the Mergui Basin (Andreason et al., 1997). Generally, the correlation of sedimentation between the Mergui Basin and the East Andaman Basin across the shelf edge area is difficult due to the subsidence history of the basins and low sedimentation rates in the Mergui Ridge area (Morley, 2015). However, a profile located about 80km north of our working area (Morley, 2015) defines units that are deposited in the shelf edge area: A Late Miocene to recent sedimentary unit is unconformably overlying middle Miocene sediments that are characterized by indicators for sea level change such as unconformities and prograding features (Morley, 2015). The sedimentary deposits show influence by the large subsidence at the end of the Late Miocene. These are unconformably overlying sediments of Early Miocene age, corresponding to the syn-rift stage in the East Andaman Basin (Morley, 2015)

5.1.3. Modern Sediments of the Mergui Shelf area

Figure M1-2 shows the modern surface sediment distribution in the Andaman Sea, based on data from Frerichs (1967), Rodolfo (1969), SEATAR (1976), Rao et al. (2005) and Ramaswamy and Rao (2006). Whereas fine grained muds and muddy sands make up the surface sediments in the deeper part of the Andaman Sea, the sediment cover of the Mergui Shelf south of the Gulf of Martaban is dominated by relict sands. The Mergui Ridge surface sediments mainly consist of foraminiferal ooze with large grain sizes and high carbonate content and a minor fraction of clay minerals (Frerichs, 1967; Rodolfo, 1969; Tripathi, 2014). In places, surface sediment samples have revealed clastic sediments of pebble size or larger (SEATAR, 1976). In locations at the inner shelf area off western Thailand, sedimentary cover also consists in parts of coarse sandy sediment (Feldens et al., 2012). Here also event layers and structures related to backwash of the 2004 Tsunami have been identified (Feldens et al., 2009; Sugawara et al., 2009; Sakuna et al., 2012; Sakuna-Schwarz et al., 2015).

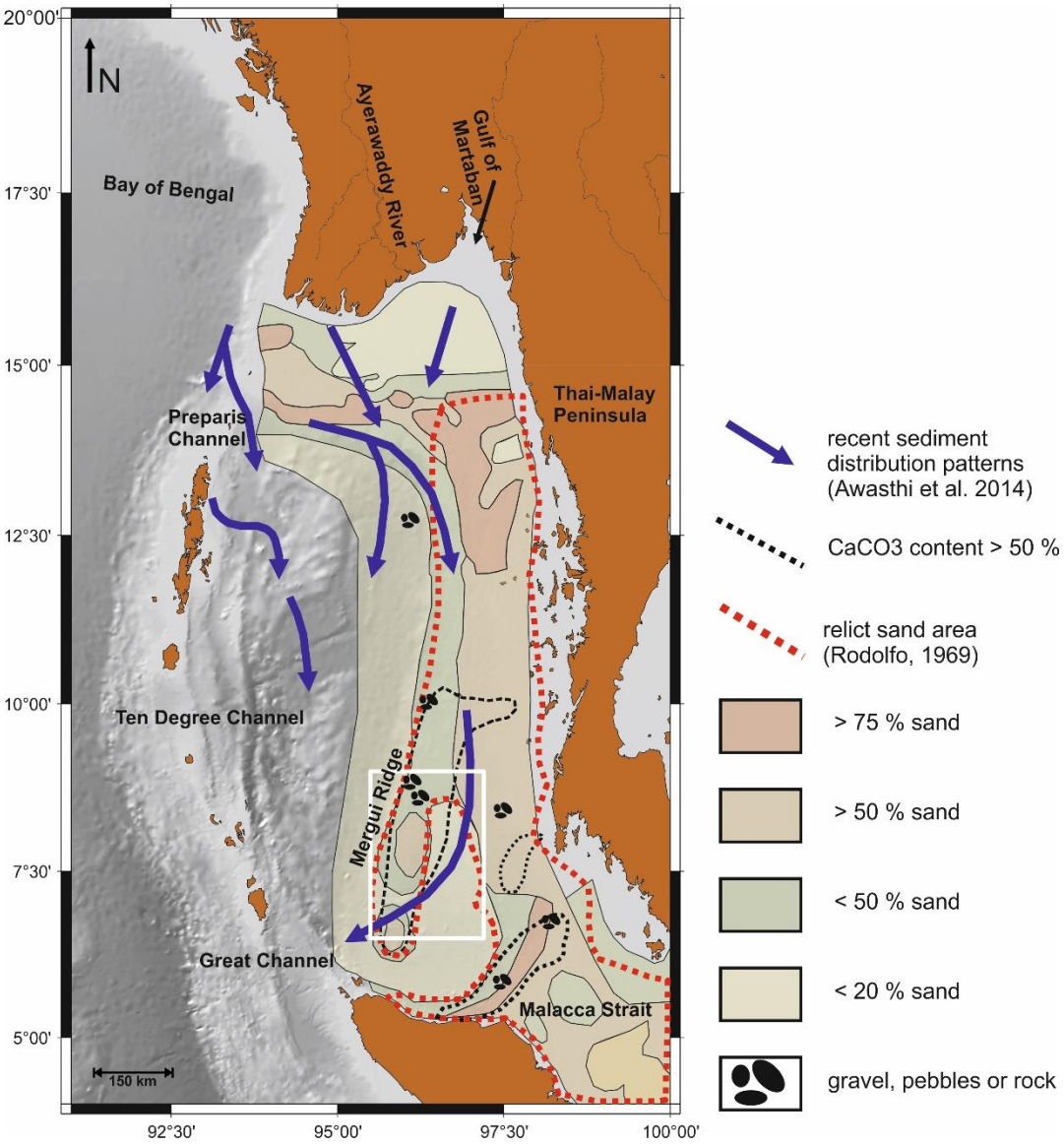

Figure M1- 2: Surface sediment distribution in the working area, with individual patches according to sand content. The locations where gravel, pebbles or rock have been sampled are from SEATAR (1977) database. Data compilation shows that the Mergui Ridge is an area of relict sand and high $CaCO^3$ content, indicating low terrestrial detrital input although modern sediment transport routes (blue arrows) are delivering fine grained material to the area. Compiled from Frerichs (1967), Rodolfo (1969), Rao et al. (2005), Ramaswamy and Rao (2006) and Awashti et al. (2014). CAB: Central Andaman Basin; EAB: East Andaman Basin; MS: Mergui Shelf.

The Ayerawaddy-Salween river system has been delivering clastic sediments into the Andaman Sea since 7Ma (Morley, 2015). It is currently the main source for terrestrial sediment in the Andaman Sea (Rodolfo, 1969; Colin et al., 1999), carrying huge quantities of freshwater and detrital material mainly in the main SW monsoon season. In total, a yearly amount of 364Mt of sediment is delivered into the Andaman Sea (Milliman and Meade, 1983; Robinson et al., 2007). Figure M1-2 shows the modern sediment transport routes that disperse this sediment southward across the Thai-Malay shelf area (Awasthi et al., 2014). Accordingly, from the analysis of two sediment cores in the working area, Bunsomboonsakul et al. (2012) identified the Ayerawaddy-Salween rivers as a main source for terrestrial clay minerals that are present in the working area. Cao et al. (2015) also identified the Ayerawaddy as main source for sediment in the southeastern Andaman Sea shelf slope area.

However, most of the sediment delivered by the Ayerawaddy River is trapped in the Gulf of Martaban (see Figure M1-2 for location) due to coastal currents influenced by tidal currents and monsoonal currents transporting the suspended load from the river mouths eastward (Ramaswamy et al., 2004). Additionally, a part of the delivered sediment is transported by gravity driven processes via the Martaban Canyon into the deeper parts of the Central Andaman Basin (Ramaswamy and Rao, 2006). Despite the huge quantity of input and the deposition of great amounts of sediments into the East Andaman Basin from the Ayerawaddy River (Morley, 2015), the Mergui Shelf area is a zone of low sedimentation (Rodolfo et al. 1969; Rao and Ramaswamy 2005; Figure M1-2), where relict sands that show indications of prolonged reworking (80-90% quartz, feldspar only in trace amounts) prevail (Rodolfo, 1969; Rao et al. 2005), and also relict foraminifera are present (Rodolfo,1969; Panchang et al., 2008), indicating low sedimentation rates and/or reworking of the sediment. This zone is starved of fine grained sediments of modern origin (Rao and Ramaswamy, 2005). Unlike in the adjacent rift basins the Mergui shelf area modern (Middle Miocene to Recent) sediment cover has a thickness of no more than 0.5 to 1km (Morley and Alvey, 2015).

5.1.4. Oceanographic setting

The hydrologic conditions in the Andaman Sea are driven by the effects of the Southeast Asian (Indian) Monsoon system, which induces a semi-annual reversal of wind directions over India/Southeast Asia. This reversal of wind directions leads to seasonal reversal of upper ocean circulation directions (Wyrtki, 1961) and controls the amount of freshwater that is shed into the Andaman Sea.
During NE monsoon winds blow from the north/north east and during SW monsoon from the southwest. The strength of winds leads to peak rainfall amounts in the Ayerawaddy catchment area in August (Rashid et al., 2007) and this in turn leads to main outflow of freshwater into the Andaman Sea in October (in total 482km^3 of freshwater per year after Millimann and Meade, 1983; Rashid et al., 2007) and to the presence of a low salinity freshwater lens in the Andaman Sea (Rodolfo, 1969) with fluctuating salinity. During SW monsoon the surface circulation in the Andaman Sea is dominated by the SW monsoon current that enters the Andaman Sea from the north (Brown, 2007). Varkey et al. (1996) and Potemra et al. (1991) describe the establishment of an anticlockwise (cyclonic) seasonal gyre, affecting also the deeper parts of the water column. During NE monsoon, the flow of the North Equatorial Current is entering the Andaman Sea from the south via the Malacca Strait (Brown et al., 2007), and the surface circulation is described to be a clockwise (anticyclonic) gyre (Varkey et al., 1996; Potemra et al., 1991) with downward effect to 500 and 1000m (Varkey et al., 1996), and current speeds of up to 12cm/s at 500m (Varkey et al., 1996). Potemra et al., (1991) modeled gyral flow in deeper layer (250 m) of the Andaman Sea with change of direction of the gyral flow from cyclonic (Jan-Mar) to anticyclonic (April-July) to cyclonic (August-October) and to anticyclonic again (November-December).

The Andaman Sea is a semi enclosed ocean basin, therefore lateral exchange with the Bay of Bengal waters is restricted and occurs solely via sills in the Andaman-Nicobar Ridge and the shallow water (<200 m) Malacca Strait (Wyrtki, 1961; Keller and Richards, 1967; see Figure M1-2 for the location of sills). The sill depth of the Preparis Channel is shallower than 250m. This means that the exchange of deeper water occurs via the Ten Degree Channel (800m) and the Great Channel (1800m) (Nozaki and Alibo, 2003). Below

1800m no lateral exchange does occur (Rodolfo, 1969; Dutta et al., 2007). Due to the large fluvial inflow into the Andaman Sea the surface water to about 70 -100m depth (Rodolfo, 1969) is made up by a high-temperature, low-salinity freshwater lens with seasonally changing salinity and extent. Beneath the surface layer water mass characteristics in the upper 1300m (Rodolfo, 1969) to 1500m (Nozaki and Alibo, 2003) are similar in the Andaman Sea and Bay of Bengal, with a salinity maximum layer between 300 and 600m water depth (Naqvi et al., 1997; Kim et al., 2015). The thickness of this layer varies seasonally (Varkey et al., 1996). Deep water characteristics start to diverge below 1250m water depth (Nozaki and Alibo, 2003). Below 1500m in the Andaman Sea uniform, well mixed water mass prevails with similar characteristics as the Bay of Bengal waters at 1250m (Varkey et al., 1996; Nozaki and Alibo, 2003; Dutta et al. 2007). This implies vigorous vertical mixing (Dutta et al., 2007) with renewal times of about 6yr (Okubo et al., 2004). The inflow of deep water from the Bay of Bengal above the sills at around 1300m might be in response to the seasonally changing surface currents, balancing the outflow out of the Andaman Sea, mainly during NE monsoon (Rodolfo, 1969).

5.2. Data and Methods

5.2.1. Multibeam bathymetry and 2D multichannel reflection seismic dataset

High resolution multibeam bathymetry data (about 3000km^2) obtained during MASS I and MASS II cruises in 2006 and 2007 were used for this study (Figure M1-3a). The data were acquired with a portable Seabeam 1050 multibeam echo sounder. This system operates at a frequency of 50Hz and provides 126 individual beams with a maximum swath width of up to 153°. The data were originally processed and published by Jintasaeranee et al. (2012). For this study a bathymetric grid with a grid cell size of 50m was applied. Moreover, a backscatter map was created with MB-system and visualized with GlobalMapper. The high resolution bathymetry was supplemented with GEBCO bathymetry (IOC et al. 2003). Data interpretation and visualization was done with GlobalMapper and GMT. This bathymetry map was used to interpret the morphological features in the working area, supplemented by the 2D multichannel high resolution data set.

A High resolution 2D multichannel reflection seismic data set (Figure M1-3a) was obtained during MASS cruise III in 2011 and partly published by Schwab et al. (2012). In total 39 seismic profiles with a total length of about 630km were collected. The data has been acquired using a micro GIGun (2×0.1l) as source and a 150m-long 96-channel digital Geometrics GeoEel streamer (12 sections with 8 channels each, channel distance 1.56m). The gun was shot every 5s at 120bar, resulting in a shotpoint distance of ~ 10m at 4kn. The main signal frequency was around 200Hz. The signals, digitized at 4kHz were converted into SEG-Y format for further processing. Vista Seismic Data Processing (Schlumberger) was used to carry out standard processing steps including setup of geometry, common midpoint sorting at bin sizes of 2m inline, normal moveout corrections and bandpass frequency filtering for frequency contents of 25/50–600/1200kHz, as well as stacking and time migration at a constant velocity of 1500m/s. IHS Kingdom Suite was used for interpretation.

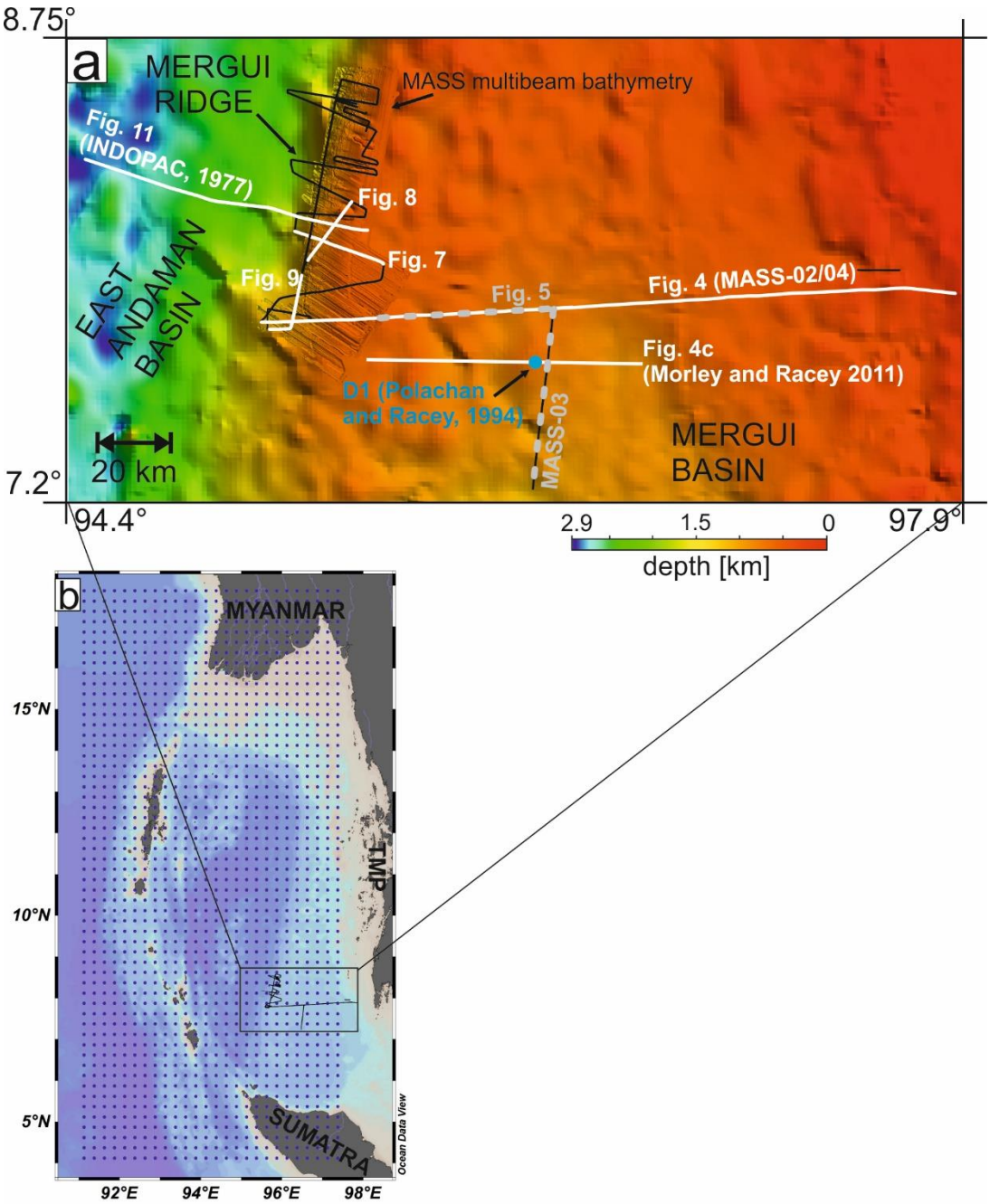

Figure M1- 3: a) Geologic dataset used in this study and location of figures shown in this study. The data used consist of multibeam bathymetry and high resolution 2D multichannel reflection seismic (black lines) acquired during MASS cruises in 2006 and 2007. They are supplemented by two profiles from one from INDOPAC 1977(NCEI, available at https://www.ngdc.noaa.gov/mgg/mggd.html) and one from Morley and Racey 2010 as well as borehole data from D-1 well in the Mergui Basin (Polachan and Racey, 1994). b) Hydrographic dataset ("ECCO2 Estimating the Circulation and Climate of the Ocean, Phase II: High Resolution Global-Ocean and Sea-Ice Data Synthesis" (Menemenlis et al. 2008, available *at http://ecco2.jpl.nasa.gov/). Blue dots represent data locations at a 0.25° grid spacing. The data were visualized with ODV (Schlitzer, 2016). Background bathymetry in both figures is from GEBCO (IOC et al. 2003).*

Additionally, water depths for the profile "INDOPAC" (see Figure M1-3b for location) were obtained from a seismic line from the INDOPAC 11 (1977) cruise (assuming a TWT of 1500 m/s) in order to get an idea of the morphology of deeper parts of the EAB shelf slope. The seismic line is available from NCEI (National Centers for Environmental Information at https://www.ngdc.noaa.gov/mgg/mggd.html. Most of the seismic lines obtained during the MASS cruises are located at the Mergui Ridge –East Andaman basin transition (Figure M1-3a). Two profiles have been acquired in the Mergui Basin, one

running E-W- across the basin (Profile MASS-02/04, Figure M1-4, see Figure M1-3a for location) and one N-S profile in the southern part of the basin (Profile MASS-03, Figure M1-5, see Figure M1-3a for location). These two profiles were used for stratigraphic correlation. The seismic and bathymetric dataset was applied in order to interpret subsurface seismic units and to deduce the sedimentary development of the working area. In addition to that, the bathymetry/backscatter map was used to interpret surface morphological features in the working area.

Stratigraphic placement of the seismic units interpreted in our dataset was obtained by correlation to borehole data of the D-1 well in the Mergui Basin (Polachan and Racey, 1994) which is located about 2.8km from profile MASS-03 (Figure M1-3a); this site was projected onto profile Mass-03. The depth for the Late Miocene/Pliocene boundary was taken from the D-1 well (Polachan and Racey, 1994; their Figure 16).

5.2.2. ECCO2 circulation velocity and direction data

The hydrographic dataset was interpreted in order to obtain an overview of the oceanographic processes (bottom currents that may influence the sedimentary development. Current velocity data from “ECCO2 Estimating the Circulation and Climate of the Ocean, Phase II: High Resolution Global-Ocean and Sea-Ice Data Synthesis” (Menemenlis et al. 2008) were used (Figure M1-3b) in order to relate the observations of the sediment dynamics to the hydrography of the working area. This data assimilation, provided by NASA (available at http://ecco2.jpl.nasa.gov/) combines global in situ and remote observational data with the global circulation model “MITgcm” (Massachusetts Institute of Technology General Circulation Model, Marshall et al., 1997) resulting in a global grid of 0.25° grid cell size of current velocities, temperature and salinity. The data are originally provided as monthly mean for each year. For this study an eleven year average (arithmetic mean) of current velocity in zonal (uvel) and meridional (vvel) direction for each month (Jan 2003 to Dec 2013) was calculated with “MathWorks® MATLAB 2011a”. The data were investigated and visualized with Ocean Data View (Schlitzer, 2016).

5.3. Results

5.3.1. Seismic Units in the Mergui Basin

High resolution 2D multichannel reflection seismic data are available from the top and the western edge of the Mergui Ridge. Only two profiles are available in the Mergui Basin area west of the Mergui Ridge. Profile MASS-02/04 (Figure M1-4, see Figure M1-3a for location) extends from the Mergui Ridge basement high in the west to the shallow shelf area in the east, imaging the transition from the Mergui Basin to the Mergui Ridge down to a subsurface depth of ~1s TWT. Profile MASS-03 (Figure M1- 5, see Figure M1-3a for location) is a N-S transect in the Mergui Basin, connected to Profile MASS-02/04. These

profiles were used to assess the stratigraphy at the edge of the Mergui Ridge by comparison to previously published data from the Mergui Basin (Polachan and Racey, 1994; Racey, 2010; Morley, 2015). We divided the sedimentary basin fill of the MB into three seismic units, MB1, MB2 and MB3. Figure M1-4 (Profile MASS-02/04) is giving an overview of the units interpreted in the Mergui Basin and Mergui Ridge areas.

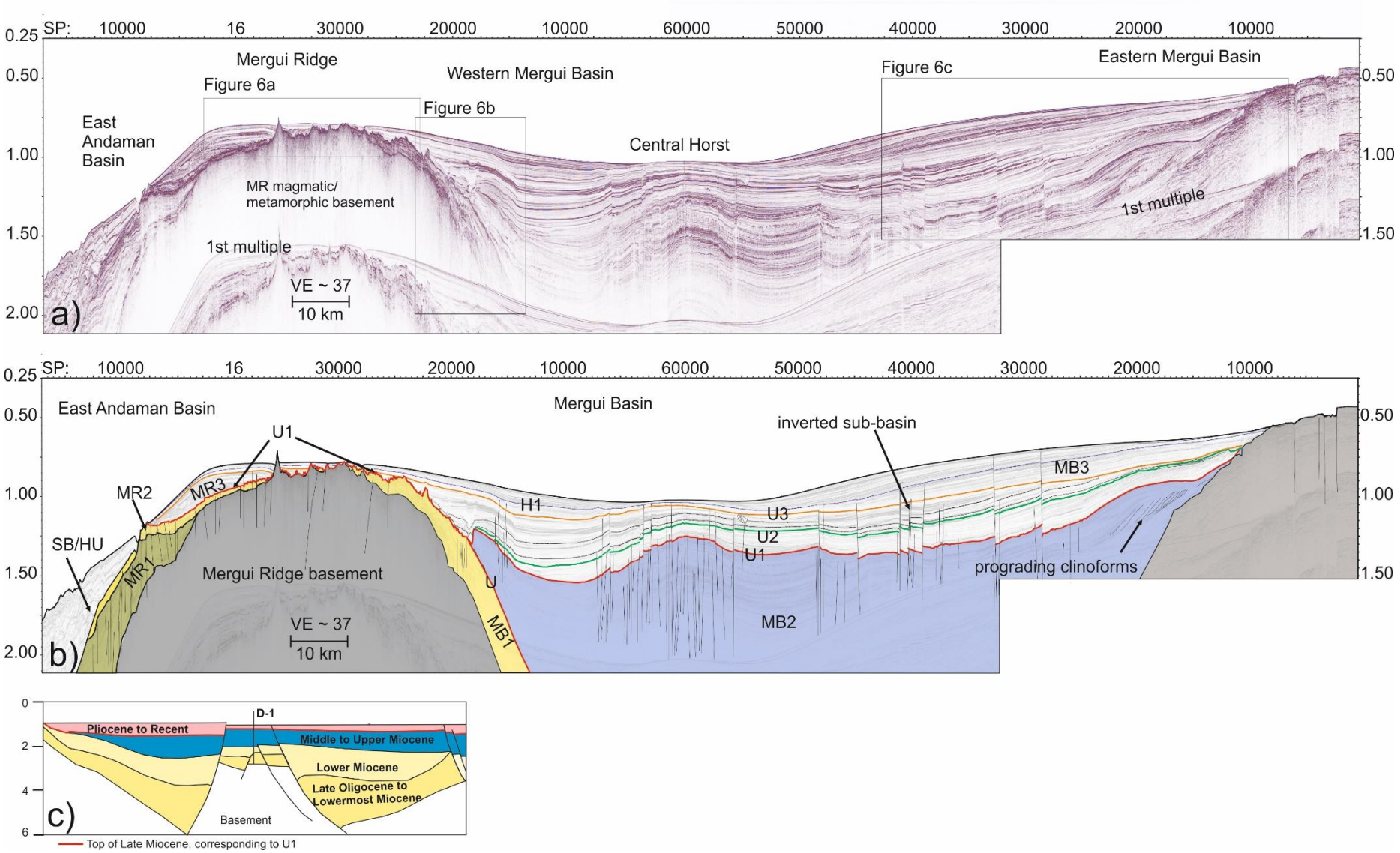
SP: 10000 16 30000 20000 10000 60000 50000 40000 30000 20000 10000
0.25
0.50
1.00
1.50
2.00
Mergui Ridge
Figure 6a
Western Mergui Basin
Figure 6b
Figure 6c
Eastern Mergui Basin
East Andaman Basin
Central Horst
MR magmatic/ metamorphic basement
1st multiple
1st multiple
VE ~ 37
10 km
a)
East Andaman Basin
Mergui Basin
U1
MR2
MR3
H1
inverted sub-basin
MB3
U3
U2
U1
SB/HU
MR1
Mergui Ridge basement
U
MB1
MB2
prograding clinoforms
VE ~ 37
10 km
b)
0
2
4
6
D-1
Pliocene to Recent
Middle to Upper Miocene
Lower Miocene
Late Oligocene to Lowermost Miocene
Basement
c)
Top of Late Miocene, corresponding to U1

Figure M1- 4: a) (previous page): high resolution 2D multichannel reflection seismic line across the Mergui Basin/Mergui Ridge area. See Figure M1-3a for location. b) Interpretation of the seismic profile. MB1: seismic unit representing the syn-rift sedimentary unit in the Mergui Basin; MB2: seismic unit representing the post rift sediments in the Mergui Basin. U1: unconformity indicating approximately the Late Miocene-Pliocene boundary. MB3: seismic unit representing the Plio-Pleistocene sediments. U2, U3: unconformities within the Plio-Pleistocene sequence, H1: continuous horizon in the uppermost part of the Plio-Pleistocene that can be traced all across the Mergui Basin to the western edge of Mergui Ridge; MR1: seismic unit representing old sediments onlapping onto the western flank of Mergui Ridge. MR3: seismic unit on the western flank of Mergui Ridge, contemporaneous/correlatable to MB1. MR3: seismic unit representing Plio-Pleistocene sediments at the western edge of Mergui Ridge. SB/HU: seismic unit representing drift deposits onlapping onto the Mergui Ridge in the East Andaman Basin. c) Interpreted profile modified from Morley and Racey (2010) for comparison. See Figure M1-3a for location.

MB1: Basin filling seismic unit onlapping on Mergui Ridge

MB1 is the lowermost seismic unit overlying the Mergui Ridge basement high (Figure M1-4). It is thinning towards the crest of Mergui Ridge, but it can be traced further eastward across the Mergui Ridge (Figure M1-6a). Seismic unit MB1 is characterized in the Mergui Ridge area by wavy high amplitude reflectors (Figure M1-6a) which form pronounced amplitude contrasts to the overlying seismic units. Amplitude strength generally decreases eastward towards the Mergui Basin (Figure M1-6b).

MB2: Seismic unit in the Mergui Basin

MB2 is overlying MB1 unconformably as indicated by onlapping of reflectors of MB2 onto the unit boundary in the deeper part of the Mergui Basin (Figure M1-6b) and gentler dip angles of reflectors of MB2 compared to MB1. MB1 and MB2 are separated by angular unconformity U (Figures M1-4, M1-5). Reflectors within this unit are of alternating high and low amplitude; they have a good continuity. The amplitudes generally increase towards a central horst area in the Mergui Basin (Figure M1-5). Several faults cut through this unit, especially in the central horst area. In the eastern Mergui Basin (Figure M1-4) prograding clinoforms can be identified within the upper part of MB2 (Figure M1-5, M1-6c). The top of MB2 is formed by U1, which is, a horizon separating high amplitude reflectors below from low amplitude reflectors above in central parts of the basin (Figure M1-4). Towards the eastern and western basin margins U1 is turning into an erosive unconformity (Figures M1- 4, M1-6). In the vicinity of the eastern flank of the Mergui Ridge MB2 is completely absent (Figure 6b). Here U1 forms the top of MB1 and U1 forms a pronounced erosive unconformity that is characterized by an irregular morphology, a high amplitude reflector and truncations of reflectors of seismic unit MB1. It may be traced be traced further eastward across the Mergui Ridge.

MB3: Uppermost seismic unit in Mergui Basin

MB3 is forming the topmost and youngest unit in the Mergui Basin area. It is unconformably overlying MB2 as indicated by reflectors onlapping onto U1 at the base of MB3 (Figures M1-4, M1-5 and M1-6b). Towards the Mergui Ridge it is unconformably overlying MB1 and reflectors of MB3 are onlapping on U1. MB3 reaches a maximum thickness of about 0.75 TWT in the Mergui Basin and thins out towards the Mergui Ridge. Internally MB3 is characterized by alternating packages of high and low continuous amplitude reflectors similar to MB2. Towards the central horst area within the Mergui Basin, amplitudes of MB2 are forming an amplitude contrast to the higher amplitude reflectors of MB2 below (Figure M1-5). Two unconformities within MB3 across the Mergui Basin have been identified (unconformities U2 and U3). They are indicated by reflector truncations towards the eastern basin margin (Figure M1-6c). Displacement at faults in seismic unit MB3 is observable, mainly in the lower part below U3, where an inverted sub-basin is present in the Eastern Mergui Basin. Horizon H1, interpreted in the topmost section of MB3 above U3 is one of several continuous reflectors that can be traced in the

entire basin. Towards the eastern basin margin at Mergui Ridge, it separates a lower low amplitude package from the uppermost package with higher amplitudes within the MB3 unit (Figure M1-6b).

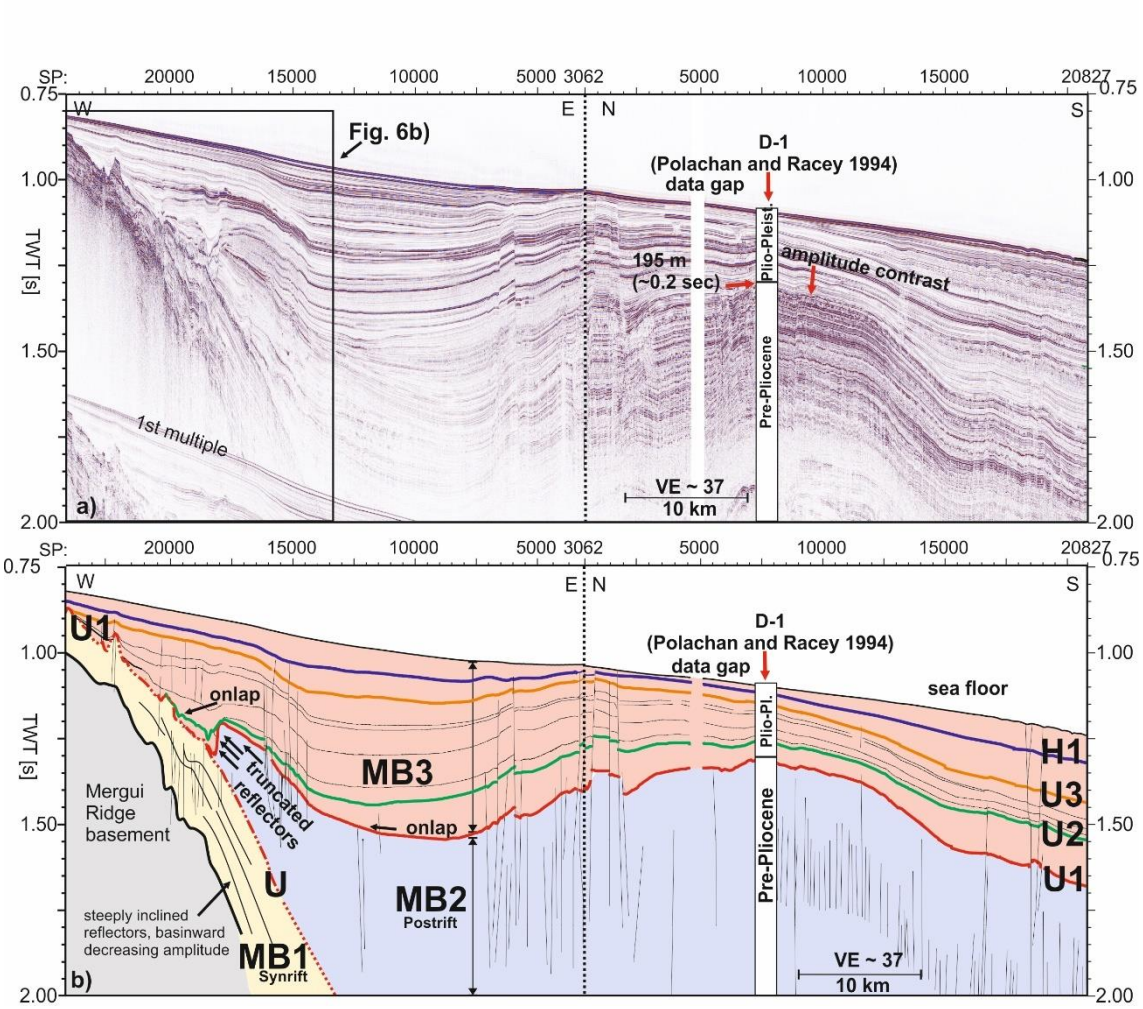

Figure M1- 5: a) 2D multichannel reflection seismic line in the Mergui Basin. D-1 borehole location with Plio-Pleistocene boundary (borehole from Polachan and Racey, 1994). See Figure M1-3a for location of profile and D-1 well. b) Interpretation of seismic units MB1, MB2 and MB3 with correlation of unconformity U3 to the D-1 well, indicating that U3 represents approximately the Late-Miocene /Pliocene boundary.

5.3.2. Seismic units at the western edge of Mergui Ridge

Seismic units at western edge of Mergui Ridge have been interpreted previously by Schwab et al. (2012). In this study the naming of seismic units, MR1, MR2, MR3, SB1/2 and HU introduced by Schwab et al. (2012) is followed (Figure 1-4), focusing on the morphology of sedimentary units that are influenced by bottom current activity in the southern part of the working area: I) Seismic unit MR2, comprising sediments outcropping at the edge of Mergui Ridge, overlying an older unit onlapping onto the Mergui Ridge (MR1); II) Carbonate platforms (here named P1, P2 and P3) on top of Mergui Ridge; III) Seismic unit MR3, consisting of a mounded body of younger sediment that is covering parts of Mergui Ridge and VI) Seismic units HU and SB1/2, the uppermost seismic unit(s) in the East Andaman Basin (Figure 1-4).

MR2: Outcropping high amplitude unit

Seismic unit MR2 can be identified at the western edge of Mergui Ridge (Figures M1-4, M1-6a). It is unconformably overlying the basement and older marine strata of seismic unit MR1 that are forming the western flank of the Mergui Ridge (Figure M1-7). It is internally characterized by parallel to subparallel high amplitude reflectors, which are discontinuous and/or wavy in places (Figures M1-6a, M1-7).

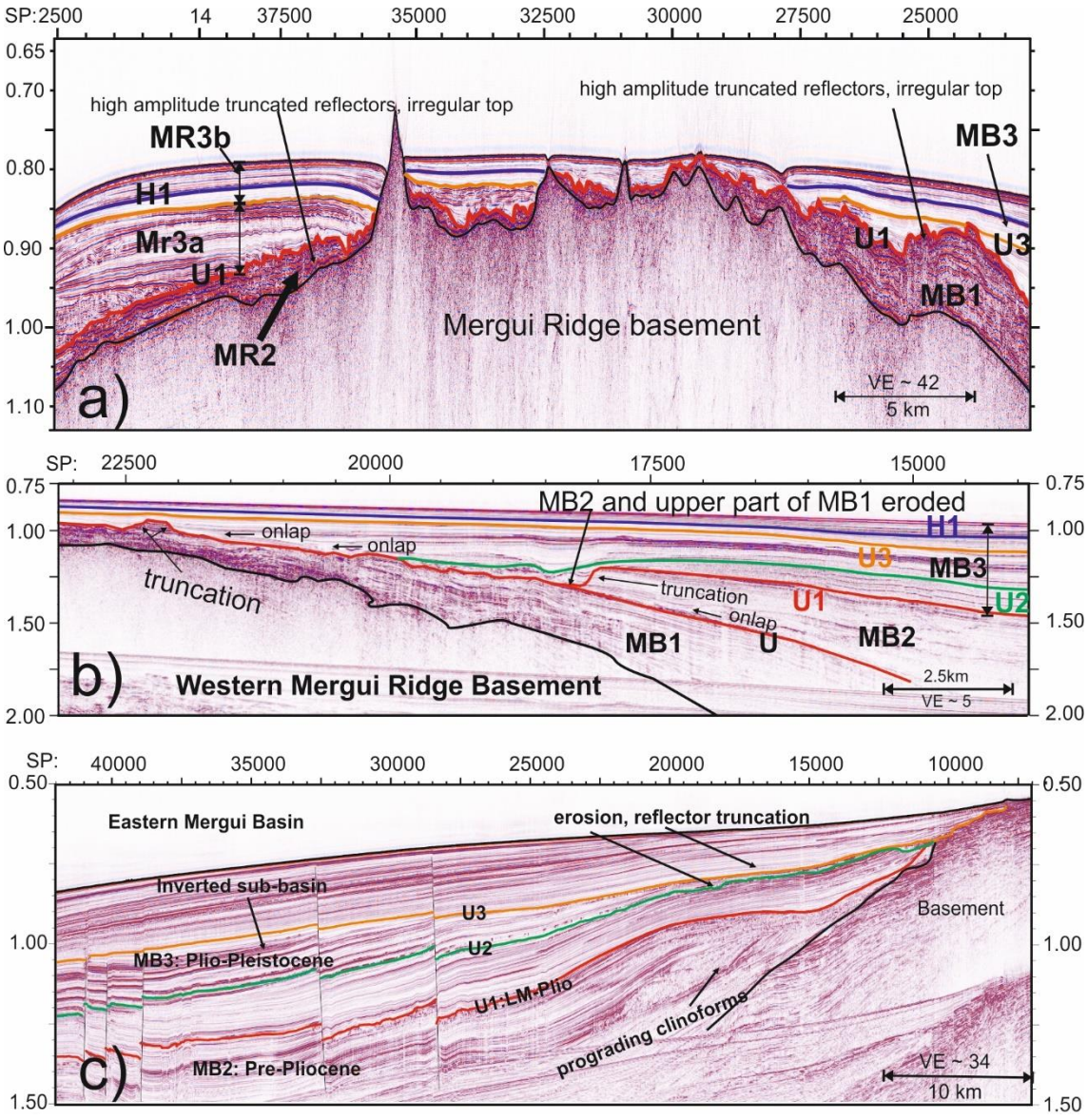

Figure M1- 6: Enlargement of parts of seismic line MASS02/04 running across the Mergui Basin. See Figure M1-4 for locations. a) Top of Mergui Ridge, showing very similar internal characteristic of seismic units MB1 and MR2, as well as continuity of unconformities U1, U3 and horizon H1 across the Mergui Ridge. b) Eastern flank of the Mergui Ridge. c) Eastern part of the Mergui Basin, showing configuration of unconformities towards the east as well as prograding clinoforms in the top part of seismic unit MB2, close to the Late Miocene-Pliocene boundary (U3). LM-Plio: Late Miocene-Pliocene boundary.

Reflection strength is decreasing towards the East Andaman Basin. The top of MR2 is formed by the erosive unconformity U1. Unconformity U1 marks the top of seismic unit MB2 in the Mergui Basin east of the Mergui Ridge and of seismic unit MB1 at the eastern flank of the Mergui Ridge. U1 is characterized by an irregular topography and truncation of reflectors in places, as well as a sharp amplitude contrast to the overlying sediments on

the western side of the Mergui Ridge (Figure M1-6a). In our data set the westward limit of MR2 is the shelf break edge of Mergui Ridge. Here MR2 is outcropping in places (Figure M1-8) and reflectors are truncated, indicating erosion of parts of this unit that originally may have extended beyond the recent shelf edge.

MR3: Mounded body on top of Mergui Ridge

The topmost seismic unit at the western side of the Mergui Ridge is MR3, which is unconformably overlying MR2 on the crest of the Mergui Ridge. Seismic units MR2 and MR3 are separated by unconformity U1 (Figure M1-7). MR3 comprises an overall wedge-shaped geometry. The crest of this wedge is running approximately parallel to the edge of Mergui Ridge. Towards the west, MR3 tapers out. MR3 has a maximum thickness of about 190m (assuming a sound velocity of 1500m/s). Two subunits within MR3 separated by U3, which is an angular unconformity in the eastern part of the Mergui Basin can be discerned (Figure M1-7). The lower seismic subunit (MR3a) comprises local unconformities, filled channels and an irregular body with chaotic internal reflections that can be traced across all profiles (Figure M1-6). This irregular body has been previously interpreted as a mass wasting deposit by Schwab et al. (2012). The upper subunit MR3b is draping MR3a and contains continuous reflectors that increase in amplitude towards the sea floor. This unit is the seaward continuation of the upper part of unit MB3 above unconformity U3 in the Mergui Basin, as Horizon H1 and unconformity U3 can be traced through the Mergui Basin to the edge of Mergui Ridge, indicating the widespread occurrence of the youngest sedimentary units in the wider Mergui Basin/Ridge area (Figure M1-4, M1-6a).

HU and SB1/2: Sediments in the EAB:

Sediments of the western part of the East Andaman Basin are onlapping onto the slope of the Mergui Ridge, namely onto seismic unit MR1 (Figure M1-9). The lower unit (SB1) comprises internally chaotic/disturbed reflector packages, which have been interpreted as mass transport by Schwab et al. (2012). In contrast, upper seismic units (SB2 and HU) are draping over these disturbed sediments and exhibit an internal reflector configuration with continuous low amplitude reflectors (Figure M1-9).

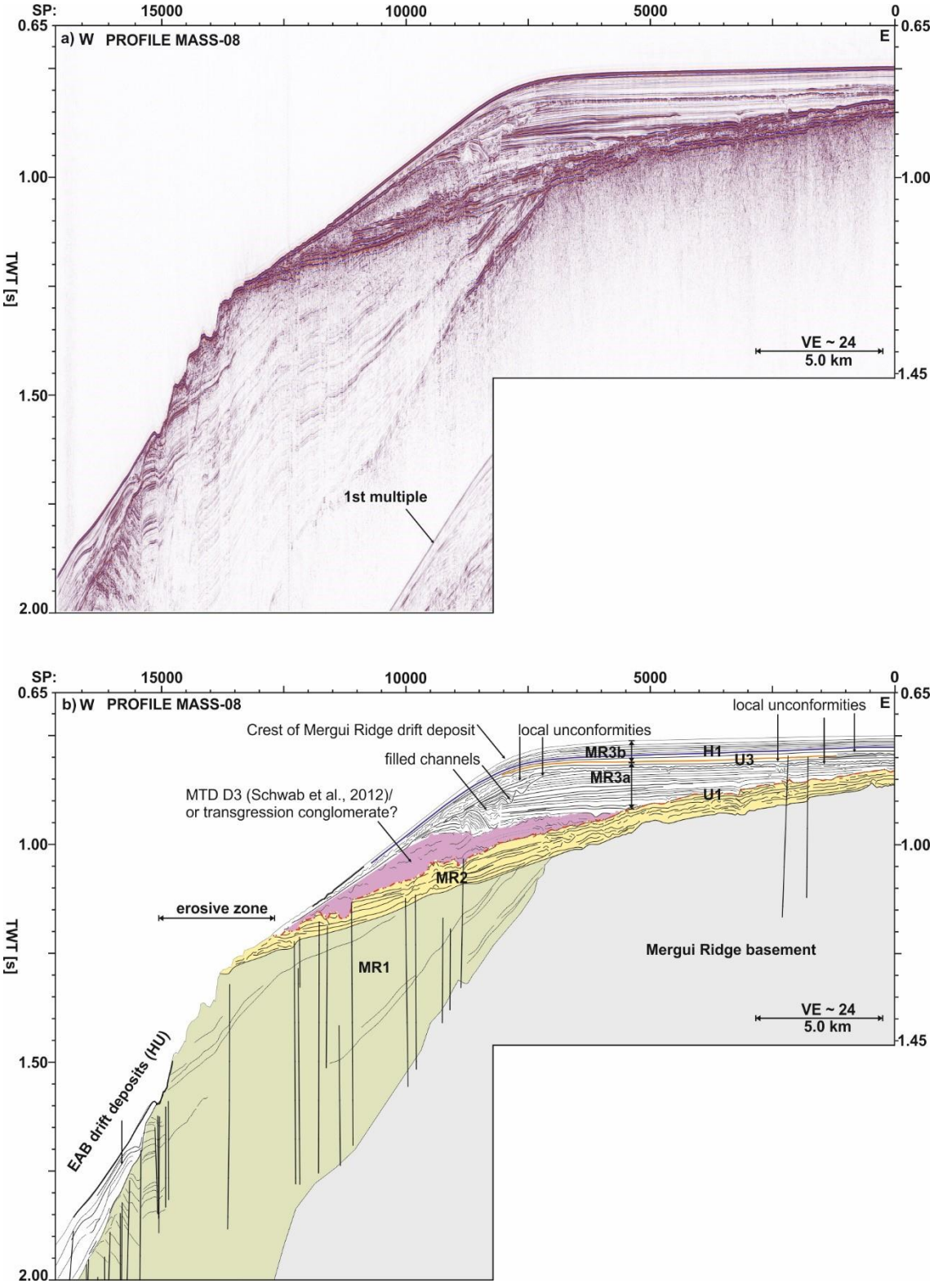

Figure M1- 7: a) High resolution 2D multichannel reflection seismic line from the Mergui Ridge-East Andaman Basin transition. See Figure M1-3a for location. b) Interpretation of the profile, showing the characteristics of seismic sub units MR3a and MR3b. MR3a is characterized by presence of a deposit (MTD D3) interpreted as landslide deposit by Schwab et al., (2012) but the deposit may also represent potentially a transgression conglomerate according to this study. Filled channels and local unconformities indicate erosion due to small scale sea level fluctuations during initial phase of subsidence of the Mergui Ridge. MR3b is draping MR3a.

Carbonate Platforms

Three E-W elongated platforms have been identified in the working area, P1, P2 and P3 (Figures M1-8, M1-10). They show (sub-)oval outlines and comprise areas between 5.5 and 17km^3. They are elevated up to 150m above the seafloor, and are not covered by stratified sediments. The platforms are characterized by flat tops, steep flanks, and a step-like incision around the tops. P1 also comprises round incisions at its top (Figure M1-8). The seismic data do not image any internal reflectors of the platforms. A sedimentary apron imaged as a zone of chaotic seismic facies is found in some areas around the platforms (Figure M1-8). The apron sediments seem to interlock with Unit MR2.

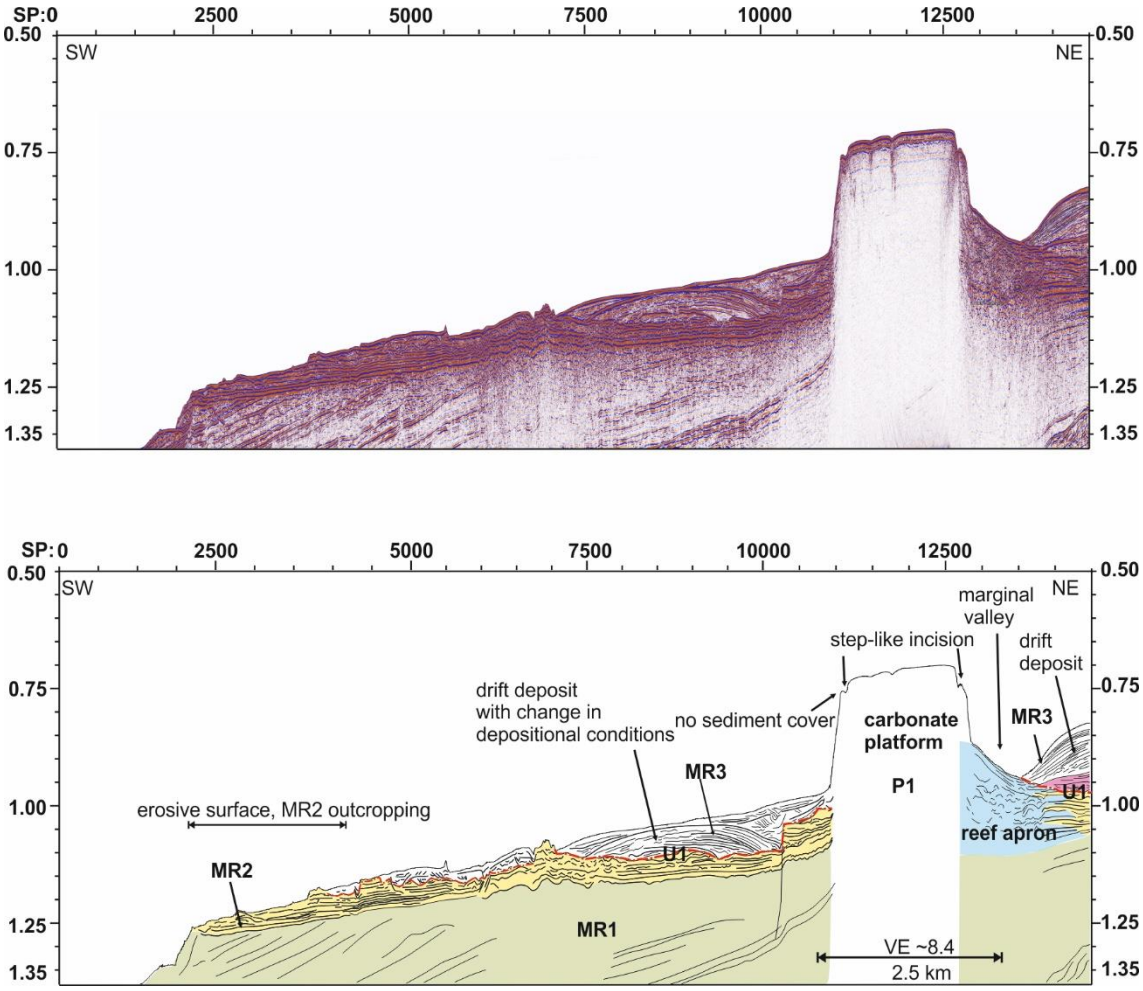

Figure M1- 8: a) High resolution 2D multichannel reflection seismic line from the top of Mergui Ridge. See Figure M1-3a for location. b) Interpretation of the profile indicating the presence of an erosive surface at the western flat top of the Mergui Ridge as well as a moat near carbonate platform P1 in the NE, and the presence of drift deposits, all indicative of the presence of bottom currents. P1 is characterized by previous subaerial erosion, as visible from the step like incision around its top. Interfingering of the reef apron with MR2 depositis may indicate platform erosion contemporaneous with deposition of MR2.

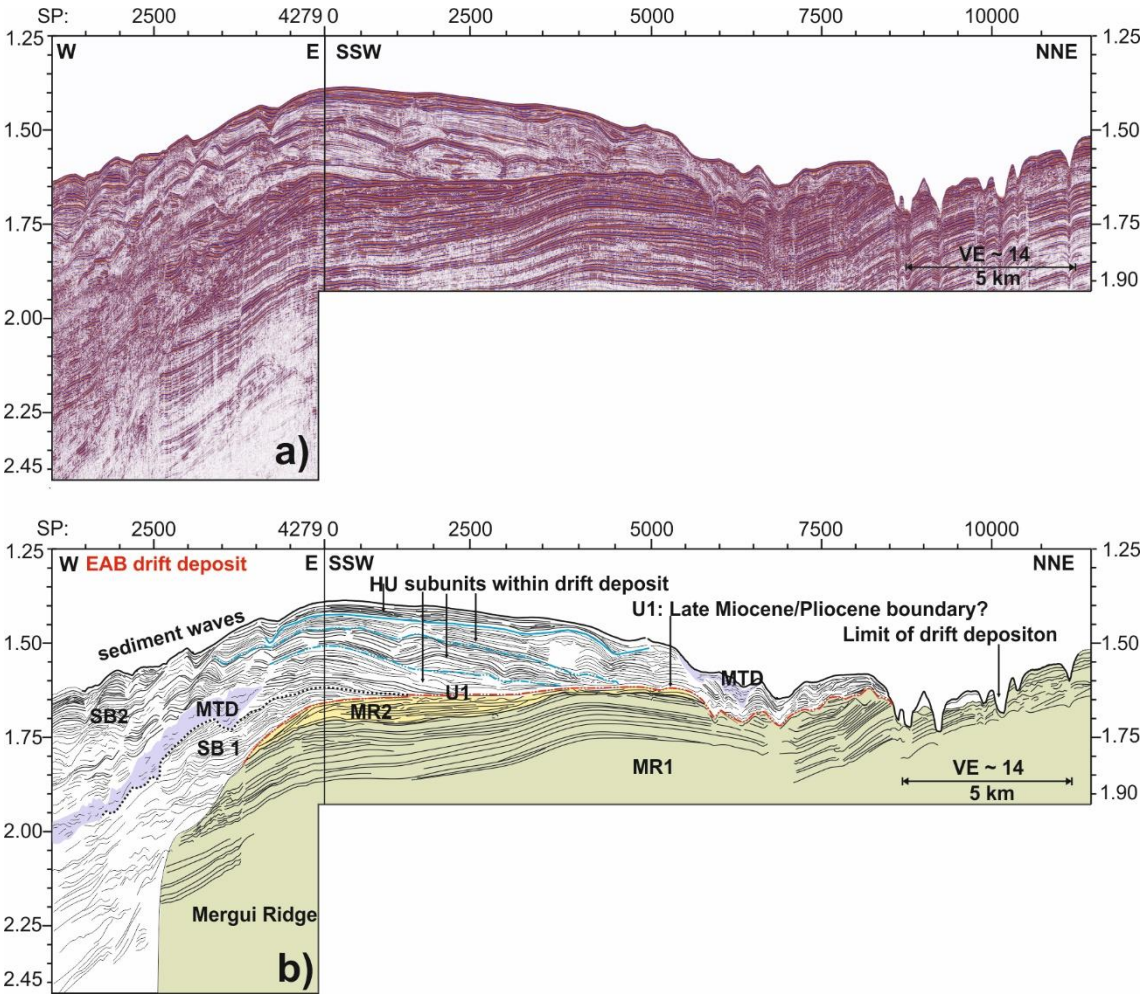

Figure M1- 9: a) High resolution 2D multichannel reflection seismic line depicting drift deposit in the East Andaman Basin onlapping onto the Mergui Ridge above unconformity U3. See Figure M1-3a for location. b) Interpretation of Profile. Interpretation of seismic units SB1, SB2 and HU as well as location of MTD (mass transport deposits) within drift deposit from Schwab et al. (2012).

5.3.3. Surface Morphology and features indicative of bottom current activity

The youngest units in the outer shelf/slope area of the western edge of the Mergui Ridge are shaped by bottom currents (see also Schwab et al., 2012). From the backscatter/multibeam data set three distinct areas (Area a, b and c, Figure M1-10) were defined based on their differing backscatter strengths and surface morphologies. They correspond to the outcropping/surfaces of the seismic units MR2, MR3, SU2/HU as defined in the previous section. Joint interpretation of seismic and multibeam bathymetry/backscatter data revealed the following units to be influenced by bottom currents (Figure M1-10): I) Drift deposits on top of the Mergui Ridge, corresponding to Unit MR3 in the subsurface; II) Moats, channels and an erosive terrace at the edge of the ridge (Corresponding to seismic unit MR2 in the subsurface); III) Bottom current-induced erosive features around the carbonate platforms that act as obstacles to the flow; VI) Drift deposits onlapping on the Mergui Ridge edge/slope from the west.

Area a: Drift deposits and erosion around platforms on top of Mergui Ridge

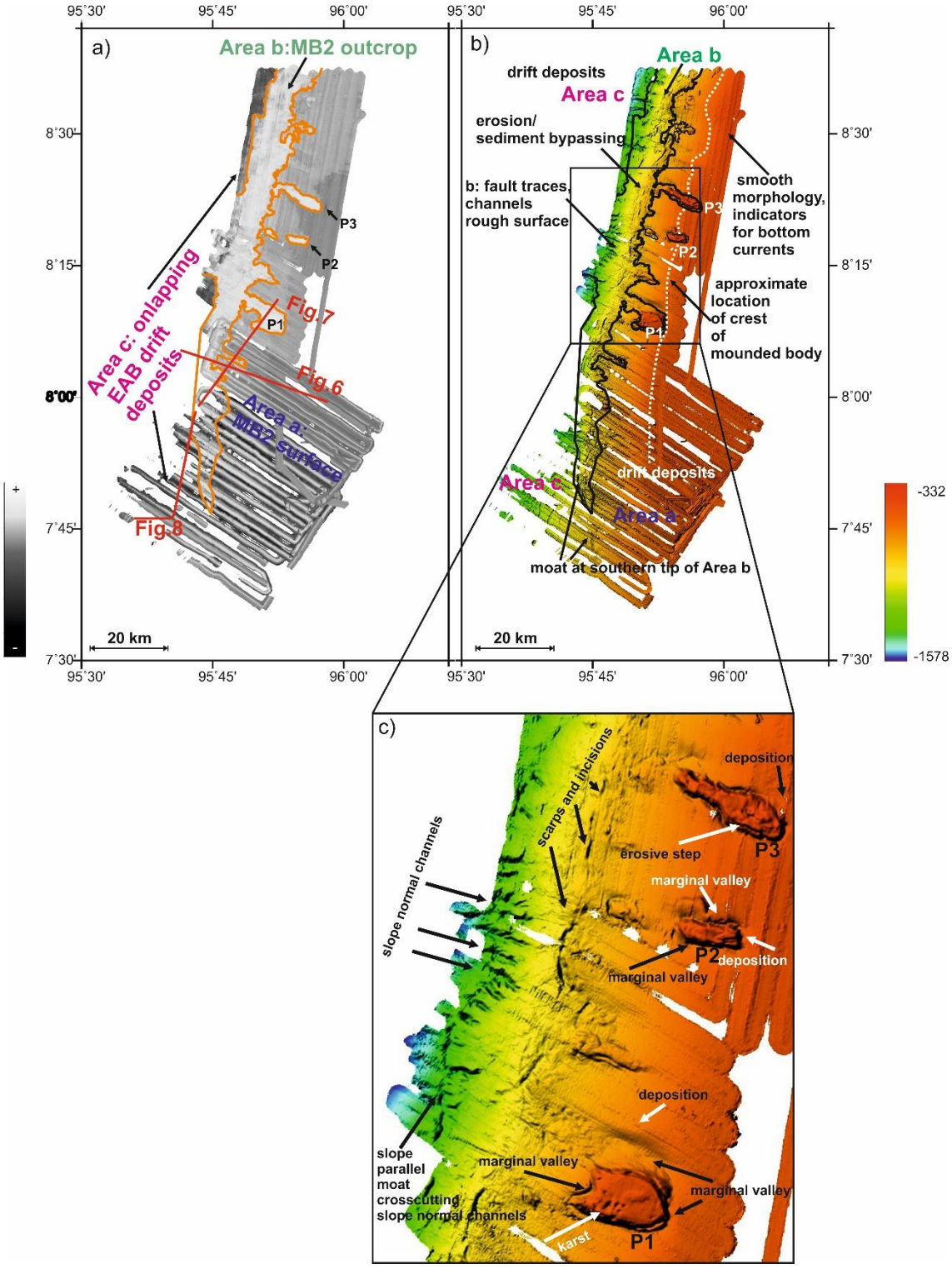

Figure M1- 10: a) Backscatter data from working area, indicating three main zones of differing backscatter strengths, striking approximately slope parallel: Area a of moderate backscatter values represents the surface of seismic unit MR3; Area b with highest backscatter values, represens outcropping surface of seismic unit MR2. Area c with lowest values represents slope area where drift deposits/seismic units SB2 and HU are onlapping onto the Mergui Ridge. b) Multibeam bathymetry, showing that the areas a, b and c differ in morphology as well. Area a is mostly smooth, whereas Area b is characterized by rugged morphology with scarps and incisions. c) Enlargement of the bathymetry showing features indicative of bottom current. Bathymetry (grid resolution 50m), originally published by Jintasaeranee et al. (2012).

This area comprises the zone where the Plio-Pleistocene to recent sediments of the seismic units MR3 are covering the Mergui Ridge. It is of moderate backscatter values (Figure M1-10a). Its western boundary was defined where the MR3 sediments are tapering out (~ 800-850m water depth). The surface of this area is generally smooth and has an overall mounded shape. The crest of the mounded body is located upward of the shelf edge at a water depth of 530-560m. The three carbonate platforms P1-P3 are aligned approximately along the western boundary of Area a. Moats have formed around the platforms (Figure M1-10b). These moats can be found all around the platforms except for their northeastern edges of P2 and P3 where sediments of unit MR3 are deposited against the platforms (Figure M1-10c). West of the platforms sediments of unit MR3 are absent or thin (Figure M1-8). Especially platform P1 exhibits a broad marginal valley (60m deep and 2.6 km wide) at its northern flank (Figure M1-8, M1-10), aligned in ESE-WNW direction. North of this moat drift sediments have been deposited (Figure M1-8).

Area b: Erosive surface, slope channels and moats

Area b is characterized by high backscatter values (Figure M1-10a), and comprises the area where older sediments of seismic unit MB2 are outcropping to the seafloor. This zone is located at the edge of Mergui Ridge and extends downward from approximately 850m to a depth of about 1300m. Area b comprises a slope parallel moat at its southern tip. This moat separates sediments from seismic unit MR3 and the seafloor deposits in the EAB (seismic unit HU; Figure M1-9b). Area b widens northward to an approximately 10km broad zone that comprises parts of the flat top of Mergui Ridge, and forms a terrace west of the mounded body of Area a/MB3a (Figure M1-8). Area b comprises also parts of the slope area toward the East Andaman BasinArea b is characterized by a rugged morphology, with numerous elongated incisions and steep scarps, roughly orientated in NNE-SSW direction (Figure M1-10c). In the west of Area b the slope is characterized by the occurrence of several subsequent slope normal channels (Figures M1-10b, c). They start all in a similar water depth and none of the canyon heads extends upslope above the -1085m depth contour. These channels have similar depths (~100-120m) and widths (~ 1km). The bathymetric dataset is limited towards the west. Hence, the downslope extent of the channels cannot be identified. However, they probably do not extent downslope further, as no channels extending further downslope could be identified in the seismic dataset reaching to larger water depths. In the southern part of the working area, a slope parallel moat is present, running alongslope at approximately 1300m water depth (Figure M1-10c). It has a depth of about 70m and an approximate width of 500m. It crosscuts the slope normal channels.

Area c: Drift deposits in the East Andaman Basin (Western slope of Mergui Ridge)

Area c is located west and downslope of Area b. It is characterized by low backscatter values (Figure M1-10a). The boundary between Area a and b is distinct. Multibeam data in this area is restricted but the seismic data (Figure M1-9) image a sedimentary body (SB2 and HU) of about 300m (at sound velocity of 1500m/s) maximum thickness that is onlapping against the Mergui Ridge. This body is characterized by the occurrence of sediment waves and generally low amplitude reflectors separated by single reflectors of higher amplitude

5.3.4. Current patterns

Figure M1-11 shows the overall current patterns for the Andaman Sea deduced from the ECCO2 dataset in 750m water depth. The ECCO2 data show, that current velocities are variable throughout the year, and that the strength and direction of currents changes with the seasons. In both peak monsoon months (Figure M1-12a, c) and in April (Figure M1-11b) a larger scale gyre is present in the northern and central part of the Andaman Sea. In October, several smaller scale gyres are present in the Andaman Sea. For both peak monsoon months (February and July) a current is entering the Andaman Sea through the Great Channel north of Sumatra (see Figure M1-2 for location), flowing along the slope of the Mergui Basin and then around the southern tip of Mergui Ridge along the Mergui slope in northward direction. Here it enters a large scale cyclonic gyre present in the central part of the Andaman Sea. Current velocities around the southern tip of Mergui Ridge are highest in the peak monsoon months (up to 8cm/s in February). For the inter monsoon months the current patterns are reversed, and current speeds are generally slower. The large scale gyre has an anticyclonic direction and water is flowing out of the Great Channel. In the inter monsoon month October several eddies with very low current speed develop. The ECCO2 data suggest a very weak southward flow along the Mergui Ridge. For the inter-monsoon months currents near the Mergui Ridge seem to be weak or absent.

Figure M1-12a shows current velocities at the Mergui Shelf slope along the “INDOPAC” profile (see Figure M1-3a for location) running from west to east from the East Andaman Basin to the Mergui Ridge for the peak monsoon month February (NE monsoon). Figure M1-12b shows the meridional current velocity component “vvel” giving an impression of the current direction along the Mergui Ridge. An overall northward directed current with mean current speeds of more than 8cm/s is present in water depths between about 300m and 800 m. Further downslope, below approximately 1000m water depth, a second counter current along the shelf margin is present, but with lower mean current speeds of around 4 cm/s maximum. The panels of Figure M1-12c and Figure M1-12d are showing current speed and vvel for the inter monsoon month April. Currents near the Mergui Ridge are absent or weaker as indicated by lower current speeds of approximately 0.25cm/s. Moreover, the overall current direction is reversed compared to the peak monsoon month during April, when the upper part of the slope is influenced by an overall southward directed current and the lower part by a northward directed current.

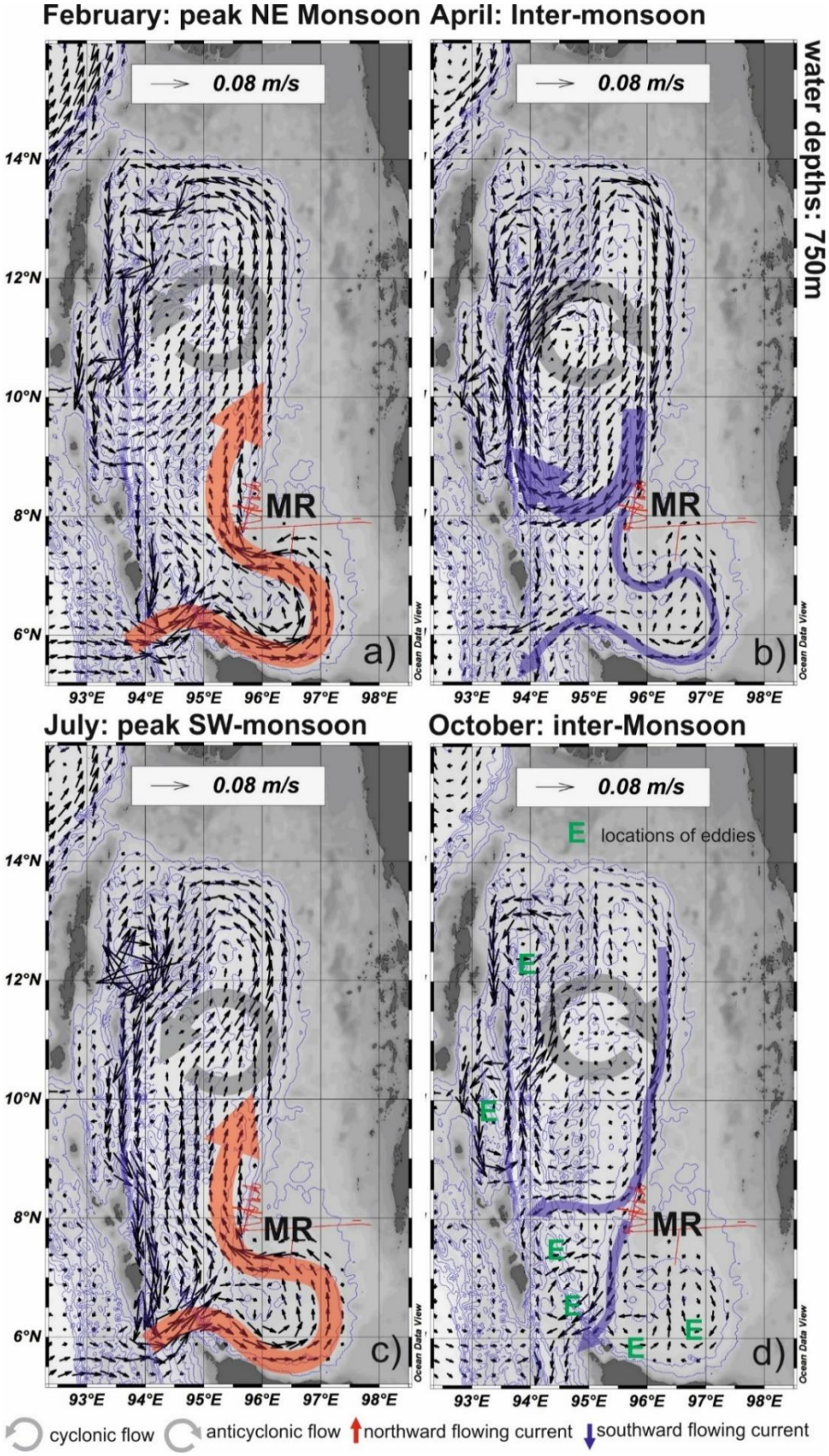

Figure M1- 11: a-d) Current patterns in the Andaman Sea during peak monsoon months February and July as well as the inter monsoon months April and October. Current velocity data re from the ECCO2 data model (Menemenlis et al. (2008); available at http://ecco2.jpl.nasa.gov/). MR: Mergui Ridge.

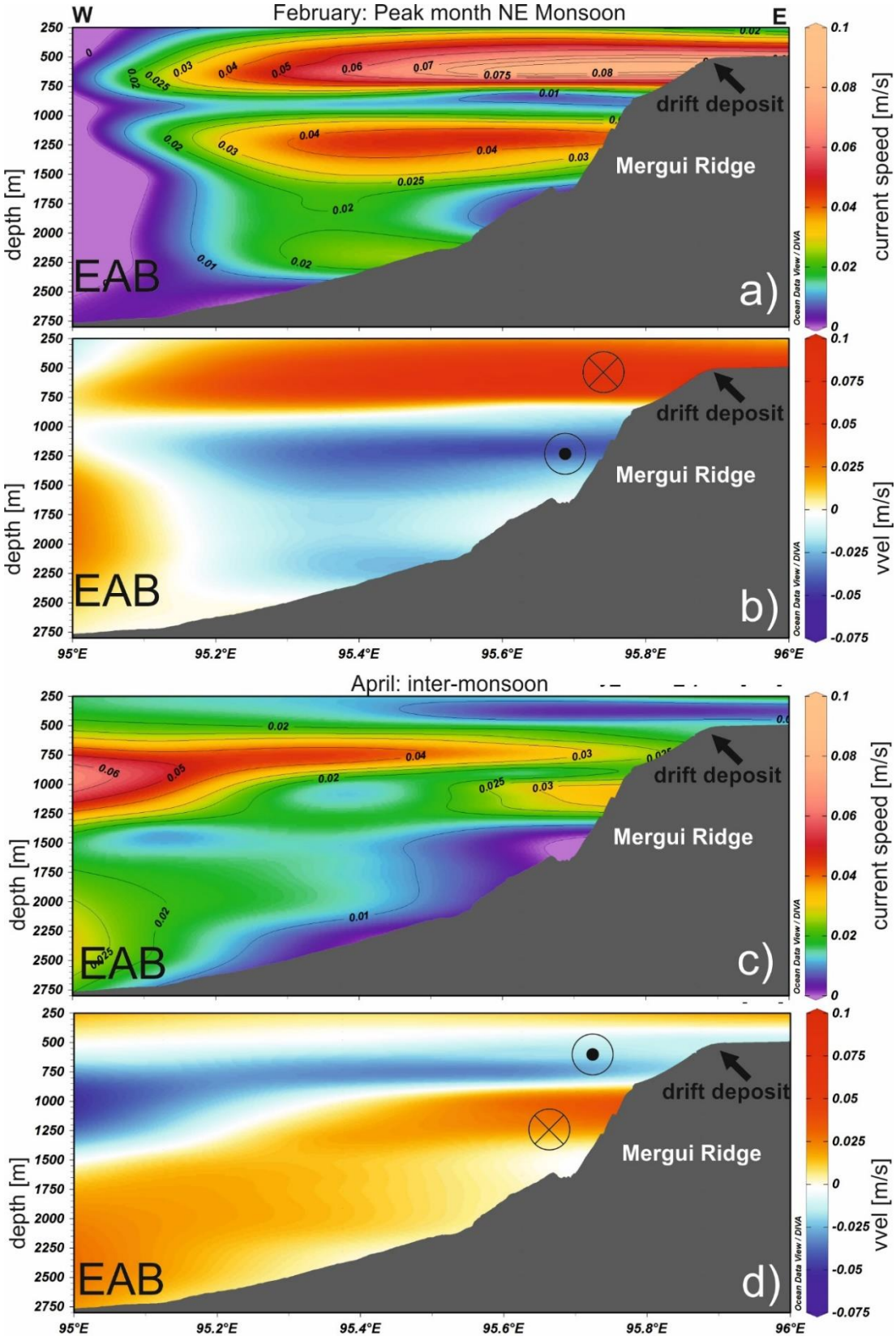

Figure M1- 12: a), b) Current velocities and meridional velocity (vvel) patterns at the western flank of the Mergui Ridge/in the EAB (East Andaman Basin) across the "INDOPAC" profile (see Figure M1-3 for location). The data for peak NE monsoon month February show a northward current at the edge of Mergui Ridge with maximum current velocity of 8cm/s and a counter current in deeper parts of the Basin. c), d) Current velocities and meridional velocity (vvel) patterns for inter-monsoon month April, showing lower current speeds and reversal of current directions. Bathymetry derived from reflection seismic line of INDOPAC 11 (NCEI, seismic line available at www.ngdc.noaa.gov)

5.4. Discussion

5.4.1. Age correlation of seismic units

Stratigraphic placement of units has been obtained by the comparison of our data to previous studies (Polachan and Racey, 1994; Morley and Racey, 2010; Racey, 2010; Morley, 2015) and by correlation of seismic data to the Miocene-Pliocene boundary in borehole data (Polachan and Racey, 1994). The D-1 well is located at a water depth of 809 m (Racey, 2010). The D-1 well contains a Plio-Pleistocene unit of about 200m thickness. This corresponds to ~0.2ms TWT at a sound velocity of 2000m/s, which is the approximate sound velocity in the upper subsurface layers within the Mergui Basin (Curray, 2005). Approximately 200m below the seafloor, the change of amplitudes from high amplitudes below within MB2 to low amplitudes above within MB3 was interpreted as the Miocene-Pliocene boundary, corresponding to unconformity U1 (Figure M1-5). U1 is the boundary between MB2 and MB3 in the Mergui Basin. Morley and Racey (2010) (Figure M1-4c) delineate the Late Miocene – Pliocene boundary between the D1 well and the Mergui Ridge between ~ 1s and 1.6s TWT total two way travel time which is in good agreement with our data. This implies that the upper part of MB2 is of Late Miocene age, and MB3 is of Plio-Pleistocene age.

5.4.2. Interpretation of seismic units in the Mergui Basin

Seismic unit MB1 predates MB2 and its steeper dip angles compared to MB2 and MB3 indicate a change in tectonic development after deposition of MB1. Proximal to the Mergui Ridge, seismic unit MB1 is overlain by seismic unit MB3 and MB2 is absent. The high amplitude of the reflectors near the crest of the Mergui Basin within MB1 and the basinward decrease in amplitude strengths may indicate a basinward transition from fluviatile/shallow marine to deeper marine depositional conditions, as it is described for the syn-rift Ranong Fm (fluviatile/shallow marine) and Yala Fm of Upper-Oligocene to early Lower Miocene age (Polachan and Racey, 1994). MB1 may be part of this syn-rift section, as previous studies describe the syn-rift section in the Mergui Basin to onlap against the Mergui Ridge in similar depth as MB1 does in in our seismic data set (Polachan and Racey 1994; Morley, 2015). Towards and on top of the Mergui Ridge only the oldest part of the syn-rift section may be present, as the younger part may have been eroded towards Mergui Ridge, indicated by erosive unconformity U1 at the top of MB1 proximal to the Mergui Ridge.

The upper boundary of MB2 is formed by the Late Miocene-Pliocene boundary marked by unconformity U1. The reflector configuration of alternating high and low amplitudes within MB2 indicates deposition in a marine environment as it has been described for the Late Miocene Thalang Formation (Polachan and Racey 1994). In the eastern Mergui Basin close to the unconformity U1, prograding clinoforms have been identified. (Figures M1-4, M1-6c). Such clinoforms are also described in Morley (2015) to be present in Late Miocene sediments in the eastern Mergui Basin margin. An uplift event during Late Miocene has been described by various authors (e.g. Andreason et al. 1997; Morley,

2015). Close to the western limit of the Mergui Ridge, Morley (2015) describes an erosive unconformity at about 1 s TWT total depth attributed to uplift during Late Miocene, which matches approximately the depth of U1. As U1 has been traced across the Mergui Ridge to its western edge, it hence may also approximately represent the Late Miocene-Pliocene transition in the Mergui Ridge area. During this uplift event, erosion of seismic unit MB2 and also MB1 near the eastern edge of Mergui Ridge may have taken place. Seismic unit MB2 hence represents sediments of the Miocene but its lower limit cannot be determined from the data set.

The internal reflector characteristics of MB3 indicate deposition in a marine environment, as it has been described for the Plio-Pleistocene Takua Pa Fm (Polachan and Racey, 1994). Reflectors in this section are largely continuous across the Mergui Basin, representing continuous sedimentation in the basin because it may have been established during/since large scale subsidence of the basin area after the Late Miocene uplift (Morley, 2015; Andreason et al., 1997). Unconformities U2 and U3 and the displacements at faults and an inverted sub-basin are present in the Plio-Pleistocene section (Figure M1-4, M1-6c). These features may have been created by smaller scale compressional events that took place during the Pliocene, either due to establishment of the modern spreading center in the EAB (Curray,2005) or due to more far field effects of the Australia Asia collision since the middle Miocene to recent (Doust and Sumner, 2007). Only minor tectonic deformation seems to have taken place above U3.

In summary, seismic unit MB1 in the Mergui Basin area represents the syn-rift section probably corresponding to the Late Oligocene - Early Miocene Ranong Fm towards the crest of Mergui Ridge and the Yala Fm toward the basin. In the Mergui Ridge area this unit was partly eroded together with seismic unit MB2, which disappears completely toward the Mergui Ridge. This erosion is possibly due to an uplift phase in the Late Miocene, marked by the presence of unconformity U1. Seismic units MB2 and MB3 correspond to overlying post-rift sediments, where MB2 represents Late Miocene (Thalang Fm) and older sediments, and MB3 represents Plio-Pleistocene (Takua Pa Fm) sediments. At the basin-ridge transition, where MB2 is eroded completely, the Plio-Pleistocene unit MB3 is deposited directly above the syn-rift sediments of unit MB1. The lower boundary of MB3 is unconformity U1, which approximately marks the Late Miocene-Pliocene boundary in the Mergui Basin. In the Mergui Ridge area it may represent subaerial exposure with severe erosion of MB2 and MB1. Afterward, unit MB3 has been deposited during relative sea level rise/high stand due to subsidence in the Pliocene.

5.4.3. Interpretation of seismic units of Mergui Ridge:

Unconformity U1 is continuous towards the west of Mergui Ridge, where it forms the base of MR3 (Figure M1-6a, M1-7). Consequently, the irregular topography and truncation of reflectors below U1 indicate subaerial exposure and erosion of the Mergui Ridge at approximately the Late Miocene-Pliocene boundary or later as well. Hence, sediments below this unconformity (seismic unit MR2 at the western edge of Mergui Ridge and seismic unit MB1 at the eastern edge of Mergui Ridge) are older than Late Miocene age. The high amplitude of reflectors and also the observation of pebble sized material in sediment samples of the outer margin (SEATAR 1976 database, Figure M1-3), where MR2 is exposed to the sea floor, may indicate that MR2 consists of fluviatile/shallow marine deposits. As they exhibit internal characteristics similar to the upper part of MB1 in

the Mergui Basin, they may have been deposited contemporaneously to the syn-rift unit in the Mergui Basin. Additionally, Jinasaeranee et al. 2012 suggested that the platforms observed in the working area are carbonate platforms. These platforms are old structures. This is indicated by the flat top and step like incisions that suggest subaerial exposure. Round incisions in carbonates indicate karst dissolution that occurs under subaerial exposure or under influence of freshwater (Betzler et al. 2011 and references therein). The interlocking of eroded material from the platforms with sediment of seismic unit MR2 (Figure M1-8) may indicate that platform erosion took place contemporaneously with the deposition of of MR2. The carbonate platforms then may correspond to carbonates that, accordingly to Srisuriyon and Morely (2014), are present on structural highs, pass laterally in deposits of the Ranong Fm and are older than carbonates in the Mergui Basin area. Moreover, Andreason et al. (1997) describe deposition of carbonates on highs prior to rifting in the Mergui Basin area and intense subaerial exposure of reefs during a sea level lowstand at 10.5Ma.

The upper part of seismic unit MR3, subunit MR3a is continuous to the uppermost undisturbed part of the MB3 Plio-Pleistocene seismic unit in the Mergui Basin, which overlies unconformity U3. The lower subunit MR3a may accordingly have been deposited during early Pliocene to the latest Plio-Pleistocene and correspond in age to seismic unit MB3 in the Mergui Basin. Andreason et al. (1997) describe that the Mergui Ridge was subaerially exposed repeatedly prior to the Late Miocene, which is in line with the formation of unconformity U1. Afterward, rapid subsidence of the Mergui Ridge started, especially since 4 Ma, when the opening at the modern spreading center in the Central Andaman Sea started (Curray, 2005). Accordingly, seismic unit MR1a may then represent sediments deposited during a transgression in response to subsidence of the Mergui Ridge. This is indicated by local unconformities within seismic unit MR1a and the presence of filled channels structure in this unit reflecting sea level variations and erosion during initial subsidence (Figure M1-7). Sea level variations may be also have been caused during the minor compressional events that are documented by the presence of the unconformities U2 and U3 within the Plio-Pleistocene as well as within the contemporaneous seismic unit MB3 in the Mergui Basin. Seismic unit MR3b is draping unit MR3a and possibly they reflect undisturbed sedimentation when the Mergui Ridge had subsided well below sea level.

Morley (2015) describes a seismic profile across the Mergui Ridge about 80km north of the survey area, where he interprets a succession of low stand systems tract, transgressive systems tracts and high stand systems tracts for the Middle Miocene to Recent shelf edge sediments. Assuming that the subsidence history is similar, the sediments of seismic unit MR3 reflect a similar development. A sedimentary body with chaotic internal reflector structure has been interpreted as a mass transport deposit within seismic unit MR3a (Schwab et al., 2012) and a similar body has been observed by Morley (2015) north of our working area at the shelf edge. In this context, these bodies may be interpreted as transgression conglomerates deposited during initial subsidence of the ridge. The presence of relict sands and relict foraminifera and coarse grained sediments in the area of Mergui Ridge/Mergui Shelf (Rodolfo, 1969; Ramaswamy et al.; 2004) may also reflect the former shallow water situation of Mergui Ridge, prior to subsidence. The age of the sediments onlapping from the East Andaman Basin onto the western flank of Mergui Ridge (seismic units SB1 and HU) are generally difficult to estimate as there is a break in sedimentation at the edge of the Mergui Ridge (represented by Area b). Nevertheless, Figure M1-9 shows that the upper part of seismic units SB2/HU is onlapping onto seismic unit MR2 and unconformity U1, indicating a deposition after the end of the Late Miocene.

5.4.4. Interpretation of the Surface Morphology

The backscatter map gives some indication of the nature of the sediments. Generally, low backscatter values, such as in the Area a (Figure M1-10a) are indicative of fine grained/softer sediment, whereas higher backscatter values are indicative of coarser grained sediment and/or harder substrate. Low backscatter values in Area c (Figure M1-10a) may indicate that the grain size of the surface sediments in this area is smaller compared to those of the Mergui Ridge area. This observation matches the observations by Rodolfo (1969) who stated that the sediments on top of Mergui Ridge area mainly consisting of sandy deposits. Accordingly, the highest backscatter values are obtained from the erosive surface Area b and from the platforms tops, supporting the assumption that no soft sediment is covering these areas where older strata of possible shallow marine/fluviatile origin are outcropping (seismic unit MB2).

The morphology of sedimentary units at the Mergui Ridge is indicative of the presence of bottom currents (see also Schwab et al., 2012). The alongslope moat (Figure M1-10) may act as a pathway for bottom currents. Generally, the flow of bottom currents may result in the formation of such erosive moats and outward of the center of such bottom currents, drift deposition takes place due to reduced current velocities (Faugères et al., 1999). According to the mounded overall shape of seismic unit MB3 and its smooth surface (Area a) it may be interpreted as a mounded drift deposit. Mounded drift deposits exhibit a mounded structure, striking in the direction of the bottom current (Faugères et al. 1999; Hernández-Molina, 2008). The crest of the sediment body indicates where the bottom current intensity is weakest, whereas the deposits are thinning out towards the core of the bottom current, where the current is strongest (Hernández-Molina, 2008). In this context, area b may represent an erosive surface. Erosive surfaces are related to the location where the erosion by the alongslope current is maximal (Hernández-Molina et al., 2008).

As also described in Schwab et al. (2012), the structure of the sediment body underlying Area c in the East Andaman Basin, downslope of Area b (Figure M1-9) exhibits internal features typical of a drift deposit, with packages of low amplitude reflectors separated by high amplitude reflectors. Such a reflector configuration indicates temporary changes in depositional conditions. The surface of this drift deposit is characterized by sediment waves, which is also typical for drift deposits (Faugères et al. 1999).

Within the mounded body on top of the Mergui Ridge the seismic unit MR3b is draping over unit MR3a and tapers out to the west. A similar configuration of a younger sedimentary unit that is draping over older eroded strata has been shown for the slope of the Campos Basin off Brazil (Viana et al., 2002). Here the establishment of a bottom current after sea level rise in the late Quaternary led to the formation of a moat running along the slope with deposition of drift deposits downslope of the moat and the formation of a drape of younger sediment over formerly subaerially exposed sedimentary layers upslope of the moat (Viana et al., 2002). Further indicators of bottom current activity in the area are pronounced moats around the platforms (Schwab et al., 2012). Such moats are typical features of bottom currents flowing around obstacles (Howe et al., 2006; Hernández-Molina et al., 2008). They develop when bottom current speed is enhanced due to flow focusing around the obstacle.

5.4.5. Link between surface morphology and circulation

The examination of the ECCO2 model data set shows that currents along the Mergui Ridge are present in the deep water. The reversal of circulation direction in the central Andaman Sea between peak and inter monsoon months as well as the reversal in directions of the along slope current at the Mergui Ridge and the occurrence of highest current speeds only in peak monsoon months suggest a dependence of the currents in the deeper water column on the monsoon. This is in line with the observations of Varkey et al. (1996) and modeling of Potemra et al. (1991), who describe the presence of a gyre in the Andaman Sea with seasonal changes in current directions, which may be present in deeper waters as well. Important for the working area of this study seems to be an inflow through the Great Channel north of Sumatra in the deeper water column, which leads to an alongslope current around the southern tip of the Mergui Ridge and therefore along the Mergui shelf to the north. Current velocities are maximal (~8cm/s) during peak monsoon months according to the ECCO2 model data. This inflow into the Andaman Sea may be due to balancing of surface water masses that leave the Andaman Sea (Rodolfo, 1969).

The establishment of a northward alongslope current during monsoon months matches the architecture of the sedimentary deposits in the working area. If the core of such a flow is located in the Area b, where non deposition and/or erosion prevails, it may lead to the formation of erosional features such as the observed slope parallel moat and prevent sedimentation, whereas in the areas adjacent to the slope the mounded drift deposit upslope (Area a) and downslope (Area c) may form. This also explains the alongslope alignment of the crest of the drift on Mergui Ridge and alignment of the erosive zone of Area b parallel to the drift body.

Regarding current velocities (maximum 8cm/s), they seem to be relatively low for the establishment of the bottom controlled sedimentary system that has been interpreted from the geophysical data set. According Stow et al. (2009), bottom currents with velocities as low as ~6cm/s may form drift deposits from sediments with up to ~1mm mean grain size, but the formation of erosive terraces requires long term stable current conditions with velocities around 0.5m/s or more. The sediments on the Mergui Ridge are generally coarse grained and contain relict sands and relict foraminifera indicative of low sedimentation rates and/or reworking of the sediment (Rodolfo, 1969). This may be due to the fact that sediments of the old shallow marine seismic unit MR2 are outcropping and were subject to reworking during the subsidence of Mergui Ridge. Fine grained material may be winnowed away by the bottom currents leaving these sands uncovered.

However, one has to take into account, that the ECCO2 model data can only give a very general overview of circulation patterns as the data are a result of modeling and rely on a coarse grid. The local circumstances may differ from the model data. For example, currents may be focused due to the topography or intensified by the Coriolis force that steers northward currents to the right on the northern hemisphere. This in turn can result in intensification of the flow, leading to erosion and channel formation (Faugères et al., 1999). Another factor that may add to the intensity of bottom currents in the area is the occurrence of internal waves. They are a frequent feature in the Andaman Sea (Osborne and Burch, 1980; Apel et al., 1985; Hyder, 2005; Jackson 2007). According to Jackson and Alpers (2002) typical wavelengths of waves in the Andaman Sea are between 6km and 15km. Waves generally “feel” the bottom at water depths shallower than half of the wave length. Therefore, internal waves at wavelengths of 6 km may interact with the seafloor at greater depths as well. This has been shown for the Dreadnought Bank just

south of the Mergui Ridge where internal waves break and overturn at 241m water depth (Vlasenko and Alpers, 2005).

5.5. Conclusions

The sedimentary units covering the Mergui Ridge area are shaped by large scale subsidence of the ridge area since around the end of the Late Miocene. An erosive unconformity was created due to previous uplift phase(s) until Late Miocene and this approximately represents the Late Miocene-Pliocene transition. Older sediments onlapping onto the Mergui Ridge were eroded during uplift and subaerial exposure of the Mergui Ridge. During the following subsidence phase, a sedimentary body was deposited at the western flank of the Mergui Ridge that contains a transgression conglomerate and several local unconformities. This setting indicates sea floor changes and erosive phases during initial subsidence. After subsidence of the Mergui Ridge below the sea level, the youngest unit has been deposited on top of the Mergui Ridge, draping older sediments of the Mergui Ridge partially. This unit is continuous to the Mergui Basin.

Today the Mergui Ridge is shaped by the occurrence of drift deposits and an erosive zone at the western edge of the ridge. Two zones of drift deposits have been identified: One on top of Mergui Ridge and one in the East Andaman Basin at the western flank of the Mergui Ridge. These two areas of drift deposits are separated by a zone of non-deposition/ erosion. Oceanographic processes shaping the margin include alongslope currents and internal waves interacting with the slope.

The alongslope currents are monsoon controlled with highest current velocities during peak monsoon months when an alongslope current flows northward along the Mergui Ridge, accompanied by a southward flowing counter current in the deeper parts of the Mergui Ridge slope.

The geological development of the Mergui Ridge indicates that drift deposition is relatively young (starting in the latest Plio-Pleistocene), and may have started only after large scale subsidence of the ridge. The thin sediment cover of the Mergui Ridge and the prevalence of coarse grained material are probably due to the subsidence history or due to winnowing of fine grained material by the bottom currents.

References

Andreason, M.W., Mudford, B., St. Onge, J.E., 1997. Geologic Evolution and Petroleum System of the Thailand Andaman Sea Basins. Proceedings of the Petroleum Systems of SE Asia and Australasia Conference.

Apel, J.R., Thompson, D.R., Tilley, D.G., van Dyke, P., 1985. Hydrodynamics and radar signatures of internal solitons in the Andaman Sea. Johns Hopkins APL Technical Digest 6 (4), 3330–3337.

Awasthi, N., Ray, J.S., Singh, A.K., Band, S.T., Rai, V.K., 2014. Provenance of the Late Quaternary sediments in the Andaman Sea: Implications for monsoon variability and ocean circulation. Geochem. Geophys. Geosyst. 15 (10), 3890–3906. 10.1002/2014GC005462.

Betzler, C., Lindhorst, S., Hübscher, C., Lüdmann, T., Fürstenau, J., Reijmer, J., 2011. Giant pockmarks in a carbonate platform (Maldives, Indian Ocean). Marine Geology 289 (1-4), 1–16. 10.1016/j.margeo.2011.09.004.

Brown, B., 2007. Coral reefs of the Andaman Sea - an integrated perspective. Oceanography and Marine Biology: an Annual Review 45, 173–194. 10.1201/9781420050943.ch5.

Brune, S., Ladage, S., Babeyko, A.Y., Müller, C., Kopp, H., Sobolev, S.V., 2010b. Supplement to: Submarine landslides at the eastern Sunda margin: Observations and tsunami impact assessment. Nat Hazards 54 (2), 547–562. 10.1007/s11069-009-9487-8.

Bunsomboonsakul, S., Liu, Z., Sompongchaiyakul, P., Snidvongs, A., Krastel S.,2012. Clay Mineralogical Records in Sediments along the Shelf Break of the Eastern Andaman Sea. American Geophysical Union, Fall Meeting.

Cao, P., Shi, X., Li, W., Liu, S., Yao, Z., Hu, L., Khokiattiwong, S., Kornkanitnan, N., 2015. Sedimentary responses to the Indian Summer Monsoon variations recorded in the southeastern Andaman Sea slope since 26 ka. Journal of Asian Earth Sciences. 10.1016/j.jseaes.2015.06.028.

Chakraborty, P.P., Khan, P.K., 2009. Cenozoic geodynamic evolution of the Andaman-Sumatra subduction margin: Current understanding. Island Arc 18 (1), 184–200. 10.1111/j.1440-1738.2008.00643.x.

Colin, C., Turpin, L., Bertaux, J., Desprairies, A., Kissel, C., 1999. Erosional history of the Himalayan and Burman ranges during the last two glacial–interglacial cycles. EPSL 171 (4), 647–660. 10.1016/S0012-821X(99)00184-3.

Curray, J.R., 2005. Tectonics and history of the Andaman Sea region. Journal of Asian Earth Sciences 25 (1), 187–232. 10.1016/j.jseaes.2004.09.001.

Curray, J.R., Moore, D.G., Lawver, L.A., Emmel, F.J., Raitt, R., Henry, M., Kieckhefer, R., 1978. Tectonics of the Andaman Sea and Burma. AAPG Bulletin, 189–197.

Diehl, T., Waldhauser, F., Cochran, J.R., Kamesh Raju, K.A., Seeber, L., Schaff, D., Engdahl, E.R., 2013. Back-arc extension in the Andaman Sea: Tectonic and magmatic processes imaged by high-precision teleseismic double-difference earthquake relocation. J. Geophys. Res. Solid Earth 118 (5), 2206–2224. 10.1002/jgrb.50192.

Doust, H., Sumner, H.S., 2007. Petroleum systems in rift basins – a collective approach inSoutheast Asian basins. Petroleum Geoscience 13 (2), 127–144. 10.1144/1354-079307-746.

Dutta, K., Bhushan, R., Somayajulu, B., 2007. Rapid vertical mixing rates in deep waters of the Andaman Basin. Science of The Total Environment 384 (1-3), 401–408. 10.1016/j.scitotenv.2007.04.041.

ECCO2: Estimating the Circulation and Climate of the Ocean, Phase II: High Resolution Global-Ocean and Sea-Ice Data Synthesis" http://ecco2.jpl.nasa.gov/

Ercilla, G., Juan, C., Hernández-Molina, F.J., Bruno, M., Estrada, F., Alonso, B., Casas, D., Farran, M., Llave, E., García, M., Vázquez, J.T., d'Acremont, E., Gorini, C., Palomino, D., Valencia, J., El Moumni, B., Ammar, A., 2015. Significance of bottom currents in deep-sea morphodynamics: An example from the Alboran Sea. Marine Geology. 10.1016/j.margeo.2015.09.007.

Faugères J. -C., Stow D. A. V., Imbert, P., Viana A., 1999. Seismic features diagnostic of contourite drifts. Marine Geology 162 (1), 1–38. 10.1016/S0025-3227(99)00068-7.

Feldens, P., Schwarzer, K., Szczucinski, W., Stattegger, K., Sakuna, D., Somgpongchaiykul, P., 2009. Impact of 2004 Tsunami on Seafloor Morphology and Offshore Sediments, Pakarang Cape, Thailand. Polish Journal of Environmental Studies 18 (1), 63–68.

Feldens, P., Schwarzer, K., Sakuna, D., Szczuciński, W., Sompongchaiyakul, P., 2012. Sediment distribution on the inner continental shelf off Khao Lak (Thailand) after the 2004 Indian Ocean tsunami. Earth Planet Sp 64 (10), 875–887. 10.5047/eps.2011.09.001.

Fitch, T.J., 1972. Plate Convergence, Transcurrent Faults, and Internal Deformation Adjacent to Southeast Asia and the Western Pacific. Journal of Geophysical Research 77 (23), 4432–4460.

Frerichs, W.E., 1967. Distribution and Ecology of Foraminifera in the Sediments of the Andaman Sea, PhD Thesis, University of Southern California, Los Angeles, 282pp.

Hernández-Molina, F.J., Llave, E., Stow, D., 2008. Continental Slope Contourites, in: M. Rebesco and A. Camerlenghi (Ed.), Developments in Sedimentology: Contourites, Volume 60. Elsevier, pp.379–408.

Hernández-Molina, F.J., Llave, E., Preu, B., Ercilla, G., Fontan, A., Bruno, M., Serra, N., Gomiz, J.J., Brackenridge, R.E., Sierro, F.J., Stow, D.A.V., Garcia, M., Juan, C., Sandoval, N., Arnaiz, A., 2014. Contourite processes associated with the Mediterranean Outflow Water after its exit from the Strait of Gibraltar: Global and conceptual implications. Geology 42 (3), 227–230. 10.1130/G35083.1.

Howe, J.A., Stoker, M.S., Masson, D.G., Pudsey, C.J., Morris, P., Larter, R.D., Bulat, J., 2006. Seabed morphology and the bottom-current pathways around Rosemary Bank seamount, northern Rockall Trough, North Atlantic. Marine and Petroleum Geology 23 (2), 165–181. 10.1016/j.marpetgeo.2005.08.003.

IOC, IHO, BODC (2003) Centenary edition of the GEBCO digital atlas, published on CDROM on behalf of the Intergovernmental Oceanographic Commission and the International Hydrographic Organization as part of the general bathymetric chart of the oceans. British Oceanographic Data Centre, Liverpool

Jha, P., 2008. Evolution and Hydrocarbon Occurrences of Rift Basins at the Western Margin of Sunda Platform and Relations with East Andaman Basin, in: Geo India 2008 Conference and Exhibition. South Asian Geosciences Exhibition and Conference, Greater Nioda, New Dheli, India. 16-19 Septemeber.

Jintasaeranee, P., Weinrebe, W., Klaucke, I., Snidvongs, A., Flueh, E.R., 2012. Morphology of the Andaman outer shelf and upper slope of the Thai exclusive economic zone. Journal of Asian Earth Sciences 46, 78–85. 10.1016/j.jseaes.2011.11.003.

Kamesh Raju, K.A., Ramprasad, T., Rao, P., Ramalingeswara Rao, B., Varghese, J., 2004. New insights into the tectonic evolution of the Andaman basin, northeast Indian Ocean. EPSL 221 (1-4), 145–162. 10.1016/S0012-821X(04)00075-5.

Keller, G.H., Richards, A.F., 1967. Sediments of the Malacca Strait, Southeast Asia. Journal of Sedimentary Petrology 37 (1), 102–127.

Khan, P.K., Chakraborty, P.P., 2005. Two-phase opening of Andaman Sea: a new seismotectonic insight. EPSL 229 (3-4), 259–271. 10.1016/j.epsl.2004.11.010.

Kim, T., Obata, H., Gamo, T., 2015. Dissolved Zn and its speciation in the northeastern Indian Ocean and the Andaman Sea. Front. Mar. Sci. 2, 2720. 10.3389/fmars.2015.00060.

Lee, T.-Y., Lawver, L.A., 1995. Cenozoic plate reconstruction of Southeast Asia: Southeast Asia Structure and Tectonics. Tectonophysics 251 (1–4), 85–138. 10.1016/0040-1951(95)00023-2.

Lin, Y.-n.N., Sieh, K., Stock, J., 2010. Submarine landslides along the Malacca Strait-Mergui Basin shelf margin: Insights from sequence-stratigraphic analysis. Journal of Geophysical Research 115 (B12), B12102.

Marshall, J., Adcroft, A., Hill, C., Perelman, L., Heisey, C., 1997. A finite-volume, incompressible Navier Stokes model for studies of the ocean on parallel computers. J. Geophys. Res. 102 (C3), 5753–5766. 10.1029/96JC02775.

Menemenlis, D., Campin, J.M., Heimbach, P., Hill, Lee, C., Nguyen, A., Schodlock, M., Zhang, H., 2008. ECCO2: High resolution Global Ocean and Sea Ice Data Synthesis. Mercator Ocean Quarterly Newsletter 31, 13–21.

Michel, G.W., Yu, Y.Q., Zhu, S.Y., Reigber, C., Becker, M., Reinhart, E., Simons, W., Ambrosius, B., Vigny, C., Chamot-Rooke, N., Le Pichon, X., Morgan, P., Matheussen, S., 2001. Crustal motion and block behaviour in SE-Asia from GPS measurements. EPSL 187 (3–4), 239–244. 10.1016/S0012-821X(01)00298-9.

Milliman, J.D., Meade, R.H., 1983. World-Wide Delivery of River Sediment to the Oceans. The Journal of Geology 91 (1), 1–21.

Morley, C.K., 2012. Discussion of tectonic models for Cenozoic strike-slip fault-affected continental margins of mainland SE Asia. Journal of Asian Earth Sciences (0). 10.1016/j.jseaes.2012.10.019.

Morley, C.K., 2015. Cenozoic structural evolution of the Andaman Sea: Evolution from an extensional to a sheared margin. Geological Society, London, Special Publications. 10.1144/SP431.1.

Morley, C.K., Alvey, A., 2015. Is spreading prolonged, episodic or incipient in the Andaman Sea? Evidence from deepwater sedimentation. Journal of Asian Earth Sciences 98, 446–456. 10.1016/j.jseaes.2014.11.033.

Morley, C.K., Racey, A., 2010. Tertiary stratigraphy, in: Ridd, M.F., Barber, A.J., Crow, M.J. (Eds.), The Geology of Thailand.

Naqvi, W.A., Charles, C.D., Fairbanks, R.G., 1994. Carbon and oxygen isotopic records of benthic foraminifera from the Northeast Indian Ocean: implications on glacial-interglacial atmospheric CO2 changes. EPSL 121 (1–2), 99–110. 10.1016/0012-821X(94)90034-5.

Nielsen, C., Chamot-Rooke, N., Rangin, C., 2004. From partial to full strain partitioning along the Indo-Burmese hyper-oblique subduction. Marine Geology 209 (1-4), 303–327. 10.1016/j.margeo.2004.05.001.

Nozaki, Y., Alibo, D.S., 2003. Importance of vertical geochemical processes in controlling the oceanic profiles of dissolved rare earth elements in the northeastern Indian Ocean. EPSL 205 (3-4), 155–172. 10.1016/S0012-821X(02)01027-0.

Okubo, A., Hajime, O., Nozaki, Y., Yamamoto, Y., Minami, H., 2004. 230 Th in the Andaman Sea: Rapid deep-sea renewal. Geophysical Research Letters 31 (22). 10.1029/2004GL020226.
Osborne, A.R., Burch, T.L., 1980. Internal Solitons in the Andaman Sea. Science 208 (4443), 451–460. 10.1126/science.208.4443.451.
Panchang, R., Nigam, R., Riedel, F., Janssen, A.W., Hla, U.K.Y., 2007. A review of the studies on pteropods from the northern Indian Ocean region with a report on the pteropods of Irrawaddy continental shelf off Myanmar. Indian Journal of Marine Sciences 36 (4), 384–398.
Polachan, S., 1988. The geological Evolution of the Mergui Basin S.E. Andaman Sea. PhD Thesis, University of London.
Polachan, S., Pradidtan, S., Tongtaow, C., Janmaha, S., Intarawijitr, K., Sangsuwan, C., 1991. Development of Cenozoic basins in Thailand. Marine and Petroleum Geology 8 (1), 84–97. 10.1016/0264-8172(91)90047-5.
Polachan, S., Racey, A., 1994. Stratigraphy of the Mergui Basin, Andaman Sea: (Implications for Petroleum Exploration). Journal of Petroleum Geology 17 (4), 373–406.
Potemra, J.T., Luther, M.E., O'Brien, J.J., 1991. The seasonal circulation of the upper ocean in the Bay of Bengal. J. Geophys. Res. 96 (C7), 12667. 10.1029/91JC01045.
Preu, B., Hernández-Molina, F.J., Violante, R., Piola, A.R., Paterlini, C.M., Schwenk, T., Voigt, I., Krastel, S., Spiess, V., 2013. Morphosedimentary and hydrographic features of the northern Argentine margin: The interplay between erosive, depositional and gravitational processes and its conceptual implications. Deep Sea Research Part I: Oceanographic Research Papers 75, 157–174.
Racey, A., 2010. Petroleum geology, in: Ridd, M.F., Barber, A.J., Crow, M.J. (Eds.), The Geology of Thailand.
Ramaswamy, V., Rao, P.S., 2006. Grain Size Analysis of Sediments from the Northern Andaman Sea: Comparison of Laser Diffraction and Sieve-Pipette Techniques. Journal of Coastal Research 224, 1000–1009. 10.2112/04-0162.1.
Ramaswamy, V., Rao, P., Rao, K., Thwin, S., Rao, N., Raiker, V., 2004. Tidal influence on suspended sediment distribution and dispersal in the northern Andaman Sea and Gulf of Martaban. Marine Geology 208 (1), 33–42. 10.1016/j.margeo.2004.04.019.
Rangin, C., Maurin, T., Masson, F., 2013. Combined effects of Eurasia/Sunda oblique convergence and East-Tibetan crustal flow on the active tectonics of Burma. Journal of Asian Earth Sciences 76 (0), 185–194. 10.1016/j.jseaes.2013.05.018.
Rao, P.S., Ramaswamy, V., Thwin, S., 2005. Sediment texture, distribution and transport on the Ayeyarwady continental shelf, Andaman Sea. Marine Geology 216 (4), 239–247. 10.1016/j.margeo.2005.02.016.
Rashid, H., Flower, B., Poore, R., Quinn, T., 2007. A ~25ka Indian Ocean monsoon variability record from the Andaman Sea. Quaternary Science Reviews 26 (19-21), 2586–2597. 10.1016/j.quascirev.2007.07.002.
Rebesco, M., Hernández-Molina, F.J., Rooij, D.v., Wåhlin, A., 2014. Contourites and associated sediments controlled by deep-water circulation processes: State-of-the-art and future considerations. Marine Geology 352, 111–154. 10.1016/j.margeo.2014.03.011.
Robinson, R.A.J., Bird, M.I., Oo, N.W., Hoey, T.B., Aye, M.M., Higgitt, D.L., X. X., L., Swe, A., Tun, T., Win, S.L., 2007. The Irrawaddy River Sediment Flux to the Indian Ocean: The Original Nineteenth-Century Data Revisited. J GEOL 115 (6), 629–640. 10.1086/521607.
Rodolfo, K.S., 1969. Sediments of the Andaman Basin, northeastern Indian Ocean. Marine Geology 7 (5), 371–402. 10.1016/0025-3227(69)90014-0.
Sakuna, D., Szczuciński, W., Feldens, P., Schwarzer, K., Khokiattiwong, S., 2012. Sedimentary deposits left by the 2004 Indian Ocean tsunami on the inner continental shelf offshore of Khao Lak, Andaman Sea (Thailand). Earth Planet Sp 64 (10), 931–943. 10.5047/eps.2011.08.010.
Schlitzer, R., Ocean Data View, http://odv.awi.de,2016
Schwab, J.M., Krastel, S., Grün, M., Gross, F., Pananont, P., Jintasaeranee, P., Bunsomboonsakul, S., Weinrebe, W., Winkelmann, D., 2012. Submarine mass wasting and associated tsunami risk offshore western Thailand, Andaman Sea, Indian Ocean. Nat. Hazards Earth Syst. Sci. 12 (8), 2609–2630. 10.5194/nhess-12-2609-2012.
Searle, M.P., Morley, C.K., 2010. Tectonic and thermal evolution of Thailand in the regional context of SE Asia, in: Ridd, M.F., Barber, A.J., Crow, M.J. (Eds.), The Geology of Thailand.
SEATAR, 1976: SIO 76-3, Sediment Descriptions from the Studies of East Asia Tectonics and Resources (SEATAR) Program, 1976 Jane Frazer, Donna Hawkins; last access: 15.08.2016.
Socquet, A., Vigny, C., Chamot-Rooke, N., Simons, W., Rangin, C., Ambrosius, B., 2006. India and Sunda plates motion and deformation along their boundary in Myanmar determined by GPS. Journal of Geophysical Research 111 (B5), B05406. 10.1029/2005JB003877.

Srisuriyon, K., Morley, C.K., 2014. Pull-apart development at overlapping fault tips: Oblique rifting of a Cenozoic continental margin, northern Mergui Basin, Andaman Sea. Geosphere 10 (1), 80–106. 10.1130/GES00926.1.

Stow, D.A., Hernandez-Molina, F.J., Llave, E., Sayago-Gil, M., Diaz del Rio, V., Branson, A., 2009. Bedform-velocity matrix: The estimation of bottom current velocity from bedform observations. Geology 37 (4), 327–330. 10.1130/G25259A.1.

Sugawara, D., Minoura, K., Nemoto, N., Tsukawaki, S., Goto, K., Imamura, F., 2009. Foraminiferal evidence of submarine sediment transport and deposition by backwash during the 2004 Indian Ocean tsunami. Island Arc 18 (3), 513–525. 10.1111/j.1440-1738.2009.00677.x.

Tripathi, S.K., 2014. Biogenic sediment distribution around south of Central Andaman Trough, Andaman Sea:signatures from micropaleontological studies. Indian Journal of Geosciences 68 (4), 337–346.

Varkey, M.J., Murty, V.S.N., Suryanarayana, A., 1996. Physical Oceanography of the Bay of Bengal and Andaman Sea. Oceanography and Marine Biology: an Annual Review 34, 1–70.

Viana, A.R., 2002. Seismic expression of shallow- to deep-water contourites along the south-eastern Brazilian margin. Marine Geophysical Researches 22 (5-6), 509–521.

Wyrtki, K., 1961. Physical Oceanography of the Southeast Asian waters: Scientific Results -Marine Investigations of the South China Sea and the Gulf of Thailand. Naga Report 2. The University of California, Scripps Institution of Oceanography, 225 pp.

6. Submarine mass wasting and associated tsunami risk offshore western Thailand, Andaman Sea, Indian Ocean

MANUSCRIPT II

Julia M. Schwab, Sebastian Krastel, Mathias Grün, Felix Gross, Passakorn Pananont, Pachoenchoke Jintasaeranee, Suratta Bunsomboonsakul, Wilhelm Weinrebe, Daniel Winkelmann

Published in in: Natural Hazards and Earth System Science 12, 2609–2630, 2012, doi:10.5194/nhess-12-2609-2012.

Nat. Hazards Earth Syst. Sci., 12, 2609–2630, 2012
www.nat-hazards-earth-syst-sci.net/12/2609/2012/
doi:10.5194/nhess-12-2609-2012

Natural Hazards and Earth System Sciences

Submarine mass wasting and associated tsunami risk offshore western Thailand, Andaman Sea, Indian Ocean

J. M. Schwab[1], S. Krastel[1], M. Grün[1], F. Gross[1], P. Pananont[2], P. Jintasaeranee[3], S. Bunsomboonsakul[4], W. Weinrebe[1], and D. Winkelmann[1]

[1]GEOMAR | Helmholtz Centre for Ocean Research Kiel, Germany
[2]Department of Earth Sciences, Faculty of Science, Kasetsart University, Bangkok, Thailand
[3]Department of Aquatic Science, Burapha University, Chonburi, Thailand
[4]Thailand Southeast Asia START Regional Center, Chulalongkorn University, Bangkok, Thailand

Correspondence to: J. M. Schwab (jschwab@geomar.de)

Received: 23 March 2012 – Revised: 30 June 2012 – Accepted: 23 July 2012 – Published: 17 August 2012

Abstract. 2-D seismic data from the top and the western slope of Mergui Ridge in water depths between 300 and 2200 m off the Thai west coast have been investigated in order to identify mass transport deposits (MTDs) and evaluate the tsunamigenic potential of submarine landslides in this outer shelf area. Based on our newly collected data, 17 mass transport deposits have been identified. Minimum volumes of individual MTDs range between 0.3 km^3 and 14 km^3. Landslide deposits have been identified in three different settings: (i) stacked MTDs within disturbed and faulted basin sediments at the transition of the East Andaman Basin to the Mergui Ridge; (ii) MTDs within a pile of drift sediments at the basin-ridge transition; and (iii) MTDs near the edge of/on top of Mergui Ridge in relatively shallow water depths (< 1000 m). Our data indicate that the Mergui Ridge slope area seems to have been generally unstable with repeated occurrence of slide events. We find that the most likely causes for slope instabilities may be the presence of unstable drift sediments, excess pore pressure, and active tectonics. Most MTDs are located in large water depths (> 1000 m) and/or comprise small volumes suggesting a small tsunami potential. Moreover, the recurrence rates of failure events seem to be low. Some MTDs with tsunami potential, however, have been identified on top of Mergui Ridge. Mass-wasting events that may occur in the future at similar locations may trigger tsunamis if they comprise sufficient volumes. Landslide tsunamis, emerging from slope failures in the working area and affecting western Thailand coastal areas therefore cannot be excluded, though the probability is very small compared to the probability of earthquake-triggered tsunamis, arising from the Sunda Trench.

1 Introduction

The extremely catastrophic tsunamis of December 2004 in the SE Indian Ocean and March 2011 in Japan, as well as many other incidents (NGDC/WDC Global Tsunami Event Database, 2012), show that tsunamis pose a major threat to low-lying coastal areas. Ocean-wide tsunamis are predominantly triggered by earthquakes, but submarine landslides are also known for their potential to trigger regional tsunamis of significant wave heights (Ward, 2001; Harbitz et al., 2006). A well-studied prehistoric example of a landslide-triggered tsunami is the Storegga Slide offshore Norway (Jansen et al., 1987; Dawson et al., 1988; Bondevik et al., 1997, 2005). Tsunami deposits associated with the Storegga Slide were reported from Iceland, Norway, Scotland and the Shetland Islands with run-up heights exceeding 20 m in places (Bondevik et al., 2003). Moreover, several recent examples for locally destructive tsunami hazards were associated with submarine landslides, such as the Grand Banks tsunami (1929, Canada) that killed 28 people (Hasegawa and Kanamori, 1987; Piper et al., 1999; Fine et al., 2005), a tsunami at Skagway Harbor (1994, Alaska) with one casualty (Kulikov et al., 1996) and the Sissano or Aitape tsunami (1998, Papua New Guinea) causing about 2000 fatalities (Tappin, 1999; Tappin et al., 2001; Matsumoto and Tappin, 2003). Extensive research and modeling of landslide tsunami generation has been undertaken (Ward, 2001; Harbitz et al., 2006; Grilli et al., 2009; Weiss et al., 2009). However, early warning of landslide tsunami hazards is difficult due to the fact that seismological (Lomax et al., 2007) or GPS (Blewitt et al., 2006; Sobolev et al., 2007) techniques,

applicable to earthquake induced tsunamis, are not useful to detect landslide-generated tsunamis due to the comparably small amount of seismic energy release and long-period-signal of submarine landslides (Brune et al., 2009, 2010). Moreover, the time lag between sediment failure and tsunami arrival at the coast in the near field of a submarine landslide might be too small to forewarn and evacuate endangered regions (Biscontin et al., 2004).

It is therefore important to gain thorough knowledge on current stability of the continental slope for individual areas, in order to estimate frequencies and dimensions of failures and rate probability of future failures. This in turn can be used to assess tsunami risk and preparedness for corresponding coastal areas, such as the Thai Andaman Sea coast. The vicinity of this coast to the seismically highly active Sunda Trench (NGDC, Global Significant Earthquake Database, 2012) makes the area vulnerable to tsunamis. The geological record reveals recurrent tsunami events of destructive dimensions that struck the Thai west coast (Jankaew et al., 2008; Fujino et al., 2009). A potentially unstable continental slope off the Thai coast may pose an additional risk from submarine landslides, whether co-seismically triggered or triggered by other factors, provided that these failures would be of tsunamigenic dimensions. Assessing this risk is the central task of the MASS-project (Morphodynamics and Slope Stability of the Andaman Sea Shelf Break) in the frame of the Thai-German cooperation TRIAS (Tracing Tsunami impacts on- and offshore in the Andaman Sea Region).

Bathymetric and sub-bottom profiler data were obtained during the first project phases MASS I and MASS II. Jintasaeranee et al. (2012) identified possible slumping areas, though these landslides are considered to be too small for having triggered a significant tsunami in the recent past. Jintasaeranee et al. (2012), however, did not investigate older slope failures. New seismic data were collected during the MASS III research cruise in January 2011. These data are used in this study to trace landslide-related features in the subsurface in order to (1) identify areas that show indications of previous slope failure, (2) estimate volumes/dimensions of slides, (3) determine pre-conditioning and trigger mechanisms, and (4) assess the tsunamigenic potential of the detected landslides. The terms “landslide” and/or “mass transport deposit (MTD)” are used in this paper in a broad sense, denoting all types of gravitational mass wasting products, irrespective of the process.

2 Regional setting

The study area is situated at the western outer Sunda shelf in the southeastern part of the Andaman Sea backarc-basin, about 250 km off Phuket (Fig. 1). A basement high, the Mergui Ridge, forms the outer shelf break, where water depths increase from 300 to 2200 m in the working area. The Mergui Ridge separates two adjacent basins, the East Andaman

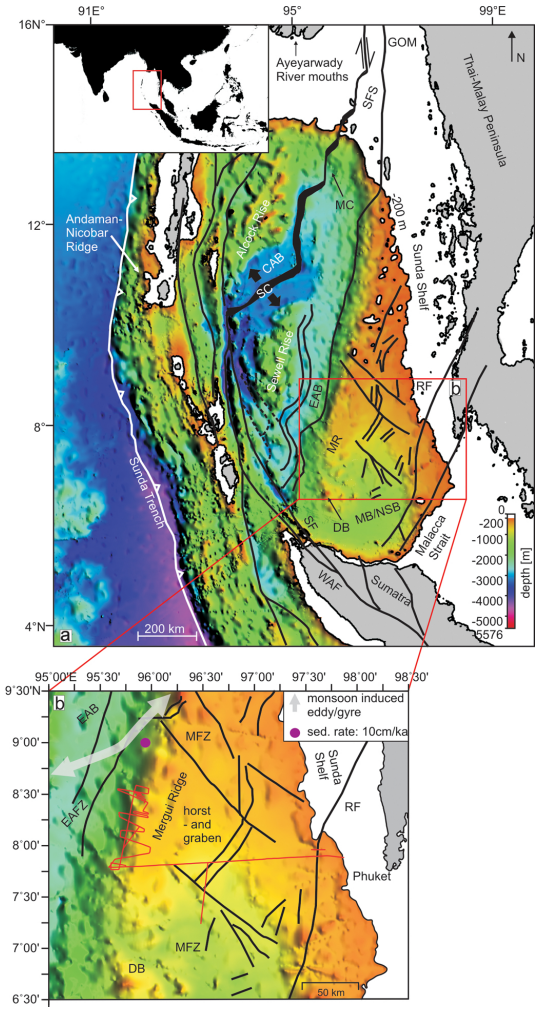

Fig. 1. **(a)** Bathymetric map and structural framework of the Andaman Sea area. The structural elements are modified from Curray (2005). Black continuous lines mark fault traces of the main fault systems: SFS: Sagaing Fault System; WAF: West Andaman Fault; RF: Ranong Fault; SF: Sumatra Fault System; GOM: Gulf of Martaban; MC: Martaban Canyon; SC: Modern spreading centre; CAB: Central Andaman Basin; EAB: East Andaman Basin; MR: Mergui Ridge; MB/NSB: Mergui Basin/North Sumatra Basin; DB: Dreadnought Bank. The bathymetry has been reproduced from GEBCO. **(b)** Close-up of the working area, situated in the western flank of Mergui Ridge. The red lines mark seismic lines of MASS III cruise. The black lines denote fault systems, modified after Curray (2005), Morley et al. (2011) and Polachan (1988). MFZ: Mergui Fault Zone (modified after Curray, 2005 and Morley et al., 2011. EAFZ: East Andaman Fault Zone (from Polachan, 1988). DB: Dreadnought Bank. EAB: East Andaman Basin. The grey arrow shows the approximate position of a monsoonal gyre that induces currents in deeper parts of the water column (modified after Varkey et al., 1996). The purple dot shows the position of a sediment core discussed by Rodolfo (1969). The bathymetry has been reproduced from SRTM30_PLUS (Becker et al., 2009).

Basin in the west and the Mergui Basin in the east and southeast (Fig. 1). The East Andaman Basin and the Mergui Basin are elongated, approximately NNE–SSW trending, sediment filled sub-basins of the Andaman Sea, located southwest of the Central Andaman Basin (Fig. 1, Curray, 2005). They have been described as rift basins (Hall and Morley, 2004; Jha et al., 2010), like numerous other Cenozoic basins across Sundaland (Polachan et al., 1991; Morley et al., 2001; Morley, 2002; Hall and Morley, 2004; Doust and Noble, 2008) and accordingly comprise a sedimentation history that is linked to typical rift stages (Doust and Noble, 2007; Doust and Sumner, 2008; Jha et al., 2010). The formation of the East Andaman Basin and the Mergui Basin results from backarc-related extensional tectonics, active throughout the area (Chakraborty and Khan, 2009; Curray, 2005). For the development of the Andaman Sea basins multi-stage models have been suggested (Kamesh Raju et al., 2004; Curray, 2005; Kamesh Raju, 2005; Chakraborty and Khan, 2009). The area of rifting moved from the Mergui Basin over the East Andaman Basin to its current position (Fig. 1) during Oligocene to Pliocene, due to increasingly oblique plate motions and changing convergence rates of Indian and Sundaland plates (Curray, 2005). In the Central Andaman Basin active sea floor spreading has occured since 4 Ma (Kamesh Raju et al., 2004; Kamesh Raju, 2005; Khan and Chakraborty, 2009). This modern spreading center links a group of N–S striking dextral strike-slip faults (Sagaing Fault, West Andaman Fault and Sumatra Fault, Fig. 1a). This system is described to accommodate the oblique convergence of the Indian and Sundaland plates (Michel et al., 2001; Nielsen et al., 2004a; Curray, 2005; Socquet et al., 2006; Chakraborty and Khan, 2009).

The East Andaman Basin has been influenced by extensional and also strike-slip faulting. Kishore et al. (2010) described NE–SW trending extensional faults, truncated by N–S trending strike slip faults. W-NW facing listric block faulting at the western flank of Mergui Ridge was reported by Curray (2005). The general trend of main strike-slip faults in the East Andaman Basin area is N–S to NE–SW (Morley et al., 2011). The East Andaman Basin is bounded towards the Mergui Basin by the East Andaman Fault Zone (EAFZ, Fig. 1b), interpreted as a branch of the Sagaing Fault System (Polachan and Racey, 1994; Jha et al., 2010). North of the working area, the NW–SE trending strike-slip Mergui Fault is cutting across Mergui Ridge (Fig. 1b). Recent reactivation at this fault has been observed (Polachan and Racey, 1994).

The establishment of the Pliocene spreading center has been given as a reason for thermal subsidence of the area (Morley et al., 2011), which is still ongoing today (Lin et al., 2010). Moreover, right lateral movement along strike slip faults in the East Andaman Basin, such as the EAFZ, took place during the Late Miocene and caused subsidence and the development of mass wasting complexes west of the Mergui Ridge (Jha et al., 2010).

Today, the East Andaman Basin comprises a total sedimentary thickness of 4600 m (Curray, 2005). It is under a shallow- to deep- water regime since the Middle to Late Miocene (Curray, 2005; Jha, 2011) and post-rift sediments up to 2500 m thick have been deposited in this environment since the Middle Miocene (Jha et al., 2010). Presently, the main source for fine grained terrigenous sediment in the Andaman Sea is the Ayeyarwady-Salween river-system (Fig. 1a, Rodolfo, 1969; Colin et al., 1999). An enormous quantity of sediment is shed into the Andaman Sea (364 MT a^{-1}, Robinson et al., 2007), and a fraction of it reaches the deeper basins of the Andaman Sea via the Martaban Canyon (Fig. 1; Rao et al., 2005; Ramaswamy et al., 2004). An additional source of terrigenous input in the southern part of the Andaman Sea is the Malacca Strait (Fig. 1), delivering fine grained terrigenous detritus to the deeper parts of the Andaman Sea basins (Keller and Richards, 1967). Transport or deposition of terrigenous sediments on the outer shelf areas along Myanmar and the Thai-Malay peninsula (Sunda shelf, Fig. 1a), between the Ayeyarwady mouth and Mergui Ridge (Fig. 1a), is not important; these areas are described to be sediment starved (Rao et al., 2005; Ramaswamy et al., 2004; Panchang et al., 2008; Rodolfo, 1969), whereas the adjacent East Andaman Basin is one of the main depocenters in the Andaman Sea (Morley et al., 2011).

The recent hydrographic regime of the Andaman Sea is dominated by the Asian Monsoon, leading to seasonal reversal of upper ocean circulation directions (Wyrtki, 1961). During Northeast Monsoon (December–March) the circulation is cyclonic, whereas during Southwestern Monsoon (June–September) anticyclonic circulation prevails (Rao et al., 2005). Seasonal upwelling (Wirtky, 1961; Buranapratheprat et al., 2010) and lowered salinity in the surface waters due to freshwater discharge during SW Monsoon (Wirtky, 1961) are consequences of the monsoonal influence on the area. Circulation in greater water depths is affected as well. A steady, seasonal gyre is reported (Varkey et al., 1996) to be located slightly northwest of the working area (Fig. 1b). Lateral exchange with Indian Ocean water masses occurs at sills in the Andaman-Nicobar Ridge (Fig. 1, Wyrtki, 1961). They comprise maximum depths of around 1800 m. Below 1800 m exchange is restricted (Rodolfo, 1969; Dutta et al., 2007). However, a very uniform well mixed water mass is present in the deepest parts throughout the Andaman Sea (Varkey et al., 1996; Dutta et al., 2007). This implies vigorous vertical mixing (Dutta et al., 2007) with renewal times of about 6 yr (Okubo et al., 2004). Dutta et al. (2007) suggest that internal waves, creating turbulence over irregular topography, may be responsible for this mixing process. Large amplitude internal waves have indeed been reported to occur repeatedly in the Andaman Sea (Osborne and Burch, 1980; Nielsen et al., 2004b; Hyder et al., 2005; Vlasenko and Alpers, 2005). They are described to be created by tidal currents near the shallow sills of the Andaman and Nicobar island arc from where they travel eastward across the Andaman sea, propagating at

Table 1. Measured properties of identified MTDs in the working area.

MTD	Interpolated areal extent (km^2)	Maximum thickness of MTD (m)	Approx volume of MTD (km^3)	Depth of shallowest point from surface (m)
A1	70	56	1.3	1130
A2	27	36	0.3	1280
A3	33	55	0.8	1350
A4	69	166	3.0	1210
B1	24	91	1.0	1850
B2	10	46	0.3	1950
B3	43	135	3.0	1570
B4	53	150	3.4	1710
B5	27	125	1.5	2020
C1	23	76	0.7	1480
C2	46	89	2.6	1420
C3	45	90	2.1	1550
C4	32	62	1.0	1530
C5	22	72	1.0	1560
D1	40	75	0.9	880
D2	33	234	4.0	830
D3	585	62	14.0	640

density interfaces (Vlasenko and Alpers, 2005); over shallowing ground they may break and form turbulence (Osbourne and Burch, 1980; Hyder et al., 2005; Vlasenko and Stashuk, 2007). Scattering of an internal wave and creation of secondary internal waves has been reported from the southern tip of Mergui Ridge (Dreadnought Bank, Vlasenko and Alpers, 2005).

3 Dataset and methods

A total of 39 seismic reflection lines were collected at the transition Mergui Basin-Mergui Ridge-East Andaman Basin within the Thai exclusive economic zone in ESE–WNW and N–S directions during cruise MASS III from 11 January 2011 to 24 January 2011 (Fig. 1b). The total length of acquired seismic lines is about 630 km and the investigated area comprises approximately 5000 km^2. High resolution seismic reflection data were acquired using a micro GI-Gun (2×0.1 l) and a 150 m-long 96-channel digital Geometrics GeoEel streamer. The gun was operated at 120 bars and shot every 5 s resulting in a shotpoint distance of 10 m at vessel speeds of 4 knots. The main frequency used was 200 Hz. The streamer consisted of 12 sections with 8 channels each. The channel distance was 1.56 m. The signals were digitized at 4 kHz and converted into SEG-Y format for further processing.

Standard processing steps were performed with Vista Seismic Data Processing (GEDCO). After setup of the geometry, common midpoint sorting and normal moveout corrections were applied as well as bandpass frequency filtering for frequency contents of 25/50–600/1200 kHz, stacking and time-migration (using a constant velocity of 1500 m s^{-1}). IHS Kingdom Suite was used for interpretation and volumetric calculations.

The bathymetry data set analysed in this study was obtained during previous cruises MASS I and MASS II in 2006 and 2007, using a portable Seabeam 1050 multibeam echo sounder. The system uses a frequency of 50 kHz, 126 individual beams and a swath width of up to 153° (Jintasaeranee et al., 2012). Resolution of the processed bathymetric grid is 50 m.

The general architecture of the background sedimentary units and the distributions and dimensions of mass transport deposits (MTDs) were deduced from the seismic dataset. MTDs were interpreted according to their external geometries and internal reflector characteristics. Examples of acoustic facies characteristics are given in Fig. 2. Lens- or wedge-shaped bodies showing a chaotic to transparent seismic facies were classified as MTDs. Precise measurements of volumes and areal extents of MTDs were not possible from our dataset, as spacing between profiles is relatively large, ranging between about 1 km and 7 km. Therefore, the geometries of the MTDs had to be interpolated over long distances of up to 7 km. An isopach grid was calculated, based on interpreted horizons of top and base for each MTD, using a constant sound velocity of 1500 m s^{-1}. Subsequently, volume and areal extent was deduced from the isopach grid. Values are summarized in Table 1. The values in Table 1, however, have to be regarded only as rough estimations due to the uncertainties mentioned above and due to the fact that the lateral boundaries of the MTDs are not present in our dataset, except for one MTD close to the sea floor, where boundaries

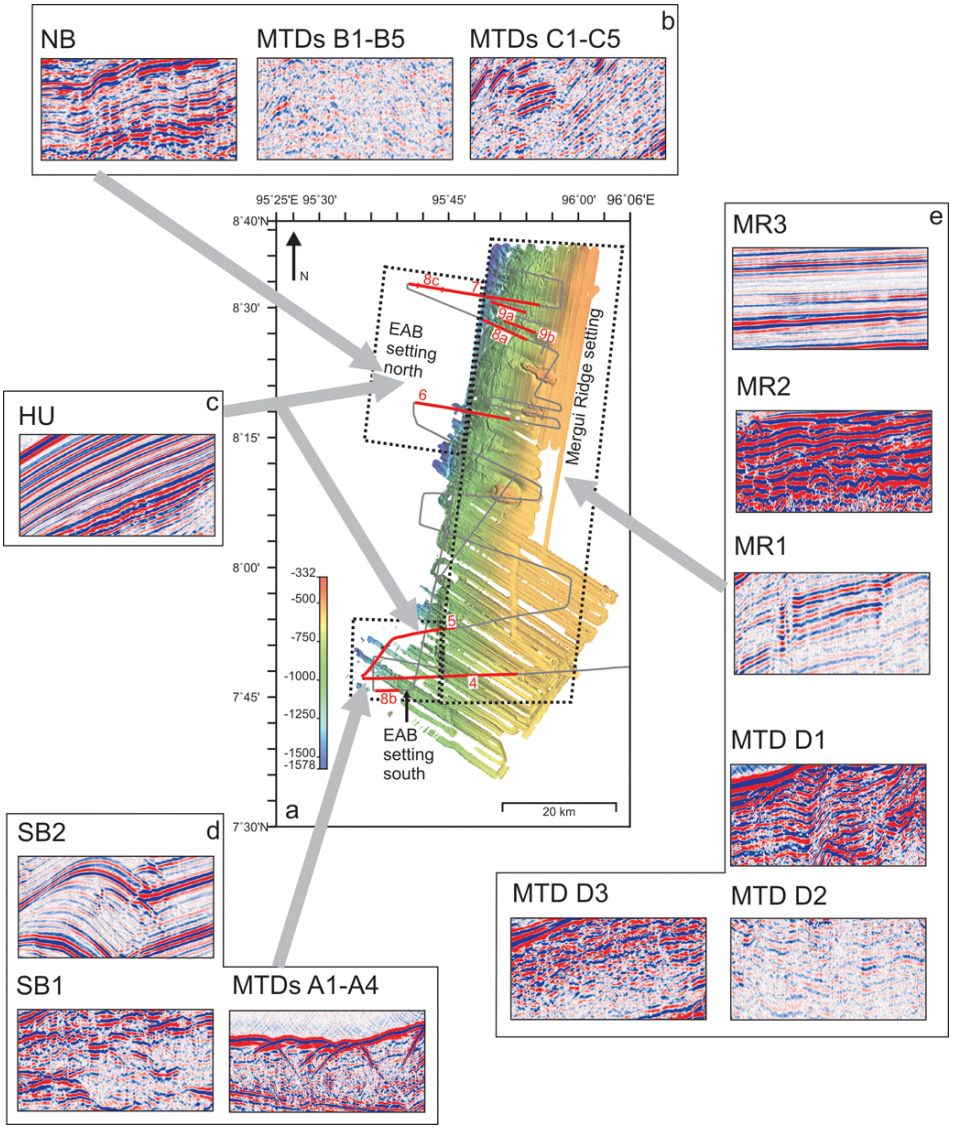

Fig. 2. (a) Bathymetric map of the working area modified after Jintasaeranee et al. (2012). The stippled black lines mark the three defined settings in the working area: Mergui Ridge, East Andaman Basin north and East Andaman Basin south. **(b)** Examples of the acoustic facies that were identified in the subsurface sediments of the northern working area, which are background sedimentary unit NB and MTDs B1–B5 and C1–C5. **(c)** Example of the acoustic facies of the surficial sedimentary unit HU identified throughout the East Andaman Basin area. **(d)** Examples of acoustic facies identified in the subsurface sediments of the southern working area, which are background sedimentary units SB1 and SB2 and MTDs A1–A4. **(e)** Examples of the acoustic facies identified in the Mergui Ridge setting, which are subsurface sedimentary units MR1 and MR2, surficial unit MR3 and MTDs D1–D3.

could be deduced from the bathymetry. Therefore, the values represent minimum estimates of individual MTDs, and actual volumes might be larger than mapped in this study. For a simple estimation of thickness of undisturbed sediment between the individual failure events, we calculated the thickness between the top and base horizon isopach grids of consecutive MTDs. For calculation of time intervals between the MTDs we used a sedimentation rate of 10 cm ka^{-1}. This sedimentation rate was established by Rodolfo (1969) from a sediment core about 50 km north of our working area (Fig. 1b, approximately 9°00′ N, 95°57′ E). The results of the calculations are given in Table 2.

4 Results

The investigated area is located at the transition from the Mergui Ridge/outer shelf area to the deep sea environment of the East Andaman Basin, and seismic profiles used in this study run across this basin-ridge transition (Figs. 1b, 2a and 3). Water depths are increasing from east (Mergui Ridge)

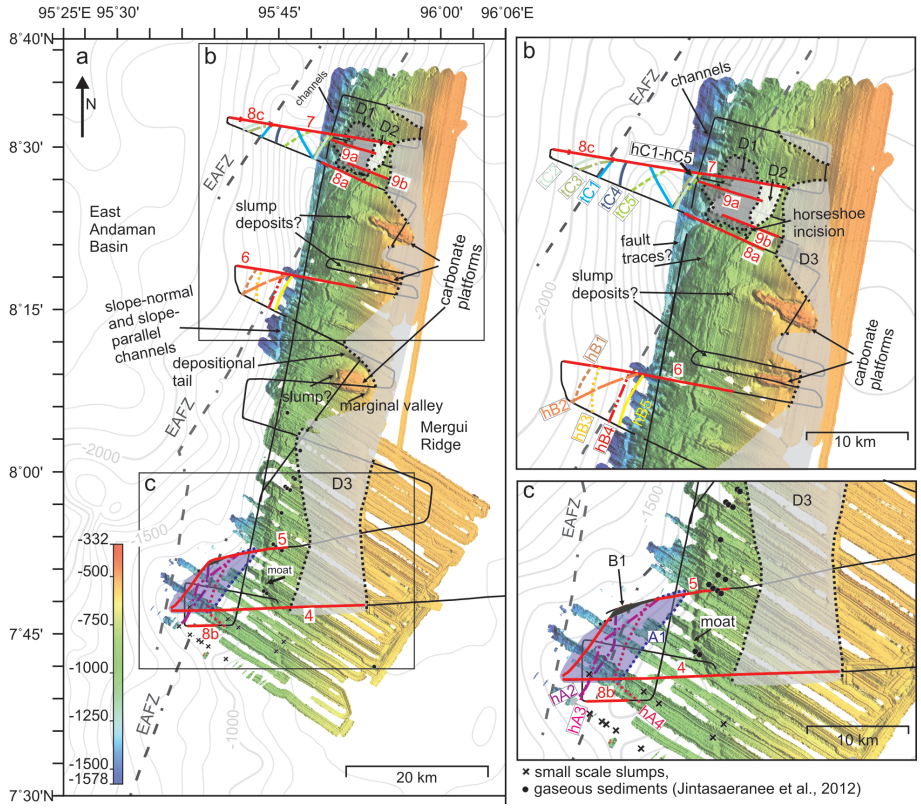

Fig. 3. (a) Bathymetric map of the working area (from Jintasearanee et al., 2012) with contour lines from SRTM30_PLUS (Becker et al., 2009). The interpretation of several morphological features, carbonate platforms, slump deposits, fault traces, as well as the positions of small scale slumps and gas-bearing sediment are taken from Jintasaeranee et al. (2012) as well. The black continuous lines show the cruise track and the red lines indicate the seismic profiles shown in this study. The grey shaded areas on the Mergui Ridge mark the areal extents of MTDs D1–D3, the black stippled lines show the slide margins where they were interpolated. The grey dotted lines indicate positions of branches of the EAFZ (from Polachan, 1988). **(b)** Close-up of the northern working area. The coloured dotted lines indicate heads (hB1–hB5 and hC1–hC5) and toes (tC1–tC5) of individual MTDs, as mapped from the seismic data. The grey shaded areas show the extents of the Mergui Ridge-MTDs D1–D3. **(c)** Close-up of the southern working area. The purple shaded area indicates the areal extent of MTD A1. The purple dotted line indicates the slide margins where they were interpolated. The dark grey block indicates the position of a potential in-situ block (B1, see also Fig. 5) or the slide margin north of A1. The coloured dotted lines denote the interpolated heads of MTDs A2–A4 (hA2–hA4).

to west (East Andaman Basin) from about 300 m to about 2200 m (Fig. 3). The western flank of Mergui Ridge forms the slope of the East Andaman Basin. Slope gradients of the basin–ridge transition are generally lower in the southern working area with values of about 1.5° (Figs. 4 and 5). Towards the north, slope angles at the edge of the Mergui Ridge are considerably higher, and reach, for example on Profile 14, values around 12° (Fig. 6). Downslope of the flank of the Mergui Ridge, the basin area is deepening towards the north (Fig. 3).

The bathymetric dataset reveals a very smooth seafloor on Mergui Ridge in the eastern part of the working area, except for three pronounced morphological highs that are pinching out from the flat top of Mergui Ridge (Fig. 3). In contrast, the sea-floor morphology is generally rough towards the western edge of the ridge. Several slope normal channels cut the edge of Mergui Ridge, and numerous elongated depressions run approximately N–S to NNE–SSW (Fig. 3). Bathymetric features that have been examined in more detail by Jintasearanee et al. (2012) are marked on Fig. 3. Seismic data reveal a smooth relief further down the slope, where sediments of the East Andaman Basin are deposited (Figs. 6 and 7).

4.1 Background sedimentary units and their architecture

Based on the architecture of the basin-ridge transition, we differentiated three settings in the working area: (1) Mergui Ridge in the western part of the working area; (2) Basin sediments of the East Andaman Basin in the southern working area; (3) Basin sediments of the East Andaman Basin in the northern working area. The location of these three settings and an overview on the acoustic facies of the seismic units identified are given in Fig. 2.

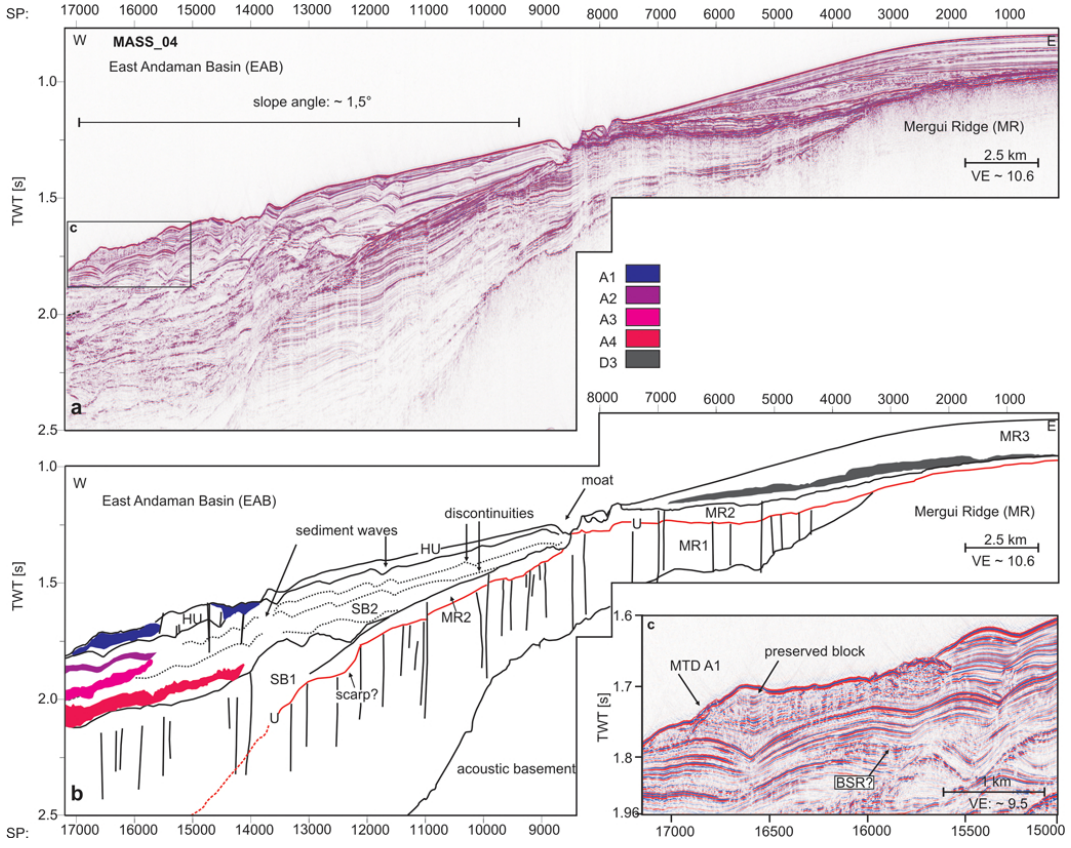

Fig. 4. **(a)** Seismic profile MASS_04 across the basin–ridge transition Mergui Ridge-East Andaman Basin in the southern working area. **(b)** Interpretation of the seismic profile showing the seismic units of Mergui Ridge in the east (MR1–MR3) and those of the southern East Andaman Basin area to the west. Faults are marked as black vertical lines. Black lines mark boundaries of seismic units. The black dashed lines mark the positions of possible discontinuities within SB2. The red line denotes the position of the unconformity *U*. The colored areas mark the position of the MTDs A1–A4. See Figs. 2 and 3 for location of profile. **(b)** Blowup of the superficial MTD A1, showing blocky structure of the deposit. The label BSR indicates the location of a potential bottom simulating reflector. See text for further explanations. See Figs. 2 and 3 for location of the profile.

Table 2. Calculated minimum time intervals between slide events, based on constant sedimentation rates of $10\,\mathrm{cm\,ka^{-1}}$ (from Rodolfo, 1969).

Interval between MTDs	Maximum thickness of undisturbed sediment between MTDs (m)	Calculated time interval (ka)
A1–A2	94	940
A2–A3	91	910
A3–A4	119	1190
B1–B2	39	390
B2–B3	22	220
B3–B4	96	960
B4–B5	147	1470
C1–C2	47	470
C2–C3	95	950
C3–C4	37	370
C4–C5	48	480

4.1.1 Mergui Ridge

The seismic units identified in the Mergui Ridge setting are laterally traceable on all profiles. We separated them into three seismic units: MR1 shows continuous parallel reflectors of variable amplitude (Fig. 2), and in the northern part towards its top a reflection pattern of transparent patches, alternating with chaotic high amplitude areas (Figs. 6 and 7); MR2 comprises high-amplitude, subparallel reflectors (Fig. 2); MR3 is characterized by parallel reflectors of variable amplitude with good lateral continuity (Fig. 2).

MR1 is overlying the acoustic basement at the western flank of Mergui Ridge (Fig. 4). It has a wedge-shaped geometry. The thinning of this unit towards the east and its reflector characteristics indicate deposition in a hemipelagic environment (Figs. 4 and 5). Deformation of MR1 is caused by numerous faults throughout the working area (Figs. 4–7). In the north, a section of MR1 sediments is exposed to the seafloor (Fig. 8a), indicating a recent erosive or non-depositional

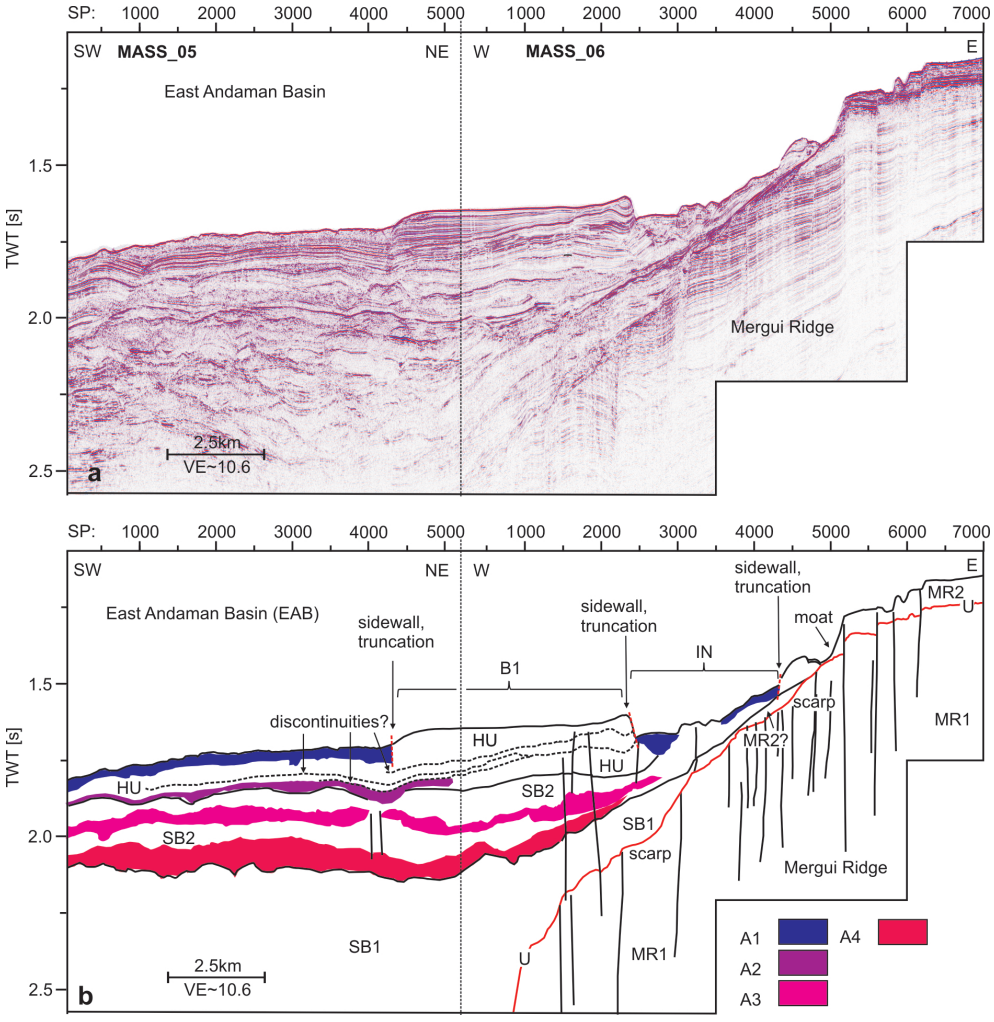

Fig. 5. (a) Seismic profiles MASS_05 and MASS_06, from the southern working area. **(b)** Interpretation of the profile, showing Mergui Ridge seismic units MR1 and MR2 in the east and basin sedimentary units SB1, SB2 and HU in the SE. The black lines mark boundaries of seismic units. The red line denotes the position of unconformity *U*. The vertical lines mark the positions of faults. The colored areas denote the position of MTDs within the basin sediments. The black dashed line marks discontinuities within the upper unit HU, indicative of drift deposits. B1 marks a stable block/slide margin, confined by steep sidewalls, and bordered by disturbed sediment bodies of superficial deposit MTD A1; "IN" indicates an incision in the sedimentary column. See Figs. 2 and 3 for the location of the profiles and text for further explanations.

environment at the western edge of Mergui Ridge. In this area, individual blocks have been displaced and faults are cutting through the surface. A smaller block is situated basinward of these deformed MR1 sediments. A pronounced erosive unconformity (*U*) bounds unit MR1 at its top. The unconformity is traceable on top of the Mergui Ridge (Figs. 4–7). In the southern working area, unconformity *U* can be traced westward into the East Andaman Basin (Figs. 4 and 5). To the north, where MR1 exhibits a more transparent/chaotic reflection pattern in its upper part, unconformity *U* is difficult to trace to the East Andaman Basin (Figs. 6 and 7). We interpret the chaotic reflection pattern of the upper part or MR1 as depositions of slope channels as such channels are visible in the bathymetric data of this area (Fig. 3). However, these depositions do not extent across the edge of Mergui Ridge. In addition, large-scale buried slope parallel channel incisions, reaching incision depths of up to ca. 200 m are identified in places within MR1 (Figs. 6 and 7). Such slope-parallel channels are identifiable from the bathymetry as well (Fig. 3).

Seismic unit MR2 is overlying the acoustic basement and unit MR1 on top of Mergui Ridge with a maximum thickness of around 100 m (Fig. 4). In places, it has an eroded irregular top with truncated reflectors (Fig. 5). This indicates an erosive phase between deposition of MR2 and the unit on top. MR2 is exposed to the seafloor at the edge of Mergui Ridge, forming an irregular topography (Figs. 5 and 6). Downslope of the edge of Mergui Ridge, eroded packages of MR2 seem

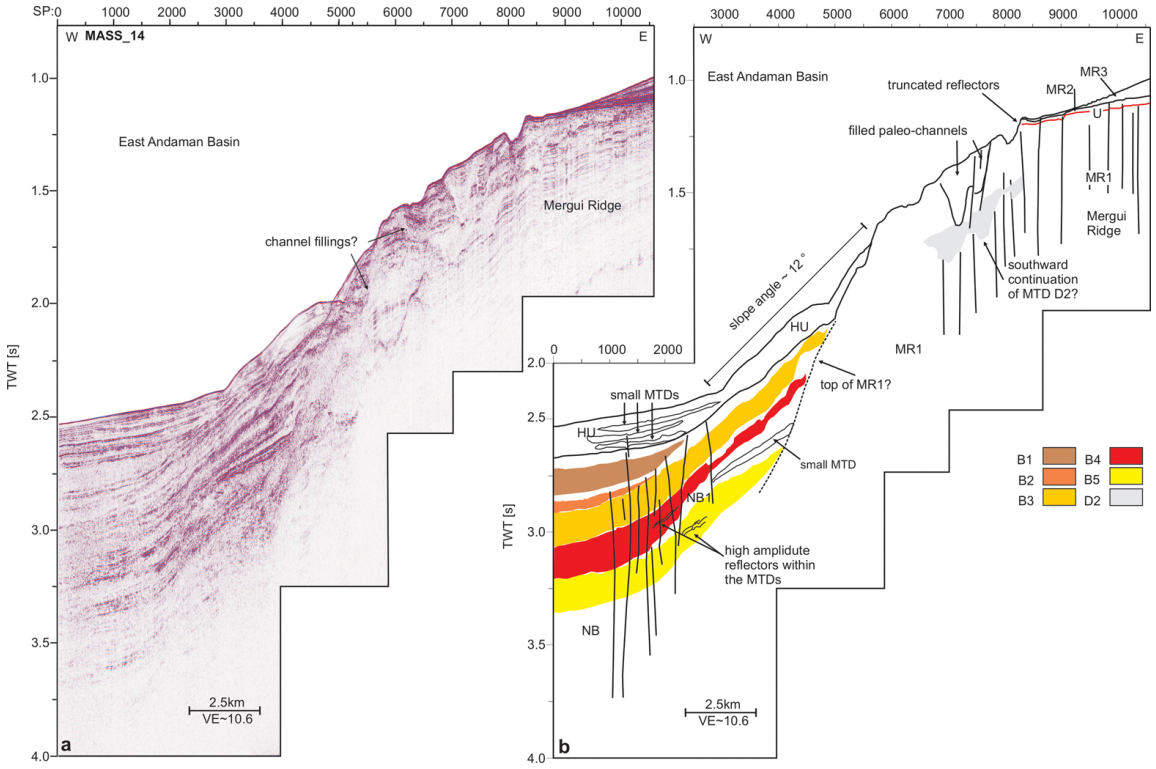

Fig. 6. (a) Seismic profile MASS_14, running across the basin-ridge transition in the northern working area, with channel-fillings indicated at the edge of Mergui Ridge. **(b)** Interpreted profile showing Mergui Ridge units MR1–MR3 in the east and basin sediments NB and HU in the west. The black lines mark boundaries between the seismic units. The red line denotes the position of unconformity *U*. The black stippled line marks the possible upper boundary of MR1. Channel fillings are present in the upper part of MR1. The reflectors of the upper Mergui Ridge units (MR2 and MR3) are truncated at the edge of the ridge. At the edge of the ridge a U-shaped structure is present, indicating an approximate slope parallel paleo-channel. The coloured areas mark the position of the stacked MTDs B1–B5 and a possible southward continuation of MTD D2. See text for further explanations and Figs. 2 and 3 for location of the profile.

to be present partially on top of the basinward continuation of unconformity *U* (Fig. 4).

Seismic unit MR3 is the youngest of the Mergui Ridge units. It is deposited on top of MR2. The thickness of this unit varies between about 120 m and 40 m; it is tapering out towards its seaward edge. Marginal valleys and mounded structures are present at the surface within MTD3 around the morphological highs on top of Mergui Ridge (Fig. 3).

4.1.2 East Andaman Basin South

Directly west of the Mergui Ridge lies the East Andaman Basin, which comprises water depths between 900 m and 2200 m. Sediments, infilling the East Andaman Basin, are resolved in the dataset to a subsurface depth of up to about 900 m. In the southern working area, we differentiate three seismic units within these basin sediments. SB1 is the oldest basin fill unit. It exhibits a disturbed acoustic character with reflectors of varying amplitude and continuity (Fig. 2). Towards its landward termination, the oldest basin fill unit SB1 is directly overlying MR1/MR2 sediments (Figs. 4 and 5).

SB1 is overlain by SB2. SB2 shows packages of well stratified, continuous to sub-continuous parallel reflectors of weak-to-moderate amplitudes, separated by pronounced reflectors of high amplitude (Fig. 2). Towards its upslope edge, SB1 onlaps against MR1/MR2 and it is confined by a moat (Figs. 4 and 5). Sediment waves are a characteristic feature of this up to 300 m thick unit (Fig. 4). Narrow vertical zones of low amplitude, crossing several reflectors, are evident within SB2 (Fig. 8b). These features may represent fluid migration pathways. At one location, a possible bottom simulating reflector (BSR) has been identified at subsurface depths around 80 m (Fig. 4c). The youngest unit HU, deposited on top of SB2, shows very regular, parallel, high-amplitude reflectors, with amplitude strengths increasing towards the seafloor (Fig. 2). Based on its reflector characteristics, it is interpreted as a hemipelagic deposit, which is undisturbed in most parts. Sediment waves have a topographic expression in this unit (Fig. 4). Towards the surface, a few zones with small scale faulting are evident within HU (Fig. 8b).

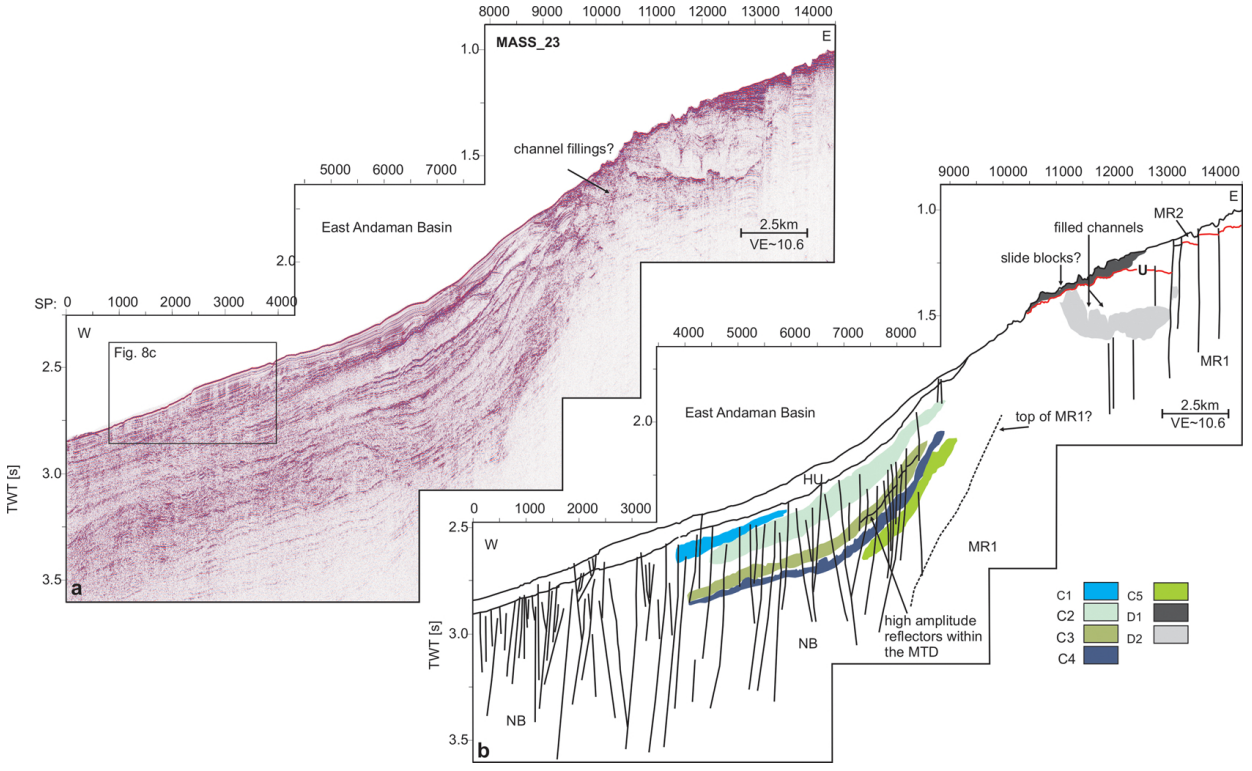

Fig. 7. (a) Slope normal seismic line MASS_23 from the basin ridge transition in the northern working area with channel fillings indicated at the edge of Mergui Ridge **(b)** Interpreted profile, showing seismic units of Mergui Ridge in the east (MR1, MR2) and seismic units of basin sediments in the west (HU, NB). The black lines indicate boundaries between units. The red line marks the position of unconformity *U*. The black dashed line marks a possible top boundary of MR1 towards the basin. The vertical lines indicate fault positions. The colored areas mark the stacked MTDs C1–C5 in the basin area and MTDs D1 and D2 on Mergui Ridge. See Figs. 2 and 3 for location of profile and text for further explanation.

4.1.3 East Andaman Basin North

We differentiated two seismic units within the northern basin sediments. The lower unit (NB) onlaps the Mergui Ridge unit MR1. Several bodies, characterized by transparent/low amplitude chaotic reflections are alternating with sediments imaged as high-amplitude reflections within NB (Figs. 6 and 7). Deformation of NB sediments is evident from numerous normal faults, dissecting the entire basin fill into blocks and leading to a rather disturbed appearance of NB (Fig. 7).

We did not correlate the lower units in the southern working area (SB1, SB2) and the lower unit in the north (NB). No seismic lines for direct lateral correlation are available. Although these units show similar characteristics, such as high amplitude reflectors alternating with low-amplitude packages, a clear correlation is not possible due to the disturbed character of NB and the lack of an internal boundary within NB, corresponding to the boundary between SB1 and SB2.

The older NB basin sediments in the north are overlain by an up to 200 m-thick hemipelagic unit characterized by parallel and fairly continuous/sub-continuous reflectors. The seismic character of this unit is very similar to the southern unit HU. Hence, we assume that this unit is the same and it is also labeled as HU (Figs. 6 and 7). HU is quite undisturbed, in contrast to the unit NB below it. However, some faults are cutting through HU to the surface. Along one of these faults, the seafloor is displaced by about 20 m (Fig. 8c). Seaward of this fault, the sediments show a wavy pattern (Fig. 8c). Vertical transparent zones, interpreted as potential fluid migration pathways, are present in the seismic unit HU (Fig. 8c)

4.2 Distribution and dimensions of mass transport deposits

Seventeen individual mass transport deposits (MTDs) were identified in the three different environments described above. Four MTDs are located in the southern basin area (MTD A1–A4), ten MTDs in the northern part (MTD B1–B5 and MTD C1–C5), and three MTDs on Mergui Ridge (MTD D1–D3). The positions of the MTDs, their boundaries and minimum areal extents, as far as they were traceable on the dataset, are illustrated on Fig. 3. The MTDs identified within the basin sediments (A1–A4, B1–B5, C1–C5) are generally characterized as lens- or wedge-shaped bodies, partially with a hummocky surface. They reveal

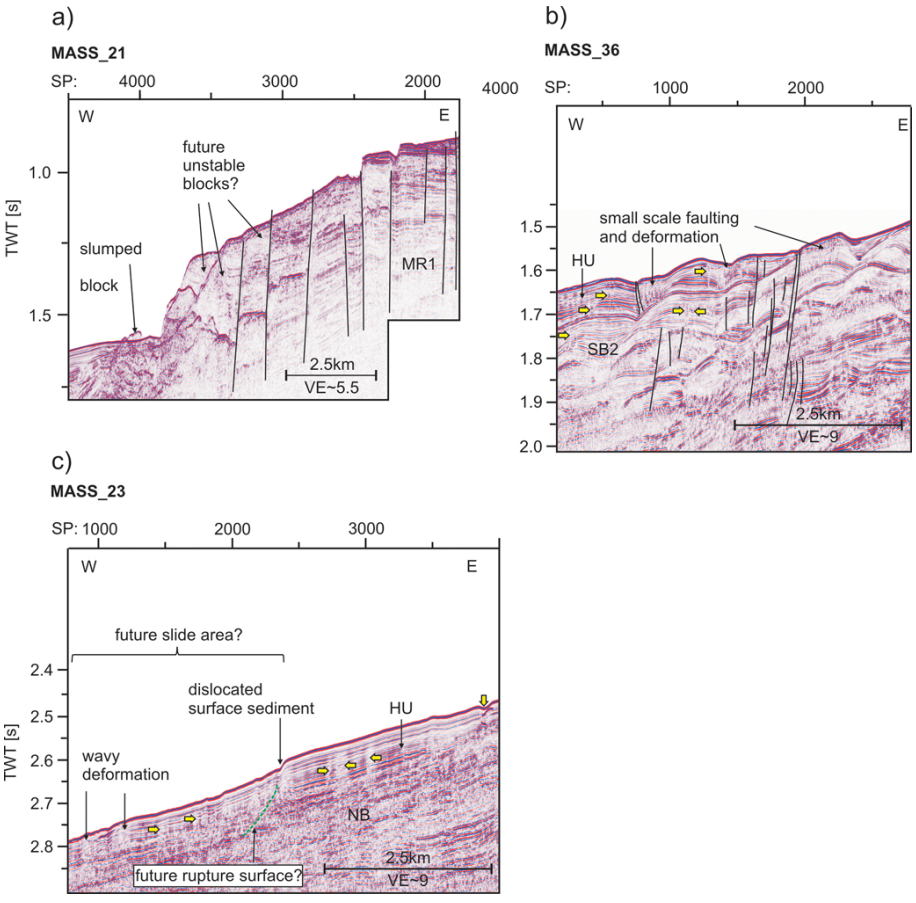

Fig. 8. Possible locations of future slope failures from the Mergui Ridge setting (MASS_23), the East Andaman Basin in the southern working area (MASS_36) and the East Andaman Basin in the northern working area. **(a)** Seismic profile from the edge of Mergui Ridge located slightly south of MTDs D1 and D2. Several faults, marked by black lines, cut to the surface and indicate recent deformation and dislocation of blocks. A small slumped block may indicate that some failure already occured. **(b)** Profile MASS_36 shows drift sediments from the southern working area. Fluid migration pathways are imaged in these sediments as transparent narrow vertical zones (yellow arrows). Small scale faulting and deformation of the upper sedimentary layers may indicate future failure of the drift deposits. **(c)** Seismic profile MASS_23 reveals numerous vertical transparent features interpreted as pathways for fluids (yellow arrows), and a fault dislocating the sea floor (green dotted line), that might act as future rupture surface. Wavy deformation of the surficial sediments downslope of this fault may indicate remobilization of the sediment. See Figs. 2 and 3 for location of profiles, and text for further explanations.

internal chaotic to transparent reflector characteristics (see Fig. 2 for examples of acoustic facies).

4.2.1 MTDs in the southern working area (A1–A4)

Four MTDs have been identified within basin sediments of unit SB2 and HU (A1–A4, Figs. 4 and 5) on the flank of the East Andaman Basin in the southern working area (see Fig. 2 for location). Estimated minimum volumes of these deposits range between 0.3 km^3 and 3 km^3 (Table 1).

At or close to the seafloor (Figs. 3, 4 and 5) we identified several bodies with disturbed internal structure, interpreted as MTDs. From our dataset we cannot clearly identify if these bodies are interconnected. As they occur in close proximity to each other and in the same stratigraphic depth, we interpreted them to belong to one failure event. Therefore, we include them all in MTD A1 for the volume estimation. Being situated at or very close to the seafloor, MTD A1 is likely one of the youngest mapped slide deposits. Within the MTD A1, partially sub-parallel reflections are preserved, indicating that movement of slide bodies caused only limited internal deformation (Fig. 4c). Individual bodies/lobes of MTD A1 are found east and southwest of an un-mobilized sediment block (B1 on Fig. 5). This block shows an undisturbed internal structure characteristic for units HU/SB2. It is truncated by steep, about 65 m–high sidewalls. Depending on the motion direction of the slides, B1 may represent a stable in-situ block within the slide area of MTD A1, or the margin of the slide (Fig. 3). Northeast of B1, a 700 m wide and up to 65 m deep incision, marked as IN in Fig. 5, is confined by truncated sidewalls at its eastern and western boundaries, which indicate erosion and removal of sediment.

This structure is interpreted as an evacuated area, which was most likely created during the failure of MTD A1. Disturbed small sediment bodies interpreted to belong to the MTD A1 are located inside the evacuated area. Volumes of MTD A1 deposits are estimated to be $\sim 1.3\,km^3$, which then is a minimum estimate for MTD A1.

MTD A2, A3 and A4 are buried mass transport deposits (Figs. 4 and 5) within seismic units HU and SB2. They are characterized by transparent to chaotic internal structures and hummocky tops. The boundaries of the individual MTDs are not easily detectable because of the overall low amplitude reflectors of the surrounding background sediment. MTD A4 is the largest slide body identified in the southern working area with an estimated volume of $3.0\,km^3$ (Figs. 4 and 5, Table 1).

4.2.2 MTDs in the northern working area (B1–B5 and C1–C5)

In the northern working area (see Fig. 2 for location), mass transport deposits were identified in two locations within seismic unit NB (Figs. 3, 6 and 7). In both settings, several stacked MTDs are located at the basin-slope transition (B1–B5 and C1–C5). Figure 3 shows positions and extents of the deposits as mapped out based on the available data set. Figure 2 gives examples of the acoustic characteristics of these bodies.

The seismic profile in Fig. 6 shows at least five stacked slide deposits (B1–B5), originating at or near the slope of Mergui Ridge within background sediments of unit NB. The volumes of the mapped parts of these deposits range from $0.3\,km^3$ to $3.4\,km^3$ (Table 1). The mapped slide bodies contain patches of higher amplitude reflections (Fig. 6). These reflections possibly result from un-deformed blocks within the MTDs. An alternative explanation for these higher amplitude reflections may be multiple failure events. The high amplitude reflectors may then represent boundaries between individual events. Several smaller MTDs are present in the vicinity of Mergui Ridge, predominantly in unit HU, but also in the deeper parts of the basin sedimentary succession (Fig. 6).

The MTDs C1–C5 (Fig. 7) are located within the same basin-slope transition setting as MTDs B1–B5 and they are also stacked slide deposits, but their thicknesses are smaller than those of B1–B5 (Table 1). It is also difficult to determine individual slide bodies at this location, because the background sediment in this part of the basin is generally disturbed and exhibits widespread irregular reflector characteristics. Hence, only chaotic to transparent areas without traceable reflectors were mapped as slide bodies. Volumes and depths are listed in Table 1.

4.2.3 MTDs on Mergui Ridge (D1–D3)

Estimated volumes of the MTDs identified in the Mergui Ridge setting (see Fig. 2 for location of setting and Fig. 3 for location of MTDs) range between $0.9\,km^3$ and $14\,km^3$ (Table 1). The individual MTDs exhibit very different characteristics in terms of external and internal structures.

MTD D1 consists of displaced sediment blocks with disturbed internal structure (Fig. 9). These blocks are located near the seafloor at the western edge of Mergui Ridge. The high amplitude reflectors inside these blocks show characteristics similar to those of MR2 sediments. This suggests that MTD D1 consists of remobilised MR2 sediment. The partly preserved stratification of the blocks implies that deformation was probably not strong and the blocks have not moved very far. As MTD D1 is situated close to the seafloor, its boundaries are deducible from seafloor morphology. The possible extent of MTD D1 therefore was deduced from the bathymetric dataset (Fig. 3).

MTD D2 is found within seismic unit MR1 (Figs. 7 and 9). Compared to the other MTDs, it shows a large maximum thickness of up to 230 m. The body of MTD D2 comprises blocks ranging from acoustic transparency to some weak internal sub-parallel layering. Its top is eroded (Figs. 7 and 9) and its slide toe is deformed (Fig. 9a). A possible rupture surface is located at the base of MTD D2 (Fig. 9). A steep depression in the seafloor morphology is located upslope of the head area of MTD D2 (Fig. 9b). This 75 m-deep incision is characterized by slope angles of up to 13.5°. The incision can also be identified on the bathymetry, where it shows an amphitheatric shape, typical for a landslide headwall (Fig. 3). The southern boundary of MTD D2 is not very clearly identifiable in the seismic dataset (Fig. 6); the MTD may therefore actually be larger than mapped.

MTD D3 is situated on the flat top of Mergui Ridge, interbedded in the strata of MR3 (Fig. 4). Due to its internal chaotic structure, we categorize it as a MTD, although no headwall or other indicators typical of slide deposits are observed. MTD D3 is traceable over a large part of the working area (about $580\,km^2$). Despite its large areal extent, it has a maximum thickness of about 60 m. MTD D3 comprises the largest volume of all identified MTDs (about $14\,km^3$). Erosive structures and channel fills at the top of MTD D3 imply that its original thickness may have been larger. Moreover, its eastward maximum extent may not be covered by our dataset, which also implies a larger original volume of the deposit.

4.3 Recurrence of failure events

Approximate time intervals between individual slide events (A1–A4, B1–B5, C1–C5) have been established for the MTDs in the southern and northern East Andaman Sea settings (see Fig. 3 for locations) following the approach described in Sect. 3. For the southern working area (A1–A4) they range between 940 ka and 1.19 Ma; for the northern working area between 220 ka and 1.47 Ma (B1–B5) and 370 and 950 ka (C1–C5), respectively (Table 2). For the MTDs on Mergui Ridge (D1–D3), no calculation of recurrence intervals have been established as information on sedimentation

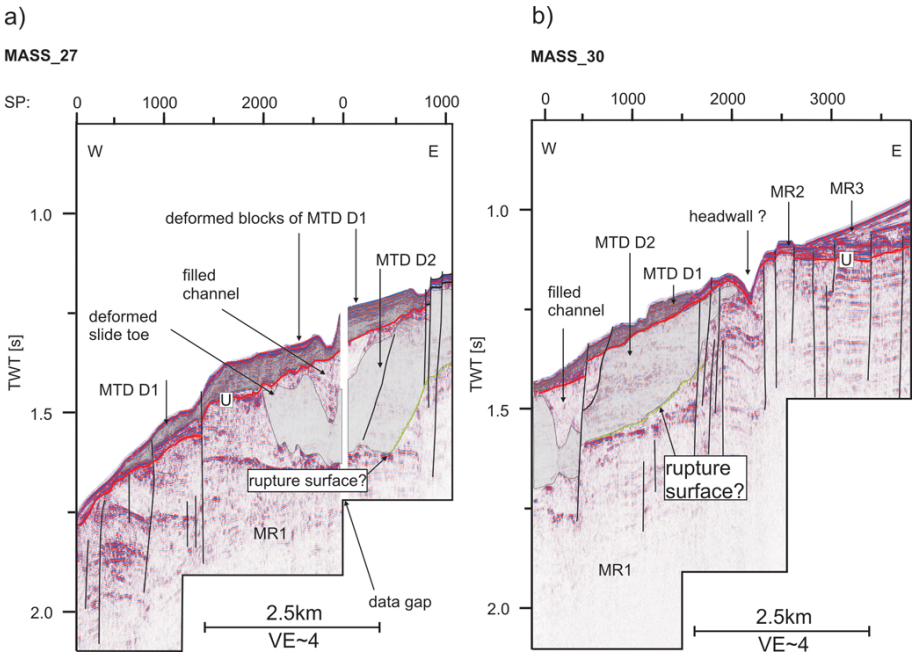

Fig. 9. Seismic profiles showing the edge of Mergui Ridge. The vertical lines indicate positions of faults. The red line marks unconformity *U*. **(a)** Deformed toe of MTD D2 (coloured in light grey). **(b)** Head area of D2 (coloured in light grey) with a steep scarp at its upper part, which may represent the modified head wall (see text for details). The green dotted line indicates the location of a possible rupture surface of D2. See Figs. 2 and 3 for the location of the profiles.

rates was not available. The subsurface depths of the uppermost MTDs in the northern working area range between 100 and 150 m for B1 and between 40 and 120 m for C1.

5 Discussion

5.1 General development and influences on background sedimentary units

5.1.1 Hemipelagic sedimentation

The reflector characteristics of the youngest seismic units HU and MR3 indicate recent hemipelagic sedimentation in the working area (Figs. 4–7). Main sedimentary components in the working area are derived from terrestrial detritus and biogenic production (Keller and Richards, 1967; Rodolfo, 1969; Colin et al., 1999). Regarding sediment type and sedimentation rates, there are differences between the area on top of Mergui Ridge and the downslope basin area of the East Andaman Basin. Whereas on top of the ridge, sediments mainly consist of foraminiferal oozes, silty clays prevail in the adjacent basin area (Keller and Richards, 1967; Rodolfo, 1969). The outer shelf of the Thai-Malay peninsula is described as sediment starved (Rodolfo, 1969; Andreason et al., 1997; Panchang et al., 2008). Rodolfo (1969) described relict foraminifera and relict corals in modern sediments of the Mergui area, implying that sedimentation rates on the Mergui Ridge are generally low and/or mainly related to biogenic input (Rodolfo, 1969). Left lateral movement along Ranong Fault (Fig. 1) is described as the cause for diversion of river systems towards the Gulf of Thailand and subsequently reduced riverine input from the Thai-Malay Peninsula since the Miocene (Andreason et al., 1997). Recent sediment starvation along the western outer shelf of the Thai-Malay peninsula is explained by Rao et al. (2005) to be due to the trapping of the Ayerawaddy riverine input in the Gulf of Martaban, and direct transfer into the deeper parts of the Andaman Sea by submarine canyons. Detritus delivered by via the Malacca Strait is also deposited only in the deeper parts of the Andaman Sea (Keller and Richards, 1967). Therefore, input of terrigenous material is largely restricted to the areas off the ridge, and sedimentation rates on top of the Mergui Ridge are low, whereas they are moderately high in the off-ridge part of the working area (around 10 cm ka^{-1}, Rodolfo, 1969, Fig. 1).

5.1.2 Sediments of Mergui Ridge

Comparison of our data set with data from the Mergui Basin (Fig. 1) east of Mergui Ridge (Polachan, 1988) suggests an approximate age of Lower Miocene for unit MR2, a large hiatus between units MR2 and MR3 and a Plio-Pleistocene age of unit MR3. MR1 reveals faulting at the western edge of Mergui Ridge (Fig. 4). Extensive faulting along the western flank of Mergui Ridge is explained by several authors by extension due to basin formation processes all over the Andaman Sea (Polachan et al., 1991; Curray, 2005; Jha et

al., 2010; Kishore et al., 2010; Morley et al., 2011). According to Morley et al. (2011), rifted sequences are deposited at the western flank of Mergui Ridge as a result of this extension. These late syn-rift deposits west of Mergui Ridge were probably deposited during formation of the East Andaman Basin in Late Oligocene/Early Miocene in an open-marine environment (Jha et al., 2010). As the deposition of MR1 clearly predates the Lower Miocene unit MR2, and its reflector characteristics indicate that the sediments are deposited in a hemipelagic environment, we speculate that the sediments of unit MR1 correspond to these synrift sequences and form an older eroded slope of Late Oligocene/Early Miocene age deposited in the marine environment that was prevailing in the area since Early Miocene (Jha et al., 2010). Younger sediments on top of Mergui Ridge (MR2/MR3) are not tectonically deformed.

5.1.3 Drift deposits in the East Andaman Basin and on top of the Mergui Ridge

Jha et al. (2011) described a post-rift sedimentary succession in the region directly west of our working area. They identified a lower sequence containing a chaotic seismic facies interpreted as mass flow complexes, and an upper sequence characterized by pelagic sedimentation since Late Miocene. This upper sequence is described to exhibit mass flow deposits in places and to be influenced by contour currents. Jha et al. (2011) attribute the mass flows within their lower sequence to subsidence in the East Andaman Basin caused by rifting in the Central Andaman Basin since Late Miocene. The presence of mass flows in their upper unit is attributed to disturbances due to modern sea-floor spreading in the Central Andaman Basin since Late Plio-Pleistocene. The sedimentary succession in the southern working area (SB1 and SB2, see Fig. 2 for location) reveals a pattern similar to that described by Jha et al. (2011). Seismic unit SB1, situated on top of the assumed synrift sediments of MR1, reveals largely disturbed sediments, possibly attributable to an older mass flow complex and correlatable to the mass flow unit described by Jha et al. (2011).

The unit SB2 comprises distinct low amplitude packages, separated by high amplitude reflectors. Sediment waves are present (Fig. 4). Rebesco and Stow (2001) described characteristics of elongated plastered drift deposits. Typical features are erosive moats at their boundaries and fields of migrating sediment waves within the deposits. Seismic characteristics of drift deposits comprise uniform low-to medium amplitude patterns (Nielsen et al., 2008). Moreover, discontinuities within drifts, marked by high amplitude reflectors, are common (Faugères et al., 1999). These criteria are met by seismic unit SB2 and we therefore interpret it as bottom current controlled sedimentary unit. SB2 may correlate to the upper, bottom current influenced unit of Jha et al. (2011). The approximate age of SB2 would then be Plio-Pleistocene.

Hérnandez-Molina et al. (2008) give examples of typical geometries of sediments deposits that develop around obstacles when bottom currents rework sediments. Regarding the current direction, a characteristic marginal valley may persist on the stoss side and a depositional tail on the lee side of the obstacle. Such structures have developed around the carbonate platforms in our working area, reworking sediments of unit MR3 (Fig. 3). We therefore conclude that bottom currents may act over a large part of the working area and influence the sediments on Mergui Ridge as well. In this context, the rugged morphology at the edge of the ridge may be attributed to erosive processes induced by bottom currents.

The presence of reversal currents in the Andaman Sea area is explained to be monsoon controlled (Wirtky, 1961). Such wind driven currents can extend to the bottom and induce sediment reworking (Hollister and McCave, 1984; Shanmugan, 2008). Northwest of our working area (Fig. 1b), a stable, monsoon-induced eddy/gyre is described by Varkey et al. (1996). Measurements revealed currents speeds of $12\,\mathrm{m\,s^{-1}}$ at 500 m and $10\,\mathrm{m\,s^{-1}}$ at 1000 m water depth (Varkey et al., 1996). In addition, internal waves and tides are able to influence deep-water bottom currents and their deposits (Shanmugan, 2008). Large amplitude internal waves have repeatedly been observed in the working area (Osburne and Burch, 1980; Nielsen et al., 2004b; Vlasenko and Alpers, 2005). They can affect the water column in the working area as deep as several hundred meters below the surface (Osburne and Burch, 1980; Nielsen et al., 2004b). Vlasenko and Alpers (2005) report in depths of up to 241 m interaction of internal waves with the Dreadnought Bank (see Fig. 1b for location). Such internal waves may be able to rework sediment (Pomar et al., 2012).

Although we do not have direct information on bottom currents, we suggest that the two processes described above may induce or influence bottom currents in our working area in the East Andaman Basin. Therefore, we interpret the character of units SB2 and HU in the southern working area and unit MR3 on top of Mergui Ridge as formed by reworking and deposition of currents.

5.1.4 Tectonically deformed sediments in the East Andaman Basin

The EAFZ is a strike slip fault zone west of the Mergui Ridge (Polachan et al., 1988; Polachan and Racey, 1994; Morley et al., 2011). Polachan (1988) reported branches of the EAFZ cutting through our working area (Fig. 3). Recent fault reactivation has been reported from the Mergui Fault north of the working area (Morley et al., 2011). Jintasearanee et al. (2012) interpreted steep NNE–SSW striking scarps in the bathymetry of our working as fault traces exposed at the sea floor. These observations let us infer that tectonic deformation in the working area is ongoing. The East Andaman Basin sediments in the northern working area (see Fig. 2 for location), especially the older deposits of seismic unit NB,

exhibit features of tectonic movement, such as the presence of numerous faults. Although the youngest basin unit HU exhibits an overall undisturbed character, a few faults cut through this unit in the northern working area (Figs. 7b and 8c). This pattern is in agreement with the description of recent deformation due to activity of fault zones near the working area, such as EAFZ and Mergui Fault.

5.2 Causes for slope instability

Causes for slope failures are manifold and may include (i) sedimentary processes, such as sedimentation at very high rates and resulting excess pore pressures, margin oversteepening, and the deposition/formation of weak layers; (ii) the presence of fluids and resulting overpressure; (iii) tectonic processes, such as fault activity and tectonic steepening; and (iv) cyclic loading by earthquakes (Hampton et al., 1996; Canals et al., 2004; Masson et al., 2006; Yamada et al., 2012 and references therein). The factors relevant for the survey area are discussed below.

5.2.1 Influence of sedimentation on slope stability

Slope channels can act as a sediment conduit from the shelf to the deep sea (Stow and Mayall, 2000). Erosion and oversteepening may also cause slope failure within canyons (Arzola et al., 2008). In our data, channels are mainly evident from the northern area and only directly at the edge of the Mergui Ridge (Figs. 3, 6 and 7). As sedimentation rates are low in the Mergui Ridge area and erosion takes place on the edge of Mergui Ridge (see above), we hypothesize that input of sediments by slope channels into the East Andaman basin may result from erosion of older sediments (MR1). The channels, however, seem to be restricted to the edge of the ridge, and no continuation of them has been detected in the basin sediments further downslope. Hence, we consider their influence on basin sedimentation and slope stability as small, but better data coverage of the basin would be needed to be confident about the distribution of canyons and their influences on slope stability. As sediment transport from the Mergui Ridge into the East Andaman Basin seems to be of minor importance and mainly results from erosion of older Mergui Ridge sediments, rapid sediment load and associated oversteepening and/or development of overpressure may play a role only in the deeper parts of the working area, basinward below the edge of Mergui Ridge (MTDs A1–C5). For the destabilization of sediments on top of Mergui Ridge (MTDs D1–D3) other preconditioning factors must be more important.

5.2.2 Tectonic influence: subsidence and fault controlled failures

Tilting of the slope due to subsidence of a margin can act as a preconditioning factor for slope failure (Masson et al., 2010). The Mergui Ridge has undergone subsidence since the onset of rifting in the Central Andaman Basin in Late Miocene (Kamesh Raju, 2005) due to dextral movement along EAFZ in Late Miocene (Jha et al., 2010) and/or due to thermal contraction (Morley et al., 2011). Jha et al. (2010) described large scale subsidence as a cause for the formation of mass flows west of our working area. These deposits may be correlatable to our seismic unit SB1 (see above). Recent subsidence rates from the shelf area of the Malacca Strait are in the range of $0.25\,\mathrm{mm\,a^{-1}}$ (Lin et al. (2010). This value is relatively small compared to areas with recent extension, for example the Corinth Basin with a subsidence rate of $1\,\mathrm{mm\,a^{-1}}$ (Lykousis et al., 2007). In addition, subsidence rates tend to decrease after termination of rifting (Prosser, 1993). Therefore, subsidence and steepening may still play a role for slope stability but its influence became probably smaller since the onset of rifting that created the large mass flows described by Jha et al. (2010).

The presence of faults has been suggested to act as controlling or preconditioning factor for slope failures (Dillon, 1993; Hampton, 1996; Anasetti et al., 2012). Except for the top unit HU, large parts of the basin fill sediments in the northern working area (unit NB, see Fig. 2 for location) are tectonically deformed. The MTDs C1–C5 and B1–B5 are located in this environment and we consider fault activity as one of the main reasons for slope failures in our working area. Episodic slope failure due to episodic fault activity has been described by Reicherter et al. (2011) to result in slide deposits interbedded in well stratified layers. A similar pattern can be observed for the MTDs in the northern working area (B1–B5 and C1–C5) (Figs. 6 and 7). Moreover, the MTDs B1–B5 seem to occur in stratigraphic depths similar to those of C1–C5. This would imply laterally contemporaneous failures in the northern working area. We therefore suggest that episodic fault activity was important for weakening the sediments along the slope.

Tectonic deformation may also play a role in development of MTDs on top of/at the edge of the Mergui Ridge (D1–D3), where sedimentation rates are low and oversteepening probably is not a preconditioning factor for slope failure. Surficial MTD D1 and buried MTD D2 are both located at the edge of the Mergui Ridge. Tectonic deformation of the top parts of unit MR1 may have caused the development of unstable blocks that were subsequently dislocated. Internal structures of these blocks are still preserved; therefore, run out distances of blocks seem to be small.

In conclusion, weakening of the sediments due to tectonic activity is considered as a main pre-conditioning factor for slope failure, especially at the basin-ridge transition.

5.2.3 Instable drift deposits

Drift deposits are present in the southern working area (see Fig. 2 for location). Laberg and Camerlenghi (2008) show an interrelation between contourite features and slope instabilities: Drifts generally tend to be prone to liquefaction during seismic loading due to good sorting of their particles and

resulting high porosity. High sedimentation rates in drift deposits may result in rapid loading and development of excess pore pressure. The development of excess pore pressure is further facilitated by gas migration, fueled by high organic matter input from productive water masses along continental margins. (Laberg and Camerlenghi, 2008). All these factors increase the susceptibility of drift sediments for failure (Laberg and Camerlenghi, 2008). Migrating fluids can especially cause build-up of excess pore pressure in upper sediment layers, a process which is well known to be capable for destabilizing slope sediments (Vorren et al., 1998; Stigall and Dugan, 2010). Sediments that build drift deposits in the southern working area contain terrigenous material from the Ayeyawady River and/or the Malacca Strait, whereas sediment input from the Mergui Ridge seems unlikely (see above). Off the ridge, sedimentation rates are high (10 cm ka^{-1}, Rodolfo, 1969). An unusually high content of terrestrial organic carbon has been reported for these sediments (Keller and Richards, 1967; Colin et al., 1999; Bird et al., 2008; Ramaswamy et al., 2008,), which may be favorable of formation of gas within the drift deposits. Jintasaeranee et al. (2012) reported gas-charged sediment at the Mergui Ridge slope area from subbottom profiler data (Fig. 3). Several possible gas migration pathways are imaged on our seismic data as vertical zones of acoustic transparency (see Fig. 8). A possible bottom simulating reflector (BSR) was identified in the southern working area (Fig. 4c). Therefore, we consider that build-up of excess pore-pressure due to migrating fluids and instability of drift deposits was an important pre-conditioning factor for the failure events in the southern working area (MTDs A1–A4).

5.2.4 Final trigger mechanism

An important factor for the formation and recurrence of submarine landslides is the presence of a final trigger leading to the failure of potentially unstable sediments (e.g. Masson et al., 2006). Seismic activity is common along the Sunda trench and also within the Andaman Sea (Lay et al., 2005; Ornthammarath et al., 2011; Khan, 2012; NGDC, Global Significant Earthquake Database, 2012). Neotectonic activities have been reported from many structures in the Andaman Sea, such as the modern spreading centre (Kamesh Raju et al., 2004), the Sagaing Fault (Wang et al., 2011), the Andaman Arc (Radhakrishna et al., 2008), or the West Andaman Fault (Kamesh Raju et al., 2007). Ongoing tectonic activity is also documented in our data as faults reaching the surface. Therefore, earthquakes are likely final triggers for slope failures.

In summary, several concurring factors have contributed to past slope failures. We consider migrating fluids, instability of drift sediments and tectonic activity as most important preconditioning factors. Regular earthquakes may act as final trigger for slope failure.

5.3 Recurrence of mass transport deposits

In the East Andaman Basin, several MTDs were detected at different stratigraphic depths at the basin-ridge transition. The stacking of MTDs in the East Andaman Basin sediments implies recurrent slide events. The ages and hence the recurrence rates for the slides in the working area are difficult to estimate. No age data are published; hence, direct age determinations are not possible. The thickness of undisturbed sediments between individual slide events can be used to estimate the recurrence rates of landslides if accumulation rates are known. However, information on accumulation rates in or close to the working area are sparse. The most reliable value is given by Rodolfo (1969), who suggested an average sedimentation rate of 10 cm ka^{-1} for the basin sediments west of Mergui Ridge. Using this accumulation rate and the mapped sediment thickness between individual slide deposits, calculations of recurrence rates result in values around 100 ka. We would like to point out that the estimates for landslide recurrence intervals contain very large error bars. This simple calculation, however, shows that recurrence rates are several 10 000 to 100 000 yr and not 100 to 1000 yr.

The values are similar for the different settings of the basin sediments. Only one slide in the basin area (MTD A1) is found close to or at the seafloor, while all other slides are deeply buried. However, the presence of several MTDs throughout the working area lets us deduce that landslides occurred repeatedly and that the slope area has been generally unstable and prone to failure.

5.4 Estimation of tsunamigenic potential and indicators for failure susceptibility

5.4.1 Past failures and likelihood of tsunamis

Important criteria that control the tsunamigenic potential of a landslide are volume, stiffness/cohesiveness of the slide material, water depth, and initial acceleration of the landslide (Løvholt et al., 2005; Haugen et al., 2005; Grilli and Watts, 2005; Ward, 2001; Greene et al., 2006). We have no knowledge on the initial acceleration and only sparse information on sediment properties, but we can analyse water depths and volumes of the identified MTDs leading to a qualitative assessment of the likelihood of tsunami generation in the past. Generally, the critical water depth for tsunami generation is given as maximum 1000 m, while the minimum volume sufficient to create a tsunami from a submarine landslide is $\sim 2\,km^3$ (Greene et al., 2006). We would like to point out these values can only be used as guidelines; large landslides in water depths deeper than 1000 m (Tappin et al., 2001) and small landslides ($< 2\,km^3$) in very shallow water (Rahiman et al., 2007) have triggered tsunamis in the past.

The volumes of the MTDs detected in our working area (0.3–14 km^3, Table 1) are small compared to giant landslides on active and passive margins, which may reach volumes

of several hundreds of cubic kilometers (Hühnerbach et al., 2004; Geersen et al., 2011; Krastel et al., 2012).

In the southern working area (see Fig. 2 for location), only one MTD (A4) comprises a volume $> 2\,km^3$ (Table 1), while the others are less than $2\,km^3$. The presence of discontinuities within background unit SB2 indicates erosive events. Such erosive events are common in drift deposits, due to short term changes of boundary conditions (Faugères et al., 1999). This implies that MTDs identified within SB2 may originally have been larger.

All MTDs in the southern area are located at water depths deeper than 1000 m. Subsidence in the working area is ongoing, but rates have been moderate since cessation of rifting, and therefore the water depth at the time of failure was most likely below 1000 m.

The situation is different for superficial MTD A1. Its source area (see depth of evacuated area IN, Fig. 5) is located at water depths around 1000 m. The mapped volume of MTD A1 is smaller than $2\,km^3$ (Table 1). However, the true extent of this MTD is not known and might be larger than $2\,km^3$. Therefore, MTD A1 may fall in the range of tsunamigenic landslides. In the northern working area, four slide deposits with volumes greater than $2\,km^3$ were found, but none of these MTDs shows a volume of more than $3.5\,km^3$ (MTDs B3, B4, C2 and C3, Table 1). As all of these slides are situated in water depths significantly deeper than 1000 m, it seems unlikely that the relatively small MTDs B3, B4, C2 or C3 triggered a tsunami.

On top of Mergui Ridge all detected MTDs (D1, D2 and D3) are located above/near 1000 m water depth, and MTD D2 and MTD D3 comprise volumes $> 2\,km^3$, whereas MTD D1 which is located near the surface, has a volume below $2\,km^3$ and therefore it has probably not been a tsunamigenic landslide.

MTD D2 comprises a volume of $4\,km^3$. Its toe region is deformed. Similar structures have been described by Frey-Martinez et al. (2006) to occur near the frontal ramp of slides that do not leave the scarp area and are frontally confined. A horseshoe incision is located on the landward side of this deposit (Fig. 3b). In contrast to most landslide scarps, this feature is more similar to an incision than a morphological step (Fig. 9b). The landward flank of the incision, however, is significantly higher than the seaward side. Such shapes of landslide scarps are reported from other areas. Krastel et al. (2011) suggest that such scarps were modified by post-failure processes, especially strong bottom currents. This seems plausible, as bottom currents are acting in the working area. Hence, we interpret the incision as headwall of MTD D2. This headwall is the location of slide initiation and located at around 830 m water depth. Therefore, D2 potentially falls in the range of tsunamigenic slides.

MTD D3 shows the largest (mapped) volume of the slides detected in our working area ($14\,km^3$, Table 1). MTD D3 has a somewhat outstanding position among the MTDs on Mergui Ridge. It is located within the tectonically undisturbed bottom current influenced unit MR3. A possible source area is not evident from our dataset. Although the conditions for slide initiation and evolution cannot be reconstructed, we can infer that this slide definitely falls in the range of tsunamigenic landslides.

5.4.2 Possible locations of future slope failures and their tsunamigenic potential

Three locations of possible future slope failures were identified in our data set. Slightly south of the location of MTD D2 (see Fig. 3 for location), faults cut through the seafloor (Fig. 8a). As fault reactivation and deformation in the region seems plausible, these deformed back rotated blocks may fail in the future. Moreover, a slumped block is located basinward of this deformed area, which may indicate, that some disintegration and failure already occurred. Masson et al. (2006) suggest that thick slide blocks with a steep headwall (rotational slides) might be particularly effective in tsunami generation even without large displacements. Therefore, future slope failures at this location in relatively shallow water depths between 700 m and 1100 m may definitively be tsunamigenic. Regarding MTD D3 that is also located on Mergui Ridge, we cannot reconstruct initiation or evolution of this MTD, as outlined above. However, we can infer that a potential future failure of the same dimensions at the same water depths of about 500–700 m definitely falls in the range of tsunamigenic landslides.

An area in water depths near 1000 m close to MTD A1 in the southern working area may be prone to future failures (Fig. 8b). Widespread sediment waves in combination with small scale faulting and indications for fluid migration pathways suggest a potentially unstable slope. Jintasaeranee et al. (2012) described numerous small scale failures in this area. Therefore, we conclude that future failures in this area are likely. A failure of significant volume of this part of the slope may be tsunamigenic. However, the area comprises large structural complexity and ongoing tectonic activity. Slope failures from areas with regular seismic activities are expected to be small in size, due to frequent triggers in the form of earthquakes, subsequently, not leaving sufficient time to accumulate large amounts of material for voluminous slides (Völker et al., 2009). Therefore, we would rather expect several small failures of individual sediment packages instead of voluminous failures. Hence, we consider the tsunami hazard emerging from this area as low.

Figure 8c shows an enlargement of the topmost sediment layers of profile MASS_23 in the northern working area. A listric fault cuts and dislocates parts of the superficial sediment of unit HU. This fault may be interpreted as possible future failure surface. Downslope of the surface expression of the fault, the sediment is deformed and destabilization may be indicated by the wavy deformation patterns visible on the seismic data. Migrating fluids may further contribute to future slope instability. However, within the northern working

area, all MTDs as well as the area of potential future slope failure are situated well below 1000 m water depth. Consequently, future slides in the northern part of the East Andaman Basin area may occur but probably do not pose a tsunami hazard.

In summary, the same settings that induced slope failures in the past may also lead to slope failure in the future, but only a few slides show volume and depth values typical for tsunamigenic slides. However, it has to be taken into account that our volume estimations are minimum values, as the lateral boundaries of the MTDs in most cases are not covered by the seismic dataset. Moreover, we cannot exclude a correlation between the stacked MTDs (B1–B5 and C1–C5) in the northern working area, as the settings where they occur show great similarity regarding characteristics, amount and architecture of the MTDs. This implies that more slides than outlined above may have triggered tsunamis in the past. However, even then their number would be small as suggested by the time intervals between the slides.

5.5 Recurrence of landslide tsunamis compared to earthquake tsunamis in the Andaman Sea

The Mergui Ridge–East Andaman Basin transition seems to be unstable and slides seem to occur repeatedly. Most of the identified slides are relatively small ($\sim 2\,km^3$) and occur at relatively large water depths (> 1000 m); hence, it is unlikely that these slides triggered significant tsunamis. Though numerous slides were found throughout the working area, their recurrence rate is definitely very long, exceeding 100 ka.

The recurrence rates of major tsunamigenic earthquakes occurring in the Sumatra–Andaman area, which triggered tsunamis also affecting the coast off Thailand, were estimated by Monecke et al. (2008). These authors analysed a 1000-yr sediment record off Northern Sumatra. They identified two older extensive sand sheets with similar sediment characteristics as the sand sheet deposited by the 2004 tsunami and concluded that the 2004 Indian Ocean tsunami is separated from its youngest full predecessor by ~ 600 yr. Similar values for major tsunamis are reported by Jankaew et al. (2008) for the Andaman Sea coast in Thailand suggesting recurrence rates of major earthquake tsunamis in the range of 400–600 yr for the Thai coast. Our estimations of time intervals between individual MTDs suggest that they are in the hundred ka to Ma range and only four potential tsunamigenic landslides were identified in the sedimentary record. Hence, the risk of submarine landslide tsunamis is negligible compared to earthquake-generated tsunamis. Landslide-triggered tsunamis, however, would hit the coast with almost no warning time.

6 Conclusions

We investigated the top and the western slope of Mergui Ridge and the Andaman Basin and found that older background sediments in the working area show clear indications for tectonic deformation and rifting processes, leading to extension and faulting. Younger sediments in the East Andaman Basin and on top of Mergui Ridge are mainly shaped by bottom currents.

Special attention was drawn to the occurrence of MTDs and the related tsunami hazard. Several MTDs as well as potential future slope failure locations were identified within sediments of the Mergui Ridge and East Andaman Basin. Generally, the slope area seems to be unstable and landslides occur repeatedly, mainly because of occurrence of potentially unstable drift sediments, the presence of fluids, and ongoing tectonic activity that produces deformation and generates earthquakes that are most likely the final trigger for the destabilization of the sediments.

Tsunami generation in the past by most of these slope failures is unlikely due to their relatively small size and their occurrence at large water depths. Recurrence rate of (tsunamigenic) landslides is small compared to the frequency of tsunamigenic earthquakes in the area. Hence, we consider the risk of landslide-generated tsunamis for the Thai west coast as very low. Triggering of tsunamis by submarine landslides, however, cannot be excluded, especially for slope instabilities at the edge of or on top of Mergui Ridge, and such a tsunami would hit the Thai coast almost without warning time.

Acknowledgements. We thank the scientists and crew of MASS III cruise for their help in collecting the data. Logistic support by the Phuket Marine Biological Center and the Thailand Southeast Asia START Regional Center is greatly appreciated. We thank Deniz Cukur for his support during seismic data analysis. Constructive reviews by Aggeliki Georgiopoulou and an anonymous reviewer significantly improved the quality of the manuscript. Our work is funded in the frame of German-Thai TRIAS-project funded by the Deutsche Forschungsgemeinschaft (Grant KR2222-8) and the National Research Council of Thailand (NRCT).

The service charges for this open access publication have been covered by a Research Centre of the Helmholtz Association.

Edited by: K. Schwarzer
Reviewed by: A. Georgiopoulou and one anonymous referee

References

Anasetti, A., Winkelmann, D., Krastel, S., Bialas, J., and Brückmann, W.: The BGR slide off Costa Rica: Preconditioning factors, trigger, and slide dynamics, in: Submarine mass movements and their consequences, edited by: Yamada, Y., Kawamura, K., Ikehara, K., Ogawa, Y., Urgeles, R., Mosher, D., Chaytor, J., and Strasser, M., Advances in natural and technological hazards research, Springer, Netherlands, 289–299, 2012.

Andreason, W. M., Mudford, B., and Onge, E. S. J.: Geologic evolution and petroleum system of the Thailand Andaman Sea basins, in: Indonesian Petroleum Association Proceedings of the Petroleum System of SE Asia and Australasia Conference, May 1997, 337–350, 1997.

Arzola, R. G., Wynn, R. B., Lastras, G., Masson, D. G., and Weaver, P. P. E.: Sedimentary features and processes in the Nazaré and Setúbal submarine canyons, west Iberian margin, Mar. Geol., 250, 64–88, doi:10.1016/j.margeo.2007.12.006, 2008.

Becker, J. J., Sandwell, D. T., Smith, W. H. F., Braud, J., Binder, B., Depner, J., Fabre, D., Factor, J., Ingalls, S.,Kim, S-H., Ladner, R., Marks, K., Nelson, S., Pharaoh, A., Trimmer, R., Von Rosenberg, J., Wallace, G., and Weatherall,P.: Global Bathymetry and Elevation Data at 30 Arc Seconds Resolution: SRTM30_PLUS, Mar. Geod., 32, 4, 355–371, doi:10.1080/01490410903297766, 2009.

Bird, M. I., Robinson, R. A. J., Win Oo, N., Maung Aye, M., Lu, X. X., Higgitt, D. L., Swe, A., Tun, T., Lhaing Win, S., Sandar Aye, K., Mi Mi Win, K., and Hoey, T. B.: A preliminary estimate of organic carbon transport by the Ayeyarwady (Irrawaddy) and Thanlwin (Salween) rivers of Myanmar, Quaternary Int., 186, 113–122, doi:10.1016/j.quaint.2007.08.003, 2008.

Biscontin, G., Pestana, J. M., and Nadim, F.: Seismic triggering of submarine slides in soft cohesive soil deposits, Mar. Geol., 203, 341–354, doi:10.1016/s0025-3227(03)00314-1, 2004.

Blewitt, G., Kreemer, C., Hammond, W. C., Plag, H.-P., Stein, S., and Okal, E.: Rapid determination of earthquake magnitude using GPS for tsunami warning systems, Geophys. Res. Lett., 33, L11309, doi:10.1029/2006gl026145, 2006.

Bondevik, S., Svendsen, J. I., and Mangerud, J.: Tsunami sedimentary facies deposited by the Storegga tsunami in shallow marine basins and coastal lakes, western Norway, Sedimentology, 44, 1115–1131, doi:10.1046/j.1365-3091.1997.d01-63.x, 1997.

Bondevik, S., Mangerud, J., Dawson, S., Dawson, A. G., and Lohne, O.: Record-breaking height for 8000-year-old tsunami in the North Atlantic, EOS, Transactions American Geophysical Union, 84, 289–293, 2003.

Bondevik, S., Løvholt, F., Harbitz, C., Mangerud, J., Dawson, A., and Inge Svendsen, J.: The Storegga slide tsunami–comparing field observations with numerical simulations, Mar. Petrol. Geol., 22, 195–208, 2005.

Brune, S., Babeyko, A. Y., and Sobolev, S. V.: Are tilt measurements useful in detecting tsunamigenic submarine landslides?, Geochem. Geophy. Geosy., 10, Q06002, doi:10.1029/2009gc002491, 2009.

Brune, S., Babeyko, A., Gaedicke, C., and Ladage, S.: Hazard assessment of underwater landslide-generated tsunamis: A case study in the Padang region, Indonesia, Nat. Hazards, 53, 205–218, doi:10.1007/s11069-009-9424-x, 2010.

Buranapratheraprat, A., Laongmanee, P., Sukramongkol, N., Prommas, R., Promjinda, S., and Yanagi, T.: Upwelling induced by meso-scale cyclonic eddies in the Andaman Sea, Coast. Mar. Sci., 34, 68–73, 2010.

Canals, M., Lastras, G., Urgeles, R., Casamor, J. L., Mienert, J., Cattaneo, A., De Batist, M., Haflidason, H., Imbo, Y., Laberg, J. S., Locat, J., Long, D., Longva, O., Masson, D. G., Sultan, N., Trincardi, F., and Bryn, P.: Slope failure dynamics and impacts from seafloor and shallow sub-seafloor geophysical data: Case studies from the COSTA project, Mar. Geol., 213, 9–72, 2004.

Chakraborty, P. P. and Khan, P. K.: Cenozoic geodynamic evolution of the Andaman–Sumatra subduction margin: Current understanding, Isl. Arc, 18, 184–200, doi:10.1111/j.1440-1738.2008.00643.x, 2009.

Colin, C., Turpin, L., Bertaux, J., Desprairies, A., and Kissel, C.: Erosional history of the Himalayan and Burman ranges during the last two glacial-interglacial cycles, Earth Planet. Sc. Lett., 171, 647–660, 1999.

Curray, J. R.: Tectonics and history of the Andaman Sea region, J. Asian Earth Sci., 25, 187–232, 2005.

Dawson, A. G., Long, D., and Smith, D. E.: The Storegga slides: Evidence from eastern Scotland for a possible tsunami, Mar. Geol., 82, 271–276, 1988.

Dillon, W. P., Risch, J. S., Scanlon, K. M., Valentine, P. C., and Huggett, Q. J.: Ancient crustal fractures control the location and size of collapsed blocks at the Blake escarpment, east of Florida, in: Submarine landslides: Selected Studies in the U.S. Exclusive Economic Zone, edited by: Schwab, W. C., Lee, H. J., and Twichell, D. C., US Geological Survey Bulletin, 54–59, 1993.

Doust, H. and Noble, R. A.: Petroleum systems of Indonesia, Mar. Petrol. Geol., 25, 103–129, doi:10.1016/j.marpetgeo.2007.05.007, 2008.

Doust, H. and Sumner, H. S.: Petroleum systems in rift basins – a collective approach in southeast Asian basins, Petrol. Geosci., 13, 127–144, doi:10.1144/1354-079307-746, 2007.

Dutta, K., Bhushan, R., and Somayajulu, B. L. K.: Rapid vertical mixing rates in deep waters of the Andaman Basin, Sci. Total Environ., 384, 401–408, doi:10.1016/j.scitotenv.2007.04.041, 2007.

Faugères, J.-C., Stow, D. A. V., Imbert, P., and Viana, A.: Seismic features diagnostic of contourite drifts, Mar. Geol., 162, 1–38, doi:10.1016/s0025-3227(99)00068-7, 1999.

Fine, I. V., Rabinovich, A. B., Bornhold, B. D., Thomson, R. E., and Kulikov, E. A.: The Grand Banks landslide-generated tsunami of November 18, 1929: Preliminary analysis and numerical modeling, Mar. Geol., 215, 45–57, 2005.

Frey-Martínez, J., Cartwright, J., and James, D.: Frontally confined versus frontally emergent submarine landslides: A 3D seismic characterisation, Mar. Petrol. Geol., 23, 585–604, doi:10.1016/j.marpetgeo.2006.04.002, 2006.

Fujino, S., Naruse, H., Matsumoto, D., Jarupongsakul, T., Sphawajruksakul, A., and Sakakura, N.: Stratigraphic evidence for pre-2004 tsunamis in southwestern Thailand, Mar. Geol., 262, 25–28, 2009.

GEBCO 2008: General Bathymetric Chart of the Oceans (GEBCO), available at: http://www.bodc.ac.uk/data/onlinedelivery/gebco/, last access: 28 June 2012.

Geersen, J., Völker, D., Behrmann, J. H., Reichert, C., and Krastel, S.: Pleistocene giant slope failures offshore Arauco peninsula, southern Chile, J. Geol. Soc. London, 168, 1237–1248, doi:10.1144/0016-76492011-027, 2011.

Greene, H. G., Murai, L. Y., Watts, P., Maher, N. A., Fisher, M. A., Paull, C. E., and Eichhubl, P.: Submarine landslides in the Santa Barbara Channel as potential tsunami sources, Nat. Hazards Earth Syst. Sci., 6, 63–88, doi:10.5194/nhess-6-63-2006, 2006.

Grilli, S. T. and Watts, P.: Tsunami generation by submarine mass failure, I: Modeling, experimental validation, and sensitivity analyses, J. Waterw. Port C.-ASCE, 131, 283–297, 2005.

Grilli, S. T., Taylor, O.-D. S., Baxter, C. D. P., and Maretzki, S.: A probabilistic approach for determining submarine landslide tsunami hazard along the upper east coast of the United States, Mar. Geol., 264, 74–97, 2009.

Hall, R. and Morley, C. K.: Sundaland basins, in: Continent-Ocean Interactions within the East Asian Marginal Seas, edited by: Clift, P., Wang, P., Kuhnt, W., and Hayes, D., American Geophysical Union, Geophysical Monograph, 149, Washington DC, 55–85, 2004.

Hampton, M. A., Lee, H. J., and Locat, J.: Submarine landslides, Rev. Geophys., 34, 33–59, doi:10.1029/95rg03287, 1996.

Harbitz, C. B., Lovholt, F., Pedersen, G., and Masson, D. G.: Mechanisms of tsunami generation by submarine landslides: A short review, Norw. J. Geol., 86, 255–264, 2006.

Hasegawa, H. S. and Kanamori, H.: Source mechanism of the magnitude 7.2 Grand Banks earthquake of November 1929: Double couple or submarine landslide?, B. Seismol. Soc. Am., 77, 1984–2004, 1987.

Haugen, K. B., Løvholt, F., and Harbitz, C. B.: Fundamental mechanisms for tsunami generation by submarine mass flows in idealised geometries, Mar. Petrol. Geol., 22, 209–217, 2005.

Hernández-Molina, F. J., Maldonado, A., and Stow, D. A. V.: Abyssal plain contourites, in: Contourites, Developments in Sedimentology, edited by: Rebesco, M. and Camerlenghi, A., Elsevier, Amsterdam, Netherlands, 345–378, 2008.

Hollister, C. D. and McCave, I. N.: Sedimentation under deep-sea storms, Nature, 309, 220–225, 1984.

Hühnerbach, V. and Masson, D. G.: Landslides in the North Atlantic and its adjacent seas: An analysis of their morphology, setting and behaviour, Mar. Geol., 213, 343–362, doi:10.1016/j.margeo.2004.10.013, 2004.

Hyder, P., Jeans, D. R. G., Cauquil, E., and Nerzic, R.: Observations and predictability of internal solitons in the northern Andaman Sea, Appl. Ocean Res., 27, 1–11, doi:10.1016/j.apor.2005.07.001, 2005.

Jankaew, K., Atwater, B. F., Sawai, Y., Choowong, M., Charoentitirat, T., Martin, M. E., and Prendergast, A.: Medieval forewarning of the 2004 Indian Ocean tsunami in Thailand, Nature, 455, 1228–1231, 2008.

Jansen, E., Befring, S., Bugge, T., Eidvin, T., Holtedahl, H., and Sejrup, H. P.: Large submarine slides on the norwegian continental margin: Sediments, transport and timing, Mar. Geol., 78, 77–107, doi:10.1016/0025-3227(87)90069-7, 1987.

Jha, P., Ros, D., degli Alessandrini, A., and Kishore, M.: Speculative petroleum system and play model of East Andaman Basin from regional geology and basin evolution concepts: Addressing the exploration challenges of an extreme frontier area, 8th Biennial International Conference and Exposition on Petroleum Geophysics, Hyderabad, India, P-261, 2010.

Jha, P., Ros, D., and Kishore, M.: Seismic and sequence stratigraphic framework and depositional architecture of shallow and deepwater postrift sediments in East Andaman Basin: An overview, GeoIndia 2011, Greater Noida, New Dheli, India, 12–14 January, 2011.

Jintasaeranee, P., Weinrebe, W., Klaucke, I., Snidvongs, A., and Flueh, E. R.: Morphology of the Andaman outer shelf and upper slope of the Thai exclusive economic zone, J. Asian Earth Sci., 46, 78–85, doi:10.1016/j.jseaes.2011.11.003, 2012.

Kamesh Raju, K. A.: Three-phase tectonic evolution of the Andaman Backarc Basin, Curr. Sci. India, 89, 1932–1937, http://drs.nio.org/drs/handle/2264/339, 2005.

Kamesh Raju, K. A., Ramprasad, T., Rao, P. S., Ramalingeswara Rao, B., and Varghese, J.: New insights into the tectonic evolution of the Andaman Basin, northeast Indian Ocean, Earth Planet. Sc. Lett., 221, 145–162, 2004.

Kamesh Raju, K. A., Murty, G. P. S., Amarnath, D., and Kumar, M. L. M.: The West Andaman Fault and its influence on the aftershock pattern of the recent megathrust earthquakes in the Andaman-Sumatra region, Geophys. Res. Lett., 34, L03305, doi:10.1029/2006gl028730, 2007.

Keller, G. H. and Richards, A. F.: Sediments of the Malacca Strait, Southeast Asia, J. Sediment. Res., 37, 102–127, doi:10.1306/74d7166d-2b21-11d7-8648000102c1865d, 1967.

Khan, A.: Seismogenic sources in the bay of bengal vis-à-vis potential for tsunami generation and its impact in the northern bay of bengal coast, Nat. Hazards, 61, 1127–1141, doi:10.1007/s11069-011-9970-x, 2012.

Kishore, M., Jha, P., and Ros, D.: Structural modeling and seismic attributes analysis of synrift sequences in East Andaman Basin: A qualitative approach towards fault seal analysis in a frontier exploration area, 8th Biennial International Conference and Exposition on Petroleum Geophysics, Hyderabad, India, P-262, 2010.

Krastel, S., Wefer, G., Hanebuth, T., Antobreh, A., Freudenthal, T., Preu, B., Schwenk, T., Strasser, M., Violante, R., Winkelmann, D., and M78/3 shipboard scientific party: Sediment dynamics and geohazards off Uruguay and the de la Plata River region (northern Argentina and Uruguay), Geo-Mar. Lett., 31, 271–283, doi:10.1007/s00367-011-0232-4, 2011.

Krastel, S., Wynn, R. B., Georgiopoulou, A., Geersen, J., Henrich, R., Meyer, M., and Schwenk, T.: Large-scale mass wasting on the Northwest African continental margin: Some general implications for mass wasting on passive continental margins, in: Submarine mass movements and their consequences, edited by: Yamada, Y., Kawamura, K., Ikehara, K., Ogawa, Y., Urgeles, R., Mosher, D., Chaytor, J., and Strasser, M., Advances in natural and technological hazards research, Springer, Netherlands, 189–199, 2012.

Kulikov, E. A., Rabinovich, A. B., Thomson, R. E., and Bornhold, B. D.: The landslide tsunami of November 3, 1994, Skagway Harbor, Alaska, J. Geophys. Res., 101, 6609–6615, doi:10.1029/95jc03562, 1996.

Laberg, J. S. and Camerlenghi, A.: The significance of contourites for submarine slope stability, in: Contourites, Developments in sedimentology, edited by: Rebesco, M., and Camerlenghi, A., Elsevier, Amsterdam, Nertherlands, 537–556, 2008.

Lay, T., Kanamori, H., Ammon, C. J., Nettles, M., Ward, S. N., Aster, R. C., Beck, S. L., Bilek, S. L., Brudzinski, M. R., Butler, R., DeShon, H. R., Ekström, G., Satake, K., and Sipkin, S.: The great Sumatra-Andaman earthquake of 26 December 2004, Science, 308, 1127–1133, doi:10.1126/science.1112250, 2005.

Lin, Y.-n. N., Sieh, K., and Stock, J.: Submarine landslides along the Malacca Strait-Mergui Basin shelf margin: Insights from sequence-stratigraphic analysis, J. Geophys. Res., 115, B12102, doi:10.1029/2009jb007050, 2010.

Lomax, A., Michelini, A., and Piatanesi, A.: An energy-duration procedure for rapid determination of earthquake magnitude and tsunamigenic potential, Geophys. J. Int., 170, 1195–1209, doi:10.1111/j.1365-246X.2007.03469.x, 2007.

Løvholt, F., Harbitz, C. B., and Haugen, K. B.: A parametric study of tsunamis generated by submarine slides in the Ormen Lange/Storegga area off western Norway, Mar. Petrol. Geol., 22, 219–231, doi:10.1016/j.marpetgeo.2004.10.017, 2005.

Lykousis, V., Sakellariou, D., Moretti, I., and Kaberi, H.: Late Quaternary basin evolution of the Gulf of Corinth: Sequence stratigraphy, sedimentation, fault–slip and subsidence rates, Tectonophysics, 440, 29–51, doi:10.1016/j.tecto.2006.11.007, 2007.

Masson, D. G., Harbitz, C. B., Wynn, R. B., Pedersen, G., and Lovholt, F.: Submarine landslides: Processes, triggers and hazard prediction, Philos. T. R. Soc. A, 364, 2009–2039, doi:10.1098/rsta.2006.1810, 2006.

Masson, D. G., Wynn, R. B., and Talling, P. J.: Large landslides on passive continental margins: Processes, hypotheses and outstanding questions, in: Submarine mass movements and their consequences, edited by: Mosher, D. C., Moscardelli, L., Baxter, C. D. P., Urgeles, R., Shipp, R. C., Chaytor, J. D., and Lee, H. J., Advances in natural and technological hazards research, Springer, Netherlands, 153–165, 2010.

Matsumoto, T. and Tappin, D. R.: Possible coseismic large-scale landslide off the northern coast of Papua New Guinea in July 1998: Geophysical and geological results from SOS cruises, Pure Appl. Geophys., 160, 1923–1943, 2003.

Michel, G. W., Yu, Y. Q., Zhu, S. Y., Reigber, C., Becker, M., Reinhart, E., Simons, W., Ambrosius, B., Vigny, C., Chamot-Rooke, N., Le Pichon, X., Morgan, P., and Matheussen, S.: Crustal motion and block behaviour in SE-Asia from GPS measurements, Earth Planet. Sc. Lett., 187, 239–244, doi:10.1016/s0012-821x(01)00298-9, 2001.

Monecke, K., Finger, W., Klarer, D., Kongko, W., McAdoo, B. G., Moore, A. L., and Sudrajat, S. U.: A 1,000-year sediment record of tsunami recurrence in northern Sumatra, Nature, 455, 1232–1234, doi:10.1038/nature07374, 2008.

Morley, C. K.: A tectonic model for the Tertiary evolution of strike-slip faults and rift basins in SE Asia, Tectonophysics, 347, 189–215, doi:10.1016/s0040-1951(02)00061-6, 2002.

Morley, C. K., Woganan, N., Sankumarn, N., Hoon, T. B., Alief, A., and Simmons, M.: Late Oligocene-recent stress evolution in rift basins of northern and central Thailand: Implications for escape tectonics, Tectonophysics, 334, 115–150, doi:10.1016/s0040-1951(00)00300-0, 2001.

Morley, C. K., Charusiri, P., and Watkinson, I.: Structural geology of Thailand during the Cenozoic, in: The geology of Thailand, edited by: Barber, A. J. and Ridd, F. D., Geological Society of London, London, United Kingdom, 539–571, 2011.

National Geophysical Data Center/World Data Center (NGDC/WDC), Significant Earthquake Database, Boulder, CO, USA, available at: http://www.ngdc.noaa.gov/nndc/struts/form?t=101650\&s=1\&d=1, last access: 28 June 2012.

National Geophysical Data Center/World Data Center (NGDC/WDC), Global Historical Tsunami Database, Boulder, CO, USA, available at: http://www.ngdc.noaa.gov/hazard/tsu_db.shtml, last access: 28 June 2012.

Nielsen, C., Chamot-Rooke, N., and Rangin, C.: From partial to full strain partitioning along the Indo-Burmese hyper-oblique subduction, Mar. Geol., 209, 303–327, doi:10.1016/j.margeo.2004.05.001, 2004a.

Nielsen, T. G., Bjørnsen, P. K., Boonruang, P., Fryd, M., Hansen, P. J., Janekarn, V., Limtrakulvong, V., Munk, P., Hansen, O. S., Satapoomin, S., Sawangarreruks, S., Thomsen, H. A., and Østergaard, J. B.: Hydrography, bacteria and protist communities across the continental shelf and shelf slope of the Andaman Sea (NE Indian Ocean), Mar. Ecol. Prog. Ser., 274, 69–86, doi:10.3354/meps274069, 2004b.

Nielsen, T., Knutz, P. C., and Kuijpers, A.: Seismic expression of contourite depositional systems, in: Contourites, Developments in sedimentology, edited by: Rebesco, M. and Camerlenghi, A., Elsevier, Amsterdam, Netherlands, 301–321, 2008.

Okubo, A., Obata, H., Nozaki, Y., Yamamoto, Y., and Minami, H.: 230th in the Andaman Sea: Rapid deep-sea renewal, Geophys. Res. Lett., 31, L22306, doi:10.1029/2004gl020226, 2004.

Ornthammarath, T., Warnitchai, P., Worakanchana, K., Zaman, S., Sigbjörnsson, R., and Lai, C.: Probabilistic seismic hazard assessment for Thailand, B. Earthq. Eng., 9, 367–394, doi:10.1007/s10518-010-9197-3, 2011.

Osborne, A. R. and Burch, T. L.: Internal solitons in the Andaman Sea, Science, 208, 451–460, doi:10.1126/science.208.4443.451, 1980.

Panchang, R., Nigam, R., Raviprasad, G. V., Rajagopalan, G., Ray, D. K., and Hla, U. K. Y.: Relict faunal testimony for sea-level fluctuations off Myanmar (Burma), J. Palaeon. Soc. India, 53, 185–195, 2008.

Piper, D. J. W., Cochonat, P., and Morrison, M. L.: The sequence of events around the epicentre of the 1929 Grand Banks earthquake: Initiation of debris flows and turbidity current inferred from sidescan sonar, Sedimentology, 46, 79–97, 1999.

Polachan, S.: The geological evolution of the Mergui Basin SE Andaman area, Thailand, Ph.D thesis, University of London, London, 218 pp., 1988.

Polachan, S. and Racey, A.: Stratigraphy of the Mergui Basin, Andaman Sea: Implications for petroleum exploration, J. Petrol. Geol., 17, 373–406, doi:10.1111/j.1747-5457.1994.tb00147.x, 1994.

Polachan, S., Pradidtan, S., Tongtaow, C., Janmaha, S., Intarawijitr, K., and Sangsuwan, C.: Development of cenozoic basins in thailand, Mar. Petrol. Geology, 8, 84–97, doi:10.1016/0264-8172(91)90047-5, 1991.

Pomar, L., Morsilli, M., Hallock, P., and Bádenas, B.: Internal waves, an under-explored source of turbulence events in the sedimentary record, Earth-Sci. Rev., 111, 56–81, doi:10.1016/j.earscirev.2011.12.005, 2012.

Prosser, S.: Rift-related linked depositional systems and their seismic expression, Geological Society, London, Special Publications, 71, 35–66, doi:10.1144/gsl.sp.1993.071.01.03, 1993.

Radhakrishna, M., Lasitha, S., and Mukhopadhyay, M.: Seismicity, gravity anomalies and lithospheric structure of the Andaman Arc, NE Indian Ocean, Tectonophysics, 460, 248–262, doi:10.1016/j.tecto.2008.08.021, 2008.

Rahiman, T. I. H., Pettinga, J. R., and Watts, P.: The source mechanism and numerical modelling of the 1953 Suva tsunami,

Fiji, Mar. Geol., 237, 55–70, doi:10.1016/j.margeo.2006.10.036, 2007.

Ramaswamy, V., Rao, P. S., Rao, K. H., Thwin, S., Rao, N. S., and Raiker, V.: Tidal influence on suspended sediment distribution and dispersal in the northern Andaman Sea and Gulf of Martaban, Mar. Geol., 208, 33–42, doi:10.1016/j.margeo.2004.04.019, 2004.

Rao, P. S., Ramaswamy, V., and Thwin, S.: Sediment texture, distribution and transport on the Ayeyarwady continental shelf, Andaman Sea, Mar. Geol., 216, 239–247, doi:10.1016/j.margeo.2005.02.016, 2005.

Rebesco, M. and Stow, D.: Seismic expression of contourites and related deposits: A preface, Mar. Geophys. Res., 22, 303–308, 2001.

Reicherter, K., Hoffmann, N., Lindhorst, K., Krastel, S., Fernández-Steeger, T., Grützner, C., and Wiatr, T.: Active basins and neotectonics: Morphotectonics of the Lake Ohrid Basin (FYROM and Albania), Z. Dtsch Ges. Geowiss., 162, 217–234, 2011.

Robinson, R., Bird, M., Oo, N., Hoey, T., Aye, M., Higgitt, D., Lu, X., Swe, A., Tun, T., and Win, S.: The Irrawaddy river sediment flux to the Indian Ocean: The original nineteenth-century data revisited, J. Geol., 115, 629–640, 2007.

Rodolfo, K. S.: Sediments of the Andaman Basin, northeastern Indian Ocean, Mar. Geol., 7, 371–402, 1969.

Shanmugam, G.: Deep-water bottom currents and their deposits, in: Contourites, Developments in sedimentology, edited by: Rebesco, M., and Camerlenghi, A., Elsevier, Amsterdam, Netherlands, 59–81, 2008.

Sobolev, S. V., Babeyko, A. Y., Wang, R., Hoechner, A., Galas, R., Rothacher, M., Sein, D. V., Schröter, J., Lauterjung, J., and Subarya, C.: Tsunami early warning using GPS-shield arrays, J. Geophys. Res., 112, B08415, doi:10.1029/2006jb004640, 2007.

Socquet, A., Vigny, C., Chamot-Rooke, N., Simons, W., Rangin, C., and Ambrosius, B.: India and Sunda plates motion and deformation along their boundary in Myanmar determined by GPS, J. Geophys. Res., 111, B05406, doi:10.1029/2005jb003877, 2006.

Stigall, J. and Dugan, B.: Overpressure and earthquake initiated slope failure in the Ursa region, northern Gulf of Mexico, J. Geophys. Res., 115, B04101, doi:10.1029/2009jb006848, 2010.

Stow, D. A. V. and Mayall, M.: Deep-water sedimentary systems: New models for the 21st century, Mar. Petrol. Geol., 17, 125–135, 2000.

Tappin, D. R.: Sediment slump likely caused Papua New Guinea tsunami, EOS Transactions American Geophysical Union, 80, 1999.

Tappin, D. R., Watts, P., McMurtry, G. M., Lafoy, Y., and Matsumoto, T.: The Sissano, Papua New Guinea tsunami of July 1998 – offshore evidence on the source mechanism, Mar. Geol., 175, 1–23, 2001.

Varkey, M. J., Murty, V. S. N., and Suryanarayana, A.: Physical oceanography of the Bay of Bengal and Andaman Sea, Oceanography and Marine Biology: An Ann. Rev., 34, 1–70, 1996.

Vlasenko, V. and Alpers, W.: Generation of secondary internal waves by the interaction of an internal solitary wave with an underwater bank, J. Geophys. Res., 110, C02019, doi:10.1029/2004jc002467, 2005.

Vlasenko, V. and Stashchuk, N.: Three-dimensional shoaling of large-amplitude internal waves, J. Geophys. Res., 112, C11018, doi:10.1029/2007jc004107, 2007.

Völker, D., Weinrebe, W., Behrmann, J. H., Bialas, J., and Klaeschen, D.: Mass wasting at the base of the south central Chilean continental margin: The Reloca slide, Adv. Geosci., 22, 155-167, doi:10.5194/adgeo-22-155-2009, 2009.

Vorren, T. O., Laberg, J. S., Blaume, F., Dowdeswell, J. A., Kenyon, N. H., Mienert, J., Rumohr, J. A. N., and Werner, F.: The Norwegian–Greenland sea continental margins: Morphology and late Quaternary sedimentary processes and environment, Quaternary Sci. Rev., 17, 273–302, doi:10.1016/s0277-3791(97)00072-3, 1998.

Wang, Y., Sieh, K., Aung, T., Min, S., Khaing, S. N., and Tun, S. T.: Earthquakes and slip rate of the southern Sagaing Fault: Insights from an offset ancient fort wall, lower Burma (Myanmar), Geophys. J. Int., 185, 49–64, doi:10.1111/j.1365-246X.2010.04918.x, 2011.

Ward, S. N.: Landslide tsunami, J. Geophys. Res.-Sol. Ea., 106, 11201–11215, 2001.

Weiss, R., Fritz, H. M., and Wünnemann, K.: Hybrid modeling of the mega-tsunami runup in Lituya Bay after half a century, Geophys. Res. Lett., 36, L09602, doi:10.1029/2009gl037814, 2009.

Wyrtki, K.: Physical oceanography of the southeast Asian waters, NAGA Report, Volume 2, Scientific Results of Marine Investigations of the South China Sea and the Gulf of Thailand 1959–1961,The University of California, Scripps Institution of Oceanography, La Jolla, California, 195 pp., 1961.

Yamada, Y., Kawamura, K., Ikehara, K., Ogawa, Y., Urgeles, R., Mosher, D., Chaytor, J., and Strasser, M. (Eds.): Submarine mass movements and their consequences, Advances in natural and technological hazards research, Springer, Dordrecht, Netherlands, 2012.

7. Modeling of Potential Landslide Tsunami Hazards Off Western Thailand (Andaman Sea)

MANUSCRIPT III

Julia Schwab, Sebastian Krastel, Mohammad Heidarzadeh, Mathias Grün, Felix Gross, Passakorn Pananont, Pachoenchoke Jintasaeranee, Suratta Bunsomboonsakul, Wilhelm Weinrebe and Daniel Winkelmann

Published in: S. Krastel et al. (Eds.): Submarine Mass Movements and Their Consequences, Advances in Natural and Technological Hazards Research, 37, Springer International Publishing Switzerland, 2014, doi: 10.1007/978-3-319-00972-8.

ERRATUM

Chapter 46
Modeling of Potential Landslide Tsunami Hazards Off Western Thailand (Andaman Sea)

Julia Schwab, Sebastian Krastel, Mohammad Heidarzadeh, and Sascha Brune

S. Krastel et al. (eds.), *Submarine Mass Movements and Their Consequences*, Advances in Natural and Technological Hazards Research 37, DOI 10.1007/978-3-319-00972-8,

DOI 10.1007/978-3-319-00972-8_62

Abstract We model several scenarios of potential submarine landslide tsunamis in the Andaman Sea off the Thai west coast. Our results suggest that landslides may be capable of producing significant tsunamis. Two categories of submarine landslide scenarios were evaluated. Geometry parameters of the first category are taken from identified mass transport deposits (MTDs); the second category considers a potentially unstable block identified in seismic data. Our preliminary modeling approach shows, that run-up values may reach significant tsunami heights for some scenarios. We point out that our results have to be regarded as only preliminary due to several limitations in our modeling approach. Our results, however, show the need for more sophisticated modeling of landslide tsunamis, especially regarding the failure process and inundation on dry land.

Unfortunately this chapter was published without authors' corrections. The revised version is published as Erratum.

J. Schwab (✉)
Helmholtz Centre for Ocean Research, GEOMAR, Kiel, Germany
e-mail: jschwab@geomar.de

S. Krastel
Institute of Geosciences, Christian-Albrechts-Universität zu Kiel, Kiel, Germany

M. Heidarzadeh
Cluster of Excellence "The Future Ocean", Institute of Geosciences, Christian-Albrechts Universität zu Kiel, Kiel, Germany

S. Brune
GFZ German Research Centre for Geosciences, Potsdam, Germany

The online version of the original chapter can be found at http://dx.doi.org/10.1007/978-3-319-00972-8_46

E3

46.1 Introduction

Due to its vicinity to the highly seismic Sunda Trench, the Thai west coast is vulnerable to tectonic tsunamis (e.g. Jankaew et al. 2008). Earthquakes, however, are not the only source of tsunami waves. Seismically triggered submarine slope failures are also known for producing large wave heights in the near field (Synolakis et al. 2002). However, tsunami warning is problematic, as landslides may initiate within minutes or hours of an earthquake (e.g. Fritz et al. 2012), and a seismic signal may not even be detectable prior to a landslide.

Schwab et al. (2012) identified several MTDs and indicators for potential future failures at the western edge of Mergui Ridge, which forms a part of the outer Thai shelf. By minimum volume estimations and submergence depth of identified deposits, they concluded that only a few slope failures may have been tsunamigenic, resulting in a low estimate for landslide tsunami hazards. In order to obtain a more detailed picture of the tsunamigenic potential that may arise from these slope failures, this study aims to quantitatively understand the landslide tsunami hazards off western Thailand by numerical modeling.

46.2 Geological Background

Schwab et al. (2012) examined 2D reflection seismic profiles across the Mergui Ridge-East Andaman Basin transition (Fig. 46.1a), and high resolution bathymetric data from the top of Mergui Ridge. They identified several stacked MTDs west of Mergui Ridge (Figs. 46.1b and 46.2a) indicating recurrent slope failures. Based on the thickness of undisturbed sediment packages between individual MTDs, long time intervals (hundreds of kyrs) were estimated between succeeding events. Possible causes for slope failures include ongoing tectonic activity, occurrence of potentially unstable drift deposits and the presence of fluids and resulting overpressure. Additionally, indicators for potential future failures were identified (Fig. 46.2b) at the faulted western edge of Mergui Ridge (Schwab et al. 2012).

46.3 Modeling and Dataset

Based on geometrical parameters derived from seismic and bathymetric dataset (Figs. 46.1b and 46.2), different hypothetical scenarios of landslide tsunami generation were modeled. The dimensions of the modeled slides are comparable to those described by Brune et al. (2010a, b) from neighboring areas. We follow the modeling approach of these authors, which takes into account that small landslides do not fulfill the applicability conditions for more realistic source models (see Brune et al. 2010b for a discussion of the approach). Therefore initial wave heights are calculated by a set of semi-empirical formulas (Watts et al. 2005; Grilli and Watts 2005). These formulas describe the sea surface response to a simplified coherent rotational slump failure. Compared to other more realistic landslide formulas

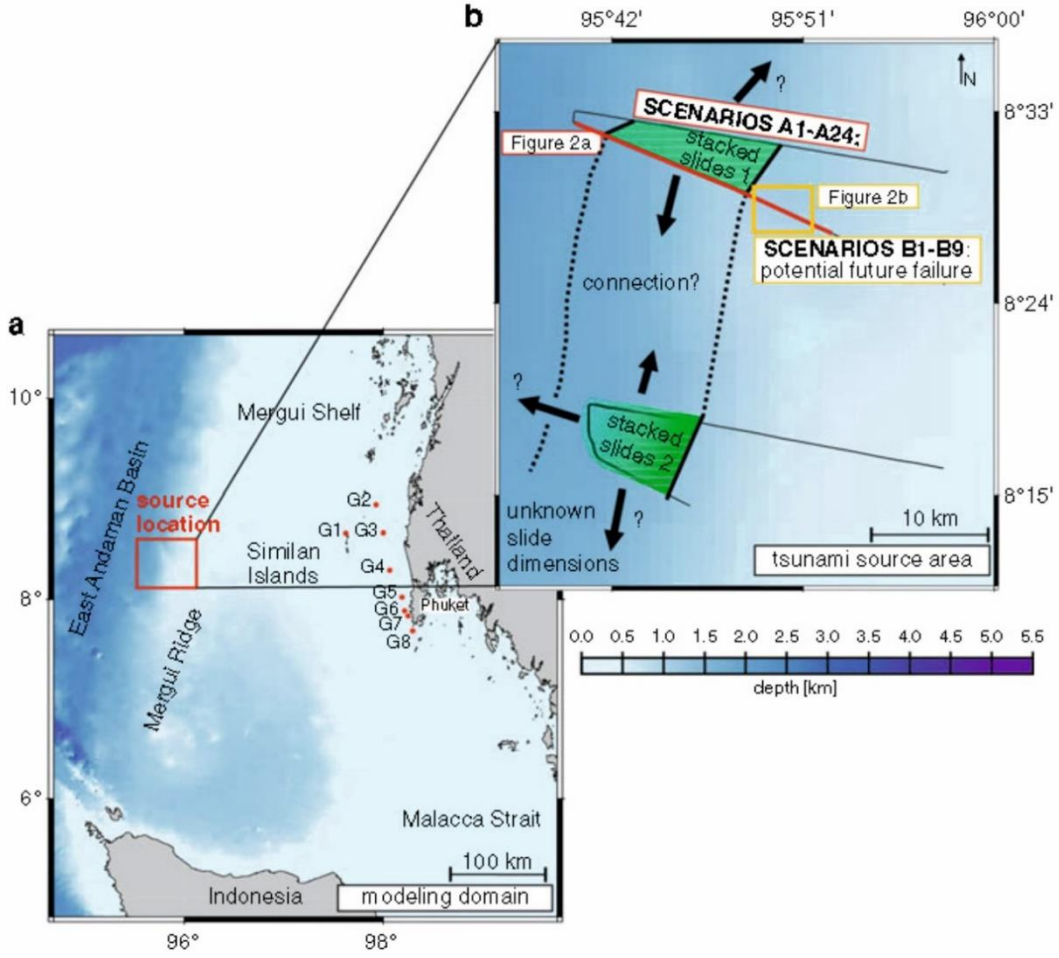

Fig. 46.1 (**a**) Bathymetric map of modeling domain and main structural features. G1–G8 indicate "artificial gauge stations" near the coast (20–50 m water depth) where maximum wave heights of tsunami are derived from. (**b**) Source location for chosen scenarios. *Green* areas indicate the locations where stacked slides have been identified in the basin on seismic profiles (*thin black lines*). *Black arrows* indicate the uncertainty in slide width

(e.g. Mohammed and Fritz 2012) they do not account for the deformation of the slide during the failure process. For calculating tsunami propagation, the TUNAMI-N2 numerical code (e.g. Goto et al. 1997) was applied, and an extension of this code (Brune et al. 2010b) was used to test stability conditions of input parameters and to calculate initial wave heights as described above. The simulations were performed for a total time of 25,200 s for all scenarios with a time step of 0.5 s using the GEBCO bathymetric grid (IOC et al. 2003) resolved to 32 arc sec.

Calculated maximum wave heights are regarded at eight artificial gauge stations G1–G8 (Fig. 46.1a, Table 46.1) placed offshore at water depths of about 20 m (G1) and about 50 m (G2–G8). Empirical formulas were applied to obtain a first estimate of potential run-up heights R1 (Ward and Asphaug 2003) and R2 (Ward and Day 2008) from the maximum offshore wave heights at G1–G8. R1 depends only on water depth and tsunami wave height at an offshore location, whereas for R2 also the slope angle between offshore location and shore line is included.

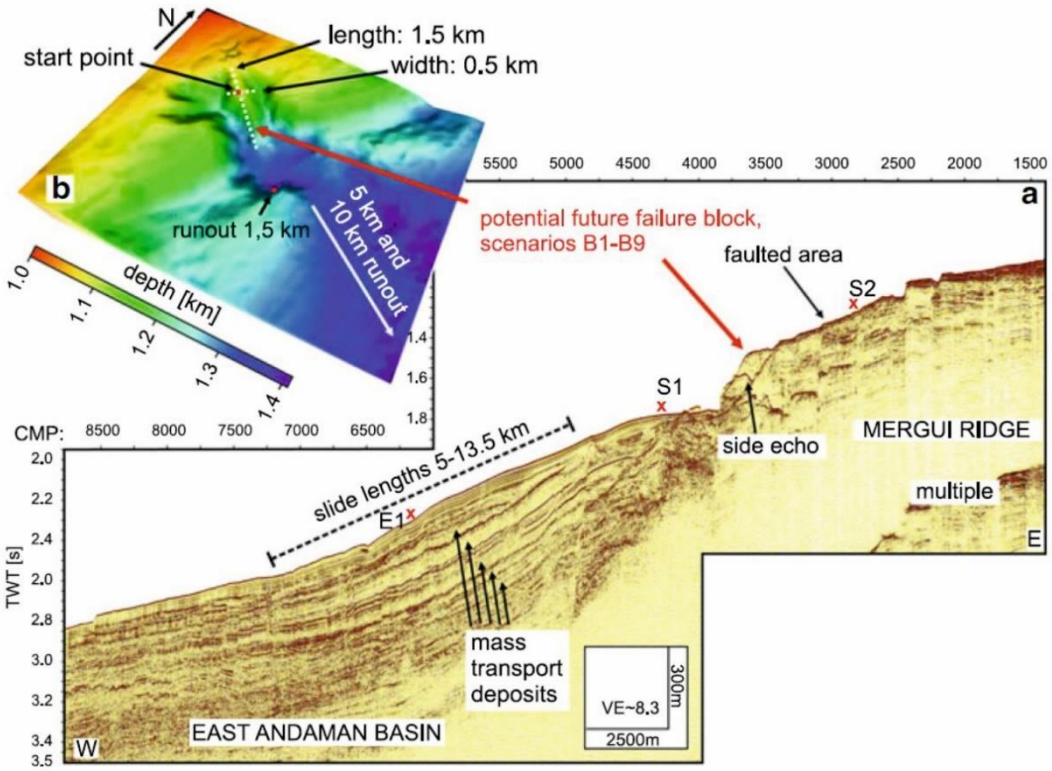

Fig. 46.2 (**a**) 2D reflection seismic profiles across the two source areas, "stacked slides location" and "potentially unstable block". *S1*: start point for slides of scenarios A1–A12, *S2*: start point for slides of scenarios A13–A24. *E1*: Endpoint for slides of scenarios A13–A24. (**b**) Bathymetry of the "potentially unstable block" (scenarios B1–B9). *CMP* Common Midpoint (See Fig. 46.1b for locations)

Table 46.1 Artificial gauge stations

Gauge	G1	G2	G3	G4	G5	G6	G7	G8
Lat [°]	8.6636	8.8639	8.6405	8.2704	8.011	7.8888	7.8404	7.7609
Long [°]	97.6254	98.2577	98.2286	98.27	98.2853	98.2524	98.284	98.3228
Water depth [m]	24	49	50	49	51	48	46	48
Coastal location	Similan Islands	Bang Muang	Khue-kakk	Khok Kloe	Chueng Tao	Patong	Karon	Rawai

46.3.1 Modeled Scenarios

We chose two source locations based on information derived from seismic and bathymetric data (Fig. 46.1). Scenarios A1–A24 correspond to a location of previously-identified, stacked MTDs. Scenarios B1–B9 consider a potentially unstable block (Fig. 46.2, Schwab et al. 2012).

46.3.1.1 Scenarios A1–A24, "Stacked Slides Location"

The "stacked slides location" is situated west of the Mergui Ridge (Fig. 46.1b). Four parallel seismic reflection profiles show a similar pattern of five stacked MTDs (Fig. 46.2a). Geometrical properties of the modeled slides were varied according to the dimensions of identified slides with lengths between 5 and 13.5 km. Widths of 5, 7 and 30 km were chosen, the latter width value assuming that the two areas of stacked MTDs are connected, while the smaller values imply separate failure events. The slide thickness applied for these scenarios was 150 m, which is the maximum thickness measured for all detected MTDs. We use slope angles of 3° and 6°, corresponding to the range of slope angles in the source area. The origin of the MTDs is unknown, therefore we assume two different locations for slide initiation at the edge of the ridge in about 880 m water depth (run-out distance 15.5 km) and at the upper boundary of the basin in about 1,270 m water depth (run-out distance 7.5 km, Fig. 46.2a).

46.3.1.2 Scenarios B1–B9: "Potentially Unstable Block"

In scenarios B1–B9, we model the failure of a potentially unstable sedimentary block located at the edge of Mergui Ridge in about 1,100 m water depth (Fig. 46.2a) (Schwab et al. 2012). Its dimensions (Table 46.3) are derived from bathymetric data (Fig. 46.2b). Different run-out distances (1.5, 5 and 10 km) and slope angles (3°, 6° and 14.5) were used (Table 46.3).

46.4 Results

Initial positive wave heights (η_{plus}) for scenarios A1–A24 range between 1.5 and 118.1 m (Table 46.2). η_{plus} values larger than 40 m are reached for scenarios with long run-out distances and short slide lengths of 5 km (A13, A15, A17, A19, A21, A23). Arrival times of the first tsunami waves at the coast (32–37 min) are similar for all scenarios. A_{20max}, the maximum offshore wave height at G1, ranges between 1.3 and 22.8 m for the A-scenarios. Run-up estimations from A_{20max} range between 2.3 and 23.1 m (R1) and 8.0 and 25.8 m (R2), respectively.

For scenarios B1–B9, η_{plus} ranges between 1.7 and 28.2 m (Table 46.3). Arrival times are in the same range as for the A-scenarios (37–40 min). Compared to A1–A24, the A_{20max} values of B1–B9 are smaller (0.01–0.24 m). Run-up estimations are in the range of 0.04–0.61 m (R1) and 1.0–4.0 m (R1) respectively.

The maximum wave height distributions strongly depend on slide input parameters (Tables 46.2 and 46.3, Figs. 46.3 and 46.4). Despite its larger length, scenario A2 produces smaller wave heights compared to scenario A1 (Fig. 46.3a, b). Scenario

Table 46.2 Key modeling parameters for scenario A1–A24

Scenario	A1	A2	A3	A4	A5	A6	A7	A8	A9	A10	A11	A12
Runout [km]	7.5	7.5	7.5	7.5	7.5	7.5	7.5	7.5	7.5	7.5	7.5	7.5
SLA [°]	3	3	3	3	3	3	6	6	6	6	6	6
DIM [km × km]	5 × 5	5 × 13.5	7 × 5	7 × 13.5	30 × 5	30 × 13.5	5 × 5	5 × 13.5	7 × 5	7 × 13.5	30 × 5	30 × 13.5
Th [m]	150	150	150	150	150	150	150	150	150	150	150	150
Vol [km^3]	2.9	8.0	4.1	11.1	17.7	47.7	2.9	8.0	4.1	11.1	17.7	47.7
η_{plus} [m]	10.8	1.5	13.2	2.0	23.7	5.0	12.6	1.8	15.5	2.3	27.6	5.8
Ta [min]	36	37	36	36	33	32	36	36	36	36	33	32
A_{20max} [m]	2.3	1.3	3.0	1.8	7.7	5.6	2.6	1.5	3.5	2.1	8.7	6.6
R1 [m]	3.6	2.3	4.6	3.0	9.6	7.5	4.1	2.6	5.1	3.4	10.6	8.5
R2 [m]	10.0	8.0	11.3	9.1	16.5	14.5	10.6	8.5	11.9	9.7	17.4	15.5
Scenario	A13	A14	A15	A16	A17	A18	A19	A20	A21	A22	A23	A24
Runout [km]	15.5	15.5	15.5	15.5	15.5	15.5	15.5	15.5	15.5	15.5	15.5	15.5
SLA [°]	3	3	3	3	3	3	6	6	6	6	6	6
DIM [km × km]	5 × 5	5 × 13.5	7 × 5	7 × 13.5	30 × 5	30 × 13.5	5 × 5	5 × 13.5	7 × 5	7 × 13.5	30 × 5	30 × 13.5
Th [m]	150	150	150	150	150	150	150	150	150	150	150	150
Vol [km^3]	2.9	8.0	4.1	11.1	17.7	47.7	2.9	8.0	4.1	11.1	17.7	47.7
η_{plus} [m]	49.8	6.8	60.4	8.9	101.4	21.0	58.0	8.0	70.3	10.4	118.1	24.4
Ta[min]	36	37	36	36	33	32	36	37	36	36	32	31
A_{20max} [m]	7.3	5.2	9.2	7.1	15.9	20.3	8.2	6.1	10.2	8.3	16.5	22.8
R1 [m]	9.3	7.1	11.2	9.1	17.2	21.0	10.2	8.0	12.1	10.3	17.8	23.1
R2 [m]	16.2	14.1	17.8	16.0	22.2	24.6	17.0	15.0	18.6	17.1	22.6	25.8

SLA local slope angle, *Runout* run-out distance, *DIM* slide dimensions in width × length, *Th* thickness of slide, *Vol.* Volume of the slide, calculated as given in Grilli and Watts (2005), η_{plus} initial wave height, *Ta* arrival time, A_{20max} maximum wave height (surface elevation) at G1, *R1* run-up calculated for A_{20max} after Ward and Asphaug (2003), *R2* run-up calculated after Ward and Day (2008)

Table 46.3 Key modeling parameters for scenarios B1–B9

Scenario	B1	B2	B3	B4	B5	B6	B7	B8	B9
Runout[km]	1.5	5	10	1.5	5	10	1.5	5	10
SLA [°]	3	3	3	6	6	6	14.5	14.5	14.5
DIM [km × km]	0.5 × 1.5	0.5 × 1.5	0.5 × 1.5	0.5 × 1.5	0.5 × 1.5	0.5 × 1.5	0.5 × 1.5	0.5 × 1.5	0.5 × 1.5
Th [m]	125	125	125	125	125	125	125	125	125
Vol [km^3]	0.07	0.07	0.07	0.07	0.07	0.07	0.07	0.07	0.07
η_{plus}[m]	1.7	9.0	24.2	2.0	10.5	28.2	2.4	12.8	34.2
Ta[min]	40	37	37	40	37	37	37	39	40
A_{20max}[m]	0.01	0.06	0.17	0.01	0.070	0.20	0.01	0.09	0.24
R1[m]	0.04	0.20	0.47	0.04	0.23	0.53	0.05	0.27	0.61
R2[m]	1.0	2.3	3.5	1.0	2.4	3.7	1.1	2.7	4.0

SLA local slope angle, *Runout* run-out distance, *DIM* slide dimensions in width × length, *Th* thickness of slide, *Vol.* Volume of the slide, calculated after Grilli and Watts (2005), η_{plus} initial wave height, *Ta* arrival time, A_{20max} maximum wave height (surface elevation) at G1, *R1* run-up calculated for A_{20max} after Ward and Asphaug (2003), *R2*: run-up calculated after Ward and Day (2008)

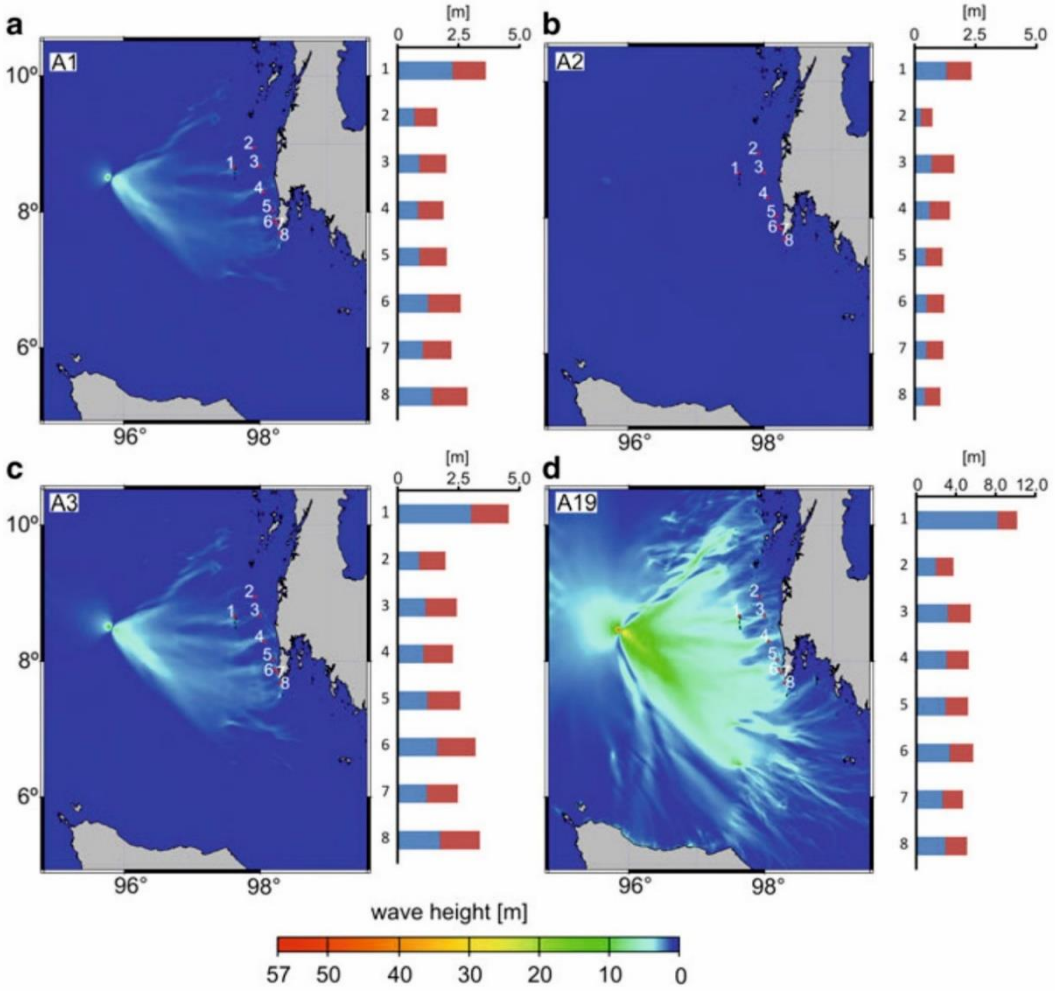

Fig. 46.3 Examples for wave height distributions from hypothetical failures at the "stacked slides location", as well as maximum wave heights (*blue bars*) and R1 run-up estimations (*red bars*) for artificial gauge stations G1–G8. Note the different scales for the wave height/run-up charts

A3 has a larger width compared to A1 and produces larger wave heights. Scenario A19 has the same slide dimensions as A1 but a larger run-out distance and larger slope angle (Fig. 46.3d, Table 46.2). This scenario also results in larger wave heights compared to A1.

Generally, largest maximum wave heights arise near the source area and in a triangular zone towards the coast. Regarding maximum wave heights at individual gauge locations, G1 records the largest run-up estimations (Fig. 46.3).

Figure 46.4 demonstrates the difference in wave heights for different run-out distances and slope angles of the B-scenarios (Table 46.3). Compared to the A-scenarios, the tsunami wave heights are smaller and not focused towards the coast, indicating reduced tsunami potential of the B-scenarios.

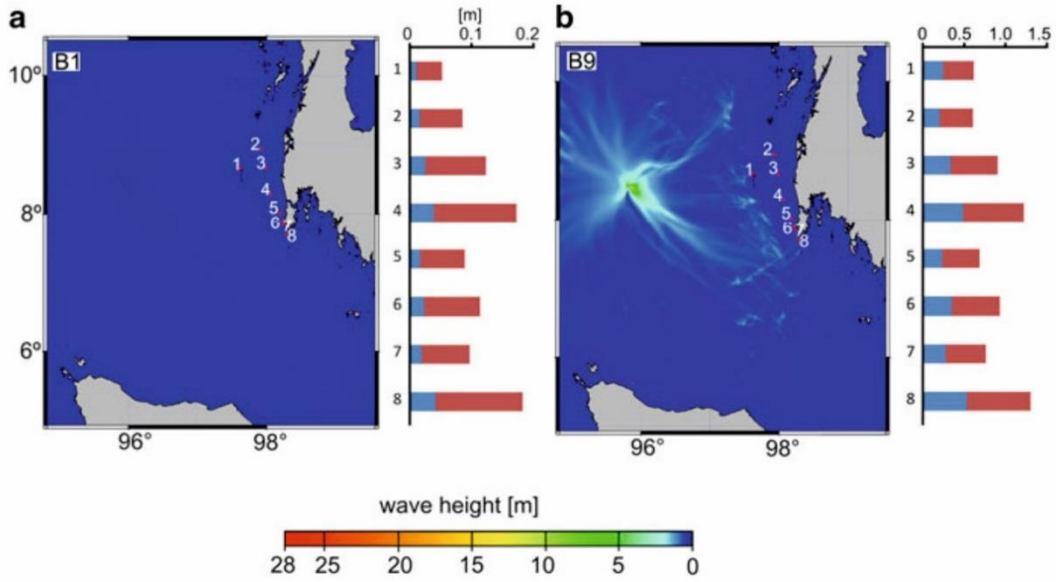

Fig. 46.4 Examples for wave height distributions from hypothetical failures at "potentially unstable block" location, as well as maximum wave heights (*blue bars*) and R1 run-up estimations (*red bars*) for artificial gauge stations G1–G8. Note the different scales for the wave height/run-up charts

46.5 Discussion and Conclusions

Our results give first insights into the tsunamigenic potential of slope failures off western Thailand. These results are only a preliminary assessment of landslide tsunami potential due to the limitations of the chosen approach:

1. The failure process that produced the MTDs in the working area is unknown. Therefore initial wave heights were calculated from failures, modeled as simplified coherent rotational slumps. More realistic failure scenarios such as translational and/or disintegrating slides or in the form of multiple events would produce smaller wave heights (Masson et al. 2006), but were not modeled in our preliminarily approach. Hence our modeled initial wave height is most likely overestimated.
2. In our numerical simulations, wave evolution beyond water depth of 20 m is prohibited, therefore run-up values were estimated by empirical equations using offshore wave heights at only a few isolated points (G1–G8), and inundation modeling was not performed at all. Empirical equations have limitations, the results vary for different equations (Tables 46.2 and 46.3), and near-shore wave phenomena reducing run-ups such as wave breaking are not considered by these empirical formulas.
3. Tsunami propagation was calculated from a coarse bathymetric grid and by shallow-water equations, which do not take into account effects such as dispersion. This may lead to inaccuracy of wave calculations.

4. The dimensions of the landslides in the A-scenarios are inferred from MTDs, as the pre-failure dimensions of the slides are not known. Thereby a thickness of 150 m was chosen for all scenarios, as thickness is the least determined value based on our seismic field data. This means that, as thickness is an important factor for wave generation, the calculation of initial wave height may contain inaccuracies.
5. The seismic images of the MTDs show clear signs of disintegration. This means that deformation occurred during the failure. According to Mohammed and Fritz (2012) deformation during the failure process leads to energy conversion and hence wave reduction. This again suggests that wave heights calculated in this study may be overestimated.

Landslide tsunamis are often described as a local phenomenon with large run-up heights limited to the near-field (Synolakis et al. 2002). Our results for the A-scenarios show such patterns (Fig. 46.3d), with a triangular zone of large maximum wave heights, presumably indicating a delimited area where tsunami hazard may occur at the coast. Some of the scenarios studied here show potential tsunami hazards comparable to the Papua New Guinea landslide tsunami of July 1998, where large run-up heights of more than 10 m were observed on a very limited coastline of about 20 km (Synolakis et al. 2002). A location especially exposed to a tsunami would then be around the gauge station G1, where the largest run-up heights were estimated.

Contrasting to the modeling results of A1–A24, the B-scenarios produce lower run-up height estimations, which are reasonable due to their smaller landslide volume and more realistic slide dimensions, and which are comparable to values described by Jintasaeranee et al. (2012).

Our results suggest that a landslide tsunami hazard for the coastal areas may exist, and wave heights and run-up estimations may increase with slope angle, run-out distance and slide volume. The width/length ratio of the slides is also affecting our preliminary results, as in most cases an increase in length leads to unexpected decrease in wave heights. This finding has to be examined in greater detail in the future.

Unlike tectonic tsunamis, landslide tsunami sources cannot not be located based on global networks and they may be located close to the shoreline (e.g. Fritz et al. 2012). Therefore landslide tsunamis are almost unpredictable making tsunami warning impossible. Short arrival times of around 30 min or less are typical for near-field tsunamis. The calculated arrival times of our model scenarios are close to this range, indicating that warning time for coastal areas would be short, adding to the unpredictability of landslide tsunamis.

Because of the previously mentioned limitations of our model approach, our results only represent worst case scenarios. This is especially true for the A-scenarios with largest volumes. Furthermore, recurrence rates for major tsunamigenic earthquakes in the area are estimated by 400 years (Monecke et al. 2008), whereas landslide recurrence is estimated to be in the range of 100 kyrs (Schwab et al. 2012). Hence, landslide tsunamis do not represent a major additional risk for the Thai coast.

However, they cannot be neglected and we recommend further geological surveys in the region to better locate sizes and distribution of submarine landslides, and sophisticated numerical modeling in order to reliably assess their hazard potential.

Acknowledgments The TUNAMI-N2 code is originally authored by Fumihiku Imamura and Nobou Shuto and copyrighted to Ahmet C. Yalciner, Fumihiku Imamura and Costas E. Synolakis. We acknowledge them for developing and making available the code. We thank the reviewers Hermann Fritz and Marc de Batist for their careful reviews and constructive comments that helped to improve the manuscript.

References

Brune S, Babeyko AY, Ladage S, Sobolev SV (2010a) Landslide tsunami hazard in the Indonesian Sunda Arc. Nat Hazards Earth Sys 10:589–604. doi:10.5194/nhess-10-589-2010

Brune S, Ladage S, Babeyko AY et al (2010b) Submarine landslides at the eastern Sunda margin: observations and tsunami impact assessment. Nat Hazards 54:547–562. doi:10.1007/s11069-009-9487-8

Fritz HM, Hillaire JV, Molière E, Wei E, Mohammed F (2012) Twin tsunamis triggered by the 12 January 2010 Haiti earthquake. Pure Appl Geophys. doi:10.1007/s00024-012-0479-3

Goto C, Ogawa Y, Shuto N, Imamura F (1997) IUGG/IOC TIME Project: Numerical method of tsunami simulation with the leap-frog scheme. In Intergovernmental Oceanographic Commission, manuals and guides no. 35, UNESCO

Grilli ST, Watts P (2005) Tsunami generation by submarine mass failure. Part I: modeling, experimental validation, and sensitivity analysis. Waterw Port C-ASCE 131(6):283–297

IOC, IHO, BODC (2003) Centenary edition of the GEBCO digital atlas, published on CD-ROM on behalf of the Intergovernmental Oceanographic Commission and the International Hydrographic Organization as part of the general bathymetric chart of the oceans. British oceanographic data centre, Liverpool

Jankaew K, Atwater BF, Sawai Y et al (2008) Medieval forewarning of the 2004 Indian Ocean tsunami in Thailand. Nature 455:1228–1231. doi:10.1038/nature07373

Jintasaeranee P, Weinrebe W, Klaucke I et al (2012) Morphology of the Andaman outer shelf and upper slope of the Thai exclusive economic zone. J Asian Earth Sci 46:78–85

Masson DG, Harbitz CB, Wynn RB et al (2006) Submarine landslides: processes, triggers and hazard prediction. Philos Trans R Soc A 364:2009–2039

Mohammed F, Fritz HM (2012) Physical modeling of tsunamis generated by three-dimensional deformable granular landslides. J Geophys Res 117(C11):C11015

Monecke K, Finger W, Klarer D et al (2008) A 1,000-year sediment record of tsunami recurrence in northern Sumatra. Nature 455:1232–1234. doi:10.1038/nature07374

Schwab JM, Krastel S, Grün M et al (2012) Submarine mass wasting and associated tsunami risk offshore western Thailand, Andaman Sea, Indian Ocean. Nat Hazards Earth Sys 12:609–2630. doi:10.5194/nhess-12-2609-2012

Synolakis CE, Bardet J-P, Borrero JC et al (2002) The slump origin of the 1998 Papua New Guinea tsunami. Proc R Soc Lond A 458:763–789

Ward SN, Asphaug E (2003) Asteroid impact tsunami of 2880 March 16. Geophys J Int 153:F6–F10. doi:10.1046/j.1365-246X.2003.01944.x

Ward SN, Day S (2008) Tsunami balls: a granular approach to tsunami runup and inundation. Commun Comput Phys 3(1):222–249

Watts P, Grilli ST, Tappin D, Fryer GJ (2005) Tsunami generation by submarine mass failure. Part II: predictive equations and case studies. Waterw Port C-ASCE 131(6):298–310

8. Conclusions and Outlook

The research carried out in the framework of this thesis aimed to investigate slope stability and landslide tsunami potential of the outer shelf slope in the Mergui Ridge area. Mainly based on high resolution 2D multichannel reflection seismic and multibeam bathymetry data the previously unknown younger sedimentary development and recent sediment dynamics of the area were investigated. Distribution and dimensions of mass transport deposits were investigated and conclusions were drawn on possible preconditioning factors/triggers for slope failures. Based on these results a preliminary modeling of landslide tsunami scenarios and run ups was carried out.

The Mergui Ridge that has already been known as a sediment starved area exhibits only a thin sedimentary cover compared to the adjacent Mergui Basin. Deposition of the oldest sedimentary unit identified in the new high-resolution seismic data started previous to the Late Miocene. These units have been subject to erosion during uplift phases when the Mergui Ridge was subaerially exposed. The top of is this sedimentary unit is formed by the approximate Late Miocene-Pliocene boundary. Afterward, during large scale subsidence in the Pliocene the Mergui Ridge was partly covered by Plio-Pleistocene sediments that show indicators of sea level fluctuations during initial subsidence. A thin layer of undisturbed sediments cover the sediments deposited during the initial sea level rise. These youngest sediments are continuous in the eastward adjacent Mergui Basin but taper out towards the west on the Mergui Ridge, forming a pronounced mounded body aligned parallel to the slope. Today parts of the old pre-Late Miocene units are still outcropping in a zone aligned parallel to the shelf slope forming an area of non-deposition or erosion. Slope sediments showing clear characteristics of drift deposits are deposited west of the Mergui Ridge.

Generally, the architecture of the sedimentary deposits on the Mergui Ridge show clear indications to be influenced by bottom currents, including the overall mounded shape of the sedimentary succession on the Mergui Ridge, the zone of outcropping pre-Late Miocene sediments, the presence of an along slope moat and the formation of moats around obstacles. Most likely these drift deposits are relatively young (Latest Plio-Pleistocene). Bottom currents that occur in the area may be monsoon controlled and potentially also enhanced by the occurrence of internal waves. During peak monsoon months, a northward along slope current is present in the area that may prevent deposition of fine grained material, and cause local erosion as well as deposition of drift deposits.

The occurrence of mass transport deposits especially on the western flank of the Mergui Ridge indicates that the slope has generally been unstable. Most of the slope failures occurred in drift deposits. Potential preconditioning factors and triggers are the general instability of drift deposits, the occurrence of fluids within these sediments and also tectonic activity. Earthquakes may act as final trigger for slope failures. Some areas show stacked mass transport deposits indicating repeated failures of specific areas. The recurrence interval of failures is long, as derived from the thickness of hemipelagic layers between the mass transport deposits, and hence the recurrence rate is low compared to tectonic tsunamis. Most mass transport deposits are of relatively small volumes between 0.3 up to 14km^3 approximately, and they occurred in large water depths. The tsunami potential arising from such failures is considered to be low, but cannot be excluded. Areas of potential future failures have been identified based on the presence of fluid migration pathways and deformation structures in young sediments.

Modeling of landslide tsunamis and nearshore run up estimations (between up to 1.0 to 25.8m), based on failure scenarios reconstructed from the bathymetric and seismic data set show that a tsunami hazard for the Thai coast may exist. Increasing wave heights are modelled with increasing slope angle, runout distance and volume of potential slope failures. However, modeled tsunamis represent worst case scenarios and wave heights may be overestimated, as for example deformation of slides is not taken into account.

In summary, the work of this thesis has shown that the Thai continental margin in the Mergui Ridge area is shaped by the interaction of bottom currents with the sea floor, leading to drift deposition in the youngest geological past, although the sedimentary input into the area is low. The identification of several mass transport deposits proofs the importance of slope failures during margin evolution, but only few of these failures may have caused a tsunami. Moreover, the recurrence of failures is long compared to tectonic tsunamis. Therefore, the risk of landslide tsunamis hitting the Andaman coast is small compared to earthquake tsunamis generated in the Sunda Trench. Landslide triggered tsunamis, however, cannot be excluded and would hit the Andaman coast with almost no warning time.

Future work should address the following topics: The current velocity data used in this thesis are from a coarse grid and mainly derived from modeling. Moreover, although internal waves have been observed and evidence for interaction of internal waves with the sea floor (Vlasenko and Alpers, 2005) and the biosphere (Wall et al. 2015; Schmidt et al. 2013; Jantzen et al., 2013) have been previously found, these studies focus on shallow shelf areas around 200m water depth. For this thesis, no measurements such as ADCP data were available for the outer continental margins. Future work aiming in this direction should focus on the acquisition of oceanographic dataset, such as ADCP measurements especially in the deeper part of the water column close to the sea floor. A monitoring over a longer period of time would allow to better constraining bottom current velocities as well as seasonal fluctuations of the bottom currents. Moreover, the occurrence of internal waves, their interaction with the topography and their dependence on the tidal cycle as they may be especially intense during spring tides (Hyder, 2005) needs to be examined. In this context, it would be useful to collect temperature/salinity data which would help to better constrain the water mass stratification in deeper parts of the water column close to the sea floor. As it has been shown for example by Preu et al. (2013), drift deposits and erosive features related to bottom current activity tend to occur related to water mass boundaries, where turbulences lead to erosive activity. A similar configuration may be present in the area of the Mergui Ridge and could be the target of further studies.

The presence and architecture of sedimentary units has been derived from high resolution 2D multichannel reflection seismic, but data coverage is limited to the southern part of the Thai EEZ and the profile spacing is large (up to 7km). Equally, the multibeam bathymetry covers only a limited area at the western edge of Mergui Ridge to water depth of maximum 2000m. Both datasets are also restricted to the boundary of the Thai EEZ towards the west, thus limiting data coverage of the transition from the Mergui Ridge slope towards the East Andaman Basin In order to better constrain sedimentary units, morphological features, as well as the frequency and the nature of slope failures in the working area, acquisition of a more extensive bathymetric and reflection seismic dataset would be necessary, especially at the western flank of Mergui Ridge, in order to constrain the location of mass wasting deposits and their extent in greater detail and over a larger area. This would help to quantify mass transported deposits more robustly regarding their volume. Moreover, a bathymetric dataset across the edge of Mergui Ridge to the west would help to identify if recent slide events are present at the basin ridge transition. Possible headwall/sidewall structures or escarpments that may be identified in such a

dataset would help to identify runout distances of individual slide events. The timing of slide events was derived from a general estimation of sedimentation rates for the area (Rodolfo, 1969). Acquisition of sediment cores in the areas where failures do occur could help to constrain their ages and hence their recurrence reliably. Sampling of mass transport deposits would allow classifying them and giving insight in failure dynamics and coherency of the landslides. Moreover, age dating of sliding events may allow a comparison/correlation with tsunami deposits that have been identified and dated on land (e.g. Brill et al. 2011; 2012), in order to determine if any landslide event really has triggered a tsunami that reached the shoreline, and also if they coincidence with earthquakes in the area. Geotechnical measurements (e.g. cone penetrometer measurements) would allow insights into shear strength of the sediment. Furthermore, potential areas of future failure have been identified in this thesis based on indications such as the presence of fluid migration pathways and the occurrence of faults. A more extensive geophysical and geotechnical data set may allow defining the occurrence of such unstable areas with more certainty.

Geological sampling in the area may also help to characterize the nature of the drift deposits including sediment types and grain size variations. Such data may give an idea of bottom current strength and variability over time. It is suggested in this thesis that the drift deposits are related to currents that are influenced by the monsoon system. As these drift deposits tend to be unstable, it would be very interesting to investigate the timing of slope failures in relation to the development of the drift deposits.

The modeling of landslide triggered tsunamis in this thesis is based on simplifying parametrization of landslides as a coherent rotational slump. The resulting tsunami heights represent worst case scenarios. Such a method is appropriate for a preliminary tsunami assessment (Watts et al., 2005) but it does not account for the deformation of the landslide mass during the failure process as more realistic landslide formulas do (e.g. Mohammed and Fritz, 2012). The modeling carried out for this thesis is not a hazard/risk assessment. The steps that need to be taken into account towards a robust hazard assessment should focus on the frequency and nature of the source events for possible tsunamis, i.e. the landslide events, an improved modeling approach and the impact on the coast. Assessing the probability of significant tsunami waves requires a statistically relevant database of historical events or sophisticated numerical modeling methods that give insight into the inundation of the coast (Burbidge and Cummins, 2008). Moreover, to know if a landslide causes a tsunami in the first place, it is important to take into account the properties of the landslide and its dynamics during failure (Løvholt et al. 2016 and references therein), which are the governing properties controlling the initial wave height. Also, a reliable recurrence rate of slope failures has to been known in order to estimate frequency of landslide tsunamis. Therefore, a better constraint of the nature of failure events and their frequency is needed toward hazard assessment. These better constrained data could then be used to model the initial tsunami wave with a modeling approach that takes into account the development of the landslide during the slide process. Another important step to be addressed is the assessment of inundation at the coast as this has been done for example for the 2004 tsunami (Kaiser et al., 2011). This is important, as the presence of coastal forests as well as topographic variations in the nearshore area and on the coast line can alter inundation and run up as has been the case during the 2004 Tsunami (Szczuciński et al., 2006; Ohira et al., 2012).

References

Brill, D., 2012. The tsunami history of southwest Thailand – Recurrence, magnitude and impact of palaeotsunamis inferred from onshore deposits.

Brill, D., Brückner, H., Jankaew, K., Kelletat, D., Scheffers, A., Scheffers, S., 2011. Potential predecessors of the 2004 Indian Ocean Tsunami — Sedimentary evidence of extreme wave events at Ban Bang Sak, SW Thailand. Sedimentary Geology 239 (3–4), 146–161.

Burbidge, D., Cummins, P., Mleczko, R., Thio, H., 2008. A Probabilistic Tsunami Hazard Assessment for Western Australia. Pure appl. geophys. 165 (11-12), 2059–2088. 10.1007/s00024-008-0421-x.

Hyder, P., Jeans, D., Cauquil, E., Nerzic, R., 2005. Observations and predictability of internal solitons in the northern Andaman Sea. Applied Ocean Research 27 (1), 1–11. 10.1016/j.apor.2005.07.001.

Jantzen, C., Schmidt, G.M., Wild, C., Roder, C., Khokiattiwong, S., Richter, C., 2013. Benthic reef primary production in response to large amplitude internal waves at the Similan Islands (Andaman Sea, Thailand). PloS one 8 (11), e81834. 10.1371/journal.pone.0081834.

Kaiser, G., Scheele, L., Kortenhaus, A., Løvholt, F., Römer, H., Leschka, S., 2011. The influence of land cover roughness on the results of high resolution tsunami inundation modeling. Nat. Hazards Earth Syst. Sci. 11 (9), 2521–2540. 10.5194/nhess-11-2521-2011.

Løvholt, F., Pedersen, G., Harbitz, C.B., Glimsdal, S., Kim, J., 2015. On the characteristics of landslide tsunamis. Philosophical transactions. Series A, Mathematical, physical, and engineering sciences 373 (2053). 10.1098/rsta.2014.0376.

Mohammed, F., Fritz, H.M., 2012. Physical modeling of tsunamis generated by three-dimensional deformable granular landslides. Journal of Geophysical Research 117 (C11), C11015. 10.1029/2011JC007850.

Ohira, W., Honda, K., Harada, K., 2012. Reduction of tsunami inundation by coastal forests in Yogyakarta, Indonesia: a numerical study. Nat. Hazards Earth Syst. Sci. 12 (1), 85–95. 10.5194/nhess-12-85-2012.

Rodolfo, K.S., 1969. Sediments of the Andaman Basin, northeastern Indian Ocean. Marine Geology 7 (5), 371–402. 10.1016/0025-3227(69)90014-0.

Schmidt, G.M., Richter, C., 2013. Coral growth and bioerosion of Porites lutea in response to large amplitude internal waves. PloS one 8 (12), e73236. 10.1371/journal.pone.0073236.

Szczuciński, W., Chaimanee, N., Niedzielski, P., Rachlewicz, G., Saisuttichai, D., Tepsuwan, T., Lorenc, S., Siepak, J., 2009. Environmental and Geological Impacts of the 26 December 2004 Tsunami in Coastal Zone of Thailand – Overview of Short and Long-Term Effects. Polish Journal of Environmental Studies 15 (5), 793–810.

Vlasenko, V., Alpers, W., 2005. Generation of secondary internal waves by the interaction of an internal solitary wave with an underwater bank. Journal of Geophysical Research 110 (C2). 10.1029/2004JC002467.

Wall, M., Putchim, L., Schmidt, G.M., Jantzen, C., Khokiattiwong, S., Richter, C., 2015. Large-amplitude internal waves benefit corals during thermal stress. Proceedings. Biological sciences / The Royal Society 282 (1799), 20140650. 10.1098/rspb.2014.0650.

Watts, P., Grilli, S.T., Tappin, D.R., Fryer, G.J., 2005. Tsunami Generation by Submarine Mass Failure. II: Predictive Equations and Case Studies. J. Waterway, Port, Coastal, Ocean Eng. 131 (6), 298–310.

Acknowledgements

Many thanks to my first supervisor Prof. Dr. Sebastian Krastel, for offering me the opportunity to conduct my PhD Thesis in the framework of the MASS project, for his support and for reviewing my thesis.

Many thanks also to my co-supervisor, Prof. Dr. Karl Stattegger for reviewing my thesis.

Many thanks to the Deutsche Forschungsgemeinschaft (Grant KR2222-8) and the National Research Council of Thailand (NRCT) for funding the MASS project in the framework of TRIAS

Many thanks to the scientists and crew of the MASS III cruise for their help in collecting the data.

Many thanks to the Phuket Marine Biological Center and the Thailand Southeast Asia START Regional Center for logistic support around the MASS cruise.

Many thanks to my co-authors for support during manuscript preparation and interesting comments and insights.

Many thanks to the reviewers of my published manuscripts for helpful comments on my work.

Thanks to my colleagues for helpful discussions and thank you for your support: Anke Schürer, Denis Cukur, Elodie Lebas, Felix Gross, Jens Schneider, Katja Lindhorst, Lili Fu, Mohammad Heidarzadeh, Peter Feldens, Philipp Held and Wei Li.

And last but certainly not least: Thanks to my friends and family for supporting me through the last years.

Thank you Christian and Hanna!